

Automated resummation of electroweak Sudakov logarithms in diboson production



Dissertation zur Erlangung des naturwissenschaftlichen
Doktorgrades an der Fakultät für Physik und Astronomie der
Julius-Maximilians-Universität Würzburg

vorgelegt von

Stefan Rode

aus Goch

Würzburg, im April 2024

Eingereicht bei der Fakultät für Physik und Astronomie am: _____

Gutachter der Dissertation

1. Gutachter: Prof. Dr. Ansgar Denner
2. Gutachter: Prof. Dr. Raimund Ströhmer

Prüfer des öffentlichen Promotionskolloquiums

1. Prüfer: Prof. Dr. Ansgar Denner
2. Prüfer: Prof. Dr. Raimund Ströhmer
3. Prüfer: _____

Tag des öffentlichen Promotionskolloquiums: _____

Doktorurkunde ausgehändigt am: _____

Abstract

The present thesis is concerned with the automated computation of integrated and differential cross sections of diboson production in proton–proton and electron–positron collisions at very high energies, including a resummation of electroweak Sudakov logarithms to all orders in the fine-structure constant using soft–collinear effective theory.

The search for new physics at future colliders such as the FCC–hh or the CLIC requires precise predictions for scattering cross sections from the theoretical high-energy physics community. Electroweak Sudakov logarithms, which currently limit the accuracy of predictions in the high-energy tails of differential distributions for LHC-like energies, are known to destroy the convergence behaviour of the fixed-order perturbative series, once sufficiently high energies are considered.

To resum these large corrections, soft–collinear effective theory has been applied to simple processes, which permits analytic calculations. Within this work, we present an automated computation within a Monte Carlo integration framework, thus facilitating the computation of fully differential cross section to complicated processes. This requires the use of the Catani–Seymour subtraction algorithm to treat the occurring infrared divergences. The machinery is applied to all diboson processes with intermediate weak gauge bosons, including the photon-induced W^+W^- -production channel.

To this end we carefully study the validity of the necessary assumptions such as the double-pole approximation and estimate the order of magnitude of neglected effects. Especially the non-doubly-resonant contributions turn out to be sizeable in several interesting phase-space regions.

For lepton collisions at 3 TeV we obtain the integrated cross sections of W-pair and Z-pair production to be shifted by more than 20% with respect to the Born value, owing to the resummation of the leading-logarithmic corrections. These effects are partly cancelled by subleading effects. For proton–proton collisions at $\sqrt{s} = 100$ TeV we observe sizeable resummation effects in the high-energy tails, while the integrated cross sections are dominated by interactions, for which soft–collinear effective theory is not applicable.

Zusammenfassung

Das Thema ist der vorliegenden Arbeit ist die automatisierte Berechnung differenzieller und integrierter Wirkungsquerschnitte der Paarerzeugung schwerer Eichbosonen bei sehr hohen Streuenergien mit Resummierung der auftretenden elektroschwachen Sudakov-Logarithmen zu allen Ordnungen in der Feinstrukturkonstanten mittels Soft-Collinear Effective Theory.

Die Suche nach Physik jenseits des Standardmodells an zukünftigen Teilchenbeschleunigern wie dem FCC oder dem CLIC erfordert hochpräzise Voraussagen für Streuquerschnitte seitens der theoretischen Physik. Es ist seit langem bekannt, dass elektroschwache Sudakov-Logarithmen, die bereits gegenwärtig die Genauigkeit der Voraussagen in den Hochenergieschwänzen von Verteilungen limitieren, die Konvergenz der konventionellen Störungsreihen vollkommen zunichte machen, wenn hinreichend hohe Energien erreicht werden.

Mittels Soft-Collinear Effective Theory wurden diese Logarithmen bereits in der Vergangenheit in einfachen Prozessen, die eine analytische Behandlung erlauben, resummiert. Im Rahmen dieser Arbeit wurden diese Methoden in ein Monte-Carlo-Integrationsprogramm implementiert, um somit vollständig differenzielle Vorhersagen präsentieren zu können. Dies erfordert die Behandlung von Infrarotdivergenzen mit Hilfe des Catani-Seymour-Algorithmus. Mit diesen Werkzeugen wurden resummierte Streuquerschnitte für verschiedene Vektorboson-Paarproduktionsprozesse berechnet, u.a. für den Photon-Photon-induzierten Produktionskanal zur W-Boson-Paarproduktion.

Auf dem Weg dorthin sind verschiedene vereinfachende Annahmen notwendig, deren Gültigkeit im Rahmen dieser Arbeit ebenfalls getestet wurde, so z.B. die Qualität der Doppelpolnäherung. Des weiteren wurden Größenordnungen vernachlässigter Effekte abgeschätzt. Dabei haben sich vor allem nicht doppelt resonante Beiträge in bestimmten Phasenraumregionen als beträchtlich herausgestellt.

Der Resummationseffekt der führend logarithmischen Korrekturen verschiebt die integrierten Paarproduktionsstreuquerschnitte um mehr als 20% bezogen auf den Bornstreuquerschnitt im Falle von Leptonkollisionen bei einer Schwerpunktsenergie von 3 TeV. Diese Effekte werden allerdings teilweise von nicht-führenden Beiträgen kompensiert. Für Proton-Proton-Kollisionen bei $\sqrt{s} = 100$ TeV finden wir deutliche Resummationseffekte in allen Hochenergieschwänzen, während die integrierten Wirkungsquerschnitte von Phasenraumregionen dominiert werden, in denen Soft-Collinear Effective Theory nicht anwendbar ist.

Contents

1. Introduction	1
2. Basics of the Standard Model	5
2.1. The Standard Model Lagrangian	5
2.2. Renormalisation	9
2.2.1. Renormalisation transformation and the on-shell scheme	10
2.2.2. $\overline{\text{MS}}$ renormalisation and the renormalisation group equations	13
3. Effective field theories and soft-collinear effective theory	15
3.1. Effective field theories and resummation	15
3.2. Soft-Collinear Effective Theory	16
3.2.1. Kinematics and conventions	17
3.2.2. The SCET Lagrangian for QCD	18
3.2.3. Label formalism and Feynman rules	21
3.2.4. Gauge invariance and Wilson lines	22
3.2.5. External Operators	26
3.2.6. n -jet scattering amplitudes in SCET	27
3.2.7. Integration of the SCET anomalous dimension	32
3.3. Generalisation to the EWSM	33
3.3.1. Treatment of longitudinally polarised gauge bosons	35
3.3.2. n -particle operators and Wilson lines	36
3.3.3. Collinear anomaly	38
3.3.4. Anomalous dimensions and running couplings in the EWSM	41
3.3.5. Collinear and soft functions, low-scale corrections and IR divergences	42
4. Fixed-order perturbation theory: Some important methods	45
4.1. Catani–Seymour subtraction	45
4.2. Treatment of unstable particles	49
4.2.1. Double-pole approximation	50
4.2.2. Complex-mass scheme	56
5. Implementation of SCET_{EW} into a Monte Carlo event generator	59
5.1. Fixed-order calculations and SCET _{EW} in complicated processes	59
5.1.1. Virtual corrections in SCET _{EW}	61
5.1.2. Modifications of the factorisation formula	62
5.1.3. Summary of the strategy	63
5.2. Ingredients of the virtual corrections	64
5.2.1. Constructing the operator basis	65
5.2.2. Tree-level matrix elements	67
5.2.3. High-scale matching contributions	69

5.2.4. Anomalous dimension	70
5.2.5. Low-scale corrections	73
5.2.6. Mixing at the low scale	76
5.3. Logarithm counting	81
5.4. Technical setup	84
6. Results for the FCC–hh setup	86
6.1. Numerical input and setup	86
6.2. Processes under consideration	88
6.2.1. W^+W^- production from fermions	88
6.2.2. W^+W^- production from photons	89
6.2.3. W^+Z production	90
6.2.4. ZZ production	91
6.3. Validation	91
6.3.1. Fiducial cross sections and DPA	92
6.3.2. Polarised leading-order results	96
6.3.3. Real and virtual corrections	104
6.3.4. SCET _{EW} vs. Fixed-Order	107
6.3.5. The individual SCET _{EW} ingredients	114
6.4. Resummed results	115
6.4.1. Virtual corrections only	118
6.4.2. Full resummed differential cross sections	123
7. Results for the CLIC setup	126
7.1. Processes, input, and setup	127
7.2. Validation	128
7.2.1. Double-pole approximation	128
7.2.2. Polarised leading-order results	132
7.2.3. Real and virtual corrections	133
7.2.4. SCET _{EW} vs. Fixed-order	140
7.2.5. Individual SCET contributions	143
7.3. Resummed results	143
7.3.1. Integrated cross sections	147
7.3.2. Differential distributions	147
7.3.3. Effect of the running couplings	155
8. Conclusion and outlook	159
A. One-loop Feynman integral calculus	161
A.1. Dimensional Regularisation	161
A.2. The scalar one-point integral	162
B. Calculation of the SCET anomalous dimension and low-scale corrections	164
B.1. Massless case	164
B.2. Massive case	172
B.2.1. Fermion jet function	172
B.2.2. Gauge boson jet function	175

B.2.3. Scalar jet function	177
B.2.4. Soft integral	177
B.2.5. Putting the results together	178
B.3. Soft and collinear functions for the Standard Model	179

Acronyms

bHQET	boosted-heavy-quark effective theory
CERN	Conseil européen pour la recherche nucléaire
CKM	Cabbibo–Kobayashi–Maskawa
CLIC	Compact Linear Collider
CMS	complex-mass scheme/Compact Muon Solenoid
COM	centre-of-mass
DL	double logarithms
DPA	double-pole approximation
EFT	effective field theory
EW	electroweak
FCC	Future Circular Collider
FCC–ee	Future Circular Collider electron–electron
FCC–hh	Future Circular Collider hadron–hadron
FO	fixed-order
FS	final state
GBET	Goldstone-boson equivalence theorem
HEPS	high-energy phase space
HQET	heavy-quark effective theory
HSM	high-scale matching
IR	infrared
IS	initial state
KLN	Kinoshita–Lee–Nauenburg
LA	logarithmic approximation
LEP	Large Electron–Positron Collider

- LHC** Large Hadron Collider
- LL** leading logarithmic
- LSM** low-scale matching
- LSZ** Lehmann–Symanzik–Zimmermann
- $\overline{\text{MS}}$** modified minimal-subtraction
- NLO** next-to-leading order
- NNLL** next-to-next-to-leading logarithmic
- NNLO** next-to-next-to-leading order
- PDF** parton-distribution function
- PR** parameter renormalisation
- QCD** quantum chromodynamics
- QED** quantum electrodynamics
- RGE** renormalisation group equation
- SCET** soft–collinear effective theory
- SCET_{EW}** soft–collinear effective theory for electroweak corrections
- SL** single logarithms
- SM** Standard Model
- SySM** symmetric Standard Model
- UV** ultraviolet
- vev** vacuum expectation value

*Everybody stutters one way or the other
So check out my message to you
As a matter of fact, don't let nothin' hold you back
If the Scatman can do it, so can you*

Scatman John

1. Introduction

Our current understanding of the fundamental constituents of matter and their interactions is based on the Standard Model (SM) of particle physics. In 2012 the SM's last undiscovered particle, the Higgs boson, was observed for the first time at the ATLAS and CMS experiments [1, 2] at CERN. The existence of the Higgs boson had been proposed independently by Brout, Englert, Guralnik, Hagen, Higgs, and Kibble [3–8] almost 60 years prior to its first observation. While the discovery of the Higgs boson rendered our picture of the SM complete, there are still unanswered questions concerning the interactions of elementary particles. Arguably, the most urgent ones concern the nature of dark matter and the matter-antimatter asymmetry in our universe. While there are, of course, intensive efforts to address these questions directly (for instance by means of proton-decay experiments), the indirect detection of physics beyond the SM is also under investigation. This approach includes the search for SM violations at current and future collider experiments, which relies on high-precision comparisons between experimental data and theoretical predictions. To this end, new methods on both the experimental and the theory side, are under development in order to reach a higher accuracy.

On the experimental side, the high-luminosity LHC [9, 10], currently under construction, is intended to collect data from the year 2029 onwards. Furthermore, several future colliders are being planned to access even higher energies. Two prominent examples are the Future Circular Collider (FCC) [11–15], which is designed as either a lepton (FCC–ee) or a hadron collider (FCC–hh), as well as the Compact Linear Collider (CLIC) [16–18] for e^+e^- collisions. The development of new colliders is supplemented with novel analysis techniques in order to obtain maximal physical insight from the expected gigantic amount of data.

On the theoretical side, the focus lies on the investigation of models for new physics and their impact on collider observables, as well as on the computation of radiative corrections, i.e. higher-order contributions to S-matrix elements, especially within the SM. This provides a vitally important piece of the research agenda, as it potentially facilitates the recognition of small deviations between SM predictions and experimental results. In the fixed-order (FO) perturbation theory approach all computations are organised as a series in the coupling constants α and α_s . In quantum chromodynamics (QCD) the relatively large numerical value of the strong coupling constant α_s (≈ 0.118 depending on the energy) necessitates at least next-to-leading order (NLO) corrections, but current research attempts to compute next-to-next-to-leading order (NNLO) and even higher corrections for increasingly complicated processes. In addition, the further development of accurate parton-shower matching methods is an important part of the theoretical research agenda.

On the other hand, electroweak (EW) radiative corrections are computed in a series in the fine-structure constant $\alpha \approx 1/137$. While NLO corrections in α are often at the level of few percent, their influence grows with energy owing to Sudakov logarithms of the form

$$\alpha^n \log^k \left(\frac{s}{M_W^2} \right), \quad k \leq 2n \quad (1.1)$$

with $\sqrt{s} \gg M_W$ denoting the energy scale of the considered process, on each order n in perturbation theory. Their universal structure at the one-loop order has been demonstrated in Refs. [19,20] and generalised to two-loop accuracy later on [21–24]. Owing to the involved structure of the EW interaction, in particular because of the numerous mass scales, calculating the complete FO EW corrections beyond NLO is presently barely possible even for simple processes. Furthermore, in the tails of certain distributions Sudakov logarithms of the form (1.1) of the order of 40% have been obtained already when considering LHC-like energies. It is therefore highly desirable to resum the corrections that are enhanced by Sudakov logarithms to all orders in the coupling constant. When considering the energy scales of future colliders, such a resummation is inevitable to obtain reliable predictions. In addition non-enhanced terms of $\mathcal{O}(\alpha)$ should be taken into account if a high precision is aimed for.

A general approach to resum logarithmically enhanced corrections in problems involving widely-separated scales is provided by effective field theories (EFTs), out of which soft-collinear effective theory (SCET) [25–33] has turned out to be particularly useful if the origins of the large logarithms involve soft or collinear physics. Originally developed in order to resum large QCD corrections in B-meson decays, SCET has been applied to many different problems such as threshold resummation [34–38], transverse-momentum resummation [39], and event shapes such as thrust [40–42]. The generalisation of SCET to EW radiative corrections, which we denote by SCET_{EW} throughout, is designed to resum the Sudakov logarithms in (1.1) and has been presented in Refs. [43–48]. Within SCET_{EW} SM scattering amplitudes are computed with the dependence on the high energy scale (of $\mathcal{O}(\sqrt{s})$) and the low scale (of $\mathcal{O}(M_W)$) being factorised into separate contributions: The high-scale matching coefficients depend only on the large energy scales and can therefore be computed with all masses set to zero. The low-scale corrections depend on the SM’s mass spectrum, but do not contain any information on the high-energy interactions. The running between these scales is governed by the renormalisation group equation (RGE), which can be solved order by order to resum the Sudakov logarithms to all orders. Similar results have been obtained using infrared evolution equations [21,49–51]. SCET_{EW} has been applied to several process such as diboson production without decays [52], vector-boson fusion [53,54], and vector-boson production in association with a jet [55]. Also processes involving weakly interacting dark matter have been considered [56].

While SCET_{EW} is conceptually well-established, it has up to now been applied on a case-by-case base to sufficiently simple processes and observables. On the other hand there is a large market of dedicated software for different parts of FO computations: Matrix element generators such as RECOLA [57,58], HELAC [59], and OPENLOOPS [60,61] have implemented automated one-loop computations to a high extent. In addition NNLO Monte Carlo programs such as MATRIX [62], parton-shower simulation software such as POWHEG [63], and parton-shower Monte Carlo programs such as PYTHIA [64] have been developed. In order to compare predictions to data these tools are orchestrated within multi-purpose event generators such as such as MADGRAPH [65], SHERPA [66], HERWIG [67], and WHIZARD [68]. Their main purpose is to make the theoretical results accessible to the experimental-physics community. To some extent the results of Refs. [19,20] have been incorporated into multi-purpose event generators [69–73], thus enabling the computation of NLO electroweak Sudakov logarithms in arbitrary processes in logarithmic approximation (LA) (i.e. neglecting non-enhanced contributions). Furthermore, complete NLO EW radiative corrections have been implemented in certain frameworks [74,75]. An approximate resummation formula for Sudakov logarithms implemented in the event generator SHERPA has been presented in Ref. [76].

An automated framework for the calculation of matrix elements including resummed Sudakov logarithms is, however, not available. In this work we demonstrate an implementation of the results of SCET_{EW} into the in-house multichannel-sampling Monte Carlo integrator MoCANLO and present integrated and differential cross sections for diboson processes including decay effects within two different setups inspired by the future-collider projects FCC–hh and CLIC. We apply the machinery to hard partonic processes of the form

$$e^+e^-/\bar{q}q/\gamma\gamma \rightarrow VV' \rightarrow 4\ell/2\ell 2\nu, \quad (1.2)$$

$V, V' \in \{W^\pm, Z\}$. A large amount of effort has been invested into scrutinising processes of the type (1.2): First experimental investigations in the LEP era [77–80] were followed by more precise measurements at the ATLAS [81–88] and CMS [89–98] experiments at the LHC. In the theoretical calculations the accuracy was increased from NLO QCD [99–103] via NLO EW and NLO QCD+EW [104–117] to NNLO QCD [118–123], NNLO QCD+NLO EW [124] and NNLOPS [125] accuracy.

Our implementation is realised with special regard to the given infrastructure: The process-specific high-scale matching corrections are computed in an operator basis of charge eigenstates, allowing for the use of the matrix-element generator RECOLA2 [58]. The other parts of the SCET_{EW} computation, i.e. the anomalous dimensions and the low-scale corrections have been shown to exhibit a universal form and are thus directly implemented into MoCANLO. The occurring loop integrals are computed using the one-loop library COLLIER [126]. The setup contains all $\mathcal{O}(\alpha)$ terms. In addition the terms from the exponentiated Sudakov logarithms can be switched on in several steps. The resummation procedure applies to virtual EW corrections only, but the obtained results are combined with real-radiation effects in the full SM in order to obtain full NLO predictions using MoCANLO. Furthermore, effects from the decay of massive particles are taken into account, which necessitates the factorisation of a process with virtual particles into a production and a decay subprocess by means of the double-pole approximation (DPA). SCET_{EW} is applied to the production part only, treating external longitudinal gauge-boson modes with the Goldstone-boson equivalence theorem (GBET) [127–130]. Concerning the polarisations of virtual vector bosons, we employ the techniques presented in Refs. [131–140]. The implementation facilitates the one-loop computation of all SM to diboson processes fully differential at the level of weighted events.

Besides making RGE-improved predictions, we carefully study the validity of the assumptions needed to be made in order to apply SCET_{EW} in the considered setups: The size of the mass-suppressed contributions, which are neglected in SCET_{EW}, is estimated by comparing the expanded SCET_{EW} result against a fixed-order computation in DPA. At the same time, this serves as a consistency check of the code. Furthermore, we quantify the error of the DPA in the interesting high-energy regions and investigate the size of the neglected interference terms between longitudinally and transversely polarised polarisation states.

This thesis is organised as follows:

- We start with a brief description of the SM and some selected basic topics of quantum field theory (Chapter 2), followed by an introduction to some general properties of EFTs and SCET, eventually introducing SCET_{EW} (Chapter 3).
- In Chapter 4 we introduce some important techniques from the field of EW precision physics, in particular the Catani–Seymour subtraction and the treatment of unstable particles by means of the DPA and the complex-mass scheme (CMS).

- In Chapter 5 we describe in detail our approach to apply SCET_{EW} diboson-production processes, which contributions we include, and their implementation into MOCANLO.
- In the following Chapters 6 and 7 we present numerical results for integrated and differential cross sections in the FCC–hh and CLIC setup, respectively. Along with the implementation described in Sec. 5, these results have been published in Ref. [141].
- Finally we give a conclusion and an outlook in Chapter 8.

2. Basics of the Standard Model

In this section we review some phenomenological properties of the SM as well as its renormalisation. The first part of the section (Sec. 2.1) deals with the field and particle content of the SM and the second one (Sec. 2.2) with some basic facts about renormalisation together with a brief discussion of the on-shell scheme and the $\overline{\text{MS}}$ renormalisation scheme.

There is a vast number of textbooks on these topics, of which the current selection is based on parts of Refs. [142–144].

2.1. The Standard Model Lagrangian

The SM is a spontaneously broken gauge theory based on a product of three gauge groups,

$$\mathcal{G}_{\text{SM}} = \text{SU}(3)_C \times \text{SU}(2)_L \times \text{U}(1)_Y, \quad (2.1)$$

of which the first one is associated with QCD and describes the strong interaction, and the other ones describe weak and electromagnetic interactions. Since this formulation provides a unified theory of weak and electromagnetic interactions, the $\text{SU}(2)_L \times \text{U}(1)_Y$ part of the SM is referred to as the electroweak (EW) sector. In this chapter, we discuss the several parts of the quantised effective SM Lagrangian in more detail. It can be decomposed as follows:

$$\mathcal{L}_{\text{SM}} = \mathcal{L}_{\text{gauge}} + \mathcal{L}_{\text{Higgs}} + \mathcal{L}_{\text{ferm}} + \mathcal{L}_{\text{fix}} + \mathcal{L}_{\text{ghost}}. \quad (2.2)$$

The first three terms describe interactions of physical particles, while the last two terms are connected to the gauge fixing. All terms are discussed further below.

Gauge part

The Yang–Mills part of the Lagrangian contains the kinetic and interaction terms between the gauge bosons and is most conveniently written as

$$\mathcal{L}_{\text{gauge}} = -\frac{1}{4} (F_{\mu\nu}^{(1)} F^{(1),\mu\nu} + F_{a,\mu\nu}^{(2)} F_a^{(2),\mu\nu} + F_{a,\mu\nu}^{(3)} F_a^{(3),\mu\nu}) \quad (2.3)$$

with the field-strength tensors $F_{\mu\nu}^{(N)}$ corresponding to the respective (S)U(N) gauge groups:

$$\begin{aligned} F_{\mu\nu}^{(1)} &= \partial_\mu B_\nu - \partial_\nu B_\mu, \\ F_{a,\mu\nu}^{(2)} &= \partial_\mu W_{a,\nu} - \partial_\nu W_{a,\mu}, \quad a = 1, \dots, 3, \\ F_{a,\mu\nu}^{(3)} &= \partial_\mu A_{a,\nu} - \partial_\nu A_{a,\mu}, \quad a = 1, \dots, 8, \end{aligned}$$

with the corresponding gauge fields B^μ , W_a^μ , and A_a^μ being the B -boson field, the W -boson fields, and the gluon fields, respectively.

Field	Q	I_w^3	Y_w	SU(3) rep.
$L_j = \begin{pmatrix} \nu_e \\ e^- \end{pmatrix}_L, \begin{pmatrix} \nu_\mu \\ \mu^- \end{pmatrix}_L, \begin{pmatrix} \nu_\tau \\ \tau^- \end{pmatrix}_L$	$\begin{pmatrix} 0 \\ -1 \end{pmatrix}$	$\begin{pmatrix} +1/2 \\ -1/2 \end{pmatrix}$	-1	1
$l_j = e_R^-, \mu_R^-, \tau_R^-$	-1	0	-2	1
$Q_j = \begin{pmatrix} u \\ d \end{pmatrix}_L, \begin{pmatrix} c \\ s \end{pmatrix}_L, \begin{pmatrix} t \\ b \end{pmatrix}_L$	$\begin{pmatrix} +2/3 \\ -1/3 \end{pmatrix}$	$\begin{pmatrix} +1/2 \\ -1/2 \end{pmatrix}$	+1/3	3 \oplus 3
$u_j = u_R, c_R, t_R$	+2/3	0	+4/3	3
$d_j = d_R, s_R, b_R$	-1/3	0	-2/3	3

Table 2.1.: Overview of the SM fermions with their quantum numbers. The electric charge is denoted by Q , the third component of the weak isospin by I_w^3 , and the hypercharge by Y_w . All antiparticles have the same quantum numbers with opposite signs. The antiquarks transform under the conjugate SU(3) representation $\bar{\mathbf{3}}$.

Fermionic part

The fermionic particle content of the SM is given by three generations of leptons, quarks, and neutrinos. They come as left- and right-handed fermions, according to their respective Lorentz-group representation. While both the strong and the electromagnetic interactions are blind to their chiralities, the $SU(2) \times U(1)_Y$ quantum numbers are different for left- and right-handed fermions: Only the left-handed ones interact via the SU(2) interaction. The hypercharges Y_w are then given such that the electric charges of the left- and right-handed fermions coincide and fulfill the Gell-Mann–Nishijima relation,

$$Q = I_w^3 + \frac{Y_w}{2}. \quad (2.4)$$

An overview of the SM fermions and their quantum numbers is shown in Tab. 2.1.

The part of the SM Lagrangian associated with the fermions and their gauge interactions reads

$$\mathcal{L}_{\text{ferm}} = \sum_{k=1}^3 \sum_{\Psi=Q,L} \bar{\Psi}'_{L,k} \not{D} \Psi'_{L,k} + \sum_{k=1}^3 \sum_{\psi=\ell,u,d} \bar{\psi}'_{R,jk} \not{D} \psi'_{R,jk} \quad (2.5)$$

with the covariant derivative

$$D_\mu = \partial_\mu + i \frac{Y_w}{2} g_1 B_\mu - i g_2 I_w^a W_\mu^a + i g_s T^a A_\mu^a. \quad (2.6)$$

In the two formulae above it is to be understood that only the left-handed quark doublets and singlets transform under SU(3) ($T^a = 0$ for leptons) and only the quark and lepton doublets transform under SU(2) ($I_w^a = 0$ for singlets).

The primes in (2.5) indicate that the fields are gauge eigenstates, which are rotated against the mass eigenstates via the Yukawa-coupling matrices, see below.

Higgs part

The missing piece to provide masses to both the weak gauge bosons and the fermions is the Higgs doublet, which can be written as

$$\Phi = \begin{pmatrix} \phi^+ \\ (H + v + i\chi)/\sqrt{2} \end{pmatrix}, \quad \phi^- = (\phi^+)^\dagger, \quad (2.7)$$

with the Higgs field H and the charged and neutral would-be Goldstone fields ϕ^+ , χ . The non-vanishing constant v denotes the vacuum expectation value (vev), which leads to masses for fields, which are coupled to the Higgs doublet via interaction terms. The Lagrangian associated with the Higgs doublet reads

$$\begin{aligned} \mathcal{L}_{\text{Higgs}} = & (D_\mu \Phi)^\dagger (D^\mu \Phi) - V(\Phi) \\ & - \sum_{i,j=1}^3 \bar{L}'_{L,i} G_{ij}^\ell \ell'_{R,j} \Phi - \sum_{i,j=1}^3 \bar{Q}'_{L,i} G_{ij}^u u'_{R,j} \Phi^c - \sum_{i,j=1}^3 \bar{Q}'_{L,i} G_{ij}^d d'_{R,j} \Phi + \text{h.c.} \end{aligned} \quad (2.8)$$

with the Higgs self-interaction potential

$$V(\Phi) = \frac{\lambda}{4} (\Phi^\dagger \Phi)^2 - \mu^2 \Phi^\dagger \Phi \quad (2.9)$$

and the Yukawa-coupling matrices G^f . The gauge-boson mass terms are contained in the gauge-interaction Lagrangian of the Higgs doublet and the masses are determined by the gauge couplings and the parameters μ and λ of the Higgs potential. While the Lagrangian is usually given in terms of the isospin eigenstates W_μ^a , B_μ , all interactions are conveniently expressed in terms of the charge and mass eigenstates. For the first two components of the SU(2) triplet one finds

$$W^\pm = \frac{1}{\sqrt{2}} (W_1 \mp W_2). \quad (2.10)$$

with the mass obtained as

$$M_W = \frac{g_2}{2} v. \quad (2.11)$$

The mass matrix in the neutral sector has to be diagonalised introducing the weak mixing angle θ_w :

$$\begin{pmatrix} A_\mu \\ Z_\mu \end{pmatrix} = \begin{pmatrix} \cos \theta_w & -\sin \theta_w \\ \sin \theta_w & \cos \theta_w \end{pmatrix} \begin{pmatrix} B_\mu \\ W_\mu^3 \end{pmatrix}, \quad (2.12)$$

defining the photon as the eigenstate of mass zero, while the Z boson acquires a mass of

$$M_Z = \frac{M_W}{\cos \theta_w}. \quad (2.13)$$

The fermion masses and mass eigenstates are obtained by diagonalising the Yukawa-coupling matrices. Because within the minimal SM all neutrinos have the same mass ($m_\nu = 0$), their mass eigenstates can be chosen to be the gauge-interaction eigenstates. As a consequence,

the lepton mass eigenstates also coincide with their interaction eigenstates and there are no generation-mixing effects in the lepton sector.

For quarks there is a non-trivial relation between mass and interaction eigenstates by means of the Cabbibo–Kobayashi–Maskawa (CKM) matrix:

$$\begin{pmatrix} d' \\ s' \\ b' \end{pmatrix} = \begin{pmatrix} V_{ud} & V_{us} & V_{ub} \\ V_{cd} & V_{cs} & V_{cb} \\ V_{td} & V_{ts} & V_{tb} \end{pmatrix} \begin{pmatrix} d \\ s \\ b \end{pmatrix}. \quad (2.14)$$

For many applications the CKM matrix can be approximated by the unit matrix, especially the off-diagonal elements describing third-generation mixing effects, $|V_{ub}|$, $|V_{cb}|$, $|V_{td}|$, and $|V_{ts}|$ are small (< 0.05).

Gauge-Fixing and Ghost Part

The quantisation of gauge theories puts up some problems related to the fact that the fundamental dynamic variables, the gauge fields, contain redundant degrees of freedom. These must be eliminated in order to obtain a well-defined quantum theory. For an Abelian theory this can be done in an ad-hoc manner by solving the classical equations of motion and identifying the physical degrees of freedom in the solution [145, 146]. For a non-Abelian gauge theory this is not sensible since the classical equation of motions are never free of interactions and can not be solved exactly. The quantisation of a Yang–Mills theory therefore has to be performed in the path-integral formalism.

The Faddeev–Popov procedure [147] allows for the quantisation of Yang–Mills theories by projecting out physically equivalent gauge configurations from the path integral, using a set of gauge-fixing functionals $C^a(\{\mathbf{A}(x), \phi(x)\})$, which depend on the gauge-boson vector fields and on the would-be Goldstone boson fields. Using a variable transformation under the path integral allows for the inclusion of the gauge-fixing effects by means of additional terms in the Lagrangian [143]:

$$\mathcal{L} \rightarrow \mathcal{L} + \mathcal{L}_{\text{fix}} + \mathcal{L}_{\text{ghost}}. \quad (2.15)$$

In the widely-used class of so-called R_ξ gauges the additional terms in the Lagrangian are given by

$$\begin{aligned} \mathcal{L}_{\text{fix}} = & - \sum_{a=1}^8 \frac{1}{2\xi^a} C^a(\{\mathbf{A}\}) C^a(\{\mathbf{A}\}) \\ & - \frac{1}{2\xi^A} C^A(A) - \frac{1}{2\xi^Z} C^Z(Z, \chi) C^Z(Z, \chi) - \frac{1}{\xi_W} C^-(W^-, \phi^-) C^+(W^+, \phi^+) \end{aligned} \quad (2.16)$$

for the gauge-fixing and

$$\begin{aligned} \mathcal{L}_{\text{ghost}} = & - \sum_{a,b,c=1}^8 \int d^4y d^4z \bar{u}^a(x) \left(\frac{\delta C^a(x)}{\delta A_\nu^c(z)} \frac{\delta A_\nu^c(z)}{\delta \theta^b(y)} + \frac{\delta C^a(x)}{\delta \phi^c(z)} \frac{\delta \phi^c(z)}{\delta \theta^b(y)} \right) u^b(y) \\ & - \sum_{a,b,c=\pm, A, Z} \int d^4y d^4z \bar{u}^a(x) \left(\frac{\delta C^a(x)}{\delta V_\nu^c(z)} \frac{\delta V_\nu^c(z)}{\delta \theta^b(y)} + \frac{\delta C^a(x)}{\delta \phi^c(z)} \frac{\delta \phi^c(z)}{\delta \theta^b(y)} \right) u^b(y) \end{aligned} \quad (2.17)$$

for the ghost part. The gauge-fixing part \mathcal{L}_{fix} projects the theory onto a specific gauge configuration (up to a normalisation factor). The ghost part $\mathcal{L}_{\text{ghost}}$ takes into account the Jacobian of the variable transformation using the auxiliary Faddeev–Popov ghost fields $\bar{u}^a(x), u^a(x)$, which appear as virtual particles in loop corrections. The gauge-fixing functionals read

$$C^a = \partial^\mu A_\mu^a, \quad a = 1, \dots, 8 \quad (2.18)$$

for gluons and

$$\begin{aligned} C^\pm &= \partial^\mu W_\mu^\pm \mp iM_W \xi'_W \phi^\pm, \\ C^Z &= \partial^\mu Z_\mu - M_Z \xi'_Z \chi, \\ C^A &= \partial^\mu A_\mu \end{aligned} \quad (2.19)$$

for the EW gauge bosons. The gauge parameters ξ_a, ξ'_a parameterise the gauge and can be chosen by convenience. Setting $\xi'_a = \xi_a$ ('t Hooft gauge) in the EW sector is particularly convenient because it removes the tree-level mixing between the W/Z bosons and the would-be Goldstone bosons ϕ^\pm, χ . With this choice the propagator of a gauge boson V with mass M_V and momentum p reads

$$G_{\mu\nu}^{VV}(p) = \frac{-ig_{\mu\nu}}{p^2 - M_V^2 + i0} + \frac{i(1 - \xi_V)p_\mu p_\nu}{(p^2 - M_V^2 + i0)(p^2 - \xi_V M_V^2 + i0)}. \quad (2.20)$$

with the symbol $i0$ being an infinitesimal imaginary part arising from the Feynman prescription. The above form holds also for the propagators of the massless photon and gluon ($M_V = 0$). In the following we often work in 't Hooft–Feynman gauge ($\xi'_a = \xi_a = 1$).

2.2. Renormalisation

The calculation of loop integrals introduces divergent integrals associated with the limit of large loop four momenta on each order in perturbation theory. In order to obtain well-defined results these ultraviolet (UV) have to be regularised, which is most conveniently done in dimensional regularisation [148, 149] (DimReg, see App. A for a brief introduction and some conventions): The number of space-time dimensions is shifted away from $D = 4$ by a small amount. In the limit $D \rightarrow 4$, any quantity is then obtained as a Laurent series with poles in $D - 4$. To get eventually rid of the divergences one has to redefine the set of input parameters, i.e. the couplings, masses and fields.

Of course, the fields are not quite input parameters. The necessity for field-renormalisation constants arises because of the different normalisation of one-particle states in free and interacting theories: In perturbation theory S-matrix elements are computed between asymptotic initial and final states, which are assumed to coincide with the corresponding free-theory states. Because the presence of interactions changes the normalisation of these states, field-renormalisation constants have to be introduced for each field. Eventually they show up as normalisation factors in the Lehmann–Symanzik–Zimmermann (LSZ) formula [150].

2.2.1. Renormalisation transformation and the on-shell scheme

The relation between bare and renormalised parameters is obtained from the renormalisation transformation. Usually, a multiplicative renormalisation transformation is employed, that is,

$$g_0 = Z_g g \approx (1 + \delta Z_g)g, \quad \psi_0 = \sqrt{Z_\psi} \psi \approx \left(1 + \frac{1}{2} \delta Z_\psi\right) \psi, \quad m_0 = Z_m m \approx m + \delta m \quad (2.21)$$

for all involved couplings g , masses m and fields ψ . The parameters g_0 , m_0 , and ψ_0 are the so-called bare parameters, which enter the Lagrangian, but, due to loop corrections, are formally infinite. The renormalised parameters g , m , and ψ remain finite because the renormalisation constants Z_g , Z_m , and Z_ψ cancel the arising divergences order by order in perturbation theory. Expanding the Lagrangian accordingly leads to

$$\mathcal{L}_0 = \mathcal{L} + \mathcal{L}_{\text{ct}}, \quad (2.22)$$

such that the renormalised Lagrangian \mathcal{L} has the same functional form in terms of the renormalised parameters as the bare Lagrangian \mathcal{L}_0 has in terms of the unrenormalised ones. The remainder \mathcal{L}_{ct} contains the renormalisation constants and is defined as the counterterm Lagrangian.

Up to the divergent parts the definition of renormalisation constants is not unique. A set of *renormalisation conditions* has to be chosen in order to fix the finite parts of the renormalisation constants. The choice of a renormalisation scheme is of great importance because it defines the relation between observables calculated in perturbation theory and measurable quantities.

On-shell scheme

The on-shell scheme [151–153] provides a natural renormalisation scheme for the EWSM, as the renormalisation conditions are defined such that the input parameters have a distinct physical meaning: The electric charge is defined via the Thomson cross section in the classical limit, while all masses correspond to the poles in the corresponding propagators and can hence be extracted from resonance peaks in differential cross sections. According to (2.21), the bare and renormalised input parameters and fields as well as the counterterms are defined via

$$\begin{aligned} e_0 &= Z_e e \approx (1 + \delta Z_e)e, & t &\approx t + \delta t, \\ V_0 &= \sqrt{Z_{VV'}} V' \approx \left(\delta_{VV'} + \frac{1}{2} \delta Z_{VV'}\right) V', & f_{i,0}^\kappa &= \sqrt{Z_{ij}^{f,\kappa}} f_j^\kappa \approx \left(1 + \frac{1}{2} \delta Z_{ij}^{f,\kappa}\right) f_j^\kappa, \\ H_0 &= \sqrt{Z_H} H \approx H + \frac{1}{2} \delta Z_H H, & M_{B,0}^2 &= (Z_{M_B} M_B)^2 \approx M^2 + \delta M_B^2, \\ m_{f,i,0} &= Z_{m_{f,i}} m_{f,i} \approx m_{f,i} + \delta m_{f,i}, \end{aligned}$$

with H denoting the Higgs boson field, V denoting the EW gauge bosons and f_i the fermion field with flavour index i and helicity $\kappa \in \{\text{L}, \text{R}\}$. The one-point function of the Higgs field (Higgs tadpole) is denoted by T . The field-renormalisation constants are matrix valued both in the case of quarks and the neutral gauge bosons A , Z , because in these cases the interaction eigenstates are rotated against the mass eigenstates. Note that there are mass counterterms for the massive boson fields $B = H, W, Z$, but not for the photon, whose mass is guaranteed to be zero by a Ward identity.

Following Ref. [154], we discuss the renormalisation conditions as well as the explicit form of the renormalisation constants briefly in the following. The first renormalisation condition concerns the Higgs-field one-point function, which after renormalisation is required to vanish:¹

$$\hat{T} \equiv \hat{\Gamma}^H = 0, \quad (2.23)$$

which defines the tadpole counterterm as

$$\delta t = -T. \quad (2.24)$$

This procedure corresponds to a renormalisation of the vev and has the effect that the renormalised vev corresponds to the actual value of the renormalised Higgs potential at its minimum. As a consequence of (2.24), all explicit tadpole diagrams can just be omitted during the calculation as a shortcut.

The renormalised two-point functions are defined by the following renormalisation conditions:

- The renormalised masses correspond to the pole positions of the respective propagators, and
- the residues of the poles are equal one. This accounts for the correct normalisation of the fields.

The former conditions read:²

$$\widetilde{\text{Re}} \hat{\Gamma}_{\mu\nu}^{VV'}(k) \varepsilon^\nu(k) \Big|_{k^2=M_V^2} = 0, \quad \widetilde{\text{Re}} \hat{\Gamma}_{ij}^f(k) u_j(k) \Big|_{k^2=m_f^2} = 0, \quad \widetilde{\text{Re}} \hat{\Gamma}^H(k) \Big|_{k^2=m_H^2} = 0, \quad (2.25)$$

which define the mass counterterms as

$$\delta M_W = \widetilde{\text{Re}} \Sigma_T^W(M_W^2), \quad \delta M_Z = \widetilde{\text{Re}} \Sigma_T^{ZZ}(M_Z^2), \quad \delta M_H = \widetilde{\text{Re}} \Sigma^H(M_H^2) \quad (2.26)$$

for the massive bosons and

$$\delta m_{f,i} = \frac{m_{f,i}}{2} \widetilde{\text{Re}} \left(\Sigma_{ii}^{f,L}(m_{f,i}) + \Sigma_{ii}^{f,R}(m_{f,i}) + 2\Sigma_{ii}^{f,S}(m_{f,i}) \right) \quad (2.27)$$

for the fermions. The respective self energies for gauge bosons and fermions have been decomposed in a covariant way:

$$\begin{aligned} \Sigma_{ij}^{f,\kappa}(k^2) &= \not{k} \Sigma_{ij}^{V,f,\kappa}(k^2) + m_{f,i} \Sigma_{ij}^{S,f,\kappa}(k^2), \\ \Sigma_{\mu\nu}^{VV'}(k^2) &= \left(g_{\mu\nu} - \frac{k_\mu k_\nu}{k^2} \right) \Sigma_T^{VV'}(k^2) + \frac{k_\mu k_\nu}{k^2} \Sigma_L^{VV'}(k^2). \end{aligned} \quad (2.28)$$

Note that the symbol $\widetilde{\text{Re}}$ denotes the real part of its argument, but with the CKM matrix remaining complex. The residues of the poles are obtained from the limit of the two-point functions with the momenta going on shell. Demanding them to equal one provides the renormalisation

¹By abuse of notation, we use the symbol “ \equiv ” as “defined to be equal” throughout.

²Note that the gauge-boson two-point function has non-trivial mixing in the case of $V, V' = A, Z$.

condition for the field renormalisation:

$$\begin{aligned}
 \lim_{k^2 \rightarrow M_V^2} \frac{1}{k^2 - M_V^2} \widetilde{\text{Re}} \hat{\Gamma}_{\mu\nu}^{VV}(k) \varepsilon^\nu(k) &= -\varepsilon_\mu(k), \\
 \lim_{k^2 \rightarrow M_H^2} \frac{1}{k^2 - M_H^2} \widetilde{\text{Re}} \hat{\Gamma}^H(k) &= 1, \\
 \lim_{k^2 \rightarrow m_{f,i}^2} \frac{k + m_{f,i}}{k^2 - m_{f,i}^2} \widetilde{\text{Re}} \hat{\Gamma}_{ii}^{f,i}(k) u_i(k) &= u_i(k), \\
 \lim_{k^2 \rightarrow m_{f,i}^2} \bar{u}_i(k) \widetilde{\text{Re}} \hat{\Gamma}_{ii}^{f,i}(k) \frac{k + m_{f,i}}{k^2 - m_{f,i}^2} &= \bar{u}_i(k),
 \end{aligned} \tag{2.29}$$

which implies that the field-renormalisation counterterms are given by derivatives of the respective fields' self energies with respect to the momentum invariant:

$$\begin{aligned}
 \delta Z_H &= -\widetilde{\text{Re}} \left. \frac{\partial \Sigma^H(k^2)}{\partial k^2} \right|_{k^2=M_H^2}, & \delta Z_{VV} &= -\widetilde{\text{Re}} \left. \frac{\partial \Sigma_T^{VV}(k^2)}{\partial k^2} \right|_{k^2=M_V^2}, \\
 \delta Z_{ZA} &= 2\widetilde{\text{Re}} \frac{\Sigma_T^{AZ}(0)}{M_Z^2}, & \delta Z_{AZ} &= -2\widetilde{\text{Re}} \frac{\Sigma_T^{ZA}(M_Z^2)}{M_Z^2},
 \end{aligned}$$

for the bosonic and

$$\begin{aligned}
 \delta Z_{ij}^{f,\kappa} &= \frac{2}{m_{f,i}^2 - m_{f,j}^2} \widetilde{\text{Re}} \left(m_{f,j}^2 \Sigma_{ij}^{f,\kappa}(m_{f,j}^2) + m_{f,i} m_{f,j} (\Sigma_{ij}^{f,\bar{\kappa}}(m_{f,i}^2) + 2\Sigma_{ij}^{S,f,\kappa}(m_{f,i}^2)) \right), \quad i \neq j \\
 \delta Z_{ii}^{f,\kappa} &= -\widetilde{\text{Re}} \Sigma_{ii}^{f,\kappa} - m_{f,i}^2 \left. \frac{\partial}{\partial k^2} \widetilde{\text{Re}} \left(\Sigma_{ii}^{f,\kappa}(k^2) + \Sigma_{ii}^{f,\bar{\kappa}}(k^2) + \Sigma_{ii}^{S,f,\kappa}(k^2) \right) \right|_{k^2=m_{f,i}^2}
 \end{aligned} \tag{2.30}$$

for the fermionic field-renormalisation constants.

As the quark mixing will be neglected in all applications throughout this thesis, we do not discuss the renormalisation of the CKM matrix. This is discussed, for instance, in Ref. [155].

From the mass counterterms for the W and Z bosons in (2.26), the counterterms for the cosine of the weak mixing angle can be deduced as

$$\frac{\delta c_w^2}{c_w^2} = \frac{\delta M_W^2}{M_W^2} - \frac{\delta M_Z^2}{M_Z^2}, \tag{2.31}$$

and from this the corresponding counterterm for the sine:

$$\frac{\delta s_w^2}{s_w^2} = -\frac{c_w^2}{s_w^2} \left(\frac{\delta M_W^2}{M_W^2} - \frac{\delta M_Z^2}{M_Z^2} \right). \tag{2.32}$$

Here we have introduced the common abbreviations

$$s_w \equiv \sin \theta_w, \quad c_w \equiv \cos \theta_w. \tag{2.33}$$

The renormalisation constants δs_w , δc_w are introduced merely for convenience, as the weak mixing angle is not an input quantity in the on-shell scheme.

2.2.2. $\overline{\text{MS}}$ renormalisation and the renormalisation group equations

The on-shell scheme described above has the advantage that all masses are directly obtained from physically measurable quantities. This is a suitable choice as long as all masses in the theory are sufficiently precisely measurable, which is not the case for the light quarks. Therefore in QCD a more naive scheme is employed, known as the $\overline{\text{MS}}$ scheme. The prescription is to subtract from the bare quantities the contributions proportional to the standard divergence

$$\Delta_{\text{UV}} = \frac{1}{\varepsilon} - \gamma_E - \log(4\pi) + \log \frac{\mu^2}{q^2}, \quad (2.34)$$

in DimReg. In the above formula $\varepsilon = (4 - D)/2$ denotes the deviation of the space-time dimensions from four and $\gamma_E \approx 0.5772$ is the Euler-Mascheroni constant. In addition to the scale μ associated with DimReg an additional reference scale q has been introduced, which is also referred to as the renormalisation point. All $\overline{\text{MS}}$ -renormalised quantities depend on the scale q ,

$$g_s = g_s(q), \quad m_q = m_q(q), \quad \psi = \psi(q), \quad (2.35)$$

with the g_s being the strong coupling constant, m_q being the quark masses, and ψ denoting the quark and gluon fields. This scale dependence is commonly referred to as parameter running.

The fact that S-matrix elements have to be independent of the scale to all orders in perturbation theory can be exploited to derive all-order relations between parameters at different scales. The scale can then obtain a physical interpretation as the energy scale the respective quantity is probed at.

All of the above is done by means of the renormalisation group equation (RGE). The independence of the S matrix of a reference scale q can be written in the form

$$\begin{aligned} 0 &= \frac{d}{d \log q} \left(R^{n/2}(g, m, q) \hat{\Gamma}^n(p_l, g, m, q) \right) \\ &= \left(\frac{\partial}{\partial \log q} + \beta \frac{\partial}{\partial g} - \gamma_m \frac{\partial}{\partial m} - n\gamma_\psi \right) \hat{\Gamma}^n(p_k, g, m, q) \end{aligned} \quad (2.36)$$

with g and m denoting the set of of all involved couplings and masses, respectively, and $\hat{\Gamma}^n$ the renormalised n -point vertex function. The above equation defines the β function, the mass coefficients, and the anomalous dimensions via

$$\begin{aligned} \beta(g, m, q) &= \frac{\partial}{\partial \log q} g(g_0, m_0, \mu, q), \\ \gamma_m(g, m, q) &= -\frac{1}{m} \frac{\partial}{\partial \log q} m(g_0, m_0, \mu, q), \\ \gamma_\psi(g, m, q) &= -\frac{1}{2Z_\psi} \frac{\partial}{\partial \log q} Z_\psi(g_0, m_0, \mu, q). \end{aligned} \quad (2.37)$$

These functions are referred to as the RGE functions. Because the scale dependence enters the RGE functions only in the context of the standard divergence (2.34), they are obtained from the UV-divergent part of the relevant loop integrals only.

Another formulation of the RGE is given by the *Callan–Symanzik Equation*,

$$\left(\frac{\partial}{\partial \log \lambda} + \beta \frac{\partial}{\partial g} - (1 + \gamma_m) \frac{\partial}{\partial m} - n_B(1 + \gamma_B) + n_f \left(\frac{3}{2} + \gamma_f \right) - 4 \right) \hat{\Gamma}^{n_B n_f}(\lambda p_k, g, m, q) = 0 \quad (2.38)$$

for a vertex function involving n_B bosons and n_f fermions. The dimensionless variable λ describes a uniform scaling of all external momenta p_k . The Callan–Symanzik Equation is obtained from (2.36) by an analysis of the mass dimensions: Since bosonic and fermionic fields have different mass dimensions, their anomalous dimensions account differently in the RGE. In order to have the correct dimension for the matrix element, one can make use of the fact that $\hat{\Gamma}^n$ has to be a homogeneous function of the p_k to obtain (2.38) from (2.36).

The form (2.38) makes it explicit that a variation of the renormalisation scale can indeed be interpreted as a change of the energy scale at which a process with external momenta p_k is probed. Note further that the solution of the RGE and hence the scaling behaviour of physical quantities can be obtained only from the UV-divergent parts of the renormalisation constants, and from some basic properties of the theory such as the number of fermions and bosons.

The solution of the RGE is obtained from the following steps: [143]

- Calculate the RGE functions in perturbation theory as functions of the couplings and masses.
- Integrate the resulting system of ordinary differential equations in $\log \mu$ to obtain the running couplings $g(\mu)$ and masses $m(\mu)$.
- The solution for the vertex function is then obtained by integrating the anomalous dimensions along the solutions $g(\mu)$, $m(\mu)$:

$$\begin{aligned} \hat{\Gamma}^{n_B n_f}(\lambda p_k, g(\mu_1), m(\mu_1)) &= \lambda^{4 - n_B - 3n_f/2} \hat{\Gamma}^{n_B n_f}(p_k, g(\mu_2), m(\mu_2)) \\ &\quad \times \exp \left(- \int_{\mu_1}^{\mu_2} d \log \mu [n_B \gamma_B(g(\mu), m(\mu)) + n_f \gamma_f(g(\mu), m(\mu))] \right). \end{aligned} \quad (2.39)$$

The above exponential now contains possibly large logarithms of μ_2/μ_1 to all orders in the coupling constant.

3. Effective field theories and soft–collinear effective theory

In this section we describe some important features of effective field theories (EFTs) in general and soft–collinear effective theory (SCET) in particular. Starting from a few general facts about EFTs in Sec. 3.1 we turn to a description of SCET in Sec. 3.2 and its generalisation to EW corrections in Sec. 3.3

3.1. Effective field theories and resummation

EFTs provide a powerful way to calculate observables involving widely separated scales. If such observables are calculated using fixed-order perturbation theory, the convergence of the series can potentially be destroyed by large logarithmic corrections. In general the interaction Lagrangian of an effective theory valid up to some energy scale Λ is based on an operator basis such as

$$\mathcal{L}_{\text{EFT}} = \mathcal{L}_{D \leq 4} + \frac{1}{\Lambda} \sum_i C_i^{(D=5)} \mathcal{O}_i^{(D=5)} + \frac{1}{\Lambda^2} \sum_i C_i^{(D=6)} \mathcal{O}_i^{D=6} + \dots, \quad (3.1)$$

with $\mathcal{L}_{D \leq 4}$ denoting the renormalisable part of the Lagrangian and the *Wilson coefficients* C_i are to be determined. Note that one has to write down all operators allowed by the symmetries of the full theory on each order in $1/\Lambda$.

The Wilson coefficients are contained in the EFT as free parameters that comprise the high-energy interactions. Their values are fixed by the requirement that the S-matrix is the same in the EFT and the full theory at any given order in both the coupling and the EFT parameter:

$$\mathcal{M}_{\text{EFT}} \stackrel{!}{=} \mathcal{M}_{\text{full}} + \mathcal{O}(\Lambda^{-1}). \quad (3.2)$$

Calculating the Wilson coefficients order by order using (3.2) is called *matching*.¹

In general, loop corrections mix operators among each other, which is why the renormalisation constants can be comprised in a matrix notation:²

$$\mathcal{O}_{0,i} = \mathbf{Z}_{ij}(\mu) \mathcal{O}_j(\mu). \quad (3.3)$$

This is referred to as *operator mixing*. Each element of the matrix \mathbf{Z} contains the field-renormalisation constants for the fields in the \mathcal{O}_i as well as an operator-specific contribution from the one-particle irreducible graphs [157]. From the fact that the all-order result for any

¹Throughout this work, all matching computations are performed employing Feynman diagrams. In many applications, performing the matching on the level of the generating functionals has turned out to be advantageous (“functional matching”). Applying this approach to SCET is still considered an open problem [156].

²In the following, we denote the scale with μ , where μ plays the role of the renormalisation point q in (2.34).

S-matrix element does not depend on the scale, it can be derived that the operators and Wilson coefficients fulfill the respective renormalisation group equations [157, 158]

$$\begin{aligned}\frac{d}{d \log \mu} \mathcal{O}_i(\mu) &= \gamma_{ij}^T(\mu) \mathcal{O}_j(\mu), \\ \frac{d}{d \log \mu} C_i(\mu) &= -\gamma_{ij}(\mu) C_j(\mu),\end{aligned}\tag{3.4}$$

with the anomalous dimension matrix γ , which can be obtained from the UV-divergent parts of the renormalisation constants comprised in \mathbf{Z} :

$$\gamma^T = -\mathbf{Z}^{-1} \frac{d\mathbf{Z}(\mu)}{d \log \mu}.\tag{3.5}$$

Note the analogy to the field anomalous dimension in (2.37). The solution of the RGE can again be used to resum large logarithmic corrections if the Wilson coefficients are matched at the high scale and run down to the low scale:

$$C_i(\mu_l) \langle \mathcal{O}_i(\mu_l) \rangle = \sum_j C_j(\mu_h) \times \left[\hat{\mathbf{P}} \exp \left(- \int_{\mu_l}^{\mu_h} d \log \mu \gamma(\mu) \right) \right]_{ij} \times \langle \mathcal{O}_i \rangle.\tag{3.6}$$

with the path-ordering operator defined via

$$\hat{\mathbf{P}} \exp \left(- \int_{\mu_l}^{\mu_h} \frac{d\mu}{\mu} \gamma(\mu) \right) = \mathbb{1} - \int_{\mu_l}^{\mu_h} \frac{d\mu}{\mu} \gamma(\mu) + \frac{1}{2} \int_{\mu_l}^{\mu_h} \frac{d\mu}{\mu} \int_{\mu_l}^{\mu} \frac{d\mu'}{\mu'} \gamma(\mu') \gamma(\mu) + \dots\tag{3.7}$$

Equation (3.6) provides the matrix-valued generalisation of (2.39) and shows one of the key ideas of EFTs that enables resummation: The separation of scale dependencies. The Wilson coefficients depend only on the high scale and the operator expectation value only on the low scale, which is why neither of them may develop large corrections in perturbation theory. In turn, all logarithmic contributions are contained in the exponential.

3.2. Soft-Collinear Effective Theory

In this section we give an introduction to some aspects of Soft-Collinear Effective Theory (SCET). Its very basic idea can be condensed in the following prescription: *Integrate out all interactions with momentum transfers larger than a given reference scale!* This results in an effective theory, which contains only dynamical degrees of freedom that are either soft or collinear with respect to a given reference direction. This approach implies two main complications:

- Such a theory turns out to be non-local. Since gauge invariance has to be taken care of, this puts up the necessity of Wilson lines, which we discuss in Sec. 3.2.4.
- Consistent power counting requires a very careful treatment of subleading effects. This point is not so much of importance for this project, as we are working at leading power only.

Originally SCET has been developed as a tool for the resummation of large logarithmic corrections related in semi-inclusive heavy-meson decays, extending heavy-quark effective theory

(HQET) [25, 26]. Since that time it has turned to be a useful tool in jet physics [40–42] and the method can also be generalised to a theory including massive gauge bosons and scalars and hence be used to resum the large logarithms of ratios the gauge boson mass and kinematic invariants in SM scattering processes of very high energy [43–48]. The crucial prerequisite for a resummation of these logarithms for a generic observable σ is to have a factorised formula, in which the dependences on the high scale and the low scale are separated,

$$\sigma = H \otimes J \otimes S, \quad (3.8)$$

with some hard function H that is independent of the low-scale physics, some jet function J that encodes collinear and a soft function S that contains the soft interactions. Each contribution depends only on a single scale and the running between the associated scales is governed by the RGE. To arrive at a formula like (3.8) we will go through several steps:

- We derive the SCET Lagrangian from the QCD Lagrangian using a consistent power counting in the scale ratios. The power counting and the kinematics are introduced in Sec. 3.2.1, while the Lagrangian is derived in Sec. 3.2.2.
- We transform to momentum space to obtain Feynman rules. For a consistent power counting this is done using the label formalism [26, 28] (Sec. 3.2.3).
- We introduce Wilson lines (Sec. 3.2.4) to ensure gauge invariance when defining external operators connecting fields at different space-time points. The construction of external operators is described in Sec. 3.2.5.
- Afterwards, we generalise the results for processes involving more than one collinear direction. This brings us to a discussion of n -jet amplitudes, we discuss the construction of the respective operators and the anomalous dimensions Sec. 3.2.6.
- The generalisation to the case of massive-boson exchange, which is needed for applications to the SM, is discussed in Sec. 3.3.

Up to the last point, the discussion is based on Ref. [159], while the last point refers to Refs. [44, 45, 47].

3.2.1. Kinematics and conventions

Consider a momentum four vector in the Sudakov parametrisation:

$$p^\mu = (n \cdot p) \frac{\bar{n}^\mu}{2} + (\bar{n} \cdot p) \frac{n^\mu}{2} + p_\perp^\mu, \quad (3.9)$$

with n being an arbitrary light-like auxiliary four vector and \bar{n} defined such that

$$n^2 = \bar{n}^2 = 0, \quad n \cdot \bar{n} = 2. \quad (3.10)$$

Denoting the light-cone components of a momentum four vector according to

$$p = (n \cdot p, \bar{n} \cdot p, |\mathbf{p}_\perp|) \equiv (p^+, p^-, p_\perp), \quad (3.11)$$

we define a momentum to have n -collinear, \bar{n} -collinear and soft scaling, respectively, according to

$$p_c^\mu \sim (\lambda^2, 1, \lambda)Q, \quad p_{\bar{c}}^\mu \sim (1, \lambda^2, \lambda)Q, \quad p_s^\mu \sim (\lambda^2, \lambda^2, \lambda^2)Q, \quad (3.12)$$

with Q being the hard energy scale. Note that the scaling of p_s is sometimes called *ultrasoft* scaling in order to distinguish it from a scaling of the form $(\lambda, \lambda, \lambda)$. However, since this scaling never occurs in our applications, we stick to the convention to use the term *soft* for $(\lambda^2, \lambda^2, \lambda^2)$.

The Sudakov parametrisation (3.9) is not restricted to momenta. In the following chapters any four vector is decomposed into its Sudakov components, if convenient. For instance, we define the components of the gluon field via

$$A^\mu = (n \cdot A) \frac{\bar{n}^\mu}{2} + (\bar{n} \cdot A) \frac{n^\mu}{2} + A_\perp^\mu \equiv A_+^\mu + A_-^\mu + A_\perp^\mu. \quad (3.13)$$

3.2.2. The SCET Lagrangian for QCD

In this section we sketch the derivation of the leading-power Lagrangian for SCET following Ref. [159]. The theory we want to arrive at is given by QCD with all off-shell interactions with order Q^2 integrated out. This is very much the same strategy as if we would consider a heavy particle to be removed as a dynamic degree of freedom. However, gauge invariance and non-locality require some special treatment, which makes SCET different from other EFTs.

The general strategy is to apply the power expansion of the previous section in a consistent way to the massless QCD action

$$S_{\text{QCD}} = \int d^4x \mathcal{L}_{\text{QCD}} = \int d^4x \left(\bar{\psi} i \not{D} \psi - \frac{1}{4} (F_{\mu\nu}^a)^2 \right) \quad (3.14)$$

with the sum over the quark flavours and colours implicit. The expansion in λ serves as an EFT parameter expansion in analogy to $1/\Lambda$ in (3.1). We will work at leading power only, meaning that we keep only terms of order λ^0 .

To this end, the power counting in λ of all fields and interactions is analysed and all subleading terms are dropped. This is done in position space using ordinary Fourier representations, an approach originally chosen in Refs. [32, 160]. We also give some results in the label formalism afterwards in order to have momentum-space Feynman rules. The derivation is also possible using the label formalism from the beginning [26].

In order to obtain the effective theory for only soft and collinear interactions, all involved fields have to be expanded into soft and collinear components:³

$$\begin{aligned} A^\mu(x) &\rightarrow A_c^\mu(x) + A_s^\mu(x), \\ \psi(x) &\rightarrow \psi_c(x) + \psi_s(x) = \xi(x) + \eta(x) + \psi_s(x) \end{aligned} \quad (3.15)$$

³Here, we assume only one collinear direction to be present. The generalisation to more than one direction is described in Sect. 3.2.6.

for the gauge-boson fields A^μ and the fermion fields ψ , respectively. For the Dirac fermions we have defined the following projections:

$$\xi_c = P_+ \psi_c = \frac{\not{n} \not{\bar{n}}}{4} \psi_c, \quad \eta_c = P_- \psi_c = \frac{\not{\bar{n}} \not{n}}{4} \psi_c. \quad (3.16)$$

We will refer to the fields in (3.15) as quark and gluon fields, even though we are in principle interested in the respective fields in the EWSM. The general method, however, will remain unchanged. The colour indices are omitted for simplicity of notation.

In order to obtain the Lagrangian in the SCET expansion, the scaling of the fields in the power counting has to be determined. The scaling of the gluon field can be obtained from the Fourier representation of its propagator using the R_ξ -gauge:⁴

$$\int d^4x e^{ikx} \langle 0 | T \{ A^\mu(x) A^\nu(0) \} | 0 \rangle = \frac{-i}{k^2} \left(g^{\mu\nu} - (1 - \xi) \frac{k^\mu k^\nu}{k^2} \right). \quad (3.17)$$

Since the scaling on both sides has to be the same, the components of the gluon fields have to scale like their associated momenta:

$$A_c^\mu \sim (\lambda^2, 1, \lambda), \quad A_s^\mu \sim (\lambda^2, \lambda^2, \lambda^2). \quad (3.18)$$

Note that the scaling of the soft field does not imply that its interactions are genuinely power suppressed. This is because the conjugate position argument scales such that $x \cdot p \sim 1$ and therefore, for instance,

$$\int \underbrace{d^4x}_{\sim \lambda^{-8}} \left(\underbrace{\partial_\mu}_{\sim \lambda^2} \underbrace{A_{\nu,s}(x)}_{\sim \lambda^2} \right)^2 \sim 1. \quad (3.19)$$

The contribution to the *action* is hence of order 1, even though the respective term in the *Lagrangian density* appears to be suppressed.

By analysing the power counting for the collinear fermion fields (3.16) in a similar manner, it can be shown that the η -contribution is power suppressed and does not contribute at leading power:

$$\xi_c(x) \sim \lambda, \quad \eta_c(x) \sim \lambda^2. \quad (3.20)$$

In contrast to A_s^μ , the position argument of the fermion component $\eta_c(x)$ has collinear scaling and the kinetic term results to be suppressed also on the level of the action. Since the Lagrangian is quadratic in η , its classical equation of motion can be solved and it can be integrated out by inserting the solution back into the Lagrangian. This procedure introduces inverse derivative operators into the Lagrangian, for instance via the equation of motion for $\bar{\eta}$:

$$\not{D}_\perp \xi = -\frac{\bar{n}}{2} n \cdot D \eta \quad \Rightarrow \quad \eta = -\frac{\not{\bar{n}}}{2\bar{n} \cdot D} \not{D}_\perp \xi, \quad (3.21)$$

⁴The gauge parameter is not to be confused with the fermion component defined in (3.16)!

where the perpendicular component of the covariant derivative is defined in analogy to (3.9). The inverse derivatives can be defined via the integral representation

$$\frac{i}{i\bar{n} \cdot \partial + i0} \phi(x) = \int_{-\infty}^0 ds \phi(x + s\bar{n}). \quad (3.22)$$

The occurrence of products of field operators evaluated at different space-time points indicates a non-local interaction along the n -collinear direction. This can be understood from the fact that any number of directional derivatives has to be considered in the effective Lagrangian:

$$\phi_c(x + s\bar{n}) = \exp(s\bar{n} \cdot \partial) \phi_c(x) = \sum_{k=0}^{\infty} \frac{s^k}{k!} (\bar{n} \cdot \partial)^k \phi_c(x). \quad (3.23)$$

Note that the first equality is the usual quantum-mechanical translation operation. Because all terms on the right-hand side of (3.23) contribute at the same order in the power counting, the general effective Lagrangian will feature non-local interactions.

Having the fields expanded in λ and having removed the η -component, we can write the Lagrangian as

$$\mathcal{L}_{\text{SCET}} = \bar{\psi}_s i \not{D}_s \psi_s + \bar{\xi} \frac{\not{\bar{n}}}{2} i n \cdot D \xi + \bar{\xi} \frac{\not{\bar{n}}}{2} \left(i \not{D}_\perp \frac{1}{i\bar{n} \cdot D} i \not{D}_\perp \right) \xi - \frac{1}{4} (F_{\mu\nu,s}^a)^2 - \frac{1}{4} (F_{\mu\nu,c}^a)^2, \quad (3.24)$$

where the expanded form of the covariant derivatives and the field strengths is still to be determined. To do this, we have to apply the same treatment to the interaction terms of the Lagrangian. Those interaction terms that involve soft or collinear fields exclusively remain unaffected by this expansion because upon integration over space-time, the interaction terms are of $\mathcal{O}(1)$ by construction. A non-trivial expansion is required only for interactions between soft and collinear modes. Consider the interaction term of two collinear fields with a soft gluon:

$$\int d^4x \phi_c^2(x) A_s^\mu(x) = \int d^4x \int \frac{d^4p_1}{(2\pi)^4} \int \frac{d^4p_2}{(2\pi)^4} \int \frac{d^4p_s}{(2\pi)^4} e^{i(p_1+p_2+p_s)x} \tilde{\phi}_c(p_1) \tilde{\phi}_c(p_2) \tilde{A}_s^\mu(p_s), \quad (3.25)$$

where ϕ_c can denote a collinear quark/antiquark or gluon pair, respectively. The sum of the momenta in the exponential has collinear scaling:

$$x(p_1 + p_2 + p_s) \sim 1, \quad x \sim \left(1, \frac{1}{\lambda^2}, \frac{1}{\lambda}\right) \frac{1}{Q}. \quad (3.26)$$

In order to remove all spurious terms from the exponent in (3.25), one makes the replacement

$$xp_s \rightarrow \left(0, \frac{1}{\lambda^2}, 0\right) \frac{1}{Q} p_s = x^- p_s^+. \quad (3.27)$$

In the same spirit, the soft gluon field is replaced by its +-component:

$$\int d^4x \phi_c^2(x) (A_c^\mu(x) + A_s^\mu(x^-)) \approx \int d^4x \phi_c^2(x) (A_c^\mu(x) + A_{+,s}^\mu(x^-)), \quad (3.28)$$

because from the scaling (3.18) one sees that

$$A_c^- \gg A_s^-, \quad A_{\perp,c} \gg A_{\perp,s}. \quad (3.29)$$

All of the above considerations are taken care by defining the covariant derivative according to

$$iD^\mu = i\partial^\mu + g \left[(n \cdot A_c^a(x) + n \cdot A_s^a(x^-)) \frac{\bar{n}^\mu}{2} + \bar{n} \cdot A_c^a(x) \frac{n^\mu}{2} + A_{\perp,c}^{a,\mu}(x) \right] T^a, \quad (3.30)$$

where we have reintroduced the colour algebra. Defining

$$\begin{aligned} iD_s^\mu &= i\partial^\mu + g A_s^{\mu,a} T^a, \\ iD_c^\mu &= i\partial^\mu + g A_c^{\mu,a} T^a, \end{aligned} \quad (3.31)$$

in addition, we can write the SCET Lagrangian in its final form

$$\mathcal{L}_{\text{SCET}} = \bar{\psi}_s i\not{D}_s \psi_s + \bar{\xi} \frac{\not{n}}{2} i n \cdot D \xi + \bar{\xi} \frac{\not{n}}{2} \left(i\not{D}_{\perp,c} \frac{1}{i\bar{n} \cdot D_c} i\not{D}_{\perp,c} \right) \xi - \frac{1}{4} (F_{\mu\nu,s}^a)^2 - \frac{1}{4} (F_{\mu\nu,c}^a)^2, \quad (3.32)$$

with the field-strength tensors being

$$F_s^{\mu\nu} = \frac{i}{g_s} [D_s^\mu, D_s^\nu], \quad F_c^{\mu\nu} = \frac{i}{g_s} [D_c^\mu, D_c^\nu]. \quad (3.33)$$

If, in addition, there is a scalar φ in the fundamental representation present, its kinetic term

$$\mathcal{L}_{\text{sc}} = (D_\mu \varphi)^\dagger (D^\mu \varphi) \quad (3.34)$$

can be expanded in a similar way [44]. After defining collinear and soft scalar fields

$$\varphi(x) \rightarrow \varphi_c(x) + \varphi_s(x), \quad (3.35)$$

and parameterising the covariant derivatives in light-cone coordinates, the Lagrangian becomes

$$\begin{aligned} \mathcal{L}_{\text{sc}} &= (D_{\mu,s} \varphi_s)^\dagger (D_s^\mu \varphi_s) + \varphi_c^\dagger \left((n \cdot D)^\dagger (\bar{n} \cdot D) + D_\perp^2 \right) \varphi_c \\ &= (D_{\mu,s} \varphi_s)^\dagger (D_s^\mu \varphi_s) + \varphi_c^\dagger \left((n \cdot \partial)^\dagger (\bar{n} \cdot \partial) + \partial_\perp^2 \right) \varphi_c + \text{interaction terms}. \end{aligned} \quad (3.36)$$

3.2.3. Label formalism and Feynman rules

Usually, given a Lagrangian in position space, the most convenient way to write down the Feynman rules is by transforming them into momentum space. In SCET, one often adopts a modified momentum space representation, which is called the label formalism first introduced in Ref. [26]. It is based on a splitting of any collinear momentum p_c into a label part and a residual part,

$$p_c \rightarrow q + r, \quad (3.37)$$

where the residual part has soft scaling,

$$r \sim (\lambda^2, \lambda^2, \lambda^2), \quad (3.38)$$

and the label momentum scales as

$$q \equiv p_- + p_\perp \sim (0, 1, \lambda). \quad (3.39)$$

The isotropic soft-momentum components are thus encoded in r , while the label momentum is designed such that it cannot be changed via collinear or soft interactions. This crucial property implies that in SCET a field can be identified with a certain label momentum q . The label of a field can be extracted with the label operator \mathcal{P} , defined via

$$\mathcal{P}^\mu \phi_q = q^\mu \phi_q. \quad (3.40)$$

The collinear fields are then rewritten as

$$\phi_c(x) \rightarrow \sum_q e^{-iqx} \phi_q(x). \quad (3.41)$$

The leading-power Lagrangian after these substitutions reads

$$\begin{aligned} \mathcal{L}_{\text{SCET}} = & \bar{\psi}_s i \not{D}_s \psi_s + \bar{\xi}_q \frac{\not{n}}{2} i n \cdot (\partial + \mathcal{A}_k) \xi_{q'} + \bar{\xi}_q \frac{\not{n}}{2} \left(i(\not{\mathcal{P}}_\perp + \mathcal{A}_{k,\perp}) \frac{1}{i\bar{n} \cdot \mathcal{P}} i(\not{\mathcal{P}}_\perp + \mathcal{A}_{k',\perp}) \right) \xi_{q'} \\ & - \frac{1}{4} (F_{\mu\nu,s}^a)^2 - \frac{1}{4} (F_{\mu\nu,c}^a)^2. \end{aligned} \quad (3.42)$$

Here the sum over the label momenta is implicit and the phase factors, which ensure the conservation of the label momentum, are also omitted. The Feynman rules following from this Lagrangian are depicted in Fig. 3.1, see Refs. [26, 28].

3.2.4. Gauge invariance and Wilson lines

The issue of gauge invariance in SCET has been treated in a systematic way in Refs. [29, 31, 32]. In this section we will recap some important results from these works.

Omitting subleading contributions in the decompositions (3.15) violates the full SU(3) gauge invariance, essentially because integrating out the hard interactions removes some non-trivial colour flow. However, the dynamic degrees of freedom left have to respect the remnant symmetries of soft and collinear gauge invariance. The respective symmetry transformations are obtained from a full gauge transformation,

$$U(x) = \exp(iT^a \theta^a(x)), \quad (3.43)$$

if the derivatives of the gauge parameters θ_a are expanded in a way consistent with (3.12):

$$\begin{aligned} U_c(x) &= \exp(iT^a \theta_c^a(x)), & \partial^\mu \theta_c^a(x) &\sim n^\mu \theta_c^a(x), \\ U_s(x) &= \exp(iT^a \theta_s^a(x)), & \partial_s^\mu \theta_s^a(x) &\sim \lambda^2 \theta_s^a(x). \end{aligned} \quad (3.44)$$

$$\begin{aligned}
 & \bullet \text{---} \overset{p}{\text{---}} \bullet = \frac{i\not{n}}{2} \frac{\bar{n}\cdot p}{p^2+i0} \\
 & \bullet \text{---} \overset{a, \mu}{\text{---}} \bullet = igT^a n_\mu \frac{\not{n}}{2} \\
 & \begin{array}{c} \bullet \text{---} \overset{a, \mu}{\text{---}} \bullet \\ | \\ \bullet \text{---} \overset{p}{\text{---}} \bullet \text{---} \overset{q}{\text{---}} \bullet \end{array} = igT^a \left(n_\mu + \frac{\gamma_\mu^\perp \not{p}_\perp}{\bar{n}\cdot p} + \frac{\not{q}_\perp \gamma_\mu^\perp}{\bar{n}\cdot q} - \frac{\not{q}_\perp \not{p}_\perp}{\bar{n}\cdot q \bar{n}\cdot p} \bar{n}_\mu \right) \frac{\not{n}}{2} \\
 & \begin{array}{c} \bullet \text{---} \overset{a, \mu}{\text{---}} \bullet \\ | \\ \bullet \text{---} \overset{p}{\text{---}} \bullet \text{---} \overset{q}{\text{---}} \bullet \\ / \quad \backslash \\ \bullet \quad \bullet \\ \backslash \quad / \\ \bullet \quad \bullet \\ | \\ \bullet \text{---} \overset{k}{\text{---}} \bullet \end{array} = \frac{ig^2 T^a T^b}{\bar{n}\cdot(p-k)} \left(\gamma_\mu^\perp \gamma_\nu^\perp - \frac{\gamma_\mu^\perp \not{p}_\perp}{\bar{n}\cdot p} \bar{n}_\nu - \frac{\not{q}_\perp \gamma_\nu^\perp}{\bar{n}\cdot q} \bar{n}_\mu + \frac{\not{q}_\perp \not{p}_\perp}{\bar{n}\cdot q \bar{n}\cdot p} \bar{n}_\mu \bar{n}_\nu \right) \frac{\not{n}}{2} \\
 & \quad + \frac{ig^2 T^b T^a}{\bar{n}\cdot(q+k)} \left(\gamma_\nu^\perp \gamma_\mu^\perp - \frac{\gamma_\nu^\perp \not{p}_\perp}{\bar{n}\cdot p} \bar{n}_\mu - \frac{\not{q}_\perp \gamma_\mu^\perp}{\bar{n}\cdot q} \bar{n}_\nu + \frac{\not{q}_\perp \not{p}_\perp}{\bar{n}\cdot q \bar{n}\cdot p} \bar{n}_\nu \bar{n}_\mu \right) \frac{\not{n}}{2} \\
 & \bullet \text{---} \overset{a, \mu}{\text{---}} \bullet \text{---} \overset{b, \nu}{\text{---}} \bullet = \frac{-ig_{\mu\nu} \delta_{ab}}{p^2+i0} \\
 & \begin{array}{c} \bullet \text{---} \overset{a, \mu}{\text{---}} \bullet \\ | \\ \bullet \text{---} \overset{b, \nu}{\text{---}} \bullet \text{---} \overset{c, \rho}{\text{---}} \bullet \end{array} = g f^{abc} n_\mu (\bar{n}\cdot p) g_{\nu\rho} \\
 & \begin{array}{c} \bullet \text{---} \overset{d, \sigma}{\text{---}} \bullet \\ / \quad \backslash \\ \bullet \quad \bullet \\ \backslash \quad / \\ \bullet \quad \bullet \\ | \\ \bullet \text{---} \overset{a, \mu}{\text{---}} \bullet \\ | \\ \bullet \text{---} \overset{b, \nu}{\text{---}} \bullet \text{---} \overset{c, \rho}{\text{---}} \bullet \end{array} = i\frac{1}{4} g^2 n_\mu n_\sigma \bar{n}_\rho \bar{n}_\nu (1 - \frac{1}{\xi}) (f^{dce} f^{abe} + f^{dbe} f^{ace}) \\
 & \begin{array}{c} \bullet \text{---} \overset{d, \sigma}{\text{---}} \bullet \\ / \quad \backslash \\ \bullet \quad \bullet \\ \backslash \quad / \\ \bullet \quad \bullet \\ | \\ \bullet \text{---} \overset{a, \mu}{\text{---}} \bullet \\ | \\ \bullet \text{---} \overset{b, \nu}{\text{---}} \bullet \text{---} \overset{c, \rho}{\text{---}} \bullet \end{array} = i\frac{1}{2} g^2 n_\sigma [f^{dae} f^{cbe} (\bar{n}_\rho g_{\mu\nu} - \bar{n}_\nu g_{\rho\mu}) \\
 & \quad + f^{dbe} f^{ace} (\bar{n}_\mu g_{\nu\rho} - \bar{n}_\rho g_{\mu\nu}) + f^{dce} f^{abe} (\bar{n}_\nu g_{\rho\mu} - \bar{n}_\mu g_{\nu\rho})
 \end{aligned}$$

Figure 3.1.: Leading-power Feynman rules for SCET in QCD in R_ξ -gauge. Curly lines represent soft gluons, while curly lines with a straight line inside represent collinear gluons. The arrows indicate the direction of the associated collinear momentum if it is not fixed by momentum conservation. Feynman rules involving only collinear or soft quarks are not shown, as they are not changed with respect to QCD.

These expressions define collinear and soft gauge transformations, respectively. Since the form of the soft interactions is the same as the full QCD Lagrangian, the soft fields transform in the same way under soft gauge transformations as QCD fields do under full gauge transformations:

$$\begin{aligned}\psi_s &\rightarrow U_s(x)\psi_s, \\ A_s^\mu &\rightarrow U_s(x)A_s^\mu U_s^\dagger(x) + \frac{i}{g_s}U_s(x) \left[\partial^\mu, U_s^\dagger(x) \right].\end{aligned}\quad (3.45)$$

Because soft particles can not emit collinear gluons while remaining soft, the collinear gauge transformation does not affect soft particles:

$$\psi_s \rightarrow \psi_s, \quad A_s^\mu \rightarrow A_s^\mu. \quad (3.46)$$

For the behaviour of collinear fields under soft gauge transformation to be consistent in the power counting, the soft gauge transformation has to be expanded in the same way as the soft field in the soft–collinear interaction term (3.25), resulting in

$$\begin{aligned}\xi_c &\rightarrow U_s(x_-)\xi_c, \\ A_c^\mu &\rightarrow U_s(x_-)A_c^\mu U_s^\dagger(x_-).\end{aligned}\quad (3.47)$$

Finally we discuss the transformation of collinear fields under collinear gauge transformations, which is given by:

$$\begin{aligned}\xi_c &\rightarrow U_c(x)\xi_c, \\ A_c^\mu &\rightarrow U_c(x)A_c^\mu U_c^\dagger(x) + \frac{1}{g_s}U_c(x) \left[i\partial^\mu + g_s \frac{\bar{n}^\mu}{2}(n \cdot A_s(x_-)), U_c^\dagger(x) \right].\end{aligned}\quad (3.48)$$

The extra contribution of the soft gluon can be motivated by the form of the covariant derivative (3.30): It is fixed such that D_μ transforms as

$$D_\mu \rightarrow U_c(x)D_\mu V_c^\dagger(x). \quad (3.49)$$

The collinear covariant derivative transforms as

$$\begin{aligned}D_c^\mu &\rightarrow U_s(x_-)D_c^\mu V_s^\dagger(x_-), \\ D_c^\mu &\rightarrow U_c(x)D_c^\mu V_c^\dagger(x)\end{aligned}\quad (3.50)$$

and hence the Lagrangian (3.32) is by construction invariant under both soft and collinear gauge transformations.

In order to construct external operators from gauge-covariant building blocks which respect the remnant gauge symmetries, we define soft and collinear Wilson lines as

$$\begin{aligned}W_n(x) &= \hat{P} \exp \left(ig_s \int_{-\infty}^0 ds \bar{n} \cdot A_c^a(x + s\bar{n}) T^a \right), \\ Y_n(x) &= \hat{P} \exp \left(ig_s \int_{-\infty}^0 ds n \cdot A_s^a(x + sn) T^a \right).\end{aligned}\quad (3.51)$$

They provide natural generalisations of the ordinary QCD Wilson line from infinity, which reads

$$W(x) = \hat{\text{P}} \exp \left(ig_s \int_{-\infty}^0 ds \bar{n} \cdot A^a(x + s\bar{n}) T^a \right). \quad (3.52)$$

Here and in the following, the symbol $\hat{\text{P}}$ denotes path ordering of the colour operators T^a , see (3.7). More generally, Wilson lines are defined as the connection of a field evaluated at two space-time points that respects gauge invariance:

$$\psi(x) = \hat{\text{P}} \exp \left(ig_s \int_y^x d\xi_\mu A^{\mu,a}(\xi^\mu) T^a \right) \psi(y) \equiv W(x, y) \psi(y), \quad (3.53)$$

where ξ is some parameterised curve connecting x and y .⁵ From a geometric point of view this corresponds to a parallel transport along the manifold of gauge-equivalent field configurations, for details see for instance Sec. 2.3.2 of Ref. [143]. Applying a gauge transformation on the ψ -fields in the above equation shows that the Wilson line's transformation behaviour under gauge transformations has to read

$$W(x, y) \rightarrow U(x) W(x, y) U^\dagger(y). \quad (3.54)$$

For a Wilson line coming from infinity, this implies

$$W(x) \rightarrow U(x) W(x) U^\dagger(-\infty) = U(x) W(x) \quad (3.55)$$

if the gauge transformation vanishes as $x \rightarrow \infty$. This is a sensible assumption, as otherwise a gauge transformation would induce non-vanishing boundary terms.

Wilson lines are especially important when constructing non-local operators since the product of two operators at different space-time points is by construction gauge invariant if they are connected via a Wilson line:

$$\begin{aligned} \bar{\psi}(x + s\bar{n}) \psi(x) &\rightarrow \bar{\psi}(x + s\bar{n}) W(x + s\bar{n}, x) \psi(x) \\ &= \bar{\psi}(x + s\bar{n}) \hat{\text{P}} \exp \left(i \int_0^s d\tau \bar{n} \cdot A^a(x + \tau\bar{n}) T^a \right) \psi(x) \\ &= \bar{\psi}(x + s\bar{n}) \hat{\text{P}} \exp \left(i \int_{-\infty}^0 d\tau \bar{n} \cdot A^a(x + s\bar{n} + \tau\bar{n}) T^a \right. \\ &\quad \left. - i \int_{-\infty}^0 d\tau \bar{n} \cdot A^a(x + \tau\bar{n}) T^a \right) \psi(x) \\ &= \bar{\psi}(x + s\bar{n}) W(x + s\bar{n}) W^\dagger(x) \psi(x), \end{aligned} \quad (3.56)$$

where the last equality shows that a single Wilson line of finite extent can be written as a product of two Wilson lines from and to infinity, respectively. This relies on the fact that all Wilson-lines considered here follow straight paths. In case of the general definition (3.53), this does not necessarily hold. Note further that both $\bar{\psi}(x + s\bar{n}) W(x + s\bar{n})$ and $W^\dagger(x) \psi(x)$ are separately gauge invariant. Non-local interactions involving collinear fermions and gauge bosons

⁵Note that Wilson lines with two arguments, as defined above, are to be distinguished from Wilson lines with a single argument defined according to (3.52). We will mostly use the type latter in the following.

can therefore be constructed using the combinations

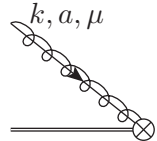
$$\chi_c(x) = W_n^\dagger(x)\xi(x), \quad \mathcal{A}^\mu(x) = W_n^\dagger(x) (iD_c^\mu W_n(x)), \quad (3.57)$$

for processes involving external n collinear quarks and gluons, respectively.

Calculating radiative corrections to operators involving these kinds of fields involves virtual gluons emitted both from the external field and from the Wilson line. The Feynman rules for the radiation from external fields can be read off Fig. 3.1, while those associated with radiation from the Wilson line are obtained via re-expanding the exponential. This is most conveniently done in momentum or label space, where the representation of the Wilson line is [27,28]

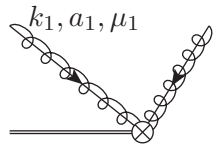
$$W_n = \sum_{\text{perms}} \exp \left(-g_s \frac{1}{\bar{n} \cdot \mathcal{P}} \bar{n} \cdot A_{c,q}(x) \right). \quad (3.58)$$

Expanding the exponential yields order by order the Feynman rules for the coupling of n -collinear gluons from the collinear Wilson line in the fundamental representation:



$$= g_s \frac{i\bar{n}^\mu}{\bar{n} \cdot k} T^a, \quad (3.59)$$

for the emission of a single collinear gluon,



$$= g_s^2 \bar{n}^{\mu_1} \bar{n}^{\mu_2} \left(\frac{T^{a_1} T^{a_2}}{\bar{n} \cdot k_2 \bar{n} \cdot (k_1 + k_2)} + \frac{T^{a_2} T^{a_1}}{\bar{n} \cdot k_1 \bar{n} \cdot (k_1 + k_2)} \right) \quad (3.60)$$

for two gluons, and so on for a higher number of emitted gluons.

3.2.5. External Operators

The SCET Lagrangian (3.32) has been obtained by expanding all QCD interactions in the SCET power counting. It is however not the most general SCET operator one can write down. In fact, to calculate observables the SCET Lagrangian alone is rather useless because it is completely independent of any hard interaction, which is usually just the interesting part of a scattering process.

In order to calculate observables one introduces supplementary external operators, which may be inserted into Green's functions. A discussion of the defining features of external operators can be found in Ref. [144], chapter 23.4.

A very basic and extensively discussed example is the Sudakov form factor. It is of particular importance for our purpose because the results serve as building blocks for SCET corrections to n -jet amplitudes, which we are going to consider. In QCD the Sudakov form factor can be defined as the expectation value of two quarks scattering from the current operator

$$J^\mu(x) = \bar{\psi}(x)\gamma^\mu\psi(x), \quad (3.61)$$

which can be matched against a suitable SCET operator. This is conveniently done in the Breit frame, where the two quarks are back-to-back. Writing down a continuous sum of all collinear gauge invariant λ^0 -operators with the above Lorentz structure yields

$$J^\mu(x) = \int ds \int dt C(s, t) \bar{\chi}_c(x + s\bar{n}) \gamma_\perp^\mu \chi_c(x + tn). \quad (3.62)$$

The integrals occur because we do not restrict ourselves to local interactions. The fact that we need only one reference vector n is a specific property of the Breit frame. Only γ_\perp^μ contributes because of the expansion of γ^μ in the Sudakov parametrisation:

$$\gamma^\mu = \not{n} \frac{\bar{n}^\mu}{2} + \not{n} \frac{n^\mu}{2} + \gamma_\perp^\mu. \quad (3.63)$$

When sandwiched between an n -collinear and an \bar{n} -collinear fermion field, only the third term gives a non-zero contribution. In the label formalism the above operator translates into

$$J^\mu(x) = \bar{\chi}_{c,q} \tilde{C}(\mathcal{P}) \gamma_\perp^\mu \chi_{\bar{c},q'}, \quad (3.64)$$

with the phases and the sum over labels again implicit. Insertions of the current (3.62) into the Green's functions enables the description of hard interactions within SCET. In Feynman diagrams, the insertion of an external operator is denoted with the symbol

$$\otimes. \quad (3.65)$$

Note that for the notation of the Wilson-line Feynman rules in (3.59), (3.60) we have already employed this notation since the Wilson lines arise in the construction of external operators.

3.2.6. n -jet scattering amplitudes in SCET

The former discussion has covered the general properties of SCET for a process with one distinct direction. The generalisation to observables involving n directions is straightforward: A set of collinear and anticollinear fields is introduced for each direction, and they interact via a single set of soft fields. Furthermore, we will see that the anomalous dimension of any n -jet amplitude is obtained as a sum over two-particle results. Studying n -jet amplitudes in SCET has proven useful to analyse the structure of infrared (IR) singularities in QCD [158, 161–164]. A systematic consideration of subleading-power n -jet operators has been worked out in Refs. [165, 166].

If a hard scattering amplitude is to be computed, any external field is to be represented by a collinear field in a certain direction, between which interactions are only possible by means of soft modes. The SCET Lagrangian is hence obtained by copying the collinear part and keeping the soft one:

$$\mathcal{L}_n = \sum_{i=1}^n \mathcal{L}_{\text{coll},i} + \mathcal{L}_{\text{soft}}. \quad (3.66)$$

A cross talk between the collinear sectors via collinear interactions is forbidden by momentum conservation.

An external operator representing an n -jet scattering amplitude has the form

$$\mathcal{O}(x) = \int dt_1 \dots dt_n \phi_1(x + t_1 \bar{n}_1) \dots \phi_n(x + t_n \bar{n}_n), \quad (3.67)$$

or, within the label formalism,

$$\mathcal{O} = \phi_{1,p_1} \dots \phi_{n,p_n}. \quad (3.68)$$

Here, each field ϕ denotes a gauge-invariant building block discussed in Sec. 3.2.4. We have to assume that colour is conserved in the interaction, that is, the colour of the ϕ_i adds up to zero if all fields are incoming. The fact that any operator can be written as in (3.68) is investigated more detail in Sec. 3.3.2.

Factorization theorem

The RGE-improved matrix element for the n -jet process involving an operator j reads

$$\mathcal{M}_j = C_i(\mu_h) \hat{\mathbb{P}} \exp \left[- \int_{\mu_1}^{\mu_h} d \log \mu \gamma(\mu) \right]_{ij} \times \prod_k J_k \times S, \quad (3.69)$$

which is precisely (3.6) with the Wilson coefficients C_i and the anomalous dimension γ . J_k and S , denoting the jet and soft functions respectively, are not discussed in detail for the case of QCD. In some cases they depend on non-perturbative low-energy physics, such as the jet algorithm, the parton-distribution functions (PDFs) or fragmentation functions. In the following we discuss the computation of the Wilson coefficients and the anomalous dimension.

Wilson coefficients

Following the considerations given in Sec. 3.1, the Wilson coefficients associated with the operators (3.68) are obtained from a matching computation between QCD and SCET with all small scales set to zero. In terms of the operators of the form (3.68), a hard n -jet matrix element reads

$$\mathcal{M}_{\text{SCET}} = C_i \langle \mathcal{O}_i \rangle, \quad (3.70)$$

where we have suppressed colour and spin indices. The values of the tree-level Wilson coefficients are inferred by demanding

$$\mathcal{M}_{\text{SCET}} \stackrel{!}{=} \mathcal{M}_{\text{QCD}} + \mathcal{O}(\lambda). \quad (3.71)$$

As the operators themselves fix the Lorentz- and colour algebra, the matching condition can be phrased as

$$\mathcal{M}_{\text{SCET}}(\{p\}) = C(\{p\}) \times (\text{“spinors and polarisation vectors”}), \quad (3.72)$$

with the latter part also containing Dirac and colour matrices. The dependence on the momenta indicates that the Wilson coefficient is in momentum space. While (3.72) is somewhat obvious at tree level, it also holds at higher orders.

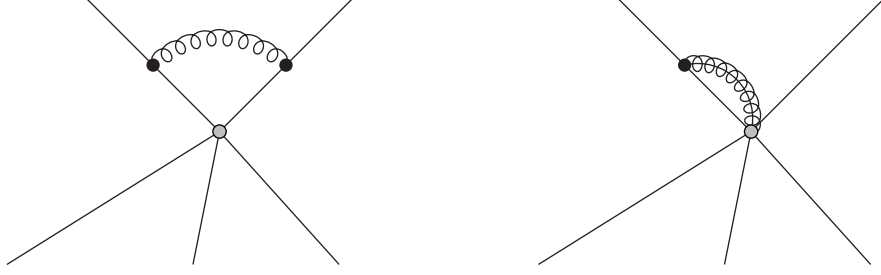


Figure 3.2.: Structure of the soft (left) and collinear (right) one-loop SCET radiative corrections to an n -jet amplitude. All lines represent collinear fields. The collinear corrections can be associated with a single external leg, while the soft ones involve two-particle correlations.

When radiative corrections are computed in SCET, both the Wilson coefficients and the operator expectation values are expanded in a perturbative series in the coupling constant:

$$\begin{aligned} C_i \mathcal{O}_i &\rightarrow \left(C_i^{(0)} + C_i^{(1)}(\mu) + \dots \right) \left(\mathcal{O}_i^{(0)} + \mathcal{O}_i^{(1)}(\mu) + \dots \right) \\ &= C_i^{(0)} \mathcal{O}_i^{(0)} + C_i^{(0)}(\mu) \mathcal{O}_i^{(1)}(\mu) + C_i^{(1)}(\mu) \mathcal{O}_i^{(0)} + \dots \end{aligned} \quad (3.73)$$

We have indicated scale dependences of the one-loop quantities $C^{(1)}$ and $\mathcal{O}^{(1)}$. The one-loop SCET matrix element is then given by

$$\mathcal{M}_{\text{SCET}}^{1\text{-loop}}(\mu) = C^{(0)} \langle \mathcal{O}^{(1)}(\mu) \rangle + C^{(1)}(\mu) \langle \mathcal{O}^{(0)} \rangle. \quad (3.74)$$

Note that by $\langle \mathcal{O}^{(1)}(\mu) \rangle$ we denote the one-loop Feynman diagrams using the EFT Lagrangian. This includes the wavefunction counterterms from the LSZ reduction formula. Imposing (3.71) at one loop, the one-loop Wilson coefficient reads

$$\frac{C^{(1)}(\mu)}{C^{(0)}} = \frac{\mathcal{M}_{\text{QCD}}^{1\text{-loop}}(\mu) - C^{(0)} \langle \mathcal{O}^{(1)}(\mu) \rangle}{\mathcal{M}_{\text{QCD}}^{\text{tree}}}. \quad (3.75)$$

Because the Wilson coefficient depends only on the hard scale, the r.h.s. above must also not depend on any low scale. Therefore the computation can be simplified by setting all of them to zero, although this possibly introduces additional IR divergences. When the low scales are put to zero, all loop corrections $\mathcal{O}^{(1)}$ in SCET vanish because they involve only scaleless integrals:

$$\mathcal{O}^{(1)}(\mu) = \sum_k \left(\frac{D_k}{\varepsilon_{\text{UV}}^k} - \frac{D_k}{\varepsilon_{\text{IR}}^k} \right), \quad (3.76)$$

with some coefficients D . This can be explained by the fact that the diagrams depicted in Fig. 3.2 do not have any dependence on momentum transfers $(p_i + p_j)^2$ and hence depend only on the external and internal masses. While this is obvious for the collinear graphs, it is also true for the soft diagrams, as the loop momentum is expanded in the soft region, see App. B for an explicit calculation.

The UV poles in the full and the effective theory can in general be different, but the IR poles have to agree [52] and hence cancel in (3.75). The Wilson coefficient is thus calculated from the IR-finite part of the full matrix element and after renormalisation one obtains (assuming (3.72) to be valid at tree level)

$$\begin{aligned} \mathcal{M}_{\text{QCD}}^{1\text{-loop, ren}}(\mu) \Big|_{\text{IR-finite}} &= \frac{C^{(1), \text{ren}}(\mu) \mathcal{M}_{\text{QCD}}^{\text{tree}}}{C^{(0)}} = C^{(1), \text{ren}}(\mu) \langle \mathcal{O}^{(0)} \rangle \\ &= C^{(1), \text{ren}}(\mu) \times (\text{“spinors and polarisation vectors”}), \end{aligned} \quad (3.77)$$

which is the version of (3.72) at one-loop. (3.77) provides a prescription to calculate Wilson coefficients from QCD matrix elements, which will play a crucial role in our automation strategy.

Anomalous dimension

If one wishes to calculate the anomalous dimension for an n -jet operator, one has to compute an IR-finite observable involving that n -jet operator in order to extract the coefficient D_1 of the UV ε -pole in (3.76). One possibility employed in Ref. [159] is to introduce small offshellnesses p_i^2 for the external legs. The computation, see App. B, then boils down to a sum over pairs of external particles. Each contribution is similar to the corrections to the Sudakov form factor. The results for the collinear functions \mathcal{J} and the soft function \mathcal{S} read

$$\begin{aligned} \mathcal{J}_q &= 1 + \frac{\alpha_s}{4\pi} C_F \left(\frac{2}{\varepsilon^2} + \frac{2}{\varepsilon} \log \frac{\mu^2}{-p^2 - i0} + \frac{3}{2\varepsilon} \right) + \mathcal{O}(1), \\ \mathcal{J}_g &= 1 + \frac{\alpha_s}{4\pi} C_A \left(\left(\frac{2}{\varepsilon^2} + \frac{2}{\varepsilon} \log \frac{\mu^2}{-p^2 - i0} \right) + \frac{\beta_0}{2\varepsilon} \right) + \mathcal{O}(1), \\ \mathcal{S} &= 1 + \frac{\alpha_s}{4\pi} \sum_{i \neq j} \frac{\mathbf{T}_i \cdot \mathbf{T}_j}{2} \left(\frac{2}{\varepsilon^2} + \frac{2}{\varepsilon} \log \frac{(-s_{ij} - i0)\mu^2}{(-p_i^2 - i0)(-p_j^2 - i0)} + \frac{\beta_0}{2\varepsilon} \right) + \mathcal{O}(1). \end{aligned} \quad (3.78)$$

Formally, the expression $\log \frac{(-s_{ij} - i0)\mu^2}{(-p_i^2 - i0)(-p_j^2 - i0)}$ should be replaced by a sum of the individual logarithms:

$$\log \frac{(-s_{ij} - i0)\mu^2}{(-p_i^2 - i0)(-p_j^2 - i0)} \equiv \log \frac{(-s_{ij} - i0)}{\mu^2} - \log \frac{(-p_i^2 - i0)}{\mu^2} - \log \frac{(-p_j^2 - i0)}{\mu^2}. \quad (3.79)$$

The expression as a fraction is used for compactness. Because of the $i\pi$ -terms, it is not allowed to cancel any minus signs against each other! The invariant s_{ij} is defined as

$$s_{ij} = 2p_i \cdot p_j = \frac{1}{2}(\bar{n}_i \cdot p_i)(\bar{n}_j \cdot p_j)(n_i \cdot n_j) + \mathcal{O}(\lambda) \quad (3.80)$$

for all momenta incoming. Note that $\bar{n}_i \cdot p_i$ are the large momentum component of the respective collinear momenta. From the divergent parts in (3.78) one can read off the anomalous dimension matrix γ as -2 times the coefficient of $1/\varepsilon$:

$$\gamma = \sum_{\langle ij \rangle} \mathbf{T}_i \cdot \mathbf{T}_j \Gamma_{\text{cusp}} \log \left(\frac{\mu^2}{-s_{ij}} - i0 \right) + \sum_i \gamma_i, \quad (3.81)$$

where the regulators p_i^2 have all cancelled. Here γ_i denotes the anomalous dimension of the field i as defined in the full theory (see 2.37). The quantity Γ_{cusp} is defined as the coefficient of the anomalous dimension in front of the logarithm and reads $\Gamma_{\text{cusp}} = \frac{\alpha_s}{\pi}$ at one loop. Eventually, we introduced the notation for the sum over pairs:

$$\sum_{\langle ij \rangle} f(i, j) = \frac{1}{2} \sum_{i \neq j} f(i, j), \quad (3.82)$$

with the factor of 1/2 avoiding a double counting of each pair. While at one-loop order the fact that the anomalous dimension is a sum over pairs is rather obvious, it has been conjectured [158] that the above form is valid to all orders in the coupling.

The anomalous dimension is a matrix in operator space. When acting on colour-singlet operators, colour conservation can be used to split the first term in (3.81) into one- and two-particle contributions by introducing $\bar{n}_i \cdot p_i$ as auxiliary scales:

$$\begin{aligned} \gamma &= \sum_{i \neq j} \frac{\mathbf{T}_i \cdot \mathbf{T}_j}{2} \Gamma_{\text{cusp}} \left(\log \left(\frac{\mu}{\bar{n}_i \cdot p_i} \right) + \log \left(\frac{\mu}{\bar{n}_j \cdot p_j} \right) + \log \left(\frac{(\bar{n}_i \cdot p_i)(\bar{n}_j \cdot p_j)}{-s_{ij}} - i0 \right) \right) + \sum_i \gamma_i \mathbb{1} \\ &= \sum_i \mathbf{T}_i \cdot \mathbf{T}_i \Gamma_{\text{cusp}} \log \left(\frac{\bar{n}_i \cdot p_i}{\mu} \right) - \sum_{\langle ij \rangle} \mathbf{T}_i \cdot \mathbf{T}_j \Gamma_{\text{cusp}} \log \left(\frac{-n_i \cdot n_j}{2} - i0 \right) + \sum_i \gamma_i \mathbb{1} \\ &= \sum_i C_i \mathbb{1} \Gamma_{\text{cusp}} \log \left(\frac{\bar{n}_i \cdot p_i}{\mu} \right) - \sum_{\langle ij \rangle} \mathbf{T}_i \cdot \mathbf{T}_j \Gamma_{\text{cusp}} \log \left(\frac{-n_i \cdot n_j}{2} - i0 \right) + \sum_i \gamma_i \mathbb{1} \\ &\equiv \underbrace{\gamma_C \mathbb{1}}_{\gamma_C} + \gamma_S \\ &\equiv \gamma_{\text{cusp}} \mathbb{1} \log \left(\frac{\bar{n}_i \cdot p_i}{\mu} \right) + \gamma_{\text{non-cusp}}, \end{aligned} \quad (3.83)$$

where C_i denotes the Casimir operator of the representation of particle i . The last lines implicitly define two ways to split up the anomalous dimension:

- The collinear (C) and soft (S) anomalous dimension with γ_C comprising the first and third term in (3.83). This distinction is convenient because the collinear anomalous dimension exponentiates naively, while for the soft anomalous dimensions has to use a matrix exponential. It should be stressed that the distinction is not the same as the distinction between the regulator-dependent collinear and soft *functions* in (3.78) connected to the Feynman diagrams of collinear and soft gluons, respectively.
- The cusp and non-cusp anomalous dimension with the cusp anomalous dimension containing solely the contribution with $\log \left(\frac{\bar{n}_i \cdot p_i}{\mu} \right)$. If the s_{ij} and the $\bar{n}_i \cdot p_i$ are of the same order of magnitude, $\log \frac{n_i \cdot n_j}{2}$ is not large and all double-logarithmic contributions arise from the cusp anomalous dimension.

The two distinctions differ only by means of the γ_i , as shown in Tab. 3.1. In the following we consider the special case of $2 \rightarrow 2$ processes, in which the large momentum components $\bar{n}_i \cdot p_i$ are given by

$$\bar{n}_i \cdot p_i = 2E_i \equiv \mu_h, \quad (3.84)$$

Quantity	Symbol	Def.	Remark
Collinear AD	γ_C	$\propto \sum_i$	$= \gamma_{\text{cusp}} + \sum_i \gamma_i \mathbb{1}$
Soft AD	γ_S	$\propto \sum_{\langle ij \rangle}$	$= \gamma_{\text{non-cusp}} - \sum_i \gamma_i \mathbb{1}$
Cusp AD	γ_{cusp}	$\propto \log \left(\frac{\bar{n}_i \cdot p_i}{\mu} \right)$	$= \gamma_C - \sum_i \gamma_i \mathbb{1}$
Non-cusp AD	$\gamma_{\text{non-cusp}}$	not $\propto \log \left(\frac{\bar{n}_i \cdot p_i}{\mu} \right)$	$= \gamma_S + \sum_i \gamma_i \mathbb{1}$

Table 3.1.: Parts of the anomalous dimension and their definitions and relations.

defining the high energy scale μ_h .

3.2.7. Integration of the SCET anomalous dimension

From the anomalous dimension, the RGE-improved scattering amplitude is obtained using (3.6). The key ingredient is the path-ordered integral of the anomalous dimension over the scale μ , as defined in (3.7):

$$\mathbf{M}(\mu_h, \mu_l) = \hat{\mathbf{P}} \exp \left(- \int_{\mu_l}^{\mu_h} \frac{d\mu}{\mu} \boldsymbol{\gamma}(\mu) \right). \quad (3.85)$$

If $\boldsymbol{\gamma}$ is brought into the form (3.83), the integration and exponentiation can be performed quite straightforwardly. This is because the actual matrix structure is μ -independent. All terms, for which the path ordering symbol $\hat{\mathbf{P}}$ in (3.85) would apply, commute with one another and we can ignore $\hat{\mathbf{P}}$ when exponentiating. If we assume α_s to be μ -independent, the integration of $\boldsymbol{\gamma}$ is completely trivial:

$$\begin{aligned} \mathbf{M}(\mu_h, \mu_l) &= \exp \left(\left[-\frac{1}{2} \sum_i C_i \Gamma_{\text{cusp}} \log \left(\frac{(\bar{n}_i \cdot p_i)^2}{\mu_h \mu_l} \right) \log \left(\frac{\mu_h}{\mu_l} \right) + \gamma_i \log \left(\frac{\mu_h}{\mu_l} \right) \right] \mathbb{1} \right) \\ &\quad \times \exp \left(\Gamma_{\text{cusp}} \log \left(\frac{\mu_h}{\mu_l} \right) \sum_{\langle ij \rangle} \log \left(\frac{-n_i \cdot n_j}{2} - i0 \right) \mathbf{T}_i \cdot \mathbf{T}_j \right) \\ &= \exp \left(\left[-\frac{1}{2} \sum_i C_i \Gamma_{\text{cusp}} \log^2 \left(\frac{\mu_h}{\mu_l} \right) + \gamma_i \log \left(\frac{\mu_h}{\mu_l} \right) \right] \mathbb{1} \right) \\ &\quad \times \exp \left(\Gamma_{\text{cusp}} \log \left(\frac{\mu_h}{\mu_l} \right) \sum_{\langle ij \rangle} \log \left(\frac{-n_i \cdot n_j}{2} - i0 \right) \mathbf{T}_i \cdot \mathbf{T}_j \right), \end{aligned} \quad (3.86)$$

where the second form holds only in the case of a $2 \rightarrow 2$ process, when (3.84) can be used.

When assuming a constant coupling, the additional coupling-counterterm contributions proportional to δg_s contain a potentially large logarithmic term. The running is determined by the β -function coefficients via

$$\frac{\partial g_s}{\partial \log \mu} = -\beta_0 \frac{g_s^3}{16\pi^2} - \beta_1 \frac{g_s^5}{(16\pi^2)^2} + \mathcal{O}(g_s^7). \quad (3.87)$$

To solve the integral over the scale one can expand Γ_{cusp} and γ_i in $\alpha_s(\mu)$:

$$\begin{aligned}\Gamma_{\text{cusp}} &= \frac{\alpha_s}{4\pi} \Gamma_{\text{cusp}}^{(1)} + \left(\frac{\alpha_s}{4\pi}\right)^2 \Gamma_{\text{cusp}}^{(2)} + \dots, \\ \gamma &= \frac{\alpha_s}{4\pi} \gamma^{(1)} + \left(\frac{\alpha_s}{4\pi}\right)^2 \gamma^{(2)} + \dots\end{aligned}\quad (3.88)$$

Using the substitution

$$\log\left(\frac{\mu}{\mu_h}\right) = \int_{g_s(\mu)}^{g_s(\mu_h)} \frac{dg'_s}{\beta(g'_s)} \quad (3.89)$$

in the anomalous dimension and expanding the β -function, the integral is given by [29, 48]

$$\begin{aligned}\int_{\mu_1}^{\mu_h} d\log \mu \gamma(\alpha_s(\mu), \mu) &= \left(\frac{f_0(z)}{\alpha_s(\mu_h)} + f_1(z)\right) \mathbb{1} \\ &+ \frac{\Gamma^{(1)} \log(z)}{\beta_0} \sum_{\langle ij \rangle} \log\left(\frac{-n_i \cdot n_j}{2} - i0\right) \mathbf{T}_i \cdot \mathbf{T}_j + \mathcal{O}(\alpha_s^2)\end{aligned}\quad (3.90)$$

with

$$\begin{aligned}z &= \frac{\alpha_s(\mu_1)}{\alpha_s(\mu_h)}, \\ f_0(z) &= \frac{\pi \Gamma_{\text{cusp}}^{(1)}}{\beta_0^2} \left(\log z + \frac{1}{z} - 1\right), \\ f_1(z) &= \frac{\beta_1 \Gamma_{\text{cusp}}^{(1)}}{\beta_0^3} \left(\log z - z - \frac{1}{2} \log^2 z + 1\right) \\ &+ \frac{\Gamma_{\text{cusp}}^{(2)}}{\beta_0^2} (z - \log z - 1) - \frac{\sum_i \gamma_i}{\beta_0} \log(z).\end{aligned}\quad (3.91)$$

Note that (3.90) is merely a more explicit form of the results in Appendix A of [48], where terms are sorted according to whether they are proportional to the unit matrix.

3.3. Generalisation to the EWSM

The strategy to generalise SCET to the EWSM has been presented in Refs. [43, 44]. Here large logarithms arise mainly due to the exchange of massive gauge bosons between external legs if kinematic invariants are much larger than the gauge-boson mass. Some applications to simple processes can be found in Refs. [53–55].

The high energy scale is given by the energy scale of the process, which is much larger than the EW scale if large EW Sudakov logarithms appear. Similar to the QCD case, the high-scale quantities are most easily calculated with the low scales set to zero. Setting all low scales, i.e. the gauge-boson, top-quark, and Higgs-boson masses, to zero implies that this is done in the symmetric phase of the Standard Model (SySM). Note that the ratios of the masses have to be kept constant to compute the matching corrections. For instance, setting the top-quark mass and the W-boson mass to zero while keeping the ratio constant yields a constant Yukawa

coupling in the SySM:

$$g_t = \frac{g_2 m_t}{\sqrt{2} M_W} \quad (3.92)$$

In turn, the low scale μ_1 is given by the EW scale which we identify with the W-boson mass M_W . Though, for simplicity we assume all EW mass scales to be of the same order of magnitude in the calculation of the running:

$$\mu_1 = M_W \approx M_Z \approx m_t \approx M_H. \quad (3.93)$$

This is certainly justified, as in the Sudakov region the ratios between the several masses are small compared to their ratios to the kinematic invariants in the Sudakov region:

$$\frac{M_W^2}{m_t^2} \gg \frac{M_W^2}{s}. \quad (3.94)$$

Assuming (3.93) implies that logarithms like $\log M_W^2/m_t^2$ are treated perturbatively and are not resummed to all orders. However, this does not mean that they are neglected. All finite terms of the type $\log(M_\alpha^2/M_\beta^2)$, with $\alpha, \beta \in \{W, Z, H, t\}$ are indeed perturbatively taken into account in the high-scale matching coefficients and the operator matrix elements.

Guided by the considerations of the previous section, we can conclude a strategy for the calculation:

- Write down the relevant SCET operators in the EWSM. For the matching computation the low scales are conveniently set to zero. The operators and Wilson coefficients are thus computed in the unbroken phase of the theory. Calculate the matching to the SySM at the scale of the large kinematic invariant s , just like in the QCD case.
- Calculate the running of the operators down to the symmetry-breaking scale. The anomalous dimension of the operators is precisely given by (3.83) because it is calculated in the unbroken phase. In addition, there are contributions from scalars which, however, do not affect the form of (3.78) and (3.83), but merely change the β -function coefficients, which enter the one-particle contributions via the γ_i .
- Calculate the one-loop corrections to the operator matrix elements in SCET with massive gauge bosons. These can be obtained using the same Feynman rules as in the massless case, but some integrals require additional regularisation techniques described in Sec. 3.3.3. Beside the treatment of the longitudinal gauge boson degrees of freedom, this is the only part that is actually different from the massless case. In the case of the EWSM, the corrections to the low scale operators also contain IR singularities due to photon exchange.

We presented the treatment of n -jet scattering amplitudes in SCET in Sec. 3.2.6. In the following we discuss in a bit more detail the construction and the structure of radiative corrections to the corresponding SCET_{EW} objects.

Factorised matrix element and Wilson coefficients

The factorised form of the matrix element obtained in QCD can directly be transferred to the EW case:

$$\mathcal{M}_j = C_i(\mu_h) \hat{\mathcal{P}} \exp \left[- \int_{\mu_1}^{\mu_h} d \log \mu \gamma(\mu) \right]_{ij} \langle \mathcal{O}_j(\mu_1) \rangle, \quad (3.95)$$

where, compared to (3.69), we merely re-introduced the low-scale contribution $\langle \mathcal{O}_j(\mu_1) \rangle$ instead of the jet and soft functions. The two scales are defined via

$$\mu_1 = \mathcal{O}(M_{W/Z}), \quad \mu_h \gg M_{W/Z}. \quad (3.96)$$

Essentially the Wilson coefficients $C(\mu_h)$ and the anomalous dimension γ are calculated precisely as in the QCD case, while the low-scale corrections contained in $\langle \mathcal{O}_j \rangle$ are specific to the EW case.

We saw that the Wilson coefficients are obtained from (3.75). As already indicated in this formula, all low scales, i.e. the EW mass scales, are set to zero. The main differences between the QCD and the EW are:

- The longitudinal degrees of freedom of the weak gauge bosons, which are not present in the unbroken phase have to be consistently related to the would-be Goldstone bosons (see Sec. 3.3.1).
- The computation of “ n -jet amplitudes” in the EW case, i.e. scattering amplitudes with a well-defined number of electroweakly interacting particles, can be computed in perturbation theory. Since the EW gauge bosons have a mass, this introduces a few computational complications associated with the collinear anomaly, compared to the massless case. These aspects are described in Secs. 3.3.2, 3.3.3.
- There are more β -functions than in the QCD case with a more complicated structure, due to the mixing of the several coupling constants. This affects the integration of the anomalous dimension, which is described in Sec. 3.3.4.
- The low-scale corrections are completely perturbative. However, due to the photon exchange they are IR divergent and the matching conditions have to be defined such that there is an exact cancellation between the real and virtual corrections. This is described in Sec. 3.3.5.

3.3.1. Treatment of longitudinally polarised gauge bosons

In the unbroken phase of the theory, where the Wilson coefficients and the anomalous dimension are computed, gauge bosons are massless and hence always transversely polarised, while in the low-energy theory with massive gauge bosons longitudinal degrees of freedom are present. These degrees of freedom can however be identified with those of the scalar would-be Goldstone bosons in the symmetric phase, which is reflected in the Goldstone-Boson equivalence theorem (GBET),

which in terms of on-shell matrix elements reads [127–130, 143]

$$\begin{aligned}
 \mathcal{M}^{\phi_1 \dots \hat{W}_L^\pm \dots \phi_n} &= \pm \left(1 - \frac{\Sigma_L^{WW}(M_W^2)}{M_W^2} - \frac{\Sigma^{W\phi}(M_W^2)}{M_W} + \frac{1}{2} \delta Z_W + \frac{\delta M_W}{M_W} \right) \mathcal{M}^{\phi_1 \dots \phi^\pm \dots \phi_n} \\
 &\quad + \mathcal{O}(\alpha^2) + \mathcal{O}\left(\frac{M_W}{E}\right), \\
 \mathcal{M}^{\phi_1 \dots \hat{Z}_L \dots \phi_n} &= i \left(1 - \frac{\Sigma_L^{ZZ}(M_Z^2)}{M_Z^2} + i \frac{\Sigma^{Z\chi}(M_Z^2)}{M_Z} + \frac{1}{2} \delta Z_{ZZ} + \frac{\delta M_Z}{M_Z} \right) \mathcal{M}^{\phi_1 \dots \chi \dots \phi_n} \\
 &\quad + \mathcal{O}(\alpha^2) + \mathcal{O}\left(\frac{M_Z}{E}\right), \tag{3.97}
 \end{aligned}$$

with E being the boson's energy. As indicated by the hats, we assume the gauge-boson field on the l.h.s. to be renormalised, which introduces the field-renormalisation constants on the r.h.s. The Goldstone-boson fields are kept unrenormalised ($\delta Z_{\phi/\chi} = 0$) by convention.

The Wilson coefficients and the anomalous dimension for a process involving longitudinally polarised gauge bosons can therefore be obtained from the respective quantities with the gauge bosons replaced by the corresponding would-be Goldstone bosons.

3.3.2. n -particle operators and Wilson lines

In this section we describe the generalisation of the treatment of n -jet scattering amplitudes of Sec. 3.2.6 to the Standard model.

As already mentioned in Secs. 3.2.4–3.2.6, by means of Wilson lines one can construct gauge invariant external operators

$$\mathcal{O} = W_{n_1}^\dagger \xi_1 \dots W_{n_n}^\dagger \xi_n, \tag{3.98}$$

containing p_i -collinear fermion fields ξ_i and a Wilson line in p_i -direction. We picked an n -fermion operator for definiteness. While in the QCD case the fermions are restricted to quarks, in SCET_{EW} the ξ field may represent any SM fermion.

The definition of a Wilson line has been given in (3.58). The generalisation to the EW gauge group $SU(2) \times U(1)$ can be written as

$$W_{n_1}(x) = \sum_{\text{perms}} \exp \left(- \sum_k g_k \frac{1}{\bar{n} \cdot \mathcal{P}} \bar{n} \cdot A_{c,p_1,(k)}^a(x) \mathbf{T}^a \right). \tag{3.99}$$

with $\hat{\mathcal{P}}$ denoting path ordering and \mathbf{T}^a generic generators of the symmetry group. The fact that in (3.98) each collinear field comes with a single Wilson line along its momentum direction is not trivial, in particular in a theory with massive gauge bosons. The Wilson line arises from hard interactions that have been integrated out in the EFT. Schematically the included interactions associated with the radiation of n_1 -collinear gauge bosons off any line other than 1 can be

sketched as follows (we consider $n = 4$ for simplicity):

$$\begin{array}{c}
 \text{Diagram 1} \\
 \text{Diagram 2} \\
 \text{Diagram 3} \\
 \dots
 \end{array}
 = \text{Diagram 4}
 \quad (3.100)$$

with the dots representing diagrams with zero, two, or more than two p_1 -collinear gauge bosons radiated, the dashed lines represent external collinear particles, and the curly lines n_1 -collinear gluons. If the loop gauge boson exchanged between particle 1 and k is p_1 -collinear, particle k becomes far off shell (indicated by a double line) and is integrated out in SCET_{EW}. The vertex on the r.h.s. contains an n_1 -collinear Wilson line and its Feynman rules are given by (3.59), (3.60). Treating the other collinear directions in an analogous way leads to (3.98).

The reasoning behind (3.100) is that the additional gauge boson factorises from the matrix element according to

$$\text{Vertex with } j \text{ radiating} = g \frac{n_j \cdot \varepsilon}{n_j \cdot k} \mathbf{T}_j \times \text{Vertex without } j \text{ radiating}
 \quad (3.101)$$

in the high-energy limit, with k and ε being the momentum and polarisation vector of the radiated boson. If both k and ε are n_i -collinear, the overall factor in (3.101) can be written as

$$g \frac{p_j \cdot \varepsilon}{p_j \cdot k} \mathbf{T}_j = g \frac{n_j \cdot \varepsilon}{n_j \cdot k} \mathbf{T}_j = g \frac{(n_i \cdot n_j)(\bar{n}_i \cdot \varepsilon)}{(n_i \cdot n_j)(\bar{n}_i \cdot k)} \mathbf{T}_j + \mathcal{O}(\lambda) = g \frac{\bar{n}_i \cdot \varepsilon}{\bar{n}_i \cdot k} \mathbf{T}_j + \mathcal{O}(\lambda)
 \quad (3.102)$$

where the j -dependence is now only in the generator. What happens in the above calculation is that both numerator and denominator are first expressed in terms of light-cone coordinates of n_j using that p_j is j -collinear. The p_j dependence then cancels. Afterwards both quantities are expressed in terms of the light-cone coordinates with reference vector n_i . Because both k and ε are n_i -collinear (recall that the collinear gluon field scales like its momentum, cf. Eq. (3.18)), the dependence on j cancels completely from the prefactor in front of the colour operator. Conservation of colour can be used to write

$$\sum_{j \neq i} \frac{n_j \cdot \varepsilon}{n_j \cdot k} \mathbf{T}_j \times \mathcal{M} = -\frac{\bar{n}_i \cdot \varepsilon}{\bar{n}_i \cdot k} \mathbf{T}_i \times \mathcal{M},
 \quad (3.103)$$

which yields the one-loop term of the Wilson line (3.99). This can be iterated for terms involving more than one gauge boson, so that at leading power all p_i -collinear emissions are combined in a single Wilson line in n_i direction, which is then contained in the effective vertex.

All above considerations hold for both massive and massless gauge-boson radiation. When calculating radiative corrections to operators of the form (3.98), one would expect an equation

like

$$\text{Diagram 1} + \text{Diagram 2} + \text{Diagram 3} = \text{Diagram 4} \quad (3.104)$$

to hold, with the l.h.s. graphs are evaluated in the SySM (using the method of regions) and the r.h.s. graph in SCET_{EW}. In the massless case, this turns out to be true. However, if the exchange of massive gauge bosons is examined beyond tree level, the collinear anomaly potentially spoils the validity of (3.104).

3.3.3. Collinear anomaly

While the basic concepts of SCET can also be applied to a spontaneously broken gauge theory, some technical complications arise due to the collinear or factorisation anomaly [37, 167]. In contrast to the Wilson coefficients and the anomalous dimension, which can be inferred from the QCD results, the low-scale corrections require the explicit computation of the UV-finite parts of the SCET_{EW}-integrals. In the following we demonstrate the regularisation mechanism of the Δ -regulator by means of the fermion jet function, which is also computed in Ref. [46]. However, the bosonic case is very similar. Both calculations are given in more detail in App. B. A single collinear graph arising from a gauge boson with mass M coupling to a fermion with coupling constant g gives rise the following integral (all loop momenta are n_i collinear):

$$\text{Diagram} \rightarrow I_{\text{coll}} = -2ig^2\mu^{4-D} \int \frac{d^D k}{(2\pi)^D} \frac{2p_i^- - k^-}{(\bar{n}_i \cdot k)(k^2 - M^2)(k^+ p_i^- - m_i^2 - i0)}. \quad (3.105)$$

For $M = 0$ the QCD result is obtained. In Ref. [46] and in more detail in App. B, it is shown that after performing the integrations over k^+ and \mathbf{k}_\perp , the loop integral I_{coll} in (3.105) leads to a divergent integral of the form

$$I_{\text{coll}} = -\frac{\alpha}{2\pi}(\mu^2)^\varepsilon \Gamma(\varepsilon) \int_0^1 dz \frac{1-z}{z} [M^2(1-z) - m_i^2 z(1-z)]^{-\varepsilon}, \quad (3.106)$$

which is ill-defined owing to the region $z \rightarrow 0$ also if $D \neq 4$. Of course for a given observable the sum of all SCET_{EW} graphs has to be finite, as explicitly shown in Ref. [46] for the Sudakov form factor by directly putting all integrands together. This is, however, only feasible if the number of diagrams is very small and the diagrams themselves are not too complicated. It is much more convenient to evaluate each diagram separately, which requires an additional regularisation of integrals of the type (3.105) on top of DimReg. The regulator has to cancel when the several collinear and soft graphs are summed up. One possibility is the Δ -regulator discussed in the following.

Δ -regularisation and zero-bin subtraction

The Δ -regulator, which regulates the divergences associated with the collinear anomaly, corresponds to a mass shift of internal propagators,

$$\frac{1}{(p_i + k)^2 - m_i^2} \rightarrow \frac{1}{(p_i + k)^2 - m_i^2 - \Delta_i}, \quad (3.107)$$

while keeping the on-shell conditions $p_i^2 = m_i^2$ unchanged. Note that the regularisation also has to be applied to the double-line propagators in (3.100)/(3.104), which modifies the factorisation formulae (3.101)/(3.102). In particular, the last propagator denominator in (3.102) is modified according to

$$\frac{1}{\bar{n}_i \cdot k} \rightarrow \frac{1}{\bar{n}_i \cdot k - \delta_{i,n_j}} \quad (3.108)$$

with δ_{i,n_j} defined as

$$\delta_{i,n_j} = \frac{2\Delta_i}{(n_i \cdot n_j)(\bar{n}_i \cdot p_i)} \quad (3.109)$$

with a reference vector n_j , which corresponds to a collinear direction of a particle $j \neq i$. Therefore, the colour identity (3.103) can not be applied anymore, which puts up the question, whether the form of the operators (3.98) is still adequate at the one-loop level. However, it turns out that after zero-bin subtraction the dependence of the loop corrections on the r.h.s. of (3.104) on the regulator direction n_j drops out. This way using an operator with a single Wilson line for each direction is justified a posteriori.

Returning to the divergent integral (3.105), we recognise that it is regulated by the δ_{i,n_j} in the eikonal factor in (3.108): After taking the limit $\Delta_i \rightarrow 0$ one obtains for the regulated j -collinear integral

$$\begin{aligned} \lim_{\Delta_i \rightarrow 0} I_{\text{coll}} &= -\frac{\alpha}{2\pi} \Gamma(\varepsilon) \left(\frac{\mu^2}{M^2} \right)^\varepsilon \int_0^1 dz \frac{1-z}{z + \delta_{i,n_j}/p_i^-} [M^2(1-z) - m_i^2 z(1-z)]^{-\varepsilon} \\ &= \frac{\alpha}{4\pi} \Gamma(1+\varepsilon) \left(\frac{\mu^2}{M^2} \right)^\varepsilon \frac{2}{\varepsilon} \log \frac{\delta_{i,n_j}}{p_i^-} + \text{finite}, \end{aligned} \quad (3.110)$$

with the finite parts depending on the internal spins and masses. Note that “finite” refers only to the expansion in the Δ -regulator and does not mean “UV-finite”.

While rendering the collinear integral finite, introducing the regulator in the denominator of the Wilson-line propagator leads to a violation of the identity sketched in (3.104) because the respective factors on the l.h.s. of (3.103) have different denominators and the colour operators can not be added to obtain the one-loop expansion of the Wilson line. This implies that the SCET_{EW} graph on the r.h.s. of (3.104) can not be sufficient for the matching computation. Furthermore, it should be noted that the regulated collinear integral now depends on the arbitrary direction n_j via the regulator δ_{i,n_j} .

Both these issues are resolved after *zero-bin subtraction*: Because the soft-collinear region (the region where k is both soft and j -collinear) is contained in the soft and the collinear integral, it is double-counted when the diagrams are added. This double-counted contribution is usually

zero in DimReg, but the introduction of the Δ -regulator breaks this behaviour. Thus, one has to explicitly subtract the soft-collinear contribution, which is obtained by neglecting the loop momentum in the numerator in (3.105),

$$\begin{aligned} I_{\text{coll},\emptyset} &= -2ig^2\mu^{4-D} \int \frac{d^D k}{(2\pi)^D} \frac{1}{(\bar{n}_i \cdot k + \delta_{i,n_j})(k^2 - M^2)(n \cdot k - \Delta_i/p_i^- + i0)} \\ &= -\frac{\alpha}{4\pi} \Gamma(1 + \varepsilon) \left(\frac{\mu^2}{M^2} \right)^\varepsilon \frac{2}{\varepsilon} \log \frac{M^2 p_i^-}{\Delta_i \delta_{i,n_j}}, \end{aligned} \quad (3.111)$$

from each collinear integral.

The difference of both does not depend on the direction of n_j anymore:

$$I_{\text{coll}} - I_{\text{coll},\emptyset} = \frac{\alpha}{4\pi} \Gamma(1 + \varepsilon) \left(\frac{\mu^2}{M^2} \right)^\varepsilon \frac{2}{\varepsilon} \log \frac{M^2}{\Delta_i} + \text{finite}. \quad (3.112)$$

The essential point of the above calculation is that the j -dependence drops out of the i -collinear functions after zero-bin subtraction. Because the i -collinear functions depend only on i , the colour-conservation identity (3.103) may be used and the formulation in terms of a single Wilson is justified. As a consequence, the relation (3.104) is also respected if the graph on the r.h.s. is understood to be zero-bin subtracted.

This property is special for the Δ -regulator. Other regularisation schemes, such as analytic regularisation [33, 167], which avoid the necessity of zero-bin subtraction, in turn require the computation of all diagrams with n_1 -collinear gauge bosons exchanged between leg 1 and any other leg. A sample computation using this strategy, which is equivalent to compute the full SM graphs using the strategy of regions, can be found in Ref. [45]. In contrast, using the Δ -regulator one can calculate the n_i -collinear function (just as in the massless case) from a single diagram as in (3.105) with a single colour generator $\mathbf{T}_k^{(i)}$ regulated using an arbitrary reference vector n_j .

Nevertheless (3.112) still depends on the Δ_i -regulator, of which any final result must not depend. The dependence drops out if soft contributions are added, which vanish in DimReg without a regulator. After introducing the Δ -regulators, however, the soft contributions yield non-vanishing contributions of the form

$$I_s = -\frac{\alpha}{4\pi} \Gamma(1 + \varepsilon) \left(\frac{\mu^2}{M^2} \right)^\varepsilon \sum_i \frac{2}{\varepsilon} \log \frac{(\bar{n}_i \cdot p_i) M^2}{\Delta_i \mu} + \text{finite}, \quad (3.113)$$

such that the Δ_i -dependence cancels in the sum of collinear and soft contribution. Instead the sum contains logarithms of the form

$$\log \frac{\bar{n}_i \cdot p_i}{\mu}, \quad (3.114)$$

which become large in the high-energy limit. This imperfection in the factorisation of the energy scales (the high scales $\bar{n}_i \cdot p_i$ enter the low-scale corrections!) is referred to as the collinear or factorisation anomaly.

3.3.4. Anomalous dimensions and running couplings in the EWSM

The calculation of the SM anomalous dimension is not affected by the gauge-boson masses because it is solely obtained from the UV poles of the relevant SCET_{EW} graphs. The one-loop SCET_{EW} anomalous dimension can thus be written in the same way as in (3.83) in the SM with only the colour operators being adjusted from the SU(3) to the SU(2)×U(1) case:

$$\begin{aligned}\gamma &= \sum_{\langle ij \rangle} \sum_{k=1,2} \mathbf{T}_i^k \cdot \mathbf{T}_j^k \Gamma_{\text{cusp},k} \log \left(\frac{\mu^2}{-s_{ij} - i0} \right) + \sum_i \gamma_i, \\ &= \sum_{\langle ij \rangle} \left[\mathbf{T}_i^{\text{SU}(2)} \cdot \mathbf{T}_j^{\text{SU}(2)} \Gamma_{\text{cusp},2} + \frac{Y_i Y_j}{4} \Gamma_{\text{cusp},1} \mathbb{1} \right] \log \left(\frac{\mu^2}{-s_{ij} - i0} \right) + \sum_i \gamma_i.\end{aligned}\quad (3.115)$$

with the respective SU(2) and U(1)_Y cusp anomalous dimensions $\Gamma_{\text{cusp},k}$, which at one-loop read

$$\Gamma_{\text{cusp},k} = \frac{\alpha_k}{\pi}, \quad \alpha_k = \frac{g_k^2}{4\pi}.\quad (3.116)$$

In complete analogy to (3.83) the anomalous dimension in (3.115) can be decomposed

- into a soft part γ_S and a collinear part γ_C , as well as
- into a cusp part γ_{cusp} and a non-cusp part $\gamma_{\text{non-cusp}}$.

The definitions given in Tab. 3.1 apply without modification.

Running couplings

As seen above, the anomalous dimension is linear in $\log \mu$. If the running of the couplings is neglected, the integrated anomalous dimension can be written as (cf. (3.86))

$$\begin{aligned}- \int_{\mu_1}^{\mu_h} d \log \mu \gamma(\alpha_1(\mu), \alpha_2(\mu), \mu) &= \\ &= \left[-\frac{1}{2} \sum_i C_i \frac{\alpha}{\pi} \log \left(\frac{(\bar{n}_i \cdot p_i)^2}{\mu_h \mu_1} \right) \log \left(\frac{\mu_h}{\mu_1} \right) + \gamma_i \log \left(\frac{\mu_h}{\mu_1} \right) \right] \mathbb{1} \\ &\quad + \frac{\alpha}{\pi} \log \left(\frac{\mu_h}{\mu_1} \right) \sum_{\langle ij \rangle} \log \left(\frac{-n_i \cdot n_j}{2} - i0 \right) \mathbf{T}_i \cdot \mathbf{T}_j\end{aligned}\quad (3.117)$$

with the EW Casimir invariants C_i comprising the SU(2)×U(1) colour factors of each particle [19]:

$$C_i = \sum_{V_a=A,Z,W^\pm} I_i^{V_a} I_i^{\bar{V}_a} = \frac{1}{c_w^2} \frac{Y_i^2}{4} + \frac{C_i^{\text{SU}(2)}}{s_w^2}.\quad (3.118)$$

The accuracy of the calculation may be increased by taking the running of the EW gauge couplings g_1 and g_2 into account. The gauge couplings obey similar RGEs as the strong coupling g_s . However, if radiative corrections in the full SM are calculated, there is a mixing between

all (!) coupling constants, including the quartic Higgs self coupling λ and all Yukawa coupling constants. Schematically, this leads to the following RGEs for the EW gauge couplings [168]:

$$\begin{aligned}\frac{\partial g_1}{\partial \log \mu} &= -\beta_{0,1} \frac{g_1^3}{16\pi^2} - \sum_j \beta_{1j,1} \frac{g_j^2 g_1^3}{(16\pi^2)^2} + \mathcal{O}(g^7), \\ \frac{\partial g_2}{\partial \log \mu} &= -\beta_{0,2} \frac{g_2^3}{16\pi^2} - \sum_j \beta_{1j,2} \frac{g_j^2 g_2^3}{(16\pi^2)^2} + \mathcal{O}(g^7).\end{aligned}\quad (3.119)$$

Here j runs over all couplings SM couplings. Nevertheless, in practical applications only the largest Yukawa couplings are taken into account: results up to $\mathcal{O}(g^9)$ including the top-quark, bottom-quark, and τ Yukawa couplings have been published in Ref. [169]. The β -function coefficients have the one-loop values

$$\beta_{0,1} = -\frac{41}{6}, \quad \beta_{0,2} = \frac{19}{6}.\quad (3.120)$$

The one-loop running can be taken into account as in QCD, thus (3.91) holds for the EWSM with a sum over the running couplings:

$$\begin{aligned}\int_{\mu_1}^{\mu_h} d \log \mu \gamma(\alpha_1(\mu), \alpha_2(\mu), \mu) &= -f_0^{\text{EWSM}}(\alpha_1, \alpha_2) + \gamma_{\text{non-cusp}} \log \left(\frac{\mu_h}{\mu_1} \right) \\ &= -\frac{f_0^{\text{SU}(2)}(z_2)}{\alpha_2(\mu_h)} - \frac{f_0^{\text{U}(1)}(z_1)}{\alpha_1(\mu_h)} + \gamma_{\text{non-cusp}} \log \left(\frac{\mu_h}{\mu_1} \right),\end{aligned}\quad (3.121)$$

with

$$\begin{aligned}z_{1/2} &= \frac{\alpha_{1/2}(\mu)}{\alpha_{1/2}(\mu_h)}, \\ f_0^{\text{U}(1)}(z) &= \sum_i \frac{\pi Y_i^2}{\beta_{0,1/2}^2} \left(\log z + \frac{1}{z} - 1 \right), \\ f_0^{\text{SU}(2)}(z) &= \sum_i \frac{4\pi C_i^{\text{SU}(2)}}{\beta_{0,1/2}^2} \left(\log z + \frac{1}{z} - 1 \right).\end{aligned}\quad (3.122)$$

From the two-loop running on, however, the RGEs for α_1 and α_2 are coupled, one can therefore not analytically perform the integration in (3.121).

3.3.5. Collinear and soft functions, low-scale corrections and IR divergences

In SCET the parts sensitive to the collinear and soft scales are the jet (or collinear) and soft functions, respectively. The precise definition of what a collinear and a soft function is depends on the observable under consideration (recall that SCET is often applied to jet observables or to differential cross sections in a specific phase-space region).

In SCET_{EW} the collinear and soft functions are obtained from the SCET_{EW} loop graphs with the EW mass scales $M_{W/Z/H/t}$ kept finite and the renormalisation scale set to the low scale μ_1 . In contrast to the anomalous dimension, which can be calculated in the symmetric phase of the EWSM, the low-scale graphs have to be evaluated in the mass eigenbasis. A set of sample

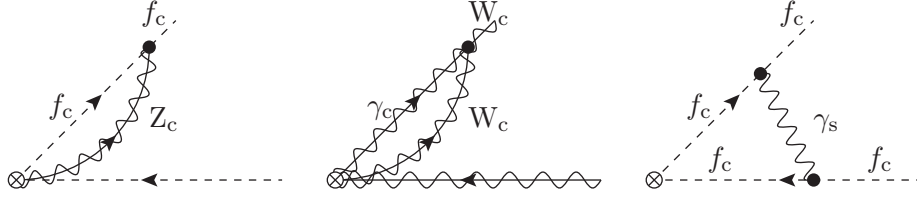


Figure 3.3.: Sample diagrams contributing to the low-scale corrections in SCET_{EW} . In the collinear graphs (first and second one) the lower line enters only via the reference direction in (3.108), (3.109). All other lines are not shown for compactness.

diagrams is displayed in Fig. 3.3. There are also collinear wavefunction-correction graphs, which remain unchanged with respect to the full SM.

The diagrams in Fig. 3.3 have similar properties as the example graph given in (3.105). Calculating these diagrams thus requires the regularisation techniques described in the previous section. The computation of all diagrams relevant for the SM is given in App. B.

The one-loop results for these diagrams have first been presented in Ref. [45] for external fermions, and in Ref. [48] for all SM particles. Since these graphs have a non-trivial $\text{SU}(2) \times \text{U}(1)$ -colour flow, they must be written as a matrices in the space of operators.

$$\langle 0 | \mathcal{O}_i^{1\text{-loop}} | p_1, \dots, p_n \rangle_{\text{SCET}_{\text{EW}}} = \mathbf{D}_{ij}^{(1)} \langle 0 | \mathcal{O}_j^{\text{tree}} | p_1, \dots, p_n \rangle_{\text{SCET}_{\text{EW}}}. \quad (3.123)$$

In our approach, the results of Refs. [47, 48] are supplemented by the IR divergent photon contributions proportional to $Q_i Q_j$.

The IR poles are not present in the literature because previous results are based on a formalism, in which the SCET_{EW} results are matched onto a version of SCET with W, Z, Higgs bosons and top quark integrated out [45, 47, 48]. The theory is called SCET_γ and can be used to resum large logarithms between the EW scale and a possibly much smaller factorisation scale. In SCET_γ both the top quark and the W boson are treated as boosted heavy quarks coupling to soft photons and gluons.

Because we identify the IR scale with the EW scale ($\mu_{\text{IR}} = \mu_1 = M_W$), we have no need to consider running effects below μ_1 . Instead we can simply add the UV-finite parts of the SCET_γ loop corrections to the IR-finite SCET_{EW} low-scale corrections to obtain both the IR-finite (SCET_{EW}) and IR-divergent (SCET_γ) contributions. The SCET_γ loop graphs contain the IR poles, but no additional finite corrections.

Since the low-scale corrections are obtained from the same diagrams as the anomalous dimension, they have very similar properties: The group-theoretical structure of the operator matrix elements can also be written in terms of one-particle (“collinear”) and two-particle (“soft”) contributions. While the soft low-scale corrections have a universal form in the colour-space formalism, the collinear low-scale corrections $D_{C,i}$ depend on the spin of particle i . The computation of the relevant integrals and all results can be found in App. B.3. One property we mention here is that for all external particles the correction factors contain logarithmic contributions of

the form

$$D_{C,i}^{\text{weak}} \sim \log \frac{\bar{n}_i \cdot p_i}{\mu_1} \log \frac{M_{W/Z}^2}{\mu_1^2} + \dots \quad (3.124)$$

in the weak part and of the form

$$D_{C,i}^{\gamma} \sim \log \frac{\bar{n}_i \cdot p_i}{\mu_1} \log \frac{\mu_{\text{IR}}^2}{\mu_1^2} + \dots \quad (3.125)$$

in the photonic part. Recalling that $\bar{n}_i \cdot p_i$ is the large component of p_i , the expressions above are logarithmically enhanced in the high-energy limit.

4. Fixed-order perturbation theory: Some important methods

In this chapter we review some techniques related to the calculation of radiative corrections using fixed-order perturbation theory. All of them are very well established for a long time. We keep the discussions short and constrain ourselves to some important formulas. The first section, Sec. 4.1, is dedicated to a discussion of the Catani–Seymour subtraction algorithm, which we use to treat IR singularities. In Sec. 4.2 we review two useful techniques to deal with phase-space singularities arising from virtual unstable particles.

4.1. Catani–Seymour subtraction

The numerical evaluation of cross sections in quantum field theory requires the disentanglement of the IR divergences that both real and virtual corrections suffer from: While the virtuals contain loop integrals diverging in the limit of vanishing loop momentum on massless propagators, $k \rightarrow 0$, or a massless loop momentum parallel to an external leg, $k \parallel p_{\text{ext}}$, the real corrections develop singularities in the integration over phase-space regions associated with soft or collinear radiation and both divergences cancel exactly in physical observables according to the Kinoshita–Lee–Nauenberg (KLN) theorem [170, 171].

Combining the two is, however, not straightforwardly possible because the two contributions are defined on different phase spaces:

$$\sigma = \int_n d\sigma_{\text{Born}} + \int_n d\sigma_{\text{virt}} + \int_{n+1} d\sigma_{\text{real}} \quad (4.1)$$

for a $2 \rightarrow n$ process, where the abbreviation

$$\int_n \equiv \int d\Phi_{\text{LIPS}}^{(n)} \quad (4.2)$$

has been introduced. Here $d\Phi_{\text{LIPS}}^{(n)}$ denotes the usual n -particle Lorentz-invariant phase-space measure. A subtraction algorithm solves this issue by introducing a local counterterm $d\sigma^{\text{sub}}$, that subtracts the IR divergent parts of the real corrections in all regions of phase space. If the counterterm can be integrated over a suitable one-particle phase space analytically, the result can be added to the virtual corrections:

$$\sigma = \int_n d\sigma_{\text{Born}} + \int_n \left(d\sigma_{\text{virt}} + \int_1 d\sigma_{\text{sub}} \right) + \int_{n+1} (d\sigma_{\text{real}} - d\sigma_{\text{sub}}) \quad (4.3)$$

In total, by introducing the subtraction term we added 0 to the total cross section and both the second and the third term in (4.3) can be integrated numerically. The subtraction term is only determined up to non-singular contributions and several implementations of the basic

idea have been proposed, including antenna subtraction [172, 173], q_T -subtractions [174], and FKS subtraction [175]. We use a version introduced by Catani and Seymour [176] for the case of massless QCD-based dipole terms. It has been extended to QED [177, 178] and QCD with massive partons [179]. While being the most frequently used subtraction method for fixed-order calculations at NLO due to its simplicity, the former methods have been successful when considering NNLO corrections (q_T , antennas) or parton-shower matching (FKS).

Within the dipole subtraction, the IR-singular behaviour is parameterised in terms of three-particle splitting functions g_{ijk} . The associated splitting processes involve the radiation of a massless (or very light) particle, the emissus, off an emitter particle in the presence of a spectator particle, which is necessary to assure momentum conservation. The soft region is given by the limit of zero emissus momentum, while the collinear limit is obtained if the emitter's and emissus' momenta are parallel. The structure of the counterterms depends, however, on whether the emitter and spectator are in the initial (IS) or final state (FS), respectively. In the following we give the results for the QED case, sticking to the case of photon emission off massless fermions:

$$f \rightarrow \gamma f, \quad \bar{f} \rightarrow \gamma \bar{f} \quad (4.4)$$

By default we use DimReg to regulate the IR divergences. In the following we collect some important results for the above cases, including explicit expressions for the subtraction dipoles as well as their integrated counterparts. The latter requires the integration over the one-particle phase space, which brings up some technical challenges: On the one hand the IR singularities have to be worked out analytically, which can be quite cumbersome. On the other hand the final n -particle phase-space integration may still contain integrable singularities, which should be avoided in order to obtain a reasonably stable integration. To this end one introduces the plus distribution, defined via

$$\begin{aligned} \int_0^1 dx [f(x)]_+ g(x) &= \int_0^1 dx f(x)(g(x) - g(1)), \\ \Rightarrow \int_0^1 dx f(x)g(x) &= \int_0^1 dx [f(x)]_+ g(x) + g(1) \int_0^1 dx f(x) \end{aligned} \quad (4.5)$$

for f singular as $x \rightarrow 1$ and a regular test function g . This distribution is used to split off the soft-collinear endpoint contributions, for a more intensive discussion see for instance [180]. In the following we collect the results for the occurring dipole terms. The total subtraction term $d\sigma_{\text{sub}}$ is obtained as the sum over all possible emitter-spectator pairs.

FS emitter and FS spectator

We consider the case of a pair of emitter i and spectator j both in the final state (FS). The splitting kernel reads

$$g_{ij}(p_i, p_j, p') = \frac{1}{p_i p' (1-y)} \left(\frac{2}{1-z(1-y)} - 1 - z \right) \quad (4.6)$$

with

$$y = \frac{p_i p'}{p_i p_j + p_i p' + p_j p'}, \quad z = \frac{p_i p'}{p_i p_j + p_j p'}. \quad (4.7)$$

The integrated subtraction term is

$$\int_1 \int_n d\sigma_{\text{sub}}^{ij} = -\frac{\alpha}{2\pi} Q_i \sigma_i Q_j \sigma_j \int d\sigma^{\text{LO,red}}(\tilde{p}_i, \tilde{p}_j) \int_0^1 dz \left(G_{ij}(P_{ij}^2) \delta(1-z) + [\mathcal{G}_{ij}(P_{ij}^2, z)]_+ \right) \quad (4.8)$$

with the reduced Born cross section $d\sigma^{\text{LO,red}}$ and the integrated splitting functions G_{ij} , \mathcal{G}_{ij} . The former is obtained from recombining emitter and missus, while rescaling the spectator and keeping emitter and spectator on-shell. This is achieved by the replacements $p_i \rightarrow \tilde{p}_i$, $p_j \rightarrow \tilde{p}_j$, with

$$\tilde{p}_i^\mu = p_i^\mu + p'^\mu - \frac{y}{1-y} p_j^\mu, \quad \tilde{p}_j^\mu = \frac{1}{1-y} p_j^\mu. \quad (4.9)$$

The sign factors σ_i in (4.8) take the values

$$\begin{aligned} \sigma_i &= +1 \text{ for incoming particles and outgoing antiparticles,} \\ \sigma_i &= -1 \text{ for incoming antiparticles and outgoing particles.} \end{aligned} \quad (4.10)$$

The integrated splitting functions are obtained from the fermion–fermion Altarelli–Parisi splitting kernel,

$$\hat{P}_{ff}(z) = \frac{1+z^2}{1-z} \quad (4.11)$$

and read

$$\begin{aligned} \mathcal{G}_{ij}(P_{ij}^2, z) &= \hat{P}_{ff}(z) \left(-\frac{(4\pi)^\varepsilon}{\varepsilon \Gamma(1-\varepsilon)} + \log \left(\frac{P_{ij}^2}{\mu_{\text{IR}}^2} \right) + \log z + 2 \log(1-z) \right) \\ &\quad + (1+z) \log(1-z) + 1-z, \\ G_{ij}(P_{ij}^2) &= \frac{(4\pi)^\varepsilon}{\Gamma(1+\varepsilon)} \left(\frac{1}{\varepsilon^2} + \frac{3}{2\varepsilon} + \frac{1}{\varepsilon} \log \left(\frac{\mu_{\text{IR}}^2}{P_{ij}^2} \right) \right) \\ &\quad + \frac{1}{2} \log^2 \left(\frac{P_{ij}^2}{\mu_{\text{IR}}^2} \right) + \frac{3}{2} \log \left(\frac{\mu_{\text{IR}}^2}{P_{ij}^2} \right) - \frac{\pi^2}{6} + \frac{7}{2}. \end{aligned} \quad (4.12)$$

Given these ingredients, the numerical evaluation of (4.8) is straightforward. It is, however, important to consistently apply the phase-space cuts: A cut which, for instance, acts on the momentum of the emitter-particle i , should be reflected in the reduced Born as a cut on the phase-space variable \tilde{p}_i .

IS emitter and FS spectator

For the emission of a photon off an initial-state (IS) fermion a in the presence of a spectator j ¹ the subtraction term reads

$$g_{ai}(p_a, p_i, p') = \frac{1}{(p_a p') x} \left(\frac{2}{2-x-z} - 1 - x \right). \quad (4.13)$$

¹Conventionally initial-state particles are labelled with a, b, \dots and final-state particles with i, j, \dots

with the splitting variables

$$x = \frac{p_a p_i + p_a p' - p_i p'}{p_a p_i}, \quad z = \frac{p_a p_i}{p_a p_i + p_a p'}. \quad (4.14)$$

In terms of those, the integrated subtraction part reads

$$\int_1 \int_n d\sigma_{\text{sub}}^{ai} = -\frac{\alpha}{2\pi} Q_i \sigma_i Q_a \sigma_a \int d\sigma^{\text{LO,red}}(\tilde{p}_i, \tilde{p}_a) \int_0^1 dx \left(G_{ai}(P_{ai}^2) \delta(1-x) + [\mathcal{G}_{ai}(P_{ai}^2, x)]_+ \right) \quad (4.15)$$

with the redefined momenta

$$\tilde{p}_i^\mu = p_i^\mu + p'^\mu - (1-x)p_a^\mu, \quad \tilde{p}_a^\mu = x p_a^\mu, \quad (4.16)$$

The variable x can thus be interpreted as the momentum fraction the emitter carries before the splitting. The integrated splitting kernels read

$$\begin{aligned} \mathcal{G}_{ai}(P_{ai}^2, x) &= \hat{P}_{ff}(x) \left(-\frac{(4\pi)^\varepsilon}{\varepsilon \Gamma(1+\varepsilon)} + \log \left(\frac{-P_{ai}^2}{\mu_{\text{IR}}^2} \right) - \log x - 1 \right) \\ &\quad - \frac{2 \log(2-x)}{1-x} + (1+x) \log(1-x) + 1 - x, \\ G_{ai}(P_{ai}^2, x) &= \frac{(4\pi)^\varepsilon}{\Gamma(1+\varepsilon)} \left(\frac{1}{\varepsilon^2} + \frac{3}{2\varepsilon} + \frac{1}{\varepsilon} \log \left(\frac{\mu_{\text{IR}}^2}{-P_{ai}^2} \right) \right) \\ &\quad + \frac{1}{2} \log^2 \left(\frac{-P_{ai}^2}{\mu_{\text{IR}}^2} \right) + \frac{3}{2} \log \left(\frac{\mu_{\text{IR}}^2}{-P_{ai}^2} \right) + \frac{\pi^2}{3} + 1. \end{aligned} \quad (4.17)$$

FS emitter and IS spectator

The subtraction term for the case of radiation off a final-state emitter with an initial-state spectator is

$$g_{ia}(p_a, p_i, p') = \frac{1}{p_a p' x} \left(\frac{2}{2-x-z} - 1 - z \right). \quad (4.18)$$

with x and z defined as in (4.14).

$$\begin{aligned} \int_1 \int_n d\sigma_{\text{sub}}^{ia} &= -\frac{\alpha}{2\pi} Q_i \sigma_i Q_a \sigma_a \int d\sigma^{\text{LO,red}}(\tilde{p}_i, \tilde{p}_a) \\ &\quad \times \int_0^1 dx \left(G_{ia}(P_{ia}^2) \delta(1-x) + [\mathcal{G}_{ia}(P_{ia}^2, x)]_+ \right) \end{aligned} \quad (4.19)$$

with \tilde{p}_i^μ and \tilde{p}_a^μ given by (4.16) and the integrated splitting functions

$$\begin{aligned}
 G_{ia}(P_{ia}^2, x) &= \frac{(4\pi)^\varepsilon}{\Gamma(1+\varepsilon)} \left(\frac{1}{\varepsilon^2} + \frac{3}{2\varepsilon} + \frac{1}{\varepsilon} \log \left(\frac{\mu_{\text{IR}}^2}{-P_{ia}^2} \right) \right), \\
 &\quad + \frac{1}{2} \log^2 \left(\frac{-P_{ia}^2}{\mu_{\text{IR}}^2} \right) + \frac{3}{2} \log \left(\frac{\mu_{\text{IR}}^2}{-P_{ia}^2} \right) - \frac{\pi^2}{3} + \frac{7}{2}, \\
 g_{ia}(P_{ia}^2, x) &= \frac{1}{1-x} \left(2 \log \frac{2-x}{1-x} - \frac{3}{2} \right).
 \end{aligned} \tag{4.20}$$

IS emitter and IS spectator

The last case concerns the constellation of both the emitter and spectator being in the initial state. The subtraction term reads

$$g_{ab}(p_a, p_b, p') = \frac{1}{p_a p' x} \left(\frac{2}{2-x} - 1 - x \right) \tag{4.21}$$

with

$$x = \frac{p_a p_b + p_a p' - p_b p'}{p_a p_b}. \tag{4.22}$$

The integration over the one-particle phase space yields

$$\begin{aligned}
 \int_1 \int_n d\sigma_{\text{sub}}^{ab} &= -\frac{\alpha}{2\pi} Q_a \sigma_a Q_b \sigma_b \int_0^1 dx \int d\sigma^{\text{LO,red}}(\tilde{p}_a, \tilde{p}_b) \\
 &\quad \times ([\mathcal{G}_{ab}(s, x)]_+ + G_{ab}(s) \delta(1-x))
 \end{aligned} \tag{4.23}$$

with the new initial momenta for the reduced matrix element

$$\tilde{p}_a^\mu = x p_a^\mu, \quad \tilde{p}_b^\mu = p_b^\mu \tag{4.24}$$

and the integrated subtraction terms

$$\begin{aligned}
 \mathcal{G}_{ab}(s, x) &= P_{ff}(x) \left(-\frac{(4\pi)^\varepsilon}{\varepsilon \Gamma(1-\varepsilon)} + \log \frac{s}{\mu^2} + 2 \log(1-x) \right) + 1 - x, \\
 G_{ab}(s) &= -\frac{(4\pi)^\varepsilon}{\Gamma(1+\varepsilon)} \left(\frac{1}{\varepsilon^2} + \frac{3}{2\varepsilon} + \frac{1}{\varepsilon} \log \left(\frac{\mu_{\text{IR}}^2}{s} \right) \right), \\
 &\quad + \frac{1}{2} \log^2 \left(\frac{-P_{ai}^2}{\mu_{\text{IR}}^2} \right) + \frac{3}{2} \log \left(\frac{\mu_{\text{IR}}^2}{s} \right) + \frac{\pi^2}{3} + 4.
 \end{aligned} \tag{4.25}$$

We write $s = P_{ab}^2$ because the invariant of the momenta p_a, p_b can be interpreted as their centre-of-mass energy.

4.2. Treatment of unstable particles

The analytical or numerical calculation of processes involving virtual massive particles requires dealing with the phase-space singularities arising when the virtual particles are exactly on shell.

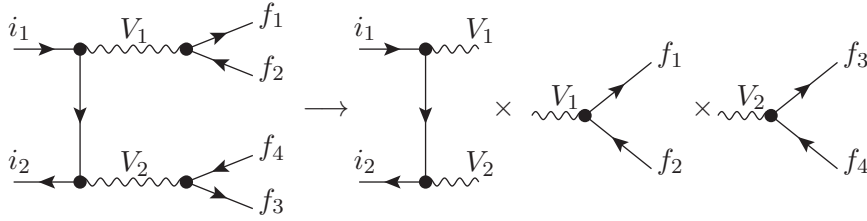


Figure 4.1.: Factorisation of the matrix element in the pole approximation. The diagram on the l.h.s. and the first diagram on the r.h.s. are understood to represent the set of all tree-level diagrams.

The propagator of the particle behaves like

$$\frac{1}{k^2 - M^2}, \quad (4.26)$$

with k being the particle's momentum and M its mass. This obviously requires a regularisation technique, which usually employs the fact that such a particle is unstable. Denoting its width with Γ , a resummation of the self-energy insertions into the propagator can be achieved by the replacement

$$M^2 \rightarrow M^2 - i\Gamma M, \quad (4.27)$$

which regularises the pole in (4.26). However, some care is required with respect to preserving gauge invariance. Several approaches are available, of which we are going to present two complementary ones in the following.

4.2.1. Double-pole approximation

In this section we discuss a widespread technique for the treatment of unstable particles in processes involving two resonances.² The basic idea of the double-pole approximation (DPA) [106, 182, 183] is to expand propagators of two vector bosons $V_{1/2}$ with off-shell momenta $k_{1/2}$ around the on-shell region. To this end, the external momenta such that the new virtual gauge-boson momenta $\tilde{k}_{1/2}$ fulfill the on-shell condition. At LO this corresponds to the replacement

$$\frac{N_1(k_1^2)}{k_1^2 - M_1^2 + i\Gamma_1 M_1} \frac{N_2(k_2^2)}{k_2^2 - M_2^2 + i\Gamma_2 M_2} \rightarrow \sum_{\lambda\lambda'} \frac{N_1^\lambda(\tilde{k}_1^2 = M_1^2)}{k_1^2 - M_1^2 + i\Gamma_1 M_1} \frac{N_2^{\lambda'}(\tilde{k}_2^2 = M_2^2)}{k_2^2 - M_2^2 + i\Gamma_2 M_2}. \quad (4.28)$$

with λ, λ' running over the internal helicity configurations and N_i denoting the numerators, which are non-singular in their on-shell behaviour. We introduced the polarisation sum in (4.28), because throughout this work we always consider matrix elements with bosons of definite internal

²It is of course also valid for only one resonance and has also been generalised to the case of more than two resonances [181]. However, since by far most applications involve not more than two resonances, we stick to this case.

polarisations. For the definition of a pole approximation alone, it is however not necessary to do so.

This procedure, sketched diagrammatically in Fig. 4.1, is manifestly gauge invariant because the on-shell numerators correspond to products of physical matrix elements: those of on-shell production and decay of the respective particles 1 and 2 in the respective helicity state,

$$N_i^\lambda(\tilde{k}_i^2) = \mathcal{M}_i^{\text{prod},\lambda}(\tilde{k}_i^2) \mathcal{M}_i^{\text{dec},\lambda}(\tilde{k}_i^2). \quad (4.29)$$

The DPA therefore achieves a factorisation of a matrix element into a production and a decay part.

Polarisation definition

The polarisation sum in (4.28) arises after decomposing the respective propagator numerators into polarisation vectors:

$$g^{\mu\nu} - \frac{\tilde{k}^\mu \tilde{k}^\nu}{M^2} = \sum_{\lambda=\pm 1,0} \varepsilon_\lambda^\mu(\tilde{k}) \varepsilon_\lambda^{*\nu}(\tilde{k}), \quad (4.30)$$

with the tildes indicating that this has to be performed after putting the momenta on shell. The above relation hold in the unitary gauge, arising from the 't Hooft–Feynman gauge in the limit $\xi_a \rightarrow \infty$, see the expression for the gauge-boson propagator (2.20). In this gauge the would-be Goldstone bosons decouple from the SM Lagrangian and the Feynman diagrams involving virtual would-be Goldstone bosons are absent.

It is clear that the polarisation of a massive particle is frame dependent. In a given frame the polarisation vectors of a massive gauge boson with helicity λ read

$$\begin{aligned} \varepsilon_{\lambda=-1}^\mu &= \frac{1}{\sqrt{2}}(0, \cos \theta \cos \phi + i \sin \phi, \cos \theta \sin \phi - i \cos \phi, -\sin \theta), \\ \varepsilon_{\lambda=+1}^\mu &= \frac{1}{\sqrt{2}}(0, -\cos \theta \cos \phi + i \sin \phi, -\cos \theta \sin \phi - i \cos \phi, \sin \theta), \\ \varepsilon_{\lambda=0}^\mu &= \frac{1}{M}(|\tilde{k}|, E \sin \theta \cos \phi, E \sin \theta \sin \phi, E \cos \theta), \end{aligned} \quad (4.31)$$

with θ and ϕ denoting the polar and azimuthal angles of the boson's three-momentum $|\tilde{k}|$ in that frame, respectively. We refer to the $\lambda = 0$ state as the longitudinal, the $\lambda = 1$ state as the left-handed transverse, and the $\lambda = -1$ state as the right-handed transverse polarisation state. Although there is a vast range of frames in principle, the following two choices appear most natural:

- the laboratory frame or the centre-of-mass (COM) frame of the incoming protons, and
- the partonic COM frame. For brevity we just refer to it as the COM frame.

The COM-frame definition of the polarisation has also been employed in recent experimental studies [86], but also laboratory-frame polarisation fractions have been considered [98]. Thus, some care is required when comparing different theoretical and experimental results. In the following we opt for the COM frame. This frame is more convenient for two reasons: On the one hand interference contributions have been found to be smaller here [134], but more importantly,

this definition implies that both bosons have high energies, which is crucial for applying the GBET.

The effects of virtual gauge-boson polarisations have first been studied in Refs. [131,184–186] at leading order. Previous NLO-accuracy studies on polarised diboson production processes can be found in Refs. [133–140]. The results have been incorporated into the event generator SHERPA [187]. NNLO QCD effects have also been studied in combination with polarisation effects [188]. The influence of the reference frame choice has been discussed in more detail in Ref. [132].

On-shell projection

The choice for the on-shell momenta \tilde{k}_i in terms of the off-shell momenta k_i is not unique. A widespread choice is to preserve the momentum sum of the two-particle system:

$$k_1 + k_2 = \tilde{k}_1 + \tilde{k}_2. \quad (4.32)$$

A drawback of this choice is the fact that all events with $\sqrt{s} < M_1 + M_2$ have to be discarded. This part of the phase space should, however, not contribute much to the cross section. Otherwise the DPA is not expected to be a good approximation, anyway.

Besides the resonance momenta, also the momenta of the decay products have to be changed to on-shell kinematics. Even after demanding (4.32), there is some freedom in how to exactly define this transformation. The precise choice of the on-shell momenta defines the on-shell projection. Usually it is constructed such that a convenient quantity is preserved under the transformation. In our application we use an on-shell projection introduced and described in more detail in Ref. [135]. It preserves the spatial direction of the decay products of the respective gauge boson in its rest frame.

To assure momentum conservation and the on-shell conditions, the vector-boson momenta are transformed as follows:

- The off-shell momenta are boosted into the two-boson rest frame.
- Their energies are rescaled to the on-shell values.
- The on-shell momenta are boosted back into the laboratory frame.

Afterwards the momenta of the decay products are treated in a similar way:

- The momenta of the decay products of the the off-shell (!) vector boson are boosted into its rest frame.
- The energies of the external particles are rescaled such that the on-shell condition is fulfilled for the vector boson.
- All momenta are boosted back along the on-shell (!) vector boson momentum.

This on-shell projection accounts for a relatively uniform deformation of the external momenta.

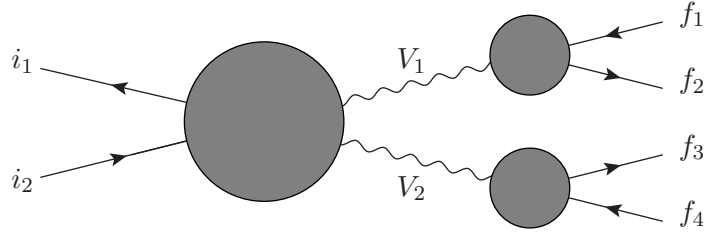


Figure 4.2.: Factorisable virtual corrections to processes with virtual unstable bosons. The blobs represent the sum of tree-level and one-loop graphs.

Factorisable and non-factorisable corrections

When considering loop correction in DPA, one has to distinguish between factorisable and non-factorisable corrections: the former arise from diagrams connecting either only the production or the decay subprocess (see Fig. 4.2), while the latter are obtained from photonic corrections that can not unambiguously be assigned to either of the subprocesses. The factorisable corrections can be straightforwardly computed using an on-shell projection like at LO. In the following we review some more detailed properties of the non-factorisable corrections, following Refs. [107, 181, 189].

Expanding the diagrams in Fig. 4.2 to $\mathcal{O}(\alpha)$ yields for the total virtual correction

$$\begin{aligned} \delta|\mathcal{M}_\lambda(\{p\})|^2 &= \delta|\mathcal{M}_{\lambda,\text{prod}}(\{p\})|^2|\mathcal{M}_{\lambda,\text{LO,Dec}}(\{p\})|^2 + |\mathcal{M}_{\lambda,\text{LO,prod}}(\{p\})|^2\delta|\mathcal{M}_{\lambda,\text{Dec}}(\{p\})|^2 \\ &\quad + 2\delta_{\text{nfact}}|\mathcal{M}_\lambda(\{p\})|^2 + \mathcal{O}\left(\frac{k^2 - M^2}{M^2}\right), \end{aligned} \quad (4.33)$$

implicitly defining the relative non-factorisable correction δ_{nfact} . In the vicinity of the doubly-resonant region, the neglected terms are of order Γ/M with Γ and M denoting the width and the mass of the virtual boson.

An example graph for a non-factorisable contribution is given in Fig. 4.3. The non-factorisable corrections originate exclusively from photon exchange [189]. In the given example graph, this can be explained by the fact that demanding both the propagator of the boson V_2 and its decay products to fulfill the on-shell condition implies that the photon loop momentum is soft, which can only happen for a massless particle. If, for instance, the photon is replaced by a Z boson, the soft region is suppressed by q^2/M_Z^2 with q denoting the soft loop momentum. This graph can therefore be neglected in the DPA.

The diagrams contributing to non-factorisable corrections can be categorised as follows:

- The photon connects initial-state and final-state particles (if case). This case is depicted in Fig. 4.3.
- The photon connects final-state particles (ff'). They have to be associated with different resonances, otherwise this is part of the factorisable decay corrections.

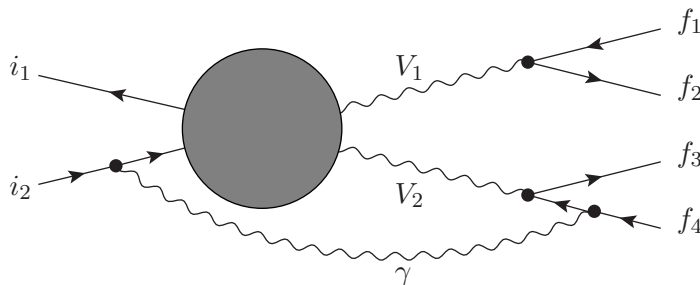


Figure 4.3.: Sample diagram contributing to the non-factorisable corrections. The blob represent all tree-level diagrams for the production subprocess.

- The photon connects the resonant bosons (mm').
- The photon connects one of the resonant bosons with itself (mm), an initial-state particle (im), one of its own decay products (mf) or with another final-state particle (mf').

At first glance, the occurrence of the cases mf , im , mm' , and mm might look surprising, as these diagrams are also contained in the factorisable corrections. But in order to account for the effects of the on-shell projection, one has to add back the difference between the on-shell and off-shell corrections, as far as the singular contributions are concerned. In the mf case, for instance, the non-factorisable contributions read in terms of Passarino–Veltman three-point functions (for the definitions of the Passarino–Veltman functions, see for instance [154, 190])

$$\Delta_{mf} \underset{\Gamma \rightarrow 0}{\sim} -2\tilde{k} \cdot q \left\{ C_0(k, q, 0, \bar{M}, m) - C_0(\tilde{k}, q, 0, M, m) \Big|_{\tilde{k}^2 = M^2} \right\}, \quad (4.34)$$

with k and \tilde{k} denoting the off-shell and on-shell gauge-boson momenta, respectively, q is the momentum of the decay product, and m its mass. In the first term, the complex mass

$$\bar{M} = \sqrt{M^2 - i\Gamma M} \quad (4.35)$$

is kept, which shields the integral from being IR divergent (assuming $m \neq 0$). The second term in brackets, which is part of the factorisable decay corrections, is IR divergent as $\tilde{k}^2 = M^2$. This superficial IR divergence has been introduced by the on-shell projection and has to be subtracted in order to match the IR structure of the real corrections, which are often computed without using the DPA. The other cases mentioned above contribute to the non-factorisable corrections by the same mechanism. The results for all cases are collected in Ref. [107].

High-energy limit

Since we are interested in processes involving energy scales much higher than the EW scale, we should investigate the behaviour of the different contributions in (4.33) in the high-energy limit. The most important result is that the factorisable decay corrections do not contain

large invariants, which is discussed in more detail in Sec. 5.1. The high-energy behaviour of the production process can be investigated using SCET_{EW}. In the following we briefly sketch the high-energy behaviour of the non-factorisable corrections. To this end, we define

$$s_{ij} = 2q_i \cdot q_j, \quad \bar{s}_{lm} = 2k_l \cdot k_m, \quad \tilde{s}_{lj} = 2k_l \cdot q_j, \quad \tilde{t}_{jk} = -2p_k \cdot k_l, \quad t_{jk} = -2q_j \cdot p_k, \quad (4.36)$$

along with the following conventions:

- Resonant bosons are indicated with l, m and their momenta are denoted by k ,
- decay products of boson l are indicated by i , decay products of boson m are indicated by j , and their momenta are denoted by q ,
- initial-state particles are indicated by k and their momenta are denoted by p .

We assume that all final-state particles result from resonant decays. Using these conventions, the high-energy behaviour has been worked out in a process-independent manner in Ref. [107] as follows:

$$\begin{aligned} \delta_{\text{nfact}} = & - \sum_l \sum_{m>l} \sum_{i=1}^{n_l} \sum_{j=1}^{n_m} Q_{li} Q_{mj} \frac{\alpha}{\pi} \text{Re}\{\Delta_1(k_l, q_i, k_m, q_j)\} \\ & - \sum_{k=1}^2 \sum_l \sum_{i=1}^{n_l} Q'_k Q_{li} \frac{\alpha}{\pi} \text{Re}\{\Delta_2(p_k, k_l, q_i)\}, \end{aligned} \quad (4.37)$$

with

$$\begin{aligned} \Delta_1(k_l, q_i, k_m, q_j) \widetilde{M^2/s \rightarrow 0} & \frac{1}{2} (s_{ij} \bar{s}_{lm} - \tilde{s}_{lj} \tilde{s}_{mj}) D_0(q_j - k_m, q_j + k_l, q_i + q_j, 0, M_m, M_l, 0) \\ & + \log\left(\frac{K_m M_l}{K_l M_m}\right) \log\left(\frac{\tilde{s}_{mi}}{\tilde{s}_{lj}}\right) + \left[2 + \log\left(\frac{s_{ij}}{\bar{s}_{lm}}\right)\right] \left[\frac{1}{\varepsilon_{\text{IR}}} + \log\left(\frac{\mu_{\text{IR}}^2 M_l M_m}{(-K_l)(-K_m)}\right)\right], \\ \Delta_2(k_l, q_i, k_m, q_j) \widetilde{M^2/s \rightarrow 0} & \left[\frac{1}{\varepsilon_{\text{IR}}} + 2 \log\left(\frac{\mu_{\text{IR}} M_l}{-K_l}\right)\right] \left[\log\left(\frac{\tilde{t}_{kl}}{\tilde{t}_{ki}}\right) - 1\right], \end{aligned} \quad (4.38)$$

with s being any of the scalar products in (4.36) and D_0 denoting the Passarino-Veltman four-point function. Note that our conventions imply that $\tilde{s}_{im}, \tilde{s}_{jl}$ are scalar products of a resonant momentum with a decay-product momentum from another resonance. The offshellnesses K_l are given by

$$K_l = k_l^2 - M_l^2. \quad (4.39)$$

The important property of these formulae is that they do not contain logarithms of the form

$$\log\left(\frac{M^2}{s}\right). \quad (4.40)$$

This property holds also for the four-point function D_0 and implies that the relative non-factorisable corrections are finite in the high-energy limit, even though they are non-analytic in M .

4.2.2. Complex-mass scheme

While the DPA is a well-suited tool in the vicinity of the resonant region, the complex-mass scheme (CMS) [105, 110, 191] provides a gauge-invariant regularisation prescription on the whole phase space, enabling the full inclusion of off-shell effects. Its basic idea is the replacement (4.27) for the W and the Z mass,³

$$\mu_W^2 = M_W^2 - i\Gamma_W M_W, \quad \mu_Z^2 = M_Z^2 - i\Gamma_Z M_Z, \quad (4.41)$$

on the level of the SM Lagrangian. This has to be set consistently including the definition of the weak mixing angle,

$$\cos^2 \theta_w = 1 - \sin^2 \theta_w = \frac{\mu_W^2}{\mu_Z^2} \quad (4.42)$$

and the renormalisation constants. In practice this implies that all mass-parameter and field-renormalisation constants are complex. In particular, the mass counterterms are defined via

$$M_{0,W}^2 = \mu_W^2 + \delta\mu_W^2, \quad M_{0,Z}^2 = \mu_Z^2 + \delta\mu_Z^2, \quad (4.43)$$

with $M_{0,V}$ denoting the bare masses, which are real and do not depend on the renormalisation scheme. Both the renormalised masses and the mass counterterms become complex, but they pick up the same imaginary part with a different sign, assuring that the bare Lagrangian remains hermitian.

With the above definition, the complex renormalised mass μ_V^2 enters the propagator and the complex mass-parameter renormalisation constant $\delta\mu_V^2$. The field-renormalisation constants are defined analogously,

$$W_0^\pm = \left(1 + \frac{1}{2}\delta\mathcal{Z}_W\right) W^\pm, \quad \begin{pmatrix} Z_{0,Z} \\ Z_{0,A} \end{pmatrix} = \begin{pmatrix} 1 + \frac{1}{2}\mathcal{Z}_{ZZ} & \frac{1}{2}\delta\mathcal{Z}_{ZA} \\ \frac{1}{2}\delta\mathcal{Z}_{ZA} & 1 + \frac{1}{2}\delta\mathcal{Z}_{AA} \end{pmatrix} \begin{pmatrix} Z \\ A \end{pmatrix}, \quad (4.44)$$

with the $\mathcal{Z}_{VV'}$ denoting complex field-renormalisation constants to be distinguished from the real ones denoted by $Z_{VV'}$. The imaginary part in the field-renormalisation condition has to be introduced because of the modified self energies:

$$\begin{aligned} \hat{\Sigma}_T^W(k^2) &= \Sigma_T^W(k^2) - \delta\mu_W^2 + (k^2 - \mu_W^2)\delta\mathcal{Z}_W, \\ \hat{\Sigma}_T^{ZZ}(k^2) &= \Sigma_T^{ZZ}(k^2) - \delta\mu_Z^2 + (k^2 - \mu_Z^2)\delta\mathcal{Z}_{ZZ}, \\ \hat{\Sigma}_T^{AA}(k^2) &= \Sigma_T^{AA}(k^2) + k^2\delta\mathcal{Z}_{AA}, \\ \hat{\Sigma}_T^{AZ}(k^2) &= \Sigma_T^{AZ}(k^2) - \delta\mu_Z^2 + (k^2 - \mu_Z^2)\delta\mathcal{Z}_{ZA}. \end{aligned} \quad (4.45)$$

Imposing the renormalisation conditions (2.25) and (2.29) without the real part with the replacement $M_V^2 \rightarrow \mu_V^2$, which is equivalent to demand

$$\hat{\Sigma}_T^W(\mu_W^2) = \hat{\Sigma}_T^{ZZ}(\mu_Z^2) = \hat{\Sigma}_T^{AZ}(\mu_Z^2) = \hat{\Sigma}_T^{AZ}(0) = 0 \quad (4.46)$$

³If processes involving resonant top quarks or Higgs bosons are considered, their masses have to be redefined similar to (4.41).

as well as

$$\hat{\Sigma}'_T{}^W(\mu_W^2) = \hat{\Sigma}'_T{}^{ZZ}(\mu_Z^2) = \hat{\Sigma}'_T{}^{AA}(0) = 0, \quad (4.47)$$

leads to the renormalisation constants for the mass parameters,

$$\delta\mu_W^2 = \Sigma_T^W(\mu_W^2), \quad \delta\mu_Z^2 = \Sigma_T^{ZZ}(\mu_Z^2), \quad (4.48)$$

and the fields renormalisation constants,

$$\begin{aligned} \delta\mathcal{Z}_W &= -\Sigma_T'^W(\mu_W^2), & \delta\mathcal{Z}_{ZZ} &= \Sigma_T'^{ZZ}(\mu_Z^2), & \delta\mathcal{Z}_{AA} &= -\Sigma_T'^{AA}(0), \\ \delta\mathcal{Z}_{AZ} &= -\frac{2\Sigma_T^{AZ}(\mu_Z^2)}{\mu_Z^2}, & \delta\mathcal{Z}_{AZ} &= -\frac{2\Sigma_T^{AZ}(0)}{\mu_Z^2}. \end{aligned} \quad (4.49)$$

For brevity we introduced the notation

$$\Sigma'(M^2) \equiv \left. \frac{\partial \Sigma(k^2)}{\partial k^2} \right|_{k^2=M^2}. \quad (4.50)$$

We note that the $\delta\mathcal{Z}_{V'V'}$ in (4.49) have indeed to be complex to fulfill (4.47)

All renormalisation constants have the same form as in the on-shell scheme, with the real arguments replaced by the complex ones. Because the gauge-boson masses enter also the fermion and Higgs-boson self energies, all other renormalisation constants also become complex. The forms of the renormalisation conditions as well their explicit forms remains the same as in the on-shell scheme [110], which is why we do not discuss them explicitly.

On-shell and pole mass definitions

We conclude this section by a brief remark on the difference between the different definitions of masses and widths in the on-shell scheme and the CMS, respectively.

Following from the renormalisation condition (2.25) and the renormalisation constants (2.26), the renormalised gauge-boson masses in the on-shell renormalisation scheme is given by

$$\left(\hat{M}_V^{\text{OS}}\right)^2 = M_{0,V}^2 - \widetilde{\text{Re}} \left\{ \Sigma_T^{VV} \left[\left(\hat{M}_V^{\text{OS}}\right)^2 \right] \right\} \quad (4.51)$$

It is worth noting that this is not the same as the real part⁴ of the pole mass in (4.41), which corresponds to the position of the pole in the complex p^2 -plane:

$$\left(\hat{M}_V^{\text{P}}\right)^2 = M_{0,V}^2 - \widetilde{\text{Re}} \left\{ \Sigma_T^{VV} \left[(\mu_V)^2 \right] \right\} - \Gamma_V^{\text{P}} M_V^{\text{P}} \widetilde{\text{Im}} \left\{ \Sigma_T^{VV} (\mu_V^{\text{P}})^2 \right\}. \quad (4.52)$$

Even though this *pole definition* appears to be a more natural definition for a physical mass, the on-shell values are usually employed because they have been measured to accurate precision.

⁴Note that the choice (4.41) is not the only one to define a mass and a width from the complex pole position, other possibilities have for instance been studied in Ref. [192].

The relation between the two,

$$M_V^P = \frac{(M_V^{\text{OS}})^2}{\sqrt{(M_V^{\text{OS}})^2 + (\Gamma_V^{\text{OS}})^2}}, \quad \Gamma_V^P = \frac{M_V^{\text{OS}} \Gamma_V^{\text{OS}}}{\sqrt{(M_V^{\text{OS}})^2 + (\Gamma_V^{\text{OS}})^2}}, \quad (4.53)$$

has been proposed in Ref. [193] and worked out in Ref. [194] and is obtained by inserting (4.51) and (4.52) into each other iteratively and using the definition of the on-shell width, which is obtained from the optical theorem as

$$\Gamma_V^{\text{OS}} = \frac{1}{M_V^2} \frac{\widetilde{\text{Im}} \left\{ \Sigma_T^V (M_V^P)^2 \right\}}{1 + \widetilde{\text{Im}} \left\{ \Sigma_T^V (M_V^P)^2 \right\}}. \quad (4.54)$$

The use of the CMS thus requires converting the on-shell values for masses and widths to the pole definitions using (4.53).

5. Implementation of SCET_{EW} into a Monte Carlo event generator

Having set the basis of both the calculation of collider observables using fixed-order techniques and SCET_{EW}, we are ready to discuss the implementation of SCET_{EW} into a Monte Carlo integration code which calculates fully differential cross sections at NLO EW accuracy. Parts of this and the two following sections are based on Ref. [141].

In the existing literature (see e.g. Refs. [52–55]), the focus has been on the analytic computation of simple processes such as four-fermion processes or vector boson pair production without decays. Within this work, in contrast, we aim for the computation of more complicated processes involving also the decays of unstable particles. In addition we want to take into account the effects of phase-space cuts. The occurring phase-space integration must therefore be performed numerically and a certain grade of automation is desirable.

The section is organised as follows: In Sec. 5.1 we sketch how to apply SCET_{EW} to LHC processes by isolating subprocesses that fulfill the SCET_{EW} condition. At the end we list all steps of the SCET_{EW} calculation. In Sec. 5.2 we discuss the implementation of all ingredients of the SCET_{EW} calculation in detail. We then proceed by discussing the logarithm counting in Sec. 5.3 and describe which of the appearing logarithmic terms are included in our calculation before closing with a brief description of the software components put to use (Sec. 5.4).

5.1. Fixed-order calculations and SCET_{EW} in complicated processes

We start from an NLO-EW-accurate computation performed using fixed-order perturbation theory. As discussed in Sec. 4.1, treating the occurring IR singularities with the subtraction scheme of Catani and Seymour implies that real and virtual corrections are integrated separately. As the logarithmically enhanced contributions arise mainly in the virtual part, we compute the real corrections in the conventional way¹. However, in order to have well-defined observables, one should assure that the IR singularities are treated in a consistent way. This issue is addressed in more detail in Sec. 5.1.2.

Since we include decay effects, any unstable particle is only detected via its decay products. We can unfortunately not apply SCET_{EW} on a process like

$$\bar{q}q \rightarrow W^+W^- \rightarrow e^- \bar{\nu}_e \mu^+ \nu_e, \quad (5.1)$$

which is dominated by phase-space regions, where invariants such as $p_e \cdot p_{\bar{\nu}_e}$ are of the order of M_W . However, when applying the DPA (see Sec. 4.2.1), the process factorises into the

¹In fact also real-radiation corrections develop logarithmic enhancement at high energies, but how to resum them relies on a certain grade of “inclusiveness” of the considered observables with respect to the real radiation of massive vector bosons [195]. Throughout this work we thus neglect these effects and do not attempt a resummation of the associated logarithms.

subprocesses

$$[\bar{q}q \rightarrow W^-W^+] \times [W^- \rightarrow e^- \bar{\nu}_e] \times [W^+ \rightarrow \mu^+ \nu_e]. \quad (5.2)$$

The $2 \rightarrow 2$ production subprocess has the kinematic invariants

$$s = 2p_q \cdot p_{\bar{q}}, \quad -t = 2p_q \cdot p_{W^+} \approx 2p_q \cdot (p_e + p_{\bar{\nu}_e}), \quad -u = 2p_{\bar{q}} \cdot p_{W^+} \approx 2p_{\bar{q}} \cdot (p_e + p_{\bar{\nu}_e}) \quad (5.3)$$

in the vicinity of the doubly-resonant region. Since these quantities become large in the high-energy limit, a SCET_{EW} expansion is sensible for the production process. In the decay subprocesses all invariants are of the order of the W mass, and there is no point in applying SCET_{EW}. It is, however, not necessary because in a process without large scale ratios no Sudakov logarithms occur on any order in perturbation theory. The corrections to the decay processes can hence reliably be calculated in fixed order.

The strategy to isolate the logarithmically enhanced corrections is thus:

- Apply the pole approximation in order to factorise the matrix element into a production and a decay part. This is sketched in diagrammatic form in Fig. 4.1.
- Calculate the decay part in the full SM. It cannot have large corrections, as the matrix element itself cannot contain any large scale ratios.
- Treat the loop corrections to the production part with SCET_{EW}. In the high-energy limit this is a process where all invariants can be considered large.
- Add the integrated subtraction counterterms (see Sec. 4.1) and the non-factorisable corrections (see Sec. 4.2.1).

The third point is the main issue of this work. The required methods have been demonstrated in Refs. [43, 45, 47, 48] and also been described in Sec. 3.3. The setup presented in this section makes use of the results of Refs. [48] as far as the anomalous dimensions and the low-scale corrections are concerned. However, our automated computation features some new properties that are desirable for the LHC and future collider predictions:

- Embedding the SCET_{EW} results into a Monte Carlo integrator enables the computation of fully differential cross sections for many different processes on a suitable fiducial phase space.
- Decay effects are taken into account properly.
- Complicated processes such as vector-boson scattering or processes with external Z bosons or photons, for which the high-scale matching coefficients contain a large number of diagrams, are also feasible.

All of the above steps are to be performed on the level of helicity amplitudes with definite polarisations of the virtual gauge bosons. This is because spin-dependent corrections occur for both fermions (left- and right-handed fermions have different EW quantum numbers) and gauge bosons (because the longitudinal polarisations are to be treated using the GBET).

5.1.1. Virtual corrections in SCET_{EW}

In the fixed-order approach the perturbative expansion of the matrix element reads

$$\begin{aligned}
 |\mathcal{M}|^2 &= \frac{1}{n_i} \left| \sum_c \sum_\lambda \mathcal{M}_{\lambda c} \right|^2 = \frac{1}{n_i} \sum_{cc'} \sum_{\lambda\lambda'} \mathcal{M}_{\lambda c} \mathcal{M}_{\lambda' c'}^* \\
 &= \frac{1}{n_i} \sum_{cc'} \sum_{\lambda\lambda'} (|\mathcal{M}_{0,\lambda c} \mathcal{M}_{0,\lambda' c'} + \mathcal{M}_{0,\lambda c} \mathcal{M}_{1\text{-loop},\lambda' c'}^* + \mathcal{M}_{1\text{-loop},\lambda c} \mathcal{M}_{0,\lambda' c'}^* \dots), \quad (5.4)
 \end{aligned}$$

where, c, c', λ and λ' run over all configurations of colour and spin, respectively, and n_i denotes the number of initial-state spin and colour configurations. The one-loop matrix element contains the large logarithmic corrections arising from massive vector-boson exchange, which we wish to resum.

Often contributions with $\lambda \neq \lambda'$ can be neglected if the phase-space cuts are sufficiently inclusive [131]. In this case the above formula simplifies to

$$|\mathcal{M}|^2 = \frac{1}{n_i} \sum_\lambda (|\mathcal{M}_{0,\lambda}|^2 + 2\text{Re}(\mathcal{M}_{0,\lambda} \cdot \mathcal{M}_{1\text{-loop},\lambda}^*) + \dots) \quad (5.5)$$

with the sum over colours now implicit. The loop matrix elements are IR divergent and after applying the Catani–Seymour dipole subtraction scheme the cross section is obtained in the form (see Sec. 4.1)

$$\sigma = \int_n d\sigma_{\text{Born}} + \int_n \left(d\sigma_{\text{virt}} + \int_1 d\sigma_{\text{sub}} \right) + \int_{n+1} (d\sigma_{\text{real}} - d\sigma_{\text{sub}}), \quad (5.6)$$

with each of the three terms being integrated separately. The term $d\sigma_{\text{Born}}$ is understood to contain the first term in (5.5) and the $d\sigma_{\text{virt}}$ the second one. We want to apply SCET_{EW} only to the virtual part, but when calculated with SCET_{EW}, the matrix element does not naturally decompose as in (5.5). Instead, the amplitude obtained from matching a set of operators contains the Born level and dominant virtual corrections to all orders. Therefore we substitute

$$\int_n \left(d\sigma_{\text{virt}} + \int_1 d\sigma_{\text{sub}} \right) \rightarrow \int_n \left(d\sigma_{\text{virt}}^{\text{SCET}} + \int_1 d\sigma_{\text{sub}} \right) \quad (5.7)$$

with $d\sigma_{\text{virt}}^{\text{SCET}}$ obtained by subtracting the tree-level result from the squared LO matrix element in the full theory:

$$d\sigma_{\text{virt}}^{\text{SCET}} = d\Phi^{(m)} (|\mathcal{M}^{\text{SCET}}|^2 - |\mathcal{M}_{\text{Born}}|^2). \quad (5.8)$$

The leading-order matrix element $|\mathcal{M}_{\text{Born}}|^2$ has to be subtracted because it is already contained in $d\sigma_{\text{Born}}$. As described in Sec. 3.3, the SCET_{EW} results are computed on the level of helicity amplitudes obtained from SCET_{EW} operators:

$$\mathcal{M}_\lambda^{\text{SCET}} = \sum_k C_{\lambda,k}(\mu) \langle \mathcal{O}_{\lambda,k}(\mu) \rangle, \quad (5.9)$$

with λ running over polarisation configurations and k over the different Lorentz/Dirac structures. To simplify the notation, we drop the subscript λ from now. As discussed in Sec. 3, the Wilson coefficients are matched at the high scale and run down to the low scale.

This procedure results in the following formula:

$$\begin{aligned} \mathcal{M}_{\text{SCET}} &= \sum_k C_k(\mu_1) \langle \mathcal{O}_k(\mu_1) \rangle \\ &= \sum_{\bar{k}, j, l} \left(\mathbf{D}_{l\bar{k}}^{(1)}(\mu_1) \left[\hat{\text{P}} \exp \left(- \int_{\mu_1}^{\mu_h} d \log \mu \gamma(\mu) \right) \right]_{l\bar{k}} \right) C_{j, k}(\mu_h) \langle \mathcal{O}_k(\mu_1) \rangle, \end{aligned} \quad (5.10)$$

with the following ingredients:

- The Wilson coefficients $C_k(\mu_h)$, matched at the high energy scale.
- The SCET_{EW} anomalous dimension denoted by γ . The matrix exponential describes the RG running from μ_h to μ_1 , the path-ordering symbol $\hat{\text{P}}$ is defined in (3.7).
- The low-scale mixing matrix \mathbf{D} , which takes the explicit SCET_{EW} loop corrections into account. It depends on the low scales, i.e. the electroweak mass spectrum.

The index k in (5.10) labels different operators contributing to the same process at tree level, while j and l denote the mixing of different operators into each other at one loop level, assembled in a way that $j = 1$ corresponds to the operators contributing already at tree-level. The anomalous dimension depends only on j and l because SCET_{EW} corrections do not mix different Lorentz or chiral structures, which are denoted by k .

The fact that we would like to use the fixed-order automation apparatus motivates us to rewrite the above expression in terms of scattering amplitudes:

$$\mathcal{M}_{\text{SCET}} = \sum_j \mathbf{D}_{1j}(\mu_1) \left[\hat{\text{P}} \exp \left(- \int_{\mu_1}^{\mu_h} d \log \mu \gamma(\mu) \right) \right]_{1j} \mathcal{M}_j(\mu_h) |_{\{M\}=0, \text{IR-finite}}, \quad (5.11)$$

where now j sums over all processes that arise, when a global SU(2) gauge transformation is applied to the external fields of the respective process, while the sum over k has disappeared, because it is contained in the \mathcal{M}_j . The fact that all mass scales have been set to zero indicates that the amplitudes are evaluated in the SySM. The connections between the operators, Wilson coefficients, and matrix elements is discussed by means of an example in Sec. 5.2.2.

5.1.2. Modifications of the factorisation formula

It is however not possible to use (5.10) as virtual matrix element in (5.7): The IR divergences, which are contained in \mathbf{D} , are multiplied with the resummed matrix element instead of the Born matrix element.

We should therefore substitute

$$\begin{aligned} \mathbf{D}_{1l}(\mu_1) \left[\hat{\text{P}} \exp \left(- \int_{\mu_1}^{\mu_h} d \log \mu \gamma(\mu) \right) \right]_{1j} &= \left(\delta_{1j} + \mathbf{D}_{1l}^{(1)}(\mu_1) \right) \left[\hat{\text{P}} \exp \left(- \int_{\mu_1}^{\mu_h} d \log \mu \gamma(\mu) \right) \right]_{1j} \\ &\rightarrow \mathbf{D}_{1j}^{(1)}(\mu_1) + \left[\hat{\text{P}} \exp \left(- \int_{\mu_1}^{\mu_h} d \log \mu \gamma(\mu) \right) \right]_{1j} \end{aligned} \quad (5.12)$$

because then the IR divergences in $\mathbf{D}^{(1)}$ are multiplied with the unresummed Born matrix element. The difference between the definitions in (5.12) are of $\mathcal{O}(\alpha^2 \log^2(M_W^2/s))$. It should clearly be said that (5.10) is the consistent way of including all terms of $\mathcal{O}(\alpha^2 \log^2(M_W^2/s))$. However, the inclusion of real-radiation effects in the full SM is more important and a treatment of the reals in the pole approximation would be beyond the scope of this work.

In addition (5.10) does not yet include the parameter renormalisation (PR) constants, which we comprise in an separate contribution:

$$\mathcal{M}_j \rightarrow \mathcal{M}_j + \delta_{\text{PR}} \mathcal{M}_j. \quad (5.13)$$

We therefore use

$$\mathcal{M}_{\text{SCET}} = \sum_j \left[\mathbf{D}^{(1)}(\mu_1) + \hat{\text{P}} \exp \left(- \int_{\mu_1}^{\mu_h} d \log \mu \gamma(\mu) \right) + \delta_{\text{PR}} \mathbb{1} \right]_{1j} \mathcal{M}_j(\mu_h) |_{\{M\}=0, \text{IR-finite}} \quad (5.14)$$

as a master formula for the MC code. We choose the high and the low scale according to

$$\mu_h = \sqrt{s}, \quad \mu_1 = M_W, \quad (5.15)$$

with \sqrt{s} denoting the centre-of-mass energy of the production subprocess. Note that if no resummation is applied, the result is completely independent of the scale choices: Changing μ_h merely shifts contributions from the high-scale matching into the anomalous dimension and vice versa, while changing μ_1 reshuffles contributions between the low-scale corrections and the anomalous dimensions. The dependence of the resummed result on the precise choice of μ_h and μ_1 is expected to be small.

5.1.3. Summary of the strategy

In more detail the strategy of applying SCET_{EW} to a generic SM process with large kinematic invariants can be summarised as follows:

- We construct all effective operators in SCET_{EW} that contribute to a specific process. By definition their expectation values reproduce the tree-level behaviour of the SM amplitude to leading power. We use an operator basis described in Sec. 5.2.1, the numerical evaluation is described in Sec. 5.2.2.
- The operators are matched (at high energies) against the SySM. Because the massless SCET_{EW} loop diagrams vanish in DimReg [52], the only object that is to be calculated is the one-loop scattering amplitude in the SySM. It does not depend on any mass scale, but depends non-trivially on the process. Therefore an automated calculation of that part is particularly desirable, especially if complicated processes are considered. This part is described in Sec. 5.2.3.
- We then calculate the SCET_{EW} anomalous dimension matrix $\gamma(\mu)$. This has been shown to be independent of the detailed structure of the process. Instead, it is a sum over contributions that depend only on quantum numbers and momenta of the external particles.
- The anomalous dimension is integrated from the low to the high scale. This always can be done using the results of Sec. 3.3.4 since the scale dependence of the anomalous di-

mension has a universal structure. We take the matrix exponential of the result. The implementation of these steps is described in Sec. 5.2.4.

- We calculate the one-loop low-scale corrections $D_\lambda^{(1)}$ to the SCET_{EW} operators in the broken phase². Because of the structure of the SCET_{EW} diagrams, they can be constructed solely from the external particles and their momenta. More details can be found in Sec. 5.2.5.
- Finally we add the corresponding coupling renormalisation constants. They are different for the Abelian and non-Abelian parts of the amplitude, respectively, which is why it is necessary to decompose each amplitude according to their corresponding powers of g_1 and g_2 . The renormalisation constants contain logarithmic corrections associated with the running of α and the weak mixing angle between the electroweak scale, where they are chosen as input parameters, and the high scale, at which the interaction takes place.
- If photons, Z bosons, or Higgs bosons are involved, all contributing processes are constructed in terms of the respective fields in the SySM. We then perform all above steps for each subamplitude individually. The anomalous dimension is most easily calculated in terms of the symmetric fields. For the low-scale SCET_{EW} corrections we apply the back transformation for each symmetric process. More details can be found in Sec. 5.2.6.

Recall that all these steps apply to the virtual corrections to the production processes of virtual gauge bosons, as discussed in Sec. 5.1. The decay corrections, the implementation of which is discussed in more detail in Sec. 5.2.6, have to be added afterwards, as well as the non-factorisable corrections, the subtracted real corrections, and the integrated dipoles. All these corrections are computed in the full SM.

5.2. Ingredients of the virtual corrections

In the following we discuss the implementation of the ingredients of (5.14) into MOCANLO. As an illustrative example we choose the four-fermion process

$$\bar{u}_L(p_1)u_L(p_2) \rightarrow e_L^+(p_3)e_L^-(p_4), \quad (5.16)$$

that contributes to the Drell–Yan cross section (a sum over the initial-state colours is implied). We choose a specific polarisation configuration (all fermions are left-handed) for simplicity. However, as mentioned above all matching and running computations have to be performed on the level of a specific polarisation configuration.

²In Refs. [45, 47, 48] these contributions have been called the low-scale matching coefficients. The motivation behind this term is that for calculating jet observables which require a treatment with SCET_{QCD}, the EW scale acts as an intermediate scale, at which one set of SCET operators is matched against another set. Since we focus on observables, for which this is not necessary, we drop this naming convention. However, we should mention that the calculation of the IR divergent photonic corrections in App. B.3 follows the strategy of the given references because the finite parts are calculated in SCET_{EW} and the divergent ones in SCET _{γ} .

5.2.1. Constructing the operator basis

From (5.14) it is obvious that the set of contributing operators (and therefore also matrix elements) to a given process

$$\phi_1\phi_2 \rightarrow \phi_3 \dots \phi_n \quad (5.17)$$

is obtained by applying the SU(2) colour operators arbitrarily often on any pair of particles. The colour operators act on an external field ψ with gauge index α according to [47]

$$\mathbf{t}_i \psi_{j,\alpha} = \sum_{a=1}^3 t_{i,\alpha\beta}^a \psi_{i,\beta} \delta_{ij}, \quad (5.18)$$

with $t_{i,\alpha\beta}^a$ denoting components of the SU(2) generators in the representation of ψ . We use the linear combinations

$$t_i^\pm = \frac{1}{\sqrt{2}} (t_i^1 \mp it_i^2) \quad \rightarrow \quad t_i^1 \cdot t_j^1 + t_i^2 \cdot t_j^2 = t_i^+ \cdot t_j^- + t_i^- \cdot t_j^+ \quad (5.19)$$

instead of the $t^{1/2}$. This basis has also been employed in Ref. [47], with a different normalisation convention. In this basis, the \mathbf{t} transform matrix elements associated with physical processes into matrix elements associated with other processes. Note that we use the lower-case \mathbf{t} for the SU(2) colour operators instead of the upper-case \mathbf{T} employed for the generic colour operators in Sec. 3.

An algorithm to compute all possible processes starting from (5.17) is implemented as follows. Starting with a list of processes that contains the initial one as its only element:

- Apply all possible two-particle transformations to the external fields. Check whether the resulting process violates charge conservation. If not, append it to the list.
- Go to the next process in the list and apply all possible two-particle transformations. Check whether the resulting process violates charge conservation. If not, check whether the process is already in the list. If not, add it.
- Repeat the above until the end of the list is reached (that is, the iteration of the last process did not produce any new ones).

Fermions

In Ref. [45] the scattering of four fermions with momenta p_1, \dots, p_4 in a spontaneously broken SU(2) gauge theory³ has been considered using the operator basis

$$\begin{aligned} \mathcal{O}_{1,\sigma\sigma'} &= \bar{\chi}_4 \frac{\tau^a}{2} \gamma^\mu \omega_\sigma \chi_3 \bar{\chi}_2 \frac{\tau^a}{2} \gamma_\mu \omega_{\sigma'} \chi_1, \\ \mathcal{O}_{2,\sigma\sigma'} &= \bar{\chi}_4 \gamma_\mu \omega_\sigma \chi_3 \bar{\chi}_2 \gamma_\mu \omega_{\sigma'} \chi_1 \end{aligned} \quad (5.20)$$

³This is basically a simplified SM without the photon. All three SU(2) gauge bosons have a common mass.

with τ^a being the Pauli matrices, the projection operators

$$\omega_{\pm} = \frac{\mathbb{1} \pm \gamma_5}{2}, \quad (5.21)$$

projecting the Dirac fermions on their component with left (−) or right (+) chirality, χ_i as defined in (3.57), but arranged in SU(2) doublets and the Wilson lines given by the EW ones (3.99). The operators correspond to SU(2) colour invariants,⁴ with $\mathcal{O}^{(1)}$ describing the interaction of two “SU(2) vector currents”, and $\mathcal{O}^{(2)}$ the interaction of SU(2) singlets. This can be extended to the SM by writing down analogous operators for the SU(3) colours. The obvious advantage of this decomposition is that a minimal set of operators is employed, hence minimising the computational effort. Additionally, the general structure is manifestly independent of the fermion species: All loop integrals that are actually different have to be computed only once.

It would certainly be possible to automate the evaluation of such colour-covariant operators. However, a vast variety of programs has been developed to calculate on-shell helicity amplitudes. These are obtained by expanding the operators into the flavour eigenstates, resulting in an overcomplete set of operators. However, at tree level they can be matched against a helicity amplitude corresponding to a physical process. This allows us to use the matrix element generator RECOLA [57, 58] to calculate the Wilson coefficients (at tree level and one-loop) and the operator expectation values of the SCET operators together.⁵

Adopting the conventions of Refs. [47, 48] to show only the colour structure and omit all Wilson lines, the relevant operators for the process (5.16) are written down as

$$\begin{aligned} \mathcal{O}_1 &= \bar{Q}_{1,L} \frac{\tau^a}{2} \gamma^\mu Q_{2,L} \bar{L}_{3,L} \frac{\tau^a}{2} \gamma_\mu L_{4,L}, \\ \mathcal{O}_2 &= \bar{Q}_{1,L} \gamma^\mu Q_{2,L} \bar{L}_{3,L} \gamma_\mu L_{4,L} \end{aligned} \quad (5.22)$$

in the colour covariant basis and as

$$\begin{aligned} \mathcal{O}_1 &= \bar{u}_{1,L} \gamma_\mu u_{2,L} \bar{e}_{3,L} \gamma_\mu e_{4,L}, \\ \mathcal{O}_2 &= \bar{d}_{1,L} \gamma_\mu d_{2,L} \bar{e}_{3,L} \gamma_\mu e_{4,L}, \\ \mathcal{O}_3 &= \bar{d}_{1,L} \gamma_\mu u_{2,L} \bar{e}_{3,L} \gamma_\mu \nu_{4,L}, \\ \mathcal{O}_4 &= \bar{u}_{1,L} \gamma_\mu d_{2,L} \bar{\nu}_{3,L} \gamma_\mu e_{4,L}, \\ \mathcal{O}_5 &= \bar{u}_{1,L} \gamma_\mu u_{2,L} \bar{\nu}_{3,L} \gamma_\mu \nu_{4,L}, \\ \mathcal{O}_6 &= \bar{d}_{1,L} \gamma_\mu d_{2,L} \bar{\nu}_{3,L} \gamma_\mu \nu_{4,L}, \end{aligned} \quad (5.23)$$

in the flavour eigenbasis we employ. In fact, this basis is used in Ref. [45] for the calculation of the low-scale matching corrections, while using the colour covariant form at the high scale. The

⁴In the following we use the term “colour” in the way as it has been introduced in Ref. [47]: That is, colour may refer to either the usual SU(3) or to the SU(2)×U(1) charges.

⁵In principle RECOLA features the computation of SU(3)-colour-stripped amplitudes in the colour flow formalism, generalising this for more than one gauge group would enable the computation in the gauge-covariant basis. This is however much more of an involved implementation than just providing a model file for the symmetric SM.

connection between fields of the bases is obvious:

$$Q_{k,L} = \begin{pmatrix} u_{k,L} \\ d_{k,L} \end{pmatrix}, \quad L_{k,L} = \begin{pmatrix} \nu_{k,L} \\ e_{k,L} \end{pmatrix}. \quad (5.24)$$

Gauge bosons

For processes with external gauge bosons we use a mixture of the symmetric and the physical base in the different contributions. For charged gauge bosons we use the charge eigenstates W^\pm rather than an SU(2)-covariant $W^{1/2}$ fields used in Ref. [47]. The form of the operator building block associated with an external gauge boson is as given in (3.57) with EW Wilson lines as in (3.99).

For neutral gauge bosons the operators are constructed in the symmetric basis W^3/B since it simplifies the anomalous dimension a lot. For the low-scale corrections one has to apply the back-transformation because they depend on the masses of the external particles. This is discussed in more detail in Sec. 5.2.6.

Scalars

The SM scalars are treated in close analogy to the neutral gauge bosons: If we denote the Higgs doublet with (see also (2.7))

$$\Phi = \begin{pmatrix} \phi^+ \\ \phi_2 \end{pmatrix} = \begin{pmatrix} \phi^+ \\ \frac{1}{\sqrt{2}}(H + v + i\chi) \end{pmatrix}, \quad (5.25)$$

then we construct the operators from the fields ϕ^\pm , ϕ_2 , and ϕ_2^* . At the low energy scale the lower components are rotated into the mass eigenstates χ , H , see again Sec. 5.2.6 for details. Since the Higgs doublet is in the same representation as the left-handed fermions, the gauge-invariant building block analogous to (3.57) has the same form as the fermionic one:

$$\Xi_n(x) = W_n^\dagger(x)\Phi_n(x), \quad (5.26)$$

with the Φ_n being composed of n -collinear scalar fields ϕ_n^\pm , $\phi_{2,n}^*$. The above expression is built into operators of the form (3.98) in the same way as for fermionic operators.

5.2.2. Tree-level matrix elements

With the considerations of the previous section the automated computation of expectation values of SCET_{EW} operators can be performed in a straightforward manner, once a program is at hand that can calculate on-shell amplitudes in the SySM. We use RECOLA2 [58] equipped with a model file of the SM in the symmetric phase to evaluate the amplitudes numerically. Starting from the SySM Lagrangian, the model file is generated using FEYNRULES [196] and afterwards renormalised and translated to a RECOLA2 model file using the in-house software REPT1L (for more details see Ref. [197]).

Given this technical toolkit, all we have to do is to express every part of the computation in a terms of matrix elements representing physical processes in the SySM, which we have achieved by obtaining (5.10) and (5.14). In the following we use our example process to elucidate the

relation between Wilson coefficients, operator expectation values, and matrix elements. In the discussed example the tree-level matching reads

$$\mathcal{M}^{\bar{u}_L u_L \bar{e}_L e_L}(\{p\}) = C_1^{(0)} \langle \mathcal{O}_1 \rangle, \quad C_1^{(0)}(\mu_h) = \frac{4\pi\alpha}{\hat{s}} (Q_u Q_e + I_{u_L}^Z I_{e_L}^Z). \quad (5.27)$$

with $\sqrt{\hat{s}}$ denoting the (partonic) CMS energy and Q_f and $I_{f_\kappa}^Z$ denoting the charge and Z-boson coupling of a fermion with chirality κ . The other operators in (5.23) are matched analogously. Note that we adopt the convention that the Wilson coefficient contains the factor $1/\hat{s}$. \mathcal{O}_1 is a dimension-6 operator, thus the product of the operator and the Wilson coefficient has mass dimension 4, as it should be at leading power.

To see that (5.27) is indeed the correct matching, we observe that $\langle \mathcal{O}_1 \rangle$ contains the spin structure of the amplitude that means all spinors and Dirac matrices:

$$\langle \mathcal{O}_1 \rangle = \bar{u}(p_{\bar{u}}) \gamma^\mu v(p_u) \bar{v}(p_{e^-}) \gamma_\mu u(p_{e^+}). \quad (5.28)$$

Note that the difference between a collinear fermion field χ_c as defined in (3.57) in SCET_{EW} and an ordinary fermion field does not matter at leading order and leading power.

Multiplied with the process-specific prefactors in $C_1^{(0)}$, (5.28) yields precisely the $\bar{u}_L u_L \rightarrow e_L^+ e_L^-$ scattering amplitude in the limit $\sqrt{\hat{s}} \gg M_Z$. Since $\sqrt{\hat{s}}$ defines the high scale μ_h , the Wilson coefficient is evaluated at μ_h .

Once the Wilson coefficient is run down to the low scale and the radiative corrections to the operator expectation value are computed, all operators in (5.23) contribute to the resummed renormalisation-group improved result even if the matching is only performed at tree level:

$$\mathcal{M}_{\text{res}}^{\bar{u}_L u_L e_L^+ e_L^-}(\{p\}) = \sum_{j=1}^6 C_j(\mu_h) \mathbf{A}_{j1}(\mu_h, \mu_l) \langle \mathcal{O}_1 \rangle, \quad (5.29)$$

where the matrix \mathbf{A} is short for the path-ordered exponential in (5.14). Since the numerical values of the spinors are not different among the \mathcal{O}_i , (5.29) can be rewritten in terms of scattering amplitudes of different processes:

$$\mathcal{M}_{\text{res}}^{\bar{u}_L u_L e_L^+ e_L^-}(\{p\}) = \sum_j \mathbf{A}_{j1}(\mu_h, \mu_l) \mathcal{M}^{f_{1j,L} f_{2j,L} f_{3j,L} f_{4j,L}}, \quad (5.30)$$

with the external fermions $f_{ij,L}$ are the respective SU(2)-transformed ones and can directly be read off from (5.23). The \mathcal{M}^{\dots} on the right-hand side of (5.30) can be evaluated using RECOLA2. It is worth noting that, since $\langle \mathcal{O} \rangle$ is a tree-level quantity, it is analytic in the massless limit. The difference between calculating it in the SySM or SM is thus just a matter of power corrections.

The generalisation to any SM process is rather obvious: The SU(2)-transformed fields are constructed in a suited basis of the respective representation and the matrix element reads

$$\mathcal{M}^{\phi_1, \dots, \phi_n}(\{p\}) = \sum_j \mathbf{A}_{1j}(\mu_h, \mu_l) \mathcal{M}^{\tilde{\phi}_1^{(j)}, \dots, \tilde{\phi}_n^{(j)}} \quad (5.31)$$

with j running up the number of processes that can be generated by applying SU(2) transformations to any number of pairs of external fields. Thus $\tilde{\phi}_i^{(j)}$ is either equal to ϕ_i or its SU(2)

partner. With a suited model file the transformed matrix elements can be evaluated for all possible combinations of fields using RECOLA2.

Identical Particles

For simplicity we have chosen a process without identical particles and hence with only a single Lorentz structure. If two or more particles are identical, there are more contributing operators. For instance, the process $\bar{u}_L u_L \rightarrow \bar{u}_L u_L$ has two contributing operators, corresponding to the t - and s -channel, respectively:

$$\mathcal{M}^{\bar{u}_L u_L \bar{u}_L u_L}(\{p\}) = C_1^{(0),t} \langle \mathcal{O}_1^t \rangle + C_1^{(0),s} \langle \mathcal{O}_1^s \rangle. \quad (5.32)$$

Even though each operator has a different tree-level Wilson coefficient, an equation similar to (5.30) still holds. Since the form of the anomalous dimension is the same for both operators (it depends only on the gauge structure of the operators) and all transformed amplitudes have the same Lorentz structure, one ends up with

$$\begin{aligned} \mathcal{M}_{\text{res}}^{\bar{u}_L u_L \bar{u}_L u_L}(\{p\}) &= \sum_j \mathbf{A}_{1j}(\mu_h, \mu_l) \left(C_j^{(0),t}(\mu_h) \langle \mathcal{O}_1^t \rangle + C_j^{(0),s}(\mu_h) \langle \mathcal{O}_1^s \rangle \right) \\ &= \sum_j \mathbf{A}_{j1}(\mu_h, \mu_l) \mathcal{M}^{f_{1j,L} f_{2j,L} f_{3j,L} f_{4j,L}}, \end{aligned} \quad (5.33)$$

once the contributions to the scattering amplitudes have been added coherently. In the first line of the above equation it is understood that for both Lorentz structures the operators are arranged in vectors like (5.23) accordingly. The above generalises to arbitrarily complicated processes.

5.2.3. High-scale matching contributions

Following the arguments in Secs. 3.2.6 and 3.3, the high-scale matching contributions are given by the IR-finite parts of the one-loop on-shell amplitudes in the SySM: the SCET_{EW} loop corrections vanish in DimReg, leaving the finite part as the one-loop matching correction to the Wilson coefficient:

$$C_1^{(1)}(\mu_h) \langle \mathcal{O}^{(0)} \rangle = \mathcal{M}(\{p\})(\mu_{UV} = \mu_{IR} = \mu_h)|_{\{M\}=0, \text{ IR-finite}}, \quad (5.34)$$

which is a SySM version of (3.77). Both C_1 and \mathcal{M} are understood to be renormalised in the $\overline{\text{MS}}$ scheme. The one-loop matching correction is hence obtained by setting all masses to zero in the full amplitude and simply take the IR-finite part. The quantity on the right-hand side of (5.34) can again directly be calculated with RECOLA2. Thus, the only thing to change is to promote all SySM matrix elements from tree-level to one loop:

$$\mathcal{M}^{\phi_1 \dots \phi_n}(\{p\}) = \sum_j \mathbf{A}_{1j}(\mu_h, \mu_l) \left(\mathcal{M}^{\text{tree}, \tilde{\phi}_{1j} \dots \tilde{\phi}_{1n}} + \mathcal{M}_{\text{IR-finite}}^{1\text{-loop}, \tilde{\phi}_{1j} \dots \tilde{\phi}_{1n}} \right). \quad (5.35)$$

Note that inserting the above into (5.14) implies cross terms between corrections associated with running and matching.

All couplings and fields are renormalised in the $\overline{\text{MS}}$ scheme, inducing a renormalisation-scale dependence. We set the renormalisation scale to

$$\mu_{\text{UV}} = \mu_{\text{h}} = \sqrt{\hat{s}}, \quad (5.36)$$

minimising corrections of the form $\log(\mu_{\text{h}}^2/\hat{s})$. The high-scale matching part is particularly desirable to be automated, as it is the only process-specific ingredient of (5.14). For four-fermion processes the respective analytical calculation has been performed in Ref. [45], while the results for diboson production can be found in Ref. [52].

5.2.4. Anomalous dimension

The form of the SCET_{EW} anomalous dimension of the SM has been analysed in Ref. [47]. At one-loop it is given by (3.115). In the following, we generalise (3.115) to the case of incoming and outgoing momenta and give some more explicit results.

Recall that we can decompose the anomalous dimension into a soft (S) and a collinear (C) part (see Sec. 3.2.6),

$$\begin{aligned} \gamma &= \gamma_{\text{C}}\mathbb{1} + \gamma_{\text{S}}, \\ \gamma_{\text{C}} &= \frac{\alpha}{\pi} \sum_i C_i \log\left(\frac{\bar{n}_i \cdot p_i}{\mu}\right) + \sum_i \gamma_i, \\ \gamma_{\text{S}} &= -\frac{\alpha}{\pi} \sum_{\langle ij \rangle} \left(\frac{1}{s_{\text{w}}^2} \mathbf{t}_i \cdot \mathbf{t}_j + \frac{1}{4c_{\text{w}}^2} \sigma_i Y_i \sigma_j Y_j \mathbb{1} \right) \log\left(-\eta_{ij} \frac{n_i \cdot n_j}{2} - i0\right), \end{aligned} \quad (5.37)$$

where we have introduced the sign factors defined in (4.10) along with η_{ij} defined as

$$\eta_{ij} = \begin{cases} 1 & \text{if both } i, j \text{ incoming or outgoing,} \\ -1 & \text{else,} \end{cases} \quad (5.38)$$

in order to obtain the correct $i\pi$ contributions if some momenta are outgoing. From now on, the hypercharges Y_i , isospin quantum numbers, and electric charges Q_i always refer to the particles. In (5.37), C_i refers to the EW Casimir invariant of particle i defined in (3.118). In the following we discuss the implementation of γ_{C} and γ_{S} separately. The terminology was introduced in Ref. [47], it should be stressed that the distinction of effects due to soft and collinear particle exchange is ambiguous on the level of Feynman diagrams: If all masses are set to zero, both soft and collinear diagrams are IR divergent and the individual diagrams depend on the IR regulator (see App. B for the computation). If the masses are kept finite, both soft and collinear diagrams are also divergent because of the collinear anomaly.

Collinear anomalous dimension

The collinear part is defined as the sum of the one-particle contributions

$$\gamma_{\text{C}}(\mu) = \sum_i \gamma_{\text{C},i}(\mu). \quad (5.39)$$

In (3.83) it can be seen clearly that γ_C contains the leading-logarithmic contribution completely. For a general gauge theory the collinear anomalous dimensions for gauge bosons and fermions are given by:

$$\gamma_{C,A_k} = \frac{\alpha_k}{4\pi} \left(4C_{A,k} \log \left(\frac{\bar{n}_i \cdot p_i}{\mu} \right) - \beta_{0,k} \right), \quad \gamma_{C,f} = \sum_{k=1}^2 \frac{\alpha_k C_{F,k}}{4\pi} \left(4 \log \left(\frac{\bar{n}_i \cdot p_i}{\mu} \right) - 3 \right), \quad (5.40)$$

with the respective Casimir invariants $C_{A,k}$, $C_{F,k}$, corresponding to the respective SU(2) Casimir representation and the hypercharge. The values for all SM particles are collected in App. B of Ref. [19].

The SM scalars are in the fundamental representation, their anomalous dimension has two modifications with respect to the fermion one:

- There is a different collinear factor for bosons [20], and
- there is an additional contribution related to the top-quark Yukawa coupling g_t .

This leads to the result:

$$\gamma_{C\Phi} = \sum_{k=1}^2 \frac{\alpha_k C_{F,k}}{4\pi} \left(4 \log \left(\frac{\bar{n}_i \cdot p_i}{\mu} \right) - 4 \right) + \frac{N_C g_t^2}{16\pi^2}. \quad (5.41)$$

The respective group-theoretical values are hard-coded for the SM.

Soft anomalous dimension

The angular-dependent logarithmic corrections to the matrix element are part of the soft anomalous dimension γ_S . It is defined as the non-trivial sum over pairs of external particles in (5.37). The matrix form is obtained by comprising all possible matrix elements in a vector,

$$\begin{pmatrix} \mathcal{M}^{\phi_1^{(1)} \dots \phi_n^{(1)}} \\ \vdots \\ \mathcal{M}^{\phi_1^{(m)} \dots \phi_n^{(m)}} \end{pmatrix}, \quad (5.42)$$

and filling the entries with the respective couplings. The neutral gauge-boson contribution to the soft anomalous dimension is hence a diagonal matrix

$$\gamma_{S,N} = -\frac{\alpha}{\pi} \text{Diag} (N_1, \dots, N_m) \quad (5.43)$$

with

$$N_k = \sigma_i \sigma_j \sum_{\langle ij \rangle} \left(\frac{Y_i^{(k)} Y_j^{(k)}}{4c_w^2} + \frac{I_i^{3(k)} I_j^{3(k)}}{s_w^2} \right) \log \left(\frac{-n_i \cdot n_j - i0}{2} \right), \quad (5.44)$$

with i, j running over the external particles and k indicating the respective transformed process. The off-diagonal elements of γ_S are obtained from the W^\pm couplings of the external particles

and the respective transformed matrix elements. In closed form they can be written as

$$(\gamma_S)_{kl} = -\frac{\alpha}{\pi s_w^2} \sum_{\langle ij \rangle} \prod_{n \neq i, j} \delta_{\phi_n^{(k)} \phi_n^{(l)}} \sum_{a=\pm} t_{\beta_i^{(k)} \beta_i^{(l)}}^a t_{\beta_j^{(k)} \beta_j^{(l)}}^{\bar{a}} \log \left(-\eta_{ij} \frac{n_i \cdot n_j}{2} - i0 \right) \quad (5.45)$$

for $k \neq l$. The indices $\beta_i^{(k)}$ denote the SU(2) indices of particle at position i of the process labelled by k . The symbol \bar{a} denotes the sign opposite to a . The expression is non-zero if W -boson couplings connect particles at positions i and j in the processes k and l . The Kronecker deltas assure that the entry is zero if more than one particle-pair transformation is needed to relate the processes k and l .

As an example, consider again the process $\bar{u}_L u_L \rightarrow e_L^+ e_L^-$. The correction can be written as

$$\delta \mathcal{M}_{\gamma_S}^{\bar{u}_L u_L e_L^+ e_L^-} = \exp \left(- \int_{\mu_1}^{\mu_h} d \log \mu \gamma(\mu) \right) \cdot \mathcal{M}_j \quad (5.46)$$

with

$$\mathcal{M} = \begin{pmatrix} \mathcal{M}^{\bar{u}_L u_L e_L^+ e_L^-} \\ \mathcal{M}^{\bar{d}_L d_L e_L^+ e_L^-} \\ \mathcal{M}^{\bar{d}_L u_L \bar{\nu}_L e_L^-} \\ \mathcal{M}^{\bar{u}_L d_L e_L^+ \nu_L} \\ \mathcal{M}^{\bar{u}_L u_L \bar{\nu}_L \nu_L} \\ \mathcal{M}^{\bar{d}_L d_L \bar{\nu}_L \nu_L} \end{pmatrix}. \quad (5.47)$$

The entries of the column vector can be recognised as the matrix elements of the operators in (5.23). Note that the last operator is not obtained from the first one via a single external-pair transformation, instead two of them are needed. Therefore, the last operator does not contribute at the one-loop level. It does nevertheless contribute to the exponential (5.14) because it is connected to the other operators via an external-pair transformation.

Using the Mandelstam variables, as usual defined via

$$s = (p_1 + p_2)^2 > 0, \quad t = (p_1 - p_3)^2 < 0, \quad u = (p_1 - p_4)^2 < 0, \quad (5.48)$$

we define the quantities [52]

$$\mathbb{L}_s = \log \left(\frac{s}{\mu_h^2} \right) - i\pi, \quad \mathbb{L}_t = \log \left(\frac{-t}{\mu_h^2} \right), \quad \mathbb{L}_u = \log \left(\frac{-u}{\mu_h^2} \right). \quad (5.49)$$

The $i\pi$ takes care of the correct analytical continuation of the complex logarithm according to the signs of s , t and u . These logarithms are used as building blocks for the off-diagonal elements of γ_S . Because in the given example the W -couplings are all identical, the matrix that is to be exponentiated has the following form:

$$\gamma_S = -\frac{\alpha}{4\pi s_w^2} \begin{pmatrix} s_w^2 N_1 & \mathbb{L}_s & \mathbb{L}_t & \mathbb{L}_t & \mathbb{L}_s & 0 \\ \mathbb{L}_s & s_w^2 N_2 & \mathbb{L}_u & \mathbb{L}_u & 0 & \mathbb{L}_s \\ \mathbb{L}_t & \mathbb{L}_u & s_w^2 N_3 & 0 & \mathbb{L}_u & \mathbb{L}_t \\ \mathbb{L}_t & \mathbb{L}_u & 0 & s_w^2 N_4 & \mathbb{L}_u & \mathbb{L}_t \\ \mathbb{L}_s & 0 & \mathbb{L}_u & \mathbb{L}_u & s_w^2 N_5 & \mathbb{L}_s \\ 0 & \mathbb{L}_s & \mathbb{L}_t & \mathbb{L}_t & \mathbb{L}_s & s_w^2 N_6 \end{pmatrix} \quad (5.50)$$

with the N_k defined according to (5.43). The off-diagonal entries can be read off by identifying the respective pair of particles that are transformed with respect to one another in the list of processes (5.23). If more than two particles have to be transformed, the entry is 0.

Path-ordered matrix exponential

As argued in Appendix A of Ref. [48], the path-ordering symbol can be ignored when exponentiating because $\gamma(\mu)$ commutes with itself for different values of μ . The key arguments are the following:

- The collinear anomalous dimension is proportional to the unit matrix and commutes with itself for different values of the scale.
- The soft anomalous dimension does not depend on μ at all.

We can therefore replace the path-ordered matrix exponential by a normal one. The matrix parts of the anomalous dimensions such as (5.50) have to be exponentiated using

$$\exp \mathbf{A} = \sum_{k=0}^{\infty} \frac{\mathbf{A}^k}{k!}. \quad (5.51)$$

To evaluate (5.51) numerically we cut off the sum at some finite order, which we choose to be $k = 6$. We have checked that the impact of including the $k = 6$ terms is already of the order of 10^{-5} with respect to the Born matrix element on the level of single phase-space points.

Integration over the scale

We have seen that, if the running of the gauge couplings is neglected, the anomalous dimension is a linear function of $\log \mu$ and thus easy to integrate, see (3.117). This formula is used if not stated otherwise. In some cases, the one-loop running of the EW gauge couplings is also be taken into account, in which case the integration is implemented via (3.121).

5.2.5. Low-scale corrections

The low-scale corrections are obtained from the one-loop operator matrix elements in SCET_{EW}. The respective Feynman graphs are of the type depicted in Fig. 3.3 with non-zero W-, Z-, Higgs-boson and top-quark masses. The regularisation techniques required for their calculation are described in Refs. [45, 46] and also in Sec. 3.3.3 of this work. The W-boson exchange graphs induce mixing between the operators, even though we are going to argue that at one-loop level the non-trivial matrix structure can be avoided.

In a given operator basis we define the one-loop matrix structure according to (3.123):

$$\langle \mathcal{O}_i^{1\text{-loop}} \rangle = \mathbf{D}_{ij}^{(1)} \langle \mathcal{O}_j^{\text{tree}} \rangle. \quad (5.52)$$

with $\mathbf{D}^{(1)}$ being composed of one-particle (“collinear”) and two-particle (“soft”) contributions. In analogy to the collinear and soft anomalous dimension we define the collinear and soft low-

scale corrections D_C and D_S , respectively:

$$\begin{aligned}
 D^{(1)}(\mu_1) &= \sum_i D_{C,i}(\mu_1) \mathbb{1} + D_S, \\
 D_S &= \sum_{\langle ij \rangle} \left[\sum_{a=\pm} \frac{\alpha}{2\pi s_w^2} \log\left(\frac{\mu_1^2}{M_W^2}\right) \mathbf{t}_i^a \cdot \mathbf{t}_j^{\bar{a}} + \frac{\alpha}{2\pi} \log\left(\frac{\mu_1^2}{M_Z^2}\right) \sigma_i I_i^Z \sigma_j I_j^Z \right. \\
 &\quad \left. + \frac{\alpha}{2\pi} \sigma_i Q_i \sigma_j Q_j \left(-\frac{1}{\epsilon_{\text{IR}}} + \log\left(\frac{\mu_1^2}{\mu_{\text{IR}}^2}\right) \right) \mathbb{1} \right] \log\left(-\eta_{ij} \frac{n_i \cdot n_j}{2} - i0\right) \quad (5.53)
 \end{aligned}$$

with Q_i and I_i^Z being the charges and Z-boson coupling of particle i , respectively. To obtain a maximally simple form for the low-scale corrections, we observe that, if the W and Z mass were equal, setting μ_1 and μ_{IR} to their mass would remove all two-particle corrections. Although this is not possible, we can choose

$$\mu_{\text{IR}} = \mu_1 = M_W. \quad (5.54)$$

With this choice the logarithms in (3.125) are removed and the only remaining logarithms in the Z-boson contributions of the $D_{C,i}$ are suppressed by a factor of $\log c_w^2 \approx 0.25$, see (3.124).

Besides this, the scale choice (5.54) has the advantage that the soft matching has no non-trivial matrix structure, as this again arises only because of the W-boson contributions in (5.53). The one-loop soft matching D_S is then only related to Z-boson exchange and becomes a unit matrix:

$$D_S = D_S \mathbb{1} = \frac{\alpha}{2\pi} \sum_{\langle ij \rangle} \log(c_w^2) \sigma_i I_i^Z \sigma_j I_j^Z \log\left(-\eta_{ij} \frac{n_i \cdot n_j}{2} - i0\right) \mathbb{1}. \quad (5.55)$$

The functions $D_{C,i}$ can be computed once for all SM particles, and the two-particle contributions can be constructed for each process in a similar way as the soft anomalous dimension.

Eventually the low-scale corrections (3.123) are implemented as

$$\mathcal{M} \rightarrow \mathcal{M} + \sum_i D_{C,i} \mathcal{M} + D_S \mathcal{M} \quad (5.56)$$

on the level of the matrix element in (5.14).

Field renormalisation and radiative corrections to the GBET

We already mentioned that the low-scale corrections contain also field-renormalisation contributions. For fermions, transverse gauge bosons, and the Higgs boson this simply means that the corresponding field-renormalisation constant $\delta Z_i/2$ is added to the loop contributions:

$$D_{C,i} = \frac{1}{2} \delta Z_i \Big|_{\mu_{\text{UV}}=\mu_1} + D_{C,i}^{\text{loop}}. \quad (5.57)$$

In the case of longitudinal gauge bosons, the δZ_i contribution is not present since the fields of the unphysical Goldstone bosons are not renormalised in our convention. Instead, one has to account for the fact that the GBET, i.e. the relations (3.97), get perturbative corrections. Therefore, the collinear matching for longitudinal gauge bosons contains the radiative correction

factors [see Eq. (3.97)]

$$\begin{aligned}
 D_{C,W_L} &= \left[-\frac{\Sigma_L^{WW}(M_W^2)}{M_W^2} - \frac{\Sigma^{W\phi}(M_W^2)}{M_W} + \frac{\delta M_W}{M_W} + \frac{1}{2}\delta Z_W \right]_{\mu_{UV}=\mu_1} + D_{C,W_L}^{\text{loop}}, \\
 D_{C,Z_L} &= \left[-\frac{\Sigma_L^{ZZ}(M_Z^2)}{M_Z^2} + i\frac{\Sigma^{Z\chi}(M_Z^2)}{M_Z} + \frac{\delta M_Z}{M_Z} + \frac{1}{2}\delta Z_{ZZ} \right]_{\mu_{UV}=\mu_1} + D_{C,Z_L}^{\text{loop}}. \quad (5.58)
 \end{aligned}$$

Sample results

As an example we give the results for D_C for left-handed up quarks and leptons, which would be necessary to calculate the process (5.16) [48]:

$$\begin{aligned}
 D_C^{\text{uL}} &= \frac{\alpha}{4\pi} \left((I_{\text{uL}}^Z)^2 D_Z + \frac{1}{2s_w^2} D_W + Q_u^2 D_\gamma \right), \\
 D_C^{\text{eL}} &= \frac{\alpha}{4\pi} \left((I_{\text{eL}}^Z)^2 D_Z + \frac{1}{2s_w^2} D_W + Q_e^2 D_\gamma \right), \quad (5.59)
 \end{aligned}$$

with the auxiliary functions

$$\begin{aligned}
 D_{W/Z} &= 2 \log \frac{M_{W/Z}^2}{\mu_1^2} \log \frac{\bar{n} \cdot p}{\mu_1} - \frac{1}{2} \log^2 \frac{M_{W/Z}^2}{\mu_1^2} - \frac{3}{2} \log \frac{M_{W/Z}^2}{\mu_1^2} - \frac{\pi^2}{2} + \frac{9}{4}, \\
 D_\gamma &= -\frac{c_\varepsilon}{\varepsilon^2} - \frac{c_\varepsilon}{\varepsilon} \left(\frac{3}{2} - \frac{1}{2} \log \frac{\bar{n} \cdot p}{\mu_{\text{IR}}} \right) + 2 \log \frac{\mu_{\text{IR}}^2}{\mu_1^2} \log \frac{\bar{n} \cdot p}{\mu_1} - \frac{1}{2} \log^2 \frac{\mu_{\text{IR}}^2}{\mu_1^2} - \frac{3}{2} \log \frac{\mu_{\text{IR}}^2}{\mu_1^2}, \quad (5.60)
 \end{aligned}$$

which occur for all fermion species. Note that the normalisation factor

$$c_\varepsilon \equiv \Gamma(1 + \varepsilon)(4\pi)^\varepsilon, \quad (5.61)$$

which is absorbed into the standard divergence following the conventions of Refs. [57, 126] leads to differences in the π^2 -terms, which is why in Ref. [48] the term $-\pi^2/2$ in $D_{W/Z}$ is replaced by $-5\pi^2/12$. This corresponds to the replacement

$$c_\varepsilon \rightarrow c'_\varepsilon = e^{-\gamma_E \varepsilon} (4\pi)^\varepsilon, \quad (5.62)$$

with γ_E denoting the Euler-Mascheroni constant.⁶

For each external up quark and electron the matrix element picks up a factor of $D_C^{\text{uL}}/D_C^{\text{eL}}$ respectively. With the choice (5.54) the two-particle contributions yield

$$D_S = \frac{\alpha}{2\pi} \log c_w^2 \left((I_{\text{eL}}^Z)^2 + (I_{\text{uL}}^Z)^2 \right) \mathbb{L}_s + 2I_{\text{eL}}^Z I_{\text{uL}}^Z (\mathbb{L}_t - \mathbb{L}_u) \mathbb{1}, \quad (5.63)$$

such that the total low-scale corrections for this process read

$$\delta \mathcal{M} = \left(2D_C^{\text{e}} + 2D_C^{\text{u}} + \frac{\alpha}{2\pi} \log c_w^2 \left((I_{\text{eL}}^Z)^2 + (I_{\text{uL}}^Z)^2 \right) \mathbb{L}_s + 2I_{\text{eL}}^Z I_{\text{uL}}^Z (\mathbb{L}_t - \mathbb{L}_u) \right) \mathcal{M}, \quad (5.64)$$

⁶Actually, at no place in Ref. [48] the convention (5.62) is explicitly formulated. In the original paper, Ref. [44], the 4π -contributions are dropped between (32) and (36), the γ_E -contributions between (36) and (37). In a similar calculation in Ref. [46], the convention (5.62) is explicitly mentioned after eq. (11).

with $L_{s/t/u}$ defined in (5.49).

5.2.6. Mixing at the low scale

In the operator basis we employ, there is one-to-one correspondence of fields in the physical basis at the low scale and fields in the symmetric basis at the high scale for all fermions and also for the W^\pm bosons. For processes with external photons, Z bosons, or Higgs bosons this not true. A mixing transformation has to be introduced, which we discuss in this section.

γ/Z -mixing

If we want to compute a process involving a photon or Z boson, the anomalous dimension and high-scale matching are conveniently expressed in terms of processes involving W^3 and B bosons. For these processes all aforementioned steps can be applied using the formulae in the previous sections. However, the low-scale contributions \mathbf{D} have to be calculated for mass eigenstates. One has to apply a forth-and-back transformation:

- Before (5.14) can be applied, a matrix element associated with external photons or Z bosons has to be decomposed into subamplitudes containing the $SU(2)$ colour eigenstates W^3/B .
- The anomalous dimension, the running, and the high-scale matching are calculated in this basis. Each subamplitude obtains its own correction factor, which depends only on the colour.
- Finally, the subamplitudes are transformed back into mass eigenstates and the low-scale corrections are calculated. They depend both on the colour and the mass eigenstate.

Repeatedly applying the transformation

$$\begin{pmatrix} A_\mu \\ Z_\mu \end{pmatrix} = \begin{pmatrix} c_w & -s_w \\ s_w & c_w \end{pmatrix} \begin{pmatrix} B_\mu \\ W_\mu^3 \end{pmatrix}, \quad (5.65)$$

one obtains for a matrix element involving n_γ photons and n_Z Z bosons

$$\begin{aligned} \mathcal{M}^{n_\gamma} &= \sum_{n_B+n_W=n_\gamma} (-s_w)^{n_W} c_w^{n_B} \mathcal{M}^{n_B n_W} = \sum_{n_B+n_W=n_\gamma} (-s_w)^{n_W} c_w^{n_B} C^{n_B n_W}(\mu_1) \langle \mathcal{O}^{n_B n_W} \rangle, \\ \mathcal{M}^{n_Z} &= \sum_{n_B+n_W=n_Z} s_w^{n_B} c_w^{n_W} \mathcal{M}^{n_B n_W} = \sum_{n_B+n_W=n_Z} s_w^{n_B} c_w^{n_W} C^{n_B n_W}(\mu_1) \langle \mathcal{O}^{n_B n_W} \rangle, \end{aligned} \quad (5.66)$$

respectively. Each contribution $\mathcal{M}^{n_B n_W}$ can now be treated completely separately. In particular, there is no cross talk between the different $\mathcal{M}^{n_B n_W}$ due to the soft anomalous dimension and soft matching, the respective matrices are block diagonal.

If both photons and Z bosons are present, the above transformations are applied successively, leading to

$$\mathcal{M}^{n_\gamma n_Z} = \sum_{n_W^{(\gamma)}+n_B^{(\gamma)}=n_\gamma} \sum_{n_W^{(Z)}+n_B^{(Z)}=n_Z} (-s_w)^{n_W^{(\gamma)}} c_w^{n_B^{(\gamma)}} s_w^{n_B^{(Z)}} c_w^{n_W^{(Z)}} \mathcal{M}^{n_W^{(\gamma)} n_B^{(\gamma)} n_B^{(Z)} n_W^{(Z)}}. \quad (5.67)$$

The one-particle low-scale SCET_{EW} corrections depend both on the SU(2) colour, which is determined by the W^3/B -field in the operator, and on the external mass, which is determined by the external momentum [48]. This leads to the following expression for the one-particle low-scale corrections associated with the photons and Z bosons:

$$\delta\mathcal{M}^{n_W^{(\gamma)} n_B^{(\gamma)} n_B^{(Z)} n_W^{(Z)}} = \left(n_W^{(Z)} D_C^{W^3 \rightarrow Z} + n_W^{(\gamma)} D_C^{W^3 \rightarrow \gamma} + n_B^{(Z)} D_C^{B \rightarrow Z} + n_B^{(\gamma)} D_C^{B \rightarrow \gamma} \right) \mathcal{M}^{n_W^{(\gamma)} n_B^{(\gamma)} n_B^{(Z)} n_W^{(Z)}} \quad (5.68)$$

with the various D_C factors collected in App. B.3.

The formula for the two-particle contributions in (5.53) can be applied in a straightforward manner on each subamplitude. Of course only the W^3 -fields in each operator get transformed. Their SU(2) partners are the W^\pm , therefore the corrections are written in terms of scattering amplitudes involving external W^\pm bosons.

Note that the above strategy is different from Ref. [19], where the mixing is taken into account by means of non-diagonal Casimir operators for the photon and the Z boson. While the two strategies are of course equivalent at any fixed order in perturbation theory, the resummation formula (5.14) can much easier be applied in the symmetric base because the collinear anomalous dimension $\gamma_C(\mu)$ is a block of unit matrices and commutes with itself for different values of μ :

$$\gamma_C(\mu) = \begin{pmatrix} \gamma_C^1(\mu)\mathbb{1} & \dots & 0 \\ \vdots & \ddots & \vdots \\ 0 & \dots & \gamma_C^n(\mu)\mathbb{1} \end{pmatrix}. \quad (5.69)$$

Here n denotes the number of processes in the symmetric basis. The exponentiation of the double logarithms can thus be performed for each subprocess individually.

Z/Higgs-mixing

The same strategy is applied for processes involving Higgs bosons or longitudinal Z-boson modes. The latter are represented by the neutral would-be Goldstone boson χ , which is the imaginary part of the lower component field of the Higgs doublet, ϕ_2 . The ϕ_2 is an I_3 - and hypercharge eigenstate, and therefore the natural choice for the construction of operators in the SySM. The transformation law reads

$$\begin{pmatrix} H \\ \chi \end{pmatrix} = \begin{pmatrix} \frac{1}{\sqrt{2}} & \frac{1}{\sqrt{2}} \\ -\frac{i}{\sqrt{2}} & \frac{i}{\sqrt{2}} \end{pmatrix} \begin{pmatrix} \phi_2 \\ \phi_2^* \end{pmatrix}. \quad (5.70)$$

Thus, a matrix element with n_H Higgs bosons and n_χ longitudinally polarised Z bosons has the hypercharge-eigenstate decomposition

$$\mathcal{M}^{n_H n_\chi} = \sum_{n_{\phi_2}^{(H)} + n_{\phi_2^*}^{(H)} = n_H} \sum_{n_{\phi_2}^{(\chi)} + n_{\phi_2^*}^{(\chi)} = n_\chi} \left(\frac{1}{\sqrt{2}} \right)^{n_{\phi_2}^{(H)}} \left(\frac{1}{\sqrt{2}} \right)^{n_{\phi_2^*}^{(H)}} \left(\frac{i}{\sqrt{2}} \right)^{n_{\phi_2}^{(\chi)}} \left(\frac{-i}{\sqrt{2}} \right)^{n_{\phi_2^*}^{(\chi)}} \mathcal{M}^{n_{\phi_2}^{(H)} n_{\phi_2^*}^{(H)} n_{\phi_2}^{(\chi)} n_{\phi_2^*}^{(\chi)}}. \quad (5.71)$$

The situation is simplified due to the fact that ϕ_2 and ϕ_2^* do not receive different low-scale corrections. Thus each subamplitude receives the correction

$$\delta\mathcal{M}^{n_{\phi_2}^{(H)} n_{\phi_2^*}^{(H)} n_{\phi_2}^{(\chi)} n_{\phi_2^*}^{(\chi)}} = \left(n_H D_C^{\phi \rightarrow H} + n_\chi D_C^{\phi \rightarrow Z_L} \right) \mathcal{M}^{n_{\phi_2}^{(H)} n_{\phi_2^*}^{(H)} n_{\phi_2}^{(\chi)} n_{\phi_2^*}^{(\chi)}}. \quad (5.72)$$

Coupling renormalisation constants

The last missing contribution needed to match the SCET_{EW} matrix element against the one in the full theory is the contribution associated with the coupling-constant renormalisation. For the renormalisation of the coupling constants as well as the weak mixing angle we adopt the on-shell scheme by default. This is in contrast to the approach in Refs. [45, 47], in which a scheme with a running electromagnetic coupling is employed. The pros and cons are:

- The logarithmic corrections associated with the running are not resummed if the on-shell scheme is used. Strictly speaking, an RGE-improved result beyond LL accuracy is not possible in the on-shell scheme.
- Within the on-shell scheme the G_F input scheme can be employed in order to use the decay constant of the muon as an input value. This is one of the most precisely measured quantities in particle physics.

It is obvious that at future colliders one is going to define an input scheme, which avoids large logarithms. Although such schemes are already under consideration (see e.g. Refs. [198, 199]), we stick to the on-shell scheme if not stated otherwise. This implies that we use the form (3.117) for the integrated anomalous dimension. The logarithmically enhanced corrections are included perturbatively in this case. Because the matching is calculated in the SySM, we introduce renormalisation constants associated with the U(1) and SU(2) coupling constants. They can be related to the usual SM renormalisation constants in an elementary way,

$$\begin{aligned} g_1 = \frac{e}{c_w} &\rightarrow \frac{\delta g_1}{g_1} = \frac{\delta e}{e} - \frac{\delta c_w}{c_w}, \\ g_2 = \frac{e}{s_w} &\rightarrow \frac{\delta g_2}{g_2} = \frac{\delta e}{e} - \frac{\delta s_w}{s_w}, \end{aligned} \quad (5.73)$$

with δs_w and δc_w being the on-shell renormalisation constants associated with the sine and cosine of the weak mixing angle. In the following we divide the calculation into two separate contributions: The logarithmically enhanced corrections and the finite remainder. The coefficients for the logarithms are related to the UV poles and can therefore be obtained from the RGE. They arise because the UV scale identified with μ_h is much larger than the EW scale. After the logarithmic part is split off, the finite part is simply obtained by setting $\mu_{UV} = \mu_1$ in the analytic expressions for the counterterms.

For some distributions we do study the influence of the running coupling, in which case the logarithmic part of δ_{PR} has to be set to zero. In turn we switch the integrated anomalous dimension to the form (3.121).

Logarithmic part

The coefficients of the logarithmically enhanced corrections can be determined from the β -function coefficients in Eq. (3.120) which are calculated from the self energies of the associated

gauge bosons according to

$$\begin{aligned}\beta_{0,1} &= -\frac{1}{3} \sum_{\varphi=\phi^{1/2}, f_L^{1/2}, f_R} \frac{\eta_\varphi Y_\varphi^2}{4}, \\ \beta_{0,2} &= \frac{11}{3} C_A - \frac{1}{3} \sum_{\varphi=\Phi, f_L} \frac{\eta_\varphi}{2},\end{aligned}\tag{5.74}$$

with Φ denoting the Higgs doublet with components $\phi^{1/2}$, f_L all left-handed doublets with components $f_L^{1/2}$, and the f_R the right-handed singlets. The η factors read $\eta_\Phi = 1$ and $\eta_{f_L} = \eta_{f_R} = 2$. Summation over the quark colours is implied.

Taking the renormalisation of the coupling constant and the weak mixing angle into account in a consistent way requires the decomposition of any SySM amplitude according to their respective power in the couplings. Using $\alpha_i = g_i^2/(4\pi)$, any subamplitude $\mathcal{M}_{n_1 n_2}$ proportional to $g_1^{n_1} g_2^{n_2}$ thus receives logarithmic corrections

$$\delta \mathcal{M}_{n_1 n_2}^{\log} = \delta_{\text{PR}, n_1 n_2}^{\log} \mathcal{M}_{n_1 n_2} = - \left(n_1 \frac{\alpha_1}{4\pi} \beta_0^{\text{U}(1)} + n_2 \frac{\alpha_2}{4\pi} \beta_0^{\text{SU}(2)} \right) \log \frac{\mu_h^2}{\mu_1^2} \mathcal{M}_{n_1 n_2}\tag{5.75}$$

from the respective counterterm contributions. Both the finite part of the field-renormalisation constants (5.57) and the radiative corrections to the GBET (5.58) are calculated using the one-loop library COLLIER [126].

Finite part

In addition, there are finite remainders

$$\delta \mathcal{M}_{n_1 n_2}^{\text{fin}} = \delta_{\text{PR}, n_1 n_2}^{\text{fin}} \mathcal{M}_{n_1 n_2} = \left((n_1 + n_2) \frac{\delta e}{e} - n_1 \frac{\delta c_w}{c_w} - n_2 \frac{\delta s_w}{s_w} \right) \Big|_{\mu_{\text{UV}} = \mu_1} \mathcal{M}_{n_1 n_2}.\tag{5.76}$$

These as well as the charge renormalisation constant δe have to be calculated in the broken phase of the SM. Finally, the contribution δ_{PR} in (5.14) is obtained as the sum of the logarithmically enhanced and the finite corrections. For processes involving the top-quark Yukawa coupling or the quartic Higgs coupling at tree level, the respective coupling constants

$$g_t = \frac{g_2 m_t}{\sqrt{2} M_W}, \quad \lambda = \frac{g_2^2 M_H^2}{2 M_W^2}\tag{5.77}$$

have to be treated analogously. The respective β -functions are somewhat more involved because several different contributions have to be considered when renormalising the respective vertex. The one-loop results read [200]

$$\frac{\beta^{g_t}}{g_t}(g_1, g_2, g_t) = -\frac{17}{12} \frac{\alpha_1}{4\pi} - \frac{9}{4} \frac{\alpha_2}{4\pi} + \frac{9}{2} \frac{g_t^2}{16\pi^2} + \mathcal{O}(g_i^4)\tag{5.78}$$

for the top-quark Yukawa coupling and [201]

$$\beta_\lambda(g_1, g_2, g_t, \lambda) = \frac{1}{4\pi} \left(\frac{3}{4}\lambda^2 + \frac{3}{2}g_t^2\lambda - 3g_t^4 + \frac{9}{16}g_2^4 + \frac{3}{8}g_1^2g_2^2 + \frac{3}{16}g_1^4 - \frac{9}{8}\lambda g_2^2 - \frac{3}{8}\lambda g_1^2 \right) + \mathcal{O}(g_i^6) \quad (5.79)$$

for the quartic scalar coupling. In analogy to (5.76) the respective finite contributions read

$$\delta\mathcal{M}_{n_t} = n_t \left(\frac{\delta e}{e} + \frac{\delta m_t}{m_t} - \frac{\delta M_W}{M_W} - \frac{\delta s_w}{s_w} \right) \Big|_{\mu_{UV}=\mu_1} \mathcal{M}_{n_t} \quad (5.80)$$

for the case of Yukawa coupling and

$$\delta\mathcal{M}_{n_\lambda} = 2n_\lambda \left(\frac{\delta e}{e} + \frac{\delta m_H}{m_H} - \frac{\delta M_W}{M_W} - \frac{\delta s_w}{s_w} + \frac{e}{2s_w} \frac{\delta t}{M_W M_H^2} \right) \Big|_{\mu_{UV}=\mu_1} \mathcal{M}_{n_\lambda} \quad (5.81)$$

in case of the Higgs self-interaction. However, we stress that both these and the Yukawa-coupling parts are not yet implemented in the code.

Decay corrections

So far, we have discussed the contributions to the production process, that are treated with SCET_{EW}. The corrections to the full processes require also the NLO corrections to the decay of the bosons. They do not contain large logarithms, but have to be evaluated using the full mass dependence (at least as far as $M_{W/Z/H/t}$ are concerned). To this end we use a second instance of RECOLA1 that works within the SM. It is, however, not required to evaluate the decay processes at NLO for every phase-space point.

For a given set of momenta $\{p\}$ in the full (production and decay) process, the corrections to the squared matrix element read (remember that interference contributions are neglected, and we suppress the non-factorisable corrections for simplicity here)

$$\delta|\mathcal{M}_\lambda(\{p\})|^2 = \delta|\mathcal{M}_{\lambda,\text{prod}}(\{p\})|^2 |\mathcal{M}_{\lambda,\text{LO,Dec}}(\{p\})|^2 + |\mathcal{M}_{\lambda,\text{LO,prod}}(\{p\})|^2 \delta|\mathcal{M}_{\lambda,\text{Dec}}(\{p\})|^2. \quad (5.82)$$

In the following, we argue that $\delta|\mathcal{M}_{\lambda,\text{Dec}}(\{p\})|^2$ can be constructed using $\{p\}$ -independent building blocks, which have to be evaluated at NLO and some $\{p\}$ -dependent tree-level quantities. Writing the square of the decay matrix element of a boson of spin λ into two massless fermions with helicities s, s' as

$$|\mathcal{M}_\lambda^{ss'}|^2 = |\mathcal{M}_{\lambda,\text{LO}}^{ss'}|^2 (1 + 2\delta_\lambda^{ss'} + \mathcal{O}(\alpha^2)), \quad (5.83)$$

we can use the following observations:

- The correction factor $\delta_\lambda^{ss'} = \delta^{ss'}$ does not depend on λ because the polarisation definitions are ambiguous in the rest frame.
- Moreover, $\delta^{ss'}$ does not depend on momenta and can be calculated in the rest frame of the boson once and for all.

While the first point is obvious, the second one requires justification. We demonstrate it by means of the Z-boson decay. Using the chiral projection operators (5.21), we can write the LO matrix element for the decay of a Z boson with momentum k into two massless left-handed (−) or right-handed (+) fermions with momenta p and q as

$$\mathcal{M}_0^\pm = \bar{u}(p)\omega_\mp \not{\epsilon}(k)(g_f^- \omega_- + g_f^+ \omega_+)\omega_\pm v(q), \quad (5.84)$$

with the left-handed and right-handed form factors g_f^- and g_f^+ . At one-loop g_f^+ and g_f^- receive different correction factors δg_f^+ and δg_f^- . Using $\omega_\pm \not{\epsilon} = \not{\epsilon} \omega_\mp$, we obtain for the ratio between the one-loop and tree-level matrix element:

$$\delta^{\pm\mp} = \frac{\mathcal{M}_1^\pm}{\mathcal{M}_0^\pm} = \frac{\bar{u}(p)\not{\epsilon}(k)\omega_\pm(\delta g_f^- \omega_- + \delta g_f^+ \omega_+)\omega_\pm v(q)}{\bar{u}(p)\not{\epsilon}(k)\omega_\pm(g_f^- \omega_- + g_f^+ \omega_+)\omega_\pm v(q)} = \frac{\delta g_f^\pm}{g_f^\pm}. \quad (5.85)$$

The last expression depends only on masses but not on any angles and can be calculated only once for each external spin configuration $ss' = \pm\mp$. For massless fermions the other configurations do not contribute.

Using this, the $\delta|\mathcal{M}_{\lambda,\text{Dec}}(\{p\})|^2$ in (5.82) are obtained as

$$\delta|\mathcal{M}_{\lambda,\text{Dec}}(\{p\})|^2 = \frac{\sum_{ss'} 2\delta^{ss'} |\mathcal{M}_{\lambda,\text{LO}}^{ss'}(\{p\})|^2}{\sum_{ss'} |\mathcal{M}_{\lambda,\text{LO}}^{ss'}(\{p\})|^2} \quad (5.86)$$

and thus depend on the external momenta only via tree-level matrix elements. Therefore, we calculate $\delta^{ss'}$ before starting the actual integration and simply add the second term in (5.82) with $\delta|\mathcal{M}_{\lambda,\text{Dec}}(\{p\})|^2$ obtained as above for each phase-space point.

On the one hand this saves computation time, there is, however, an even more important technical aspect: RECOLA1, which calculates the decay, and RECOLA2, which calculates the production matrix elements, share the same entity of the loop-integral library COLLIER. COLLIER on the other hand has to be initialised every time it is used by a new user. While it is reasonable to initialise COLLIER multiple times during before the actual phase-space integration, re-initialising it for every new momentum configuration is of course senseless.

5.3. Logarithm counting

In this section we describe the counting of large logarithms within SCET and fixed-order computations and specify which sets of terms we include in our calculations. It is important to be aware of the rather disparate conventions in the SCET and the fixed-order literature. An extensive discussion on different log-counting schemes in QCD and SCET can be found in Ref. [202].

Which terms are present?

The occurring contributions in any SM scattering amplitude computed in fixed-order perturbation theory can schematically be arranged as [45]

$$\mathcal{M} = \begin{pmatrix} 1 \\ \alpha L^2 & \alpha L & \alpha & \alpha^2 L & \alpha^2 \\ \alpha^2 L^4 & \alpha^2 L^3 & \alpha^2 L^2 & & \\ \alpha^3 L^6 & \alpha^3 L^5 & \dots & & \\ \vdots & & & & \end{pmatrix} \quad (5.87)$$

with

$$L = \log \left(\frac{s}{M_W^2} \right). \quad (5.88)$$

The notation in (5.87) implies that all entries are multiplied with some coefficients and added up. The first column of (5.87) is in fixed-order computations commonly referred to as the leading-logarithmic (LL_{FO}), the second one as the next-to-leading logarithmic (NLL_{FO}), and the n th column as the $N^{(n-1)}$ LL_{FO} contribution. Note further that within electroweak precision physics, using the notion of, for instance, NNLL does not necessarily imply that *all* terms in the second column in (5.87) are calculated. Instead the “two-loop corrections in NNLL” [21, 51] refers specifically to the $\alpha^2 L^2$ contribution. This is worth noting because both in the QCD and SCET literature the term NNLL usually implies that something is resummed.

When the SCET_{EW} approach is applied, the scattering amplitude is obtained as an exponential. Because it can completely be decomposed into sum-over-pair contributions, the expansion for its logarithm is the same as the result for the Sudakov form factor obtained in Refs. [203–205]:

$$\log \mathcal{M} = \begin{pmatrix} \alpha L^2 & \alpha L & \alpha & \alpha^2 L & \alpha^2 \\ \alpha^2 L^3 & \alpha^2 L^2 & \alpha^2 L^1 & & \\ \alpha^3 L^4 & \alpha^3 L^3 & \dots & & \\ \vdots & & & & \end{pmatrix}, \quad (5.89)$$

with the first column(s) again being defined as the LL_{SCET}, NLL_{SCET}, ..., $N^{(n-1)}$ LL_{SCET} contribution. These two log-counting schemes differ by subleading contributions: Exponentiating the first column of (5.89) does not only reproduce the first column of (5.87) but additional subleading terms that are related to the running coupling constants α_1 , α_2 . This can be seen from the fact that without the running couplings the anomalous dimension depends linearly on $\log \mu$ to all orders in α . After integrating over $\log \mu$ one is thus left with terms up to $\mathcal{O}(L^2)$ and the only term in the first column of (5.89) is the αL^2 -term, see (3.117). All terms below ($\alpha^2 L^3$, $\alpha^3 L^4$, ...) are therefore related to the running couplings.

Furthermore, one should note that in order to fix precisely which terms to include at which order in the calculation, one needs to know the hierarchy between α and L . In Ref. [45] this is sketched for two cases: First, the case of $\alpha L = \mathcal{O}(1)$ (LL regime) has been considered. This would require a full NLL_{SCET} resummation including all running effects in order to have a useful perturbation series.

The second case is $\alpha L^2 = \mathcal{O}(1)$ (LL2 regime), which naively corresponds to

$$\sqrt{s} \approx 27 \text{ TeV}. \quad (5.90)$$

However, one has to have in mind that finite prefactors in front of L can push this limit down to energy scales in the range of a few TeV. It is therefore to be expected that e.g. the CLIC collider accesses this regime. When $\alpha L^2 = \mathcal{O}(1)$, the terms in (5.87) and (5.89) are of the orders of magnitude

$$\mathcal{M} = \begin{pmatrix} 1 & & & & \\ 1 & \alpha^{1/2} & \alpha & & \\ 1 & \alpha^{1/2} & \alpha & \alpha^{3/2} & \alpha^2 \\ 1 & & & \dots & \\ \vdots & & & & \end{pmatrix}, \quad \log \mathcal{M} = \begin{pmatrix} 1 & \alpha^{1/2} & \alpha & & \\ \alpha^{1/2} & \alpha & \alpha^{3/2} & \alpha^2 & \\ \alpha & \alpha^{3/2} & \alpha^2 & \alpha^{5/2} & \alpha^3 \\ \alpha^2 & & \dots & & \\ \vdots & & & & \end{pmatrix}, \quad (5.91)$$

respectively. Here, the first columns have to be resummed, while terms of $\mathcal{O}(\alpha^{1/2})$, $\mathcal{O}(\alpha)$ have to be included at least perturbatively. A resummation of the $\alpha^{1/2}$ -terms may also be necessary to achieve high accuracy. Note also that these numbers are merely a vague order of magnitude (the actual corrections depend heavily on the finite prefactors such as s_w , 4π , the Casimir operators and more).

Which terms do we include?

To investigate the impact of the respective grades of resummation we would like to define a LL resummation scheme, which includes the single-logarithmic terms ($\mathcal{O}(\alpha^{1/2})$ in the LL2 regime) perturbatively. This is ambiguous because it depends on whether these terms are included via (5.87) or (5.89). To make this difference more explicit, consider the exponentiated form of (5.89) without running coupling,

$$\mathcal{M} = \exp(\alpha L^2 + \alpha L + \mathcal{O}(\alpha^2)) = \exp(\alpha L^2) \exp(\alpha L + \alpha + \mathcal{O}(\alpha^2)). \quad (5.92)$$

Consistently expanding the whole expression in α reproduces the terms in (5.87) order by order. If, however, only the leading term shall be resummed, there are two possibilities to add the αL and α terms:

- Expand the second factor on the r. h. s. above to $\mathcal{O}(\alpha)$: This results in

$$\mathcal{M}_{\text{NLLFO}} = \exp(\alpha L^2)(1 + \alpha L + \alpha). \quad (5.93)$$

- Set the second exponential to 1 and add the αL and α terms in directly from (5.87):

$$\mathcal{M}_{\text{LL}} = \exp(\alpha L^2) + \alpha L + \alpha. \quad (5.94)$$

The difference between the two formulae is subleading [of $\mathcal{O}(\alpha^2 L^3)$], but may still be sizeable. While (5.93) can be expected to describe the data better, (5.94) is directly related to the NLO

fixed-order result via exponentiating the respective one-loop leading logarithms.⁷ This is not always as trivial as it looks like: For processes with Z bosons or photons the one-loop leading logarithmic corrections induce mixing of different processes due to the non-diagonal Casimir operators [19]. Since (5.93) coincides with the first and second column of (5.87), we refer to it as NLL_{FO}.

We therefore investigate the following combinations of contributions:

$$\begin{aligned}
\text{LL+NLO} &= \exp(\alpha L^2) + \alpha L + \alpha, \\
\text{LL+NLO+running} &= \exp(f_0^{\text{EWSM}}(\alpha_1, \alpha_2)) + \alpha L + \alpha, \\
\text{NLL}_{\text{FO}}+\text{NLO} &= \exp(\alpha L^2)(1 + \alpha L) + \alpha, \\
\text{NLL+NLO} &= \exp(\alpha L^2 + \alpha L) + \alpha,
\end{aligned}
\tag{5.95}$$

with $f_0^{\text{EWSM}}(\alpha_1, \alpha_2)$ being defined in (3.121). The supplement “+NLO” refers to the one-loop order of matching. In the last line we also neglected the $\alpha^2 L^2$ -term associated with the two-loop anomalous dimension, which is rather involved due to the mixing of the several coupling constants of the SM. In addition its estimated impact is small ($< 1\%$ at $\sqrt{s} = 4 \text{ TeV}$ [45]).

5.4. Technical setup

In the previous section we described in detail the implementation of all ingredients of the SCET_{EW} computation. To obtain numerical predictions for collider observables, they have been integrated in the event generator MOCANLO. MOCANLO is an in-house multichannel MC integration program that can calculate NLO QCD+EW cross sections on the level of weighted events to (in principle) arbitrarily complicated SM processes. It features both off-shell and pole-approximated computations and has been used for the computation of full NLO corrections of VBS [206–209], $t\bar{t}W$ production [210], and tZj production [211].

The programs used for the different parts of the computation and their dependencies are collected in the flowchart Fig. 5.1. LHAPDF is of course only used if protons in the initial-state are considered. The most delicate issue from the interface point of view is the usage of COLLIER: It is used for the decay correction by RECOLA1, for the one-loop high-scale matching by RECOLA2, and finally explicitly by MOCANLO to evaluate the loop-integrals in the low-scale matching matrix. It has to be assured that the COLLIER parameters such as the scale variables $\mu_{\text{UV/IR}}$ are set consistently, otherwise there are inconsistent numbers without any warning (COLLIER is not “thread-safe” in the sense that it is not designed to be run by more than one instance at a time.).

One should thus conclude that this approach requires some care, especially regarding the consistent use of COLLIER, but the given resources are exploited in an efficient manner.

⁷Another source of deviation between fixed order and LL+NLO in our implementation are the NLO contributions from the transformed processes in the factorisation formula. This effect is, however, of $\mathcal{O}(\alpha^2 L)$ compared to $\mathcal{O}(\alpha^2 L^4)$ for the double-log resummation.

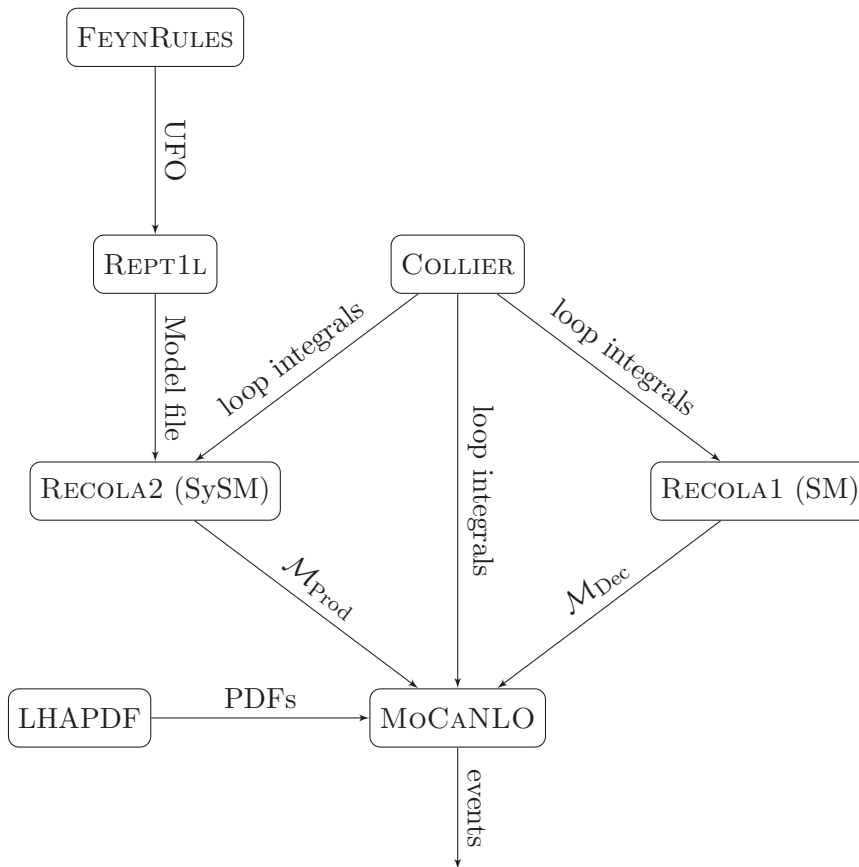


Figure 5.1.: Used software and dependencies in the setup

6. Results for the FCC–hh setup

6.1. Numerical input and setup

We use the SM input parameters

$$\begin{aligned}
 M_W^{\text{OS}} &= 80.385 \text{ GeV}, & \Gamma_W^{\text{OS}} &= 2.085 \text{ GeV}, \\
 M_Z^{\text{OS}} &= 91.1876 \text{ GeV}, & \Gamma_Z^{\text{OS}} &= 2.4952 \text{ GeV}, \\
 M_H &= 125 \text{ GeV}, & \Gamma_H &= 4.07 \cdot 10^{-3} \text{ GeV}, \\
 m_t &= 173.21 \text{ GeV}, & G_F &= 1.166138 \cdot 10^{-5} \text{ GeV}^{-2}.
 \end{aligned} \tag{6.1}$$

Note that the pole masses and widths, which are used as input parameters within the complex-mass scheme, are related to the on-shell quantities via

$$M_{W/Z}^{\text{pole}} = \frac{\left(M_{W/Z}^{\text{OS}}\right)^2}{\sqrt{\left(M_{W/Z}^{\text{OS}}\right)^2 + \left(\Gamma_{W/Z}^{\text{OS}}\right)^2}}, \quad \Gamma_{W/Z}^{\text{pole}} = \frac{M_{W/Z}^{\text{OS}}\Gamma_{W/Z}^{\text{OS}}}{\sqrt{\left(M_{W/Z}^{\text{OS}}\right)^2 + \left(\Gamma_{W/Z}^{\text{OS}}\right)^2}}, \tag{6.2}$$

see (4.53). As we use the Fermi constant as an input parameter, the EW coupling constant α is a derived quantity and is expressed in terms of the input as follows:

$$\alpha = \frac{\sqrt{2}G_F M_W^2}{\pi} \left(1 - \frac{M_W^2}{M_Z^2}\right). \tag{6.3}$$

For all diboson production processes we consider two different collider setups:

- FCC–hh setup: production in pp collisions with a centre-of-mass energy of 100 TeV.
- CLIC setup: production from an e^+e^- pair with a centre-of-mass energy of 3 TeV.

For all calculations in the FCC–hh setup, we use the NNPDF3.1QED PDF set [212] within the LHAPDF framework [213]. Within this PDF set the photon PDF is computed from the structure functions [214] obtained from deep-inelastic scattering data, according to the strategy presented in Ref. [215]. The QCD-related input parameters, i.e. the strong coupling constant, the number of flavours, and the factorisation scale read

$$\alpha_s(M_Z) = 0.118, \quad N_f = 5, \quad \mu_F = M_W^{\text{pole}}. \tag{6.4}$$

These values enter only in the PDFs. Throughout all calculations we neglect flavour-mixing effects, the CKM matrix is therefore set to unity. This allows us to directly sum production channels involving quarks of different generations via PDF merging. In the following we abbre-

viate the contributions from several partonic channels as

$$d\bar{d} + s\bar{s} + b\bar{b} \rightarrow d\bar{d}, \quad u\bar{d} + c\bar{s} \rightarrow u\bar{d}, \quad u\bar{u} + c\bar{c} \rightarrow u\bar{u}. \quad (6.5)$$

Hence, when a $d\bar{d}$ contributions is mentioned, we actually mean the sum of all down-type quark channels.

Event selection

We consider processes of the form

$$pp \rightarrow VV' \rightarrow 4\ell, \quad (6.6)$$

with $V, V' \in \{W^\pm, Z\}$. We define the fiducial phase space via the event-selection cuts

$$p_{T,\ell} > 20 \text{ GeV}, \quad |y_\ell| < 2.5, \quad m_{\text{inv},\ell\ell'} > 10 \text{ GeV}, \quad (6.7)$$

with ℓ, ℓ' denoting all charged leptons. Note that no $p_{T,\text{miss}}$ cut is applied in processes involving W bosons. In addition we imply the condition that the μ^\pm/e^\pm pairs are located around the Z resonance:

$$81 \text{ GeV} < M_{\mu^+\mu^-} < 101 \text{ GeV}, \quad 81 \text{ GeV} < M_{e^+e^-} < 101 \text{ GeV}, \quad (6.8)$$

which roughly corresponds to

$$M_Z - 5\Gamma_Z \lesssim M_{\mu^-\mu^+} \lesssim M_Z + 5\Gamma_Z, \quad M_Z - 5\Gamma_Z \lesssim M_{e^+e^-} \lesssim M_Z + 5\Gamma_Z. \quad (6.9)$$

The Z resonance is thus contained in the fiducial phase space. This cut distinguishes the Z production signal from the respective photon production process with the identical final state. A tighter cut further improves the signal-to-background ratio, but on the other hand leads to less statistics.

Photons are recombined with leptons if

$$\Delta R_{\ell\gamma} = \sqrt{(y_\ell - y_\gamma)^2 + (\Delta\phi_{\ell\gamma})^2} < 0.1, \quad (6.10)$$

where $\Delta\phi_{\ell\gamma}$ denotes the azimuthal distance of the lepton and the photon and y_ℓ, y_γ their rapidities.

For the SCET_{EW} calculations, the condition

$$s, t, u > M_W^2, \quad (6.11)$$

with s, t, u being the usual Mandelstam variables in the partonic production process

$$q\bar{q}/\gamma\gamma \rightarrow VV', \quad (6.12)$$

is enforced by means of an additional technical cut: If SCET_{EW} is applied, the event is discarded if (6.11) is not fulfilled. This effectively restricts the fiducial phase space, we define the high-

energy phase space (HEPS) to be:

$$d\Pi_{\text{HEPS}} = d\Pi_{s,t,u > M_W^2}. \quad (6.13)$$

All differential and integrated quantities calculated within SCET_{EW} are defined on the HEPS, while results evaluated in the Standard Model are computed on the full phase space.

Assumptions on the experimental setup

In order to estimate the impact of our results on actual expected experimental outcomes, we assume an integrated luminosity of [15]

$$\mathcal{L}_{\text{int}}^{\text{FCC-hh}} = 20 \text{ ab}^{-1} \quad (6.14)$$

for the FCC–hh. Hence the number of expected events in a certain phase-space region is given by

$$N_{\text{ev}} = \mathcal{L}_{\text{int}} \cdot \sigma. \quad (6.15)$$

For instance, requiring a number of $N_{\text{ev}} = 100$ events in a bin implies a minimal cross section of $\sigma = 5 \text{ ab}$ in the FCC–hh setup.

6.2. Processes under consideration

In this section we summarize some properties of the diboson processes under investigation. On this occasion we briefly discuss the status of their experimental and theoretical investigation. A more exhaustive overview over the progress of especially the calculation of EW radiative corrections can be found in Ref. [180].

6.2.1. W^+W^- production from fermions

W-boson pair production in pp collisions is predominantly mediated through partonic subprocesses of the type

$$q\bar{q} \rightarrow W^+W^- \rightarrow \mu^+\nu_\mu\bar{\nu}_e e^- \quad (6.16)$$

and has been studied extensively in the past both in theory and experiment. The closely related leptonic production process,

$$e^+e^- \rightarrow W^+W^- \rightarrow \mu^+\nu_\mu\bar{\nu}_e e^-, \quad (6.17)$$

was the first process used to directly test the non-Abelian couplings of the EW gauge bosons at LEP [77, 79, 80, 216]. Also a direct detection of longitudinally polarised W bosons was achieved [78]. Later the production cross section for (6.16) was measured to higher precision at the LHC [84, 90, 92, 217].

Decreasing experimental errors motivated the computation of higher-order corrections including both NNLO QCD and NLO EW contributions in the on-shell approximation [102, 218, 219] as well as including off-shell effects [113, 121] and matching to parton showers [125]. The combination of NNLO QCD and NLO EW corrections has been presented in Ref. [124].

The high-energy behaviour of the processes (6.16) and (6.17) has e.g. been investigated in Refs. [19, 220, 221] pointing out the large logarithmic corrections. A resummation of those by means of IR evolution equations has been presented in Refs. [21, 51].

6.2.2. W^+W^- production from photons

Besides quarks and gluons also photons have a probability to be found in the proton and thus have to be included as possible initial-state particles. We thus consider the process

$$\gamma\gamma \rightarrow W^+W^- \rightarrow \mu^+\nu_\mu\bar{\nu}_e e^- . \quad (6.18)$$

While the first QCD corrections to this partonic process arise as two-loop corrections to the photon self energy, NLO EW corrections to $\gamma\gamma \rightarrow W^+W^-$ have first been calculated in Ref. [104]. Predictions for diboson production at a hypothetical photon–photon collider including EW radiative corrections have been presented in Refs. [108, 109], and for the LHC in Refs. [111, 117, 222]. Because of its sensitivity to the quartic EW gauge couplings, it has also been studied intensively in the ATLAS [82, 87] and CMS experiments [89, 90, 94]. These studies consider mainly elastic pp scattering.

Often the photonic production channel is treated as a higher-order correction, meaning that its tree-level value is treated as part of the NLO EW contributions to the pp cross section (see for instance Ref. [113]) because of the suppression due to the small photon PDFs. In the study of W^+W^- production the γ -induced channel has occasionally been promoted to an unsuppressed partonic channel though, see for instance Ref. [117]. Throughout this work we treat the photon channel like a different process. This is motivated by several facts:

- The Sudakov corrections are particularly large for this process since it involves four gauge bosons with numerically larger EW Casimir invariants,
- It is a VBS process: Since the leading EW logarithms depend only on the external particles, results obtained for $\gamma\gamma \rightarrow W^+W^-$ might hint at what is to be expected for more complicated scattering processes, such as W^+W^+ scattering. In addition, this process has not yet been considered in the context of SCET_{EW} or IR evolution. We point out that especially the high-scale matching is much more involved than in the other diboson processes, making it particularly well-suited for an automated computation.
- In elastic pp scattering the process can actually be distinguished experimentally (classified as observed in 2020, see Ref. [87]) from the quark-induced channels: if the protons remain intact, the production of a colour-singlet final state such as two EW gauge bosons can only be mediated by colour-singlet exchange, the quark-induced production is therefore prohibited by colour conservation.
- The cross section of the production process $\gamma\gamma \rightarrow W^+W^-$ is constant in the high-energy limit, in contrast to the quark-initiated processes, which drop like $1/s$. Therefore its relevance can be expected to grow for higher energies.

In Fig. 6.1 we show the differential distributions in the four-lepton invariant mass and the $e^-\mu^+$ invariant mass for the $\gamma\gamma$ -induced channel together with the sum of the $\bar{q}q$ -induced ones.

The photon-induced process accounts for roughly one percent of the total hadronic cross section, which is dominated by the first bin. Even though the influence increases to 5–10% in

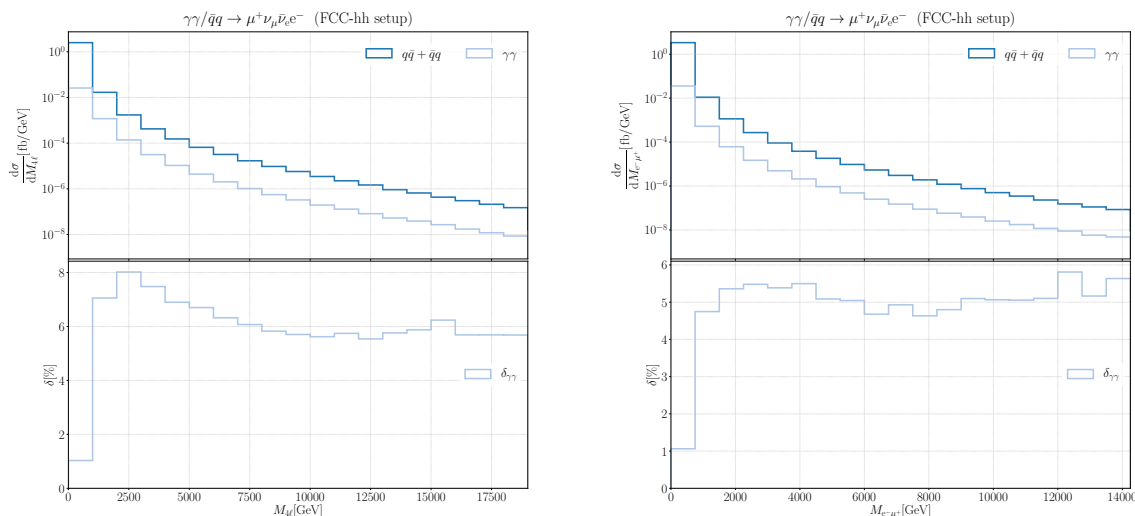


Figure 6.1.: Differential distributions in the four-lepton invariant mass and the $e^-\mu^+$ invariant mass for $\gamma\gamma \rightarrow W^+W^- \rightarrow \mu^+\nu_\mu\bar{\nu}_e e^-$, compared to the sum of all channels of $q\bar{q}/\bar{q}q \rightarrow e^-\bar{\nu}_e\mu^+\nu_\mu$. The bottom curves show the ratio of the two: $\delta_{\gamma\gamma} = \frac{d\sigma^{\gamma\gamma}/d\mathcal{O}}{d\sigma^{pp}/d\mathcal{O}}$.

the other bins, a strong enhancement in the high-energy tail does not show up. On the one hand this is an effect of the phase-space cuts: Because the photon-induced production is dominated by production along the beam axis (for a more detailed discussion of this point see Sec. 6.3.4), it is stronger affected by lepton- p_T cuts. On the other hand, in the high-energy limit non-doubly-resonant production channels can become important, which have a more complicated high-energy behaviour: In Ref. [214] the $\gamma\gamma$ -induced contributions to W^+W^- have been found to account for 35% relative to the quark-induced channels at a WW invariant mass of ~ 3 TeV at the LHC. But this has been calculated in the approximation of stable W bosons. This assumption is not quite valid for very high scattering energies as we see in Sec. 6.3.1.

6.2.3. W^+Z production

Moreover we consider the process¹

$$pp \rightarrow W^+Z \rightarrow \nu_e e^+ \mu^+ \mu^- . \quad (6.19)$$

The only partonic subprocesses have a $q\bar{q}'$ pair in the initial state, predominantly $u\bar{d}$. Despite its smaller cross section with respect to the other diboson processes, precise experimental analyses (a total error on the cross section of the order of a few percent) have been performed both with [86, 98] and without polarisation effects [83, 88, 93, 97].

On the theory side the radiative corrections of NLO QCD [101, 223] and in the following NNLO QCD [122] and NLO EW corrections [112, 116] have been calculated over the last decades.

¹The respective “conjugate” W^-Z -production process is not considered here. As its characteristics are the same, the two processes can be viewed as the same processes and for instance be summed up in an experimental analysis in order to obtain more statistics.

6.2.4. ZZ production

ZZ production at the LHC has been investigated within the ATLAS and CMS experiments [81, 85, 91, 95], taking both the decay channel with four charged leptons and the $2\ell 2\nu$ -decay channel into account. Throughout this work we focus on the process with four charged leptons in the final state:

$$pp \rightarrow ZZ \rightarrow e^+e^-\mu^+\mu^-. \quad (6.20)$$

The NLO QCD corrections have been known for a long time [99, 100, 103, 224] and have been extended to NNLO accuracy during the last decade [118, 119, 123]. EW corrections in pole approximation have been calculated in Refs. [107, 112] and with off-shell effects in Refs. [114, 115, 124]. In Ref. [76] a matching of full EW corrections against parton-shower simulations has been published, which also includes a resummation of logarithmically enhanced EW corrections. One should, however, note that the naive exponentiation prescription

$$\mathcal{M}_{\text{Born}} \rightarrow \mathcal{M}_{\text{Born}} \times (\exp(\delta_{\text{sud}}^{\text{EW}}) - 1) \quad (6.21)$$

with $\delta_{\text{sud}}^{\text{EW}}$ denoting the relative virtual correction containing the Sudakov logarithms, which is used in Ref. [76], is valid only up to LL accuracy. Strictly speaking it requires the external states to be SU(2) eigenstates. Both the non-Abelian structure of the angular-dependent logarithms and the effects due to γ/Z mixing which arise already at LL, are only approximatively taken into account if (6.21) is applied.

It should, however, be pointed out that the error due to (6.21) is not expected to have a large impact on the presented phenomenological results.²

6.3. Validation

Before presenting the actual SCET_{EW} results, we show some cross-checks related to the various different approximations and assumptions used within our framework, in particular:

- the DPA,
- the incoherent polarisation sum and the missing contributions involving mixed transverse/longitudinal polarisation configurations,
- the assumption that the bulk part of the EW corrections arises in the virtual corrections, and
- the validity of the SCET_{EW} assumption as well as the restriction of the SCET_{EW} results to the HEPS as defined in eq. (6.13).

The following four subsections deal with one of the above bullet points each.

Because SCET_{EW} requires all invariants to be much larger than the EW scale, we investigate especially the behaviour of the respective assumptions in regions of high four-lepton invariant masses, lepton transverse momenta, and dilepton invariant masses for leptons arising from different decays.

²In addition it is worth noting that there are other older publications containing wrong (or at least unclear) exponentiation prescriptions with respect to the angular and parameter renormalisation part (eq. (15) in Ref. [225], eq. (194) in Ref. [226]).

6.3.1. Fiducial cross sections and DPA

The application of SCET_{EW} relies on the factorization of a complicated process into a production and a decay part. The first validation step is thus to justify the application of the DPA. To this end, we calculate all considered processes both within the DPA and fully off shell. The quality of the approximation is estimated using the quantity

$$\Delta_{\text{DPA}} \equiv 1 - \frac{d\sigma^{\text{DPA}}/d\mathcal{O}}{d\sigma^{\text{full}}/d\mathcal{O}}. \quad (6.22)$$

If the DPA works properly, Δ_{DPA} is of the order of $\Gamma_{\text{W/Z}}/M_{\text{W/Z}}$, i.e. a few percent:

$$\frac{\Gamma_{\text{W}}}{M_{\text{W}}} = 2.6\%, \quad \frac{\Gamma_{\text{Z}}}{M_{\text{Z}}} = 2.7\%. \quad (6.23)$$

When the virtual corrections are computed, the respective relative corrections are defined as

$$\delta_{\text{DPA/full}}^{\text{virt}} = \frac{d\sigma^{\text{virt,DPA/full}}/d\mathcal{O}}{d\sigma^{\text{born,DPA/full}}/d\mathcal{O}}. \quad (6.24)$$

Of course virtual corrections alone are not well-defined due to IR singularities. We define them via their IR-finite part:

$$d\sigma^{\text{virt}} \equiv d\sigma^{\text{virt}} \Big|_{1/\varepsilon_{\text{IR}}^2=1/\varepsilon_{\text{IR}}=0, \mu_{\text{IR}}=M_{\text{W}}}. \quad (6.25)$$

The difference of the two quantities in (6.24),

$$\delta_{\text{full}}^{\text{virt}} - \delta_{\text{DPA}}^{\text{virt}}, \quad (6.26)$$

is the error if virtual corrections computed in DPA are integrated into results with all other ingredients being calculated off shell. This happens by the replacement

$$\frac{d\sigma^{\text{virt,full}}}{d\mathcal{O}} \rightarrow \frac{d\sigma^{\text{virt,DPA}}}{d\mathcal{O}} \times \frac{d\sigma^{\text{born,full}}}{d\mathcal{O}} \left(\frac{d\sigma^{\text{born,DPA}}}{d\mathcal{O}} \right)^{-1}. \quad (6.27)$$

We thus calculate and plot (6.22) and (6.26) for each process the following.

ZZ production

For ZZ production we obtain the fiducial cross sections

$$\sigma_{\text{full}} = 48.285(12) \text{ fb}, \quad \sigma_{\text{DPA}} = 47.54(6) \text{ fb}, \quad \Delta_{\text{DPA}} = 1.54(8)\% \quad (6.28)$$

in DPA and fully off shell, respectively. All numbers in parentheses are MC-integration errors. The relative virtual corrections read

$$\delta_{\text{full}}^{\text{virt}} = -3.381(7)\%, \quad \delta_{\text{DPA}}^{\text{virt}} = -3.16(3)\%, \quad \delta_{\text{full}}^{\text{virt}} - \delta_{\text{DPA}}^{\text{virt}} = -0.22(3)\%. \quad (6.29)$$

Differential distributions in several kinematic variables are shown in Fig. 6.2. The deviations Δ_{DPA} and $\delta_{\text{full}}^{\text{virt}} - \delta_{\text{DPA}}^{\text{virt}}$ show little variation over the distributions: While Δ_{DPA} fluctuates between

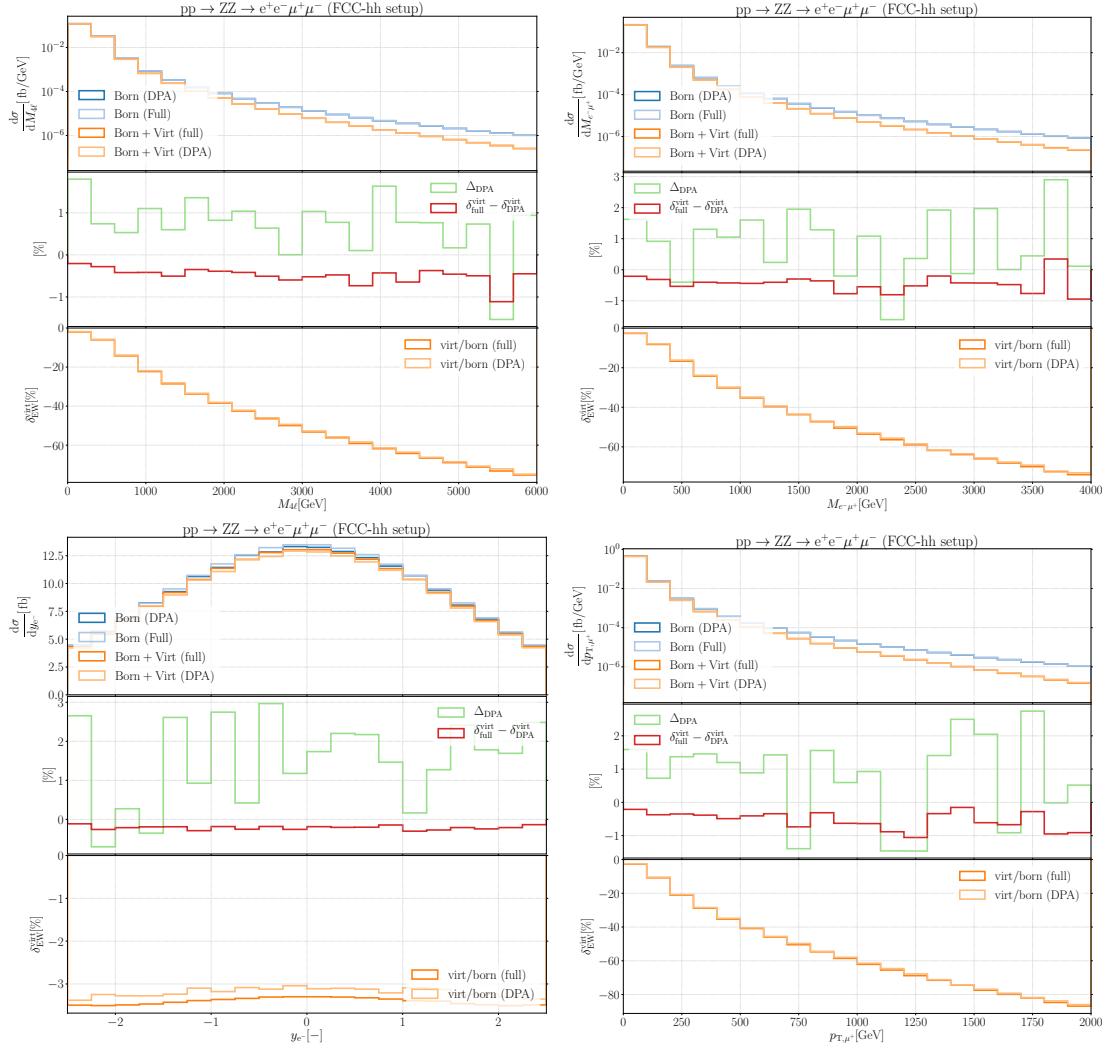


Figure 6.2.: Comparison between DPA and full off-shell calculation for $pp \rightarrow ZZ \rightarrow e^+e^-\mu^+\mu^-$: Differential distributions in the four-lepton invariant mass, the $e^-\mu^+$ invariant mass, the e^- rapidity, and the μ^+ transverse momentum. The upper panels show the differential cross sections, the middle ones the deviations due to the DPA with Δ_{DPA} as defined in (6.22), while the lower ones show the relative virtual EW corrections.

0% and 3% in all distributions, $\delta_{\text{full}}^{\text{virt}} - \delta_{\text{DPA}}^{\text{virt}}$ grows slightly from -0.2% in the bulk region towards the high-invariant-mass and high- p_{T} tails. In the particularly interesting tail regions, we find for $\delta_{\text{full}}^{\text{virt}} - \delta_{\text{DPA}}^{\text{virt}}$ values of $\sim -1\%$ in the high- $M_{e^{-}\mu^{+}}$ and the high- $p_{\text{T},\mu^{+}}$ tail and $\sim -0.5\%$ in the high- $M_{4\ell}$ tail. The DPA works thus very well for this process, which is partly a result of the phase-space cuts (6.9).

W⁺Z production

For the fiducial cross sections for W⁺Z production we obtain

$$\sigma_{\text{full}} = 102.71(5) \text{ fb} \quad \sigma_{\text{DPA}} = 100.5(2) \text{ fb}, \quad \Delta_{\text{DPA}} = 2.2(2)\%, \quad (6.30)$$

and the relative virtual corrections

$$\delta_{\text{full}}^{\text{virt}} = -1.313(6)\%, \quad \delta_{\text{DPA}}^{\text{virt}} = -1.19(3)\%, \quad \delta_{\text{full}}^{\text{virt}} - \delta_{\text{DPA}}^{\text{virt}} = -0.12(3)\%. \quad (6.31)$$

The differential results for the DPA comparison in W⁺Z production are shown in Fig. 6.3. Compared to the ZZ case, we note a worse agreement of the Born cross sections in the tails: Δ_{DPA} grows up to 20% in the high-energy and invariant-mass tails. Even stronger deviations can be found in the high- $p_{\text{T},e^{+}}$ tail (note that the positron is the decay product of the W⁺-boson!). Here the DPA cross section is not even close to the full result ($\Delta_{\text{DPA}} > 50\%$!). This is because this region is dominated by contributions originating from diagrams depicted in Fig. 6.4: Although they are not doubly resonant, they are enhanced for high electron p_{T} because the electron recoils against two or three final-state particles. This mechanism is described in more detail in Ref. [113]. In the high-antimuon- p_{T} tail, the deviation is not so strongly enhanced, reaching values of around 10%.

The values for $\delta_{\text{full}}^{\text{virt}} - \delta_{\text{DPA}}^{\text{virt}}$ also grow toward higher energies, but are in some cases considerably smaller: In the high- $M_{4\ell}$ and high- $M_{e^{-}\mu^{+}}$ tails they do not exceed $\sim 3\%$ and in the high- $p_{\text{T},\mu^{+}}$ tail they are at the subpercent level. These values are in the order of magnitude one may expect for the accuracy of the DPA. Only in the high- $p_{\text{T},e^{-}}$ tail, the difference between the virtual corrections exceeds 20%, rendering the DPA clearly a poor approximation in this region.

W⁺W⁻ production from quarks

For W-boson pair production we obtain the fiducial LO cross sections

$$\sigma_{\text{full}} = 2540(3) \text{ fb}, \quad \sigma_{\text{DPA}} = 2487(2) \text{ fb}, \quad \Delta_{\text{DPA}} = 2.09(15)\%, \quad (6.32)$$

and the relative corrections

$$\delta_{\text{full}}^{\text{virt}} = -0.759(5)\%, \quad \delta_{\text{DPA}}^{\text{virt}} = -0.617(2)\%, \quad \delta_{\text{full}}^{\text{virt}} - \delta_{\text{DPA}}^{\text{virt}} = -0.14(6)\%. \quad (6.33)$$

In the high-energy tails we can observe a similar behaviour as in the W⁺Z case: the diagrams drawn in the second row of Fig. 6.4 become large in the high- $p_{\text{T},\ell}$ tails in Fig. 6.5. In this case the effect is even stronger, leading to Δ_{DPA} values of up to 20% in the high $M_{e^{-}\mu^{+}}$ -tail, $> 30\%$ in the high- $M_{4\ell}$ tail, and even $> 60\%$ in the high- $p_{\text{T},\ell}$ tails. In the latter distributions, $\delta_{\text{full}}^{\text{virt}} - \delta_{\text{DPA}}^{\text{virt}}$ grows up to $\sim 50\%$, intimating that in the high- $p_{\text{T},\ell}$ -tail the DPA is not applicable anymore. Meanwhile, in the high- $M_{4\ell}$ and high- $M_{e^{-}\mu^{+}}$ tails, the difference of the relative correction remains below 10%. Including only the virtual corrections in DPA thus yields inaccurate,

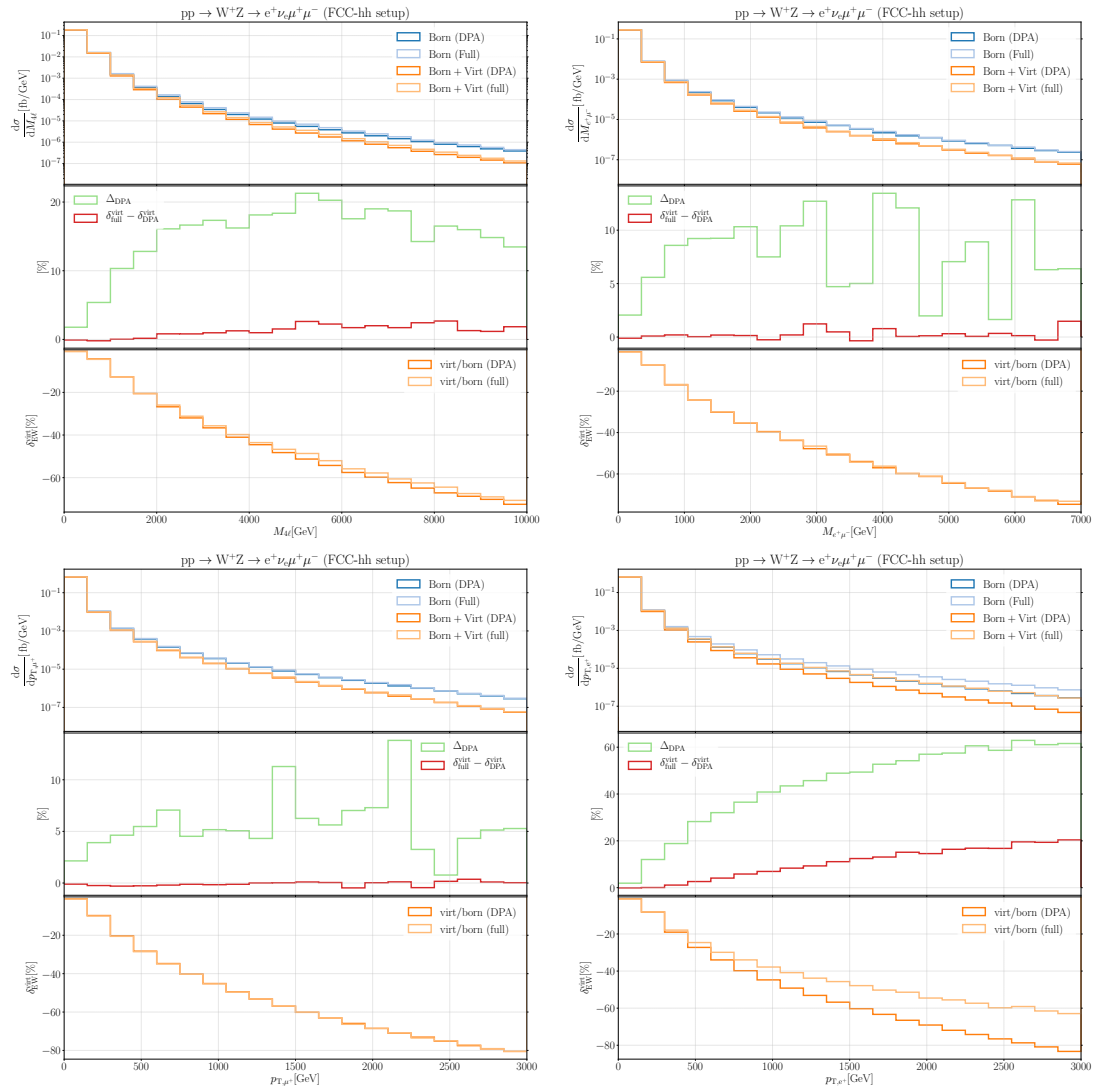


Figure 6.3.: Comparison between DPA and full off-shell calculation for $pp \rightarrow W^+Z \rightarrow e^+\nu_e\mu^+\mu^-$: Differential distributions in the four-lepton invariant mass, the $e^+\mu^-$ invariant mass, and the lepton p_{T} s. The plots are structured as in Fig. 6.2.

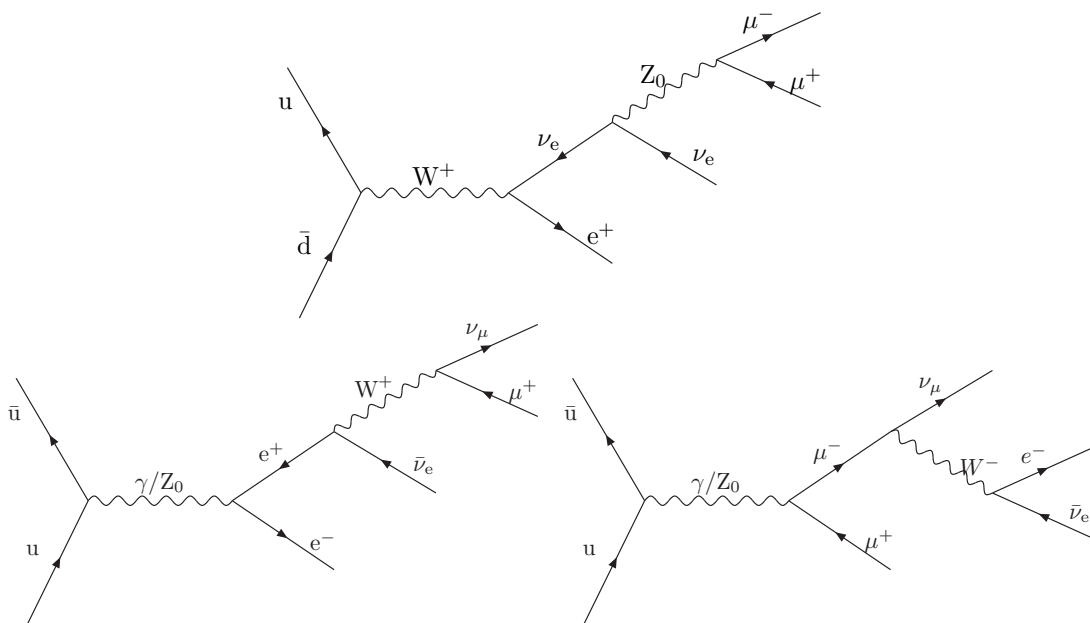


Figure 6.4.: Single-resonant diagrams that spoil the validity of the DPA in W^+Z production (top) and W^+W^- production (bottom).

but still somewhat reasonable results. However, the large Δ_{DPA} indicate strong contributions of non-doubly resonant diagrams.

W^+W^- production from photons

For photon-induced W-boson pair production we obtain the Born cross sections

$$\sigma_{\text{full}} = 27.33(2) \text{ fb} \quad \sigma_{\text{DPA}} = 27.200(16) \text{ fb}, \quad \Delta_{\text{DPA}} = 0.47(8)\%, \quad (6.34)$$

and the relative corrections

$$\delta_{\text{full}}^{\text{virt}} = 6.037(12)\%, \quad \delta_{\text{DPA}}^{\text{virt}} = 5.745(11)\%, \quad \delta_{\text{full}}^{\text{virt}} - \delta_{\text{DPA}}^{\text{virt}} = -0.219(16)\%. \quad (6.35)$$

Differential distributions in the electron p_T for the respective photon-induced channel can be found in Fig. 6.6. In the high- p_{T,e^-} tail of the distributions, a similar behaviour as in the quark-induced case can be observed. The deviations are, however, not as strong as in the quark-induced case, which can be explained by the fact that there are no single-resonant s -channel topologies for this process. Δ_{DPA} still reaches almost 40%, while $\delta_{\text{full}}^{\text{virt}} - \delta_{\text{DPA}}^{\text{virt}}$ remains below 30%. In the high- $M_{4\ell}$ and high- $M_{e^-\mu^+}$ tails one has a Δ_{DPA} of about 10%. The difference between the virtual corrections in DPA and full off-shell is about 1% up to $M_{4\ell} \approx 8 \text{ TeV}$, while ranging between 5% and 10% in the high- $M_{e^-\mu^+}$ tail.

6.3.2. Polarised leading-order results

In this section we provide some results connected to the polarisation of virtual gauge bosons. As outlined in the previous sections, we have to calculate the transverse and longitudinally polarised contribution separately because they obey different matching conditions and their RG running

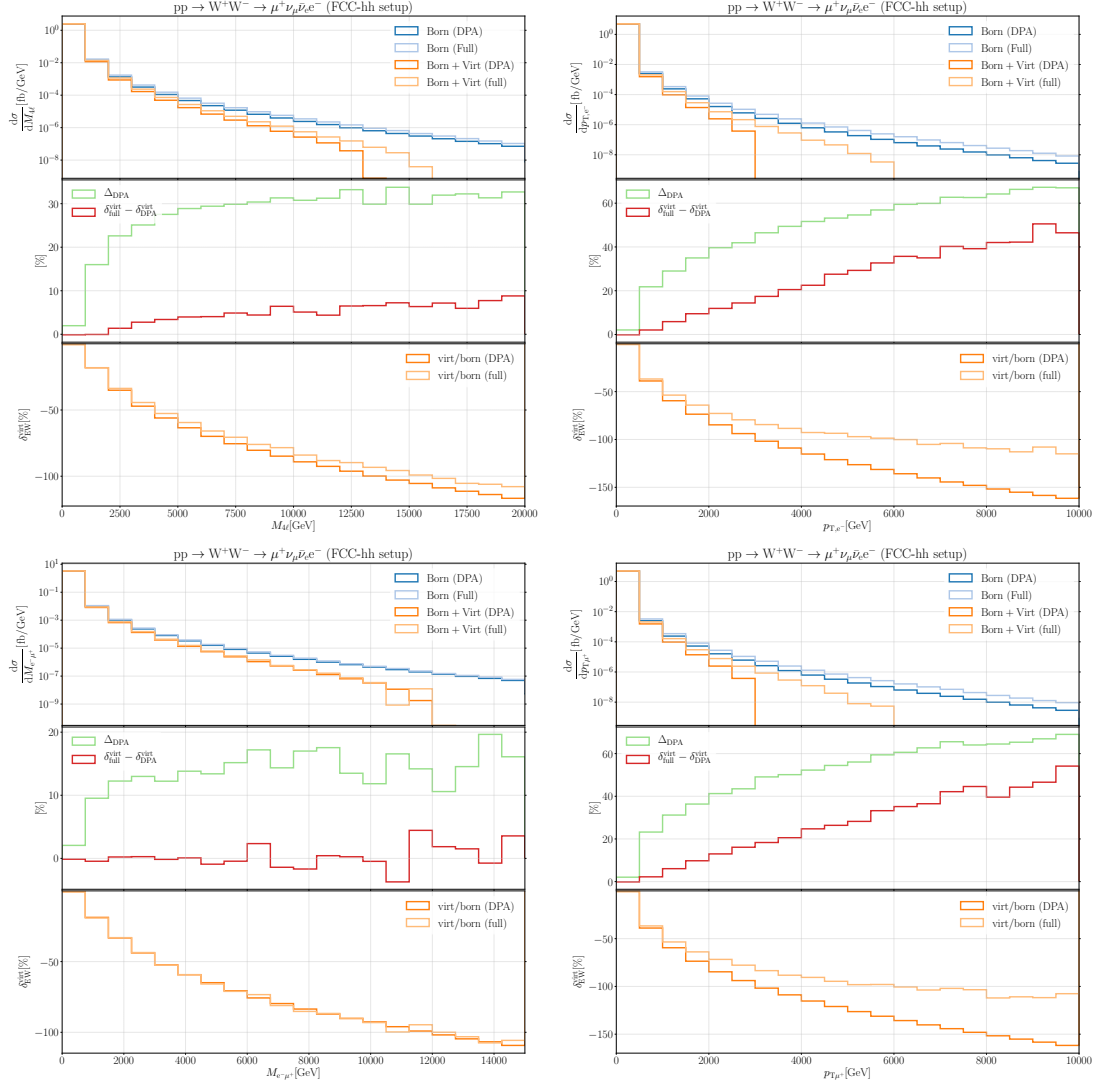


Figure 6.5.: Comparison between DPA and full off-shell calculation for $pp \rightarrow W^+W^- \rightarrow \mu^+\nu_\mu\bar{\nu}_e e^-$: Differential distributions in the four-lepton invariant mass, the $e^- \mu^+$ invariant mass, and the lepton $p_{T\text{'s}}$. The plots are structured as in Fig. 6.2.

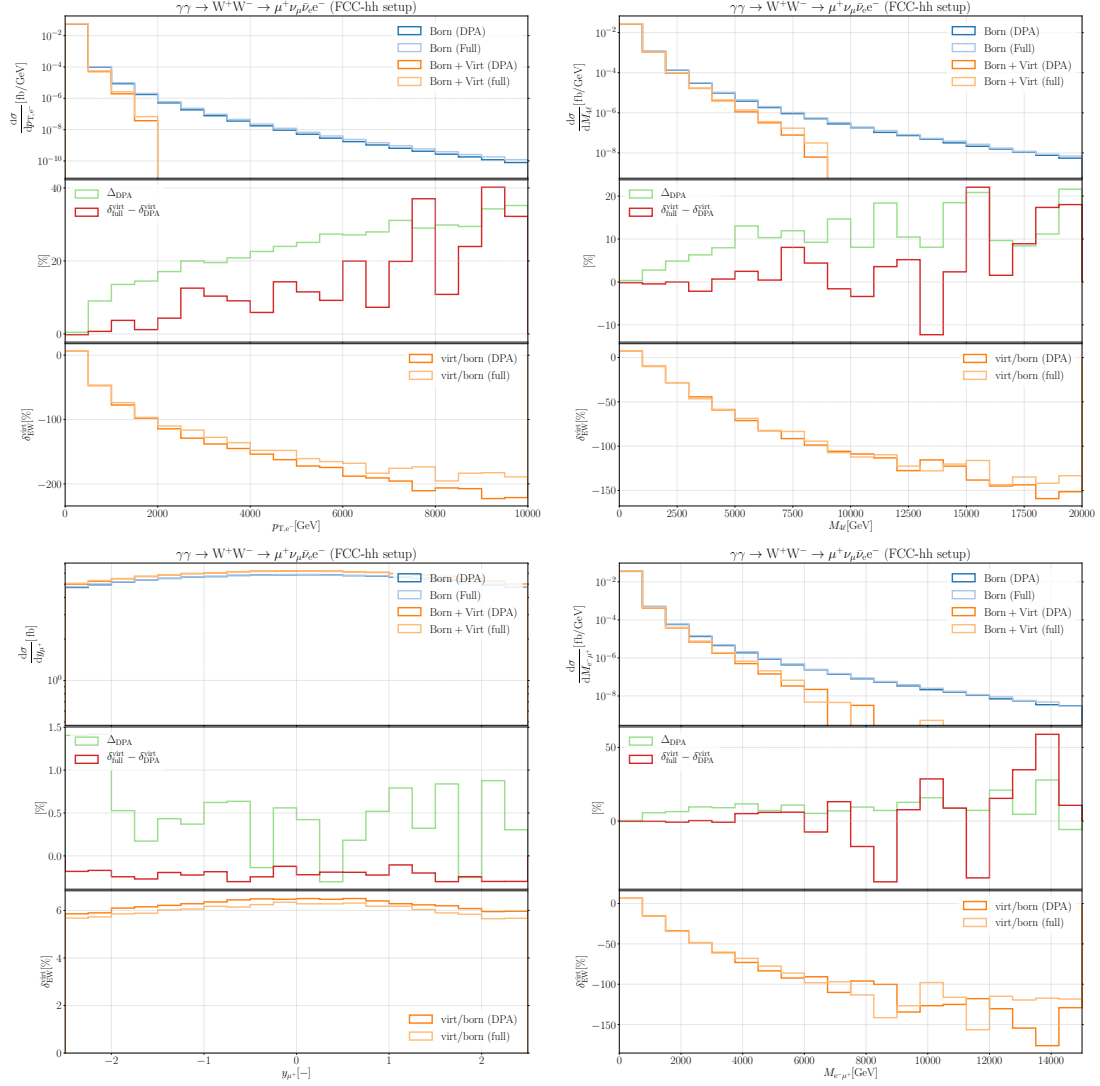


Figure 6.6.: Comparison between DPA and full off-shell calculation for $\gamma\gamma \rightarrow W^+W^- \rightarrow \mu^+\nu_\mu\bar{\nu}_e e^-$: Differential distributions in the electron p_T , the four-lepton invariant mass, the antimuon rapidity, and the $e^-\mu^+$ invariant mass. The plots are structured as in Fig. 6.2.

is different. As argued in Sec. 4.2.1, we choose the polarisation vectors of the virtual vector bosons to be defined in the partonic centre-of-mass system.

In Figs. 6.7, 6.8, 6.9, and 6.10 we show several differential distributions for $\bar{d}d + d\bar{d} \rightarrow W^+W^- \rightarrow \mu^+\nu_\mu\bar{\nu}_e e^-$, $u\bar{d} \rightarrow W^+Z \rightarrow e^+e^-\mu^+\mu^-$, $u\bar{u} \rightarrow ZZ \rightarrow e^+e^-\mu^+\mu^-$, and $\gamma\gamma \rightarrow W^+W^- \rightarrow \mu^+\nu_\mu\bar{\nu}_e e^-$. All plots are organised as follows:

- The upper panels contain the polarised differential cross sections.
- The middle panels show the curves for the quantity

$$\Delta_{\text{pol}} = 1 - \frac{d\sigma_{\text{TT}} + d\sigma_{\text{LL}}}{d\sigma_{\text{UU}}^{\text{DPA}}}, \quad (6.36)$$

which estimates the error we make by neglecting the mixed polarisation contributions³ as well as the interference terms. Here and in the following UU denotes the unpolarised cross section, while T and L denote transversely polarised cross sections. The interference terms are computed via

$$\Delta_{\text{int}} = 1 - \frac{\sum_{\lambda\lambda'} d\sigma_{\lambda\lambda'}}{d\sigma_{\text{UU}}} \quad (6.37)$$

and are shown in green, while Δ_{pol} is displayed in red. The contributions of mixed polarisation configurations alone are thus obtained from the differences between the red and the green curves.

- The lower panels show the ratios $\delta_{\lambda\lambda'} = d\sigma_{\lambda\lambda'}/d\sigma_{\text{UU}}$ of a single polarisation configuration with respect to the unpolarised result. Because the doubly-transverse polarisations often account for almost 100%, we plot $1 - \delta_{\text{TT}}$ instead of δ_{TT} .

In the muon-rapidity distribution in W^+W^- production (upper left plot in Fig. 6.7), it can be seen that Δ_{pol} is slightly below 20% in the forward and backward region and slightly above 20% in the central region. The error on the integrated cross section is hence to be estimated in this order of magnitude. Since Δ_{int} is only at the level of few percent, the bulk contribution of Δ_{pol} value originates from the mixed polarisations. In the p_{T} and invariant-mass distributions, it can be seen that these deviations contribute only in the first bins ($p_{\text{T}} < 500$ GeV, $M_{e^-\mu^+} < 750$ GeV, $M_{4\ell} < 1000$ GeV). For larger energy scales the curves for Δ_{pol} and Δ_{int} coincide, implying that the interference contributions dominate the error on the polarisation sum. Their magnitude fluctuates in the range between -0.5% and $+1\%$ in all tails.

For the other processes we show distributions in the four-lepton invariant mass and the electron p_{T} . The influence of the various contributions on the integrated level can be read off from the values of the curves in the first bins of the p_{T} distributions, as the cross section in the second bin is already smaller by at least one order of magnitude in all cases.

The picture for W^+Z production is shown in Fig. 6.8. The antimuon rapidity distribution shows a 20% contribution from mixed-polarisation and a few percent contribution from interference terms. In the energy-like distributions (p_{T,e^+} and $M_{4\ell}$) it can be seen that the mixed

³The power-suppressed mixed longitudinal/transverse are omitted per construction because the matrix elements are computed in the SySM, where there are no corresponding Feynman diagrams. In the ZZ case, this holds also for the double-longitudinal contributions.

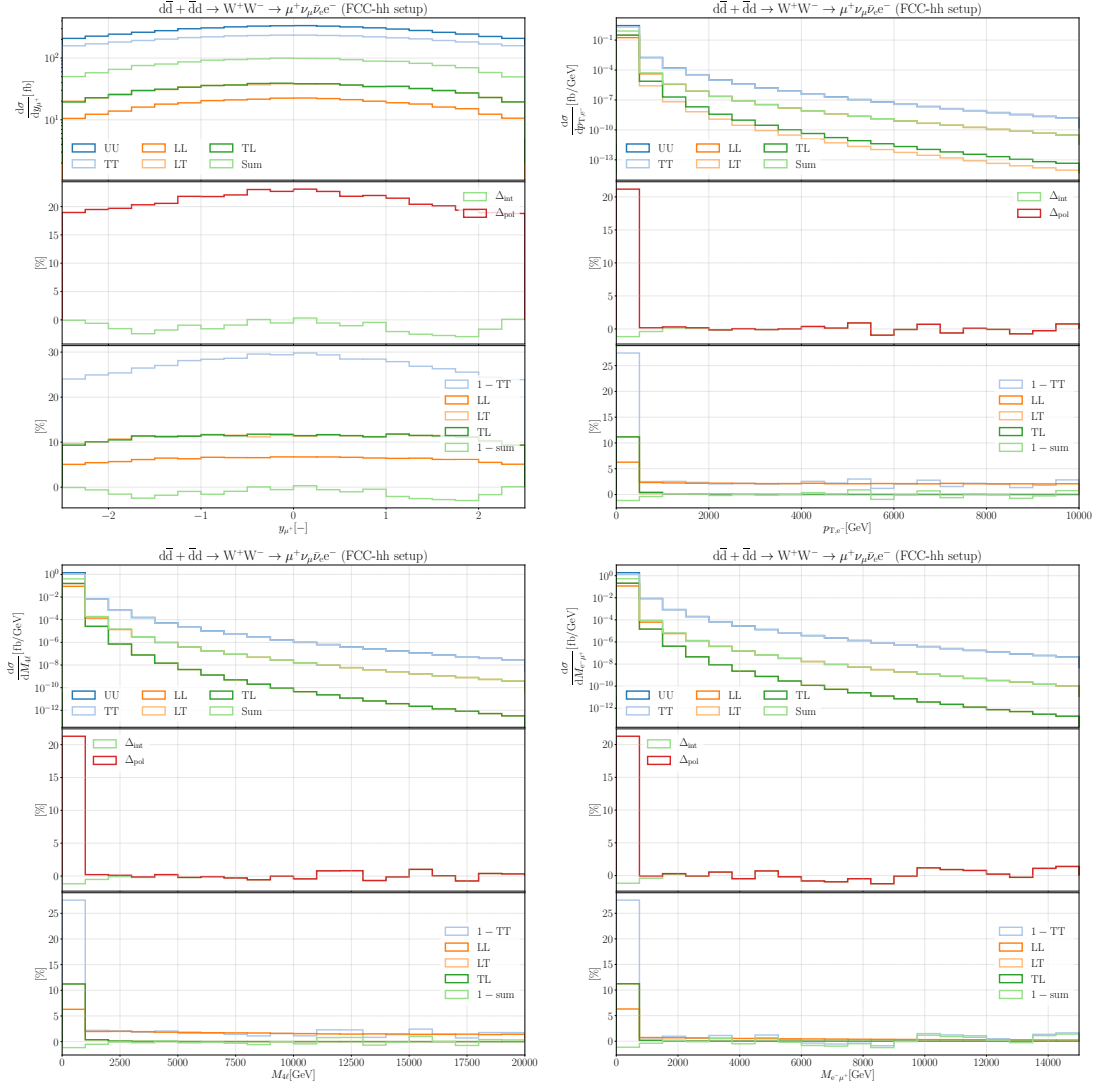


Figure 6.7.: Transversely (T), longitudinally (L) and unpolarised (U) polarised differential cross sections for $d\bar{d} \rightarrow W^+W^- \rightarrow \mu^+\nu_{\mu}\bar{\nu}_e e^-$ in the antimuon rapidity, the electron p_T , the four-lepton invariant mass, and the $e^-\mu^+$ invariant mass. The quantities $\Delta_{\text{pol/int}}$ are defined in (6.36) and (6.37), respectively. Note that both the difference between transverse and unpolarised and between TL and LT is not perceptible.

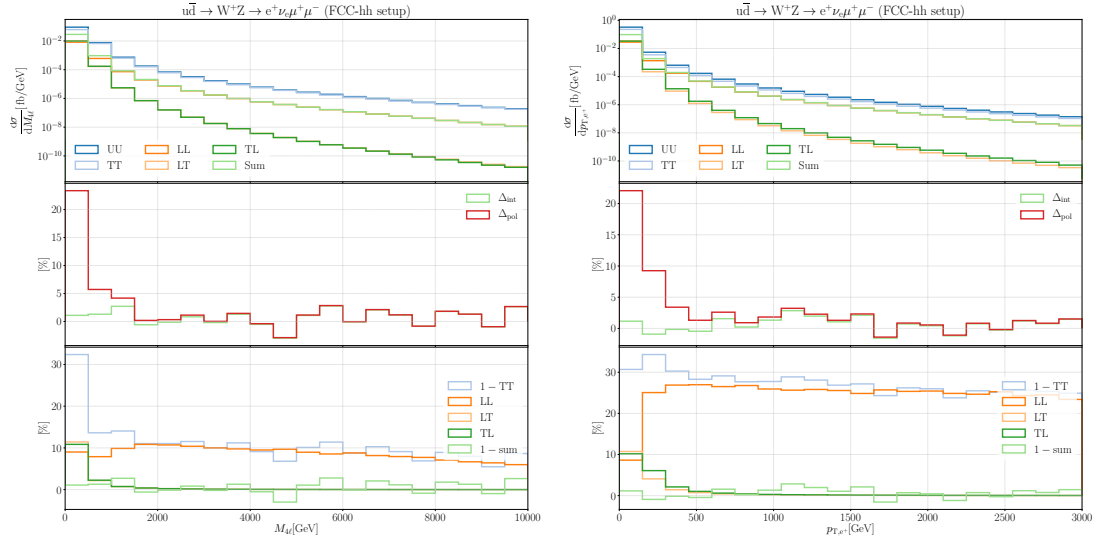


Figure 6.8.: Transversely (T), longitudinally (L) and unpolarised (U) polarised differential cross sections in the four-lepton invariant mass and the electron p_T for $u\bar{d} \rightarrow W^+Z \rightarrow e^+\nu_e\mu^+\mu^-$. The quantities $\Delta_{\text{pol/int}}$ are defined in (6.36) and (6.37), respectively.

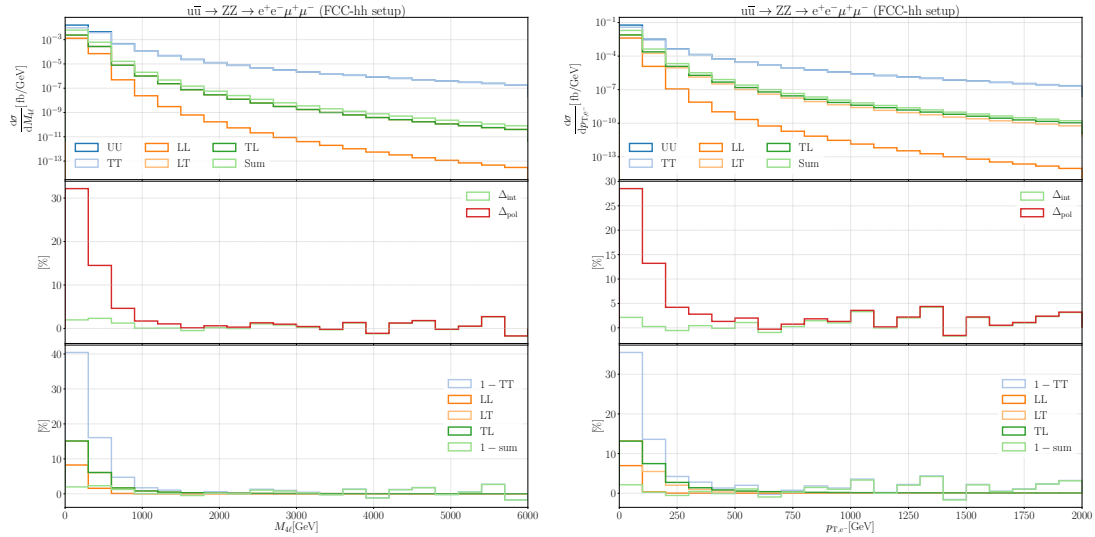


Figure 6.9.: Transversely (T), longitudinally (L) and unpolarised (U) polarised differential cross sections in the four-lepton invariant mass and the electron p_T for $u\bar{d} \rightarrow ZZ \rightarrow e^+e^-\mu^+\mu^-$. The quantities $\Delta_{\text{pol/int}}$ are defined in (6.36) and (6.37), respectively.

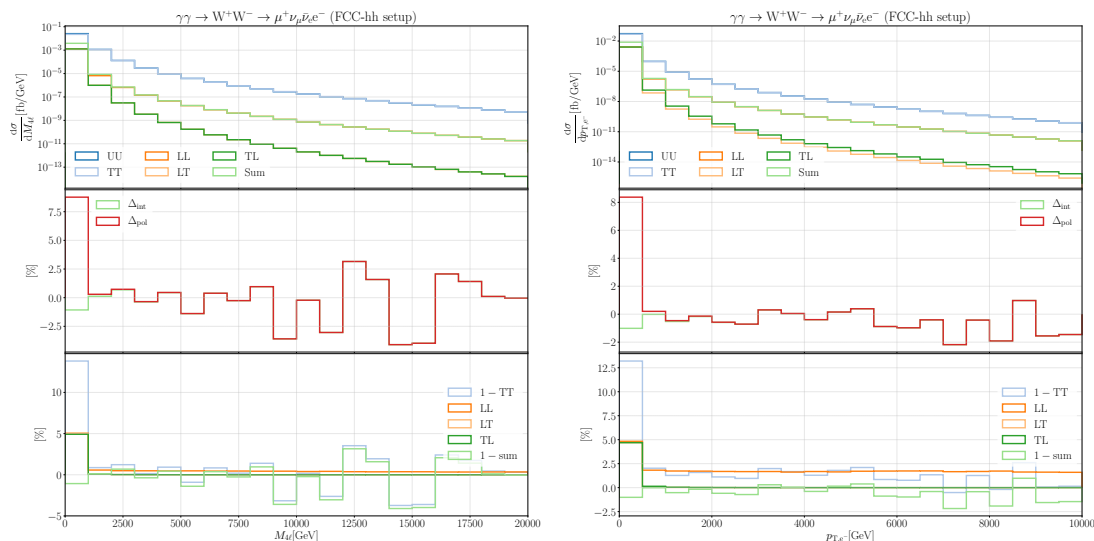


Figure 6.10.: Transversely (T), longitudinally (L) and unpolarised (U) polarised differential cross sections in the four-lepton invariant mass and the electron p_T for $\gamma\gamma \rightarrow W^+W^- \rightarrow \mu^+\nu_\mu\bar{\nu}_e e^-$. The quantities $\Delta_{\text{pol/int}}$ are defined in (6.36) and (6.37), respectively.

polarisations fall off rapidly towards the tails (note the different plot ranges between Figs. 6.7, 6.8.)

In the ZZ case (Fig. 6.9), Δ_{pol} amounts to almost 30% of the integrated cross section, but drops fast and fluctuates at the percent level for $M_{4\ell} \gtrsim 1 \text{ TeV}$ $p_{T,e^-} \gtrsim 500 \text{ GeV}$. From the green curve and its difference with the red one, it can again be seen that the bulk of the contribution to the integrated cross section arises from the neglected polarisation states and the fluctuations in the tails arise mainly from the interference terms. In Fig. 6.10, finally, we show the $M_{4\ell}$ and p_{T,e^-} distributions for photon-induced W-boson pair production. On the integrated cross section, which is again well approximated by the first bin of the p_T distribution, the interference contributions account for -1% and the mixed-polarisation contributions for $+8\%$. Again, as in the previous cases, the difference between the curves decreases rapidly, indicating the power suppression of the mixed contributions. In both tails of the presented distributions the difference between the unpolarised and the coherently summed result fluctuates at the level of few percent, which may thus be deduced as an order of magnitude for the interference contributions.

In the following we also discuss the influence of the interference terms among purely transverse polarisation states since we also neglect these in the SCET_{EW} calculation for simplicity. In Figs. 6.11 and 6.12 we present results differential in the antimuon transverse momentum and the four-lepton invariant mass in two partonic processes, $u\bar{u} \rightarrow Z_T Z_T \rightarrow e^+e^-\mu^+\mu^-$ and $\bar{u}d \rightarrow W_T^+ Z_T \rightarrow e^+\nu_e\mu^+\mu^-$, respectively. Note that within these plots Δ_{int} is redefined with respect to (6.37):

$$\Delta_{\text{int}} = 1 - \frac{\sum_{\lambda\lambda'=+,-} d\sigma_{\lambda\lambda'}}{d\sigma_{\text{TT}}}. \quad (6.38)$$

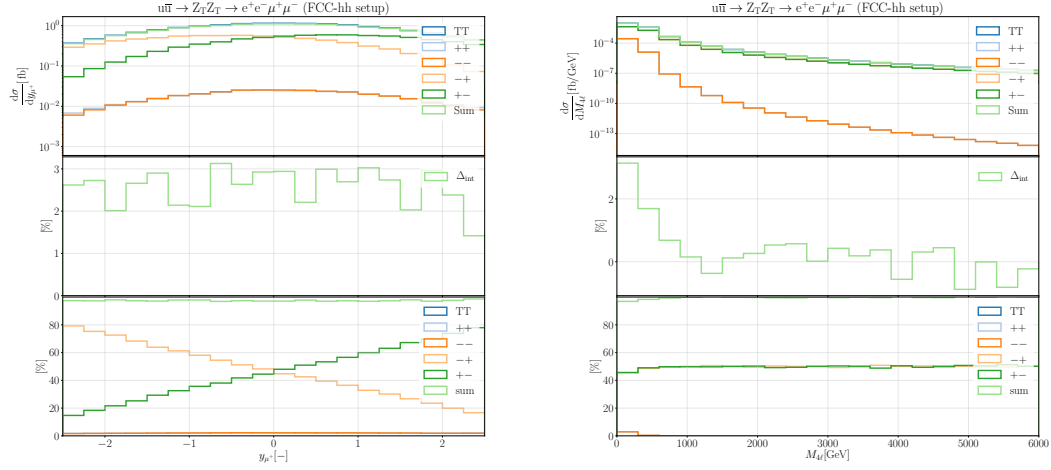


Figure 6.11.: Polarised differential cross sections in the antimuon rapidity and the four-lepton invariant mass for $u\bar{u} \rightarrow Z_T Z_T \rightarrow e^+ e^- \mu^+ \mu^-$, broken down to the individual left-handed (+) and right-handed (-) polarisation states. The curves for ++ and -- are often not to distinguish.

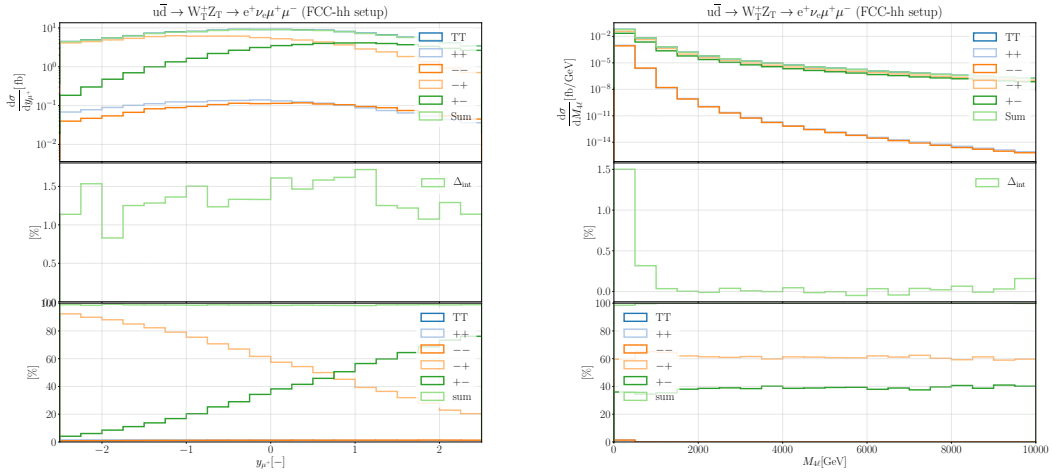


Figure 6.12.: Polarised differential cross sections in the antimuon rapidity and the four-lepton invariant mass for $u\bar{d} \rightarrow W_T^+ Z_T \rightarrow e^+ \nu_e \mu^+ \mu^-$, broken down to the individual left-handed (+) and right-handed (-) polarisation states.

In ZZ production (Fig. 6.11), Δ_{int} accounts for 3% for moderate energies and also decreases in the high- $M_{4\ell}$ tail, reaching subpercent accuracy from $M_{4\ell} \approx 1.5$ TeV. The ++ and -- configurations are strongly suppressed, while the +- and -+ configurations contribute roughly equally in the $M_{4\ell}$ distribution. The antimuon-rapidity distribution shows that the +- configuration contributes predominantly in the forward direction, while the -+ configuration dominates in the backward region.

In the W^+Z (Fig. 6.12) case, we can see that the contribution of the interference contribution is about 1.5% in the region of $M_{4\ell} < 500$ GeV, and that it is approximately constant over the antimuon rapidity. In the high-invariant-mass tail the interference contributions among the transverse polarisation quickly drop to $\sim 0.1\%$. The role of the individual polarisation configurations is similar as in the ZZ case. The curves of the +- and -+ configurations show an asymmetric behaviour owing to the mass differences of the W and Z bosons. In the $M_{4\ell}$ distribution it can be seen that the -+ configuration contributes to $\sim 60\%$ and the +- configuration to about $\sim 40\%$ of the cross section.

All in all, the plots show that the impact of interference among transversely polarised states on the integrated level is smaller compared to the interference of transversely and longitudinally polarised states: In the ZZ case the contribution to the cross section is about 2.5%, while for W^+Z it is only 0.3%

We can thus conclude that we can safely neglect all mixed-polarisation and interference contributions in the phase space regions where we expect SCET_{EW} to work: As expected, the influence of the mixed polarisation states can safely be neglected in all energy-like tails and the interference contributions fluctuate at the level of few percent.

As a final remark, we can see from Figs. 6.7, 6.8, 6.9, and 6.10 that the unpolarised results are dominated by the transverse contributions in the high-energy limit in most cases. While for W^+Z the longitudinal contributions reach a fraction of 5% – 10% of the unpolarised differential cross section in the high- $M_{4\ell}$ tail, for all other processes their contribution is below 1%. The longitudinal polarisation states seem to be enhanced in regions of high lepton p_T leading to a fraction of more than 20% of the unpolarised cross sections for W^+Z production. In the p_{T,e^+} case this phase-space region is, however, dominated by single-resonant effects, see Fig. 6.3.

6.3.3. Real and virtual corrections

The SCET_{EW} method resums only logarithmic corrections of virtual origin. Of course, any physical observable calculated on NLO has to include both real and virtual contributions. If a local subtraction scheme is applied, there are also integrated subtraction terms to include, which in the case of the Catani–Seymour subtraction method are called the integrated dipoles. Here we review some properties of the fixed-order NLO corrections to the processes we consider. As usual, we define the relative NLO correction according to

$$\delta^{\text{EW}} = \frac{d\sigma^{\text{NLO, EW}}}{d\sigma^{\text{LO}}} = \frac{d\sigma^{\text{virt}} + d\sigma^{\text{real}} + d\sigma^{\text{idip}}}{d\sigma^{\text{LO}}} \equiv \delta^{\text{virt}} + \delta^{\text{real}} + \delta^{\text{idip}}. \quad (6.39)$$

where we have split up the NLO correction into three contributions from the virtual (virt), real, and integrated dipole (idip) part. Again, the distinction between idip and virtual corrections is actually not unambiguous since both contain IR poles. The quantities are defined in analogy to

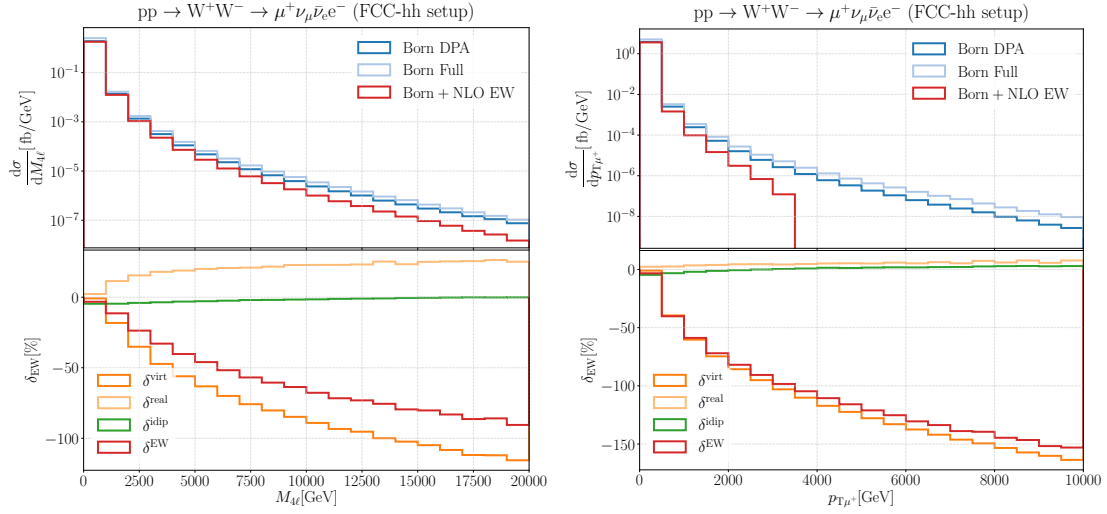


Figure 6.13.: Real, virtual, and integrated dipole (idip) NLO EW corrections for $pp \rightarrow W^+W^- \rightarrow \mu^+\nu_\mu\bar{\nu}_e e^-$ differential in the four-lepton invariant mass and the antimuon p_T . Note that the real and idip corrections are normalised by the full off-shell LO cross section, while the virtual corrections are computed in the DPA. The definition of δ^{EW} is given in (6.39). To obtain the red curves in the upper panels the rescaling (6.27) is applied for the virtuals.

(6.25):

$$d\sigma^{\text{virt}} \equiv d\sigma^{\text{virt}} \Big|_{1/\varepsilon_{\text{IR}}^2=1/\varepsilon_{\text{IR}}=0, \mu_{\text{IR}}=M_W}, \quad d\sigma^{\text{idip}} \equiv d\sigma^{\text{idip}} \Big|_{1/\varepsilon_{\text{IR}}^2=1/\varepsilon_{\text{IR}}=0, \mu_{\text{IR}}=M_W}. \quad (6.40)$$

To account for the fact that we calculate the virtual corrections in the DPA, the virtual term in (6.39) is rescaled via (6.27). As a result, the virtual and the relative corrections are in the following defined via

$$\delta^{\text{virt}} = \frac{d\sigma^{\text{virt,DPA}}/d\mathcal{O}}{d\sigma^{\text{born,DPA}}/d\mathcal{O}}, \quad \delta^{\text{real/idip}} = \frac{d\sigma^{\text{real/idip}}/d\mathcal{O}}{d\sigma^{\text{born,full}}/d\mathcal{O}}. \quad (6.41)$$

Differential results in the antimuon transverse momentum and the four-lepton invariant mass are shown Figs. 6.13, 6.14, 6.15, 6.16 for the considered processes.

For all considered processes, the bulk part of the NLO EW corrections appears to originate from virtual contributions in the high-energy tails of the distributions because of the Sudakov double logarithms.

The real corrections also grow with increasing energies. However, there is only a partial cancellation against the large Sudakov logarithms in the virtuals. This also holds when observables are defined such that real-emission contributions from undetected W or Z bosons are included, even though this leads to additional Sudakov logarithms in the reals [195, 227]. This non-cancellation of large corrections is sometimes referred to as EW Bloch-Nordsieck violation [228, 229], a somewhat misleading term, as the Bloch-Nordsieck theorem has only been stated in QED [180, 228].

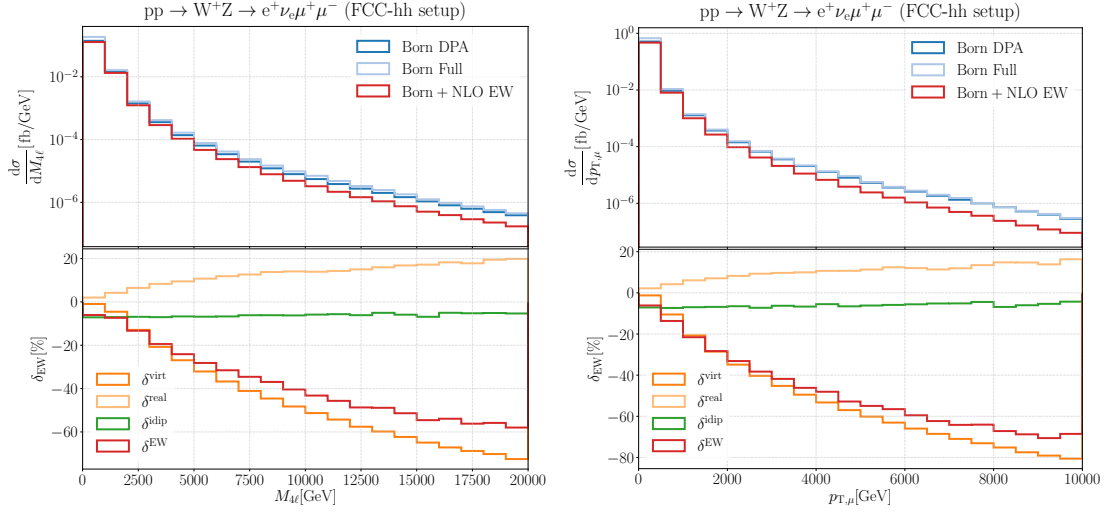


Figure 6.14.: Real, virtual, and integrated dipole (idip) NLO EW corrections for $pp \rightarrow W^+Z \rightarrow e^+\nu_e\mu^+\mu^-$ differential in the four-lepton invariant mass and the antimuon p_T . The plots are organised as in Fig. 6.13.

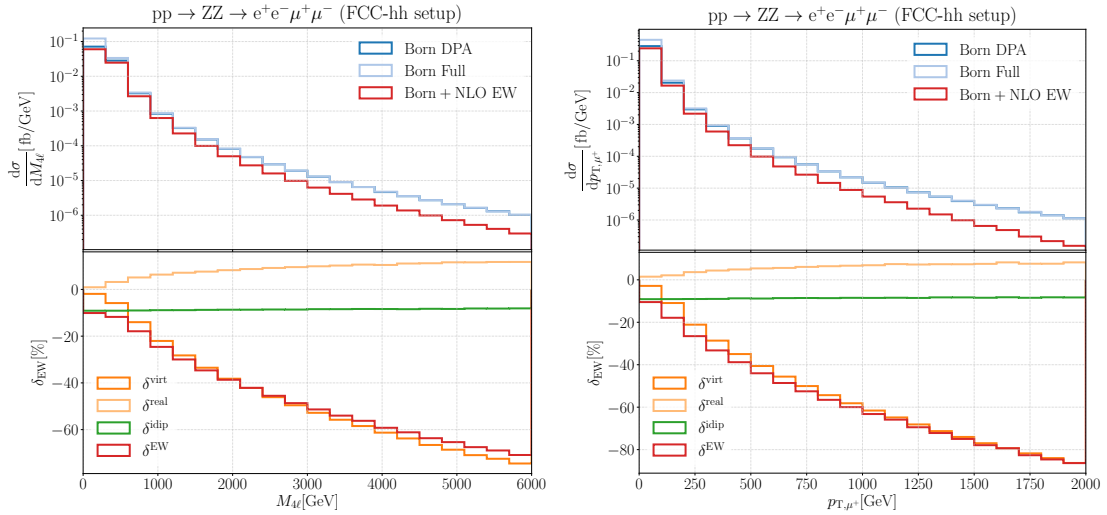


Figure 6.15.: Real, virtual, and integrated dipole (idip) NLO EW corrections for $pp \rightarrow ZZ \rightarrow e^+e^-\mu^+\mu^-$ differential in the four-lepton invariant mass and the antimuon p_T . The plots are organised as in Fig. 6.13.

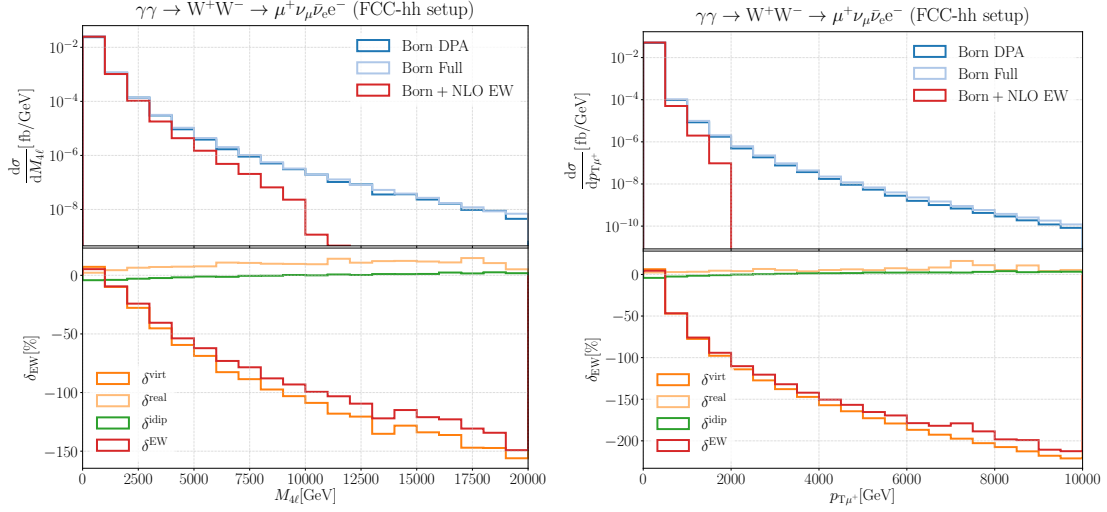


Figure 6.16.: Real, virtual, and integrated dipole (idip) NLO EW corrections for $\gamma\gamma \rightarrow W^+W^- \rightarrow \mu^+\nu_\mu\bar{\nu}_e e^-$ differential in the four-lepton invariant mass and the anti-muon p_T . The plots are organised as in Fig. 6.13.

6.3.4. SCET_{EW} vs. Fixed-Order

The validity of SCET_{EW} results is restricted to the region $s, t, u \gg M_W^2$. However, we have to expect large contributions from phase-space regions, where the condition (6.11) is not satisfied: In the high-energy limit the Born matrix elements for the dominant $\bar{q}q$ and $q\bar{q}$ production channels of transversely (T) and longitudinally (L) polarised gauge bosons can be decomposed as [19]

$$\mathcal{M}_T = \frac{\mathcal{M}_t}{t} + \frac{\mathcal{M}_u}{u}, \quad \mathcal{M}_L = \frac{\mathcal{M}_s}{s} \quad (6.42)$$

with $\mathcal{M}_s, \mathcal{M}_t, \mathcal{M}_u$ being analytical in s, t, u , and all masses. This form holds for all diboson production processes from fermions.

For $\gamma\gamma \rightarrow W^+W^-$, the amplitudes have the form [230]

$$\mathcal{M}_T = \frac{\mathcal{M}_s/us}{u} + \frac{\mathcal{M}_t^2/us^2}{us} + \frac{\mathcal{M}_u/su}{s} + \frac{\mathcal{M}_s/ts}{t} + \frac{\mathcal{M}_t/st}{s} + \frac{\mathcal{M}_u^2/ts^2}{ts} \quad (6.43)$$

in the high-energy limit for transverse gauge bosons and

$$\mathcal{M}_L = \frac{\mathcal{M}_1 u}{s} + \frac{\mathcal{M}_2 t}{s} \quad (6.44)$$

in the longitudinal case. Since the smallest invariant is relevant for estimating the quality of the SCET_{EW} assumption, we investigate the behaviour for $|t|, |u| \ll s$. In the fermionic case, squaring the matrix element yields another factor of the invariant, making the contribution of the squared matrix element behave as

$$\left| \frac{\mathcal{M}_t}{t} \right|_{|t| \ll s}^2 \sim \frac{s}{t} \quad (6.45)$$

and similar for \mathcal{M}_u . In the photon-induced case this effect is absent, and the squared matrix element scales as

$$\left| \frac{\mathcal{M}_{s/t}}{t} \right|_{|t| \ll s}^2 \sim \frac{s^2}{t^2}, \quad (6.46)$$

and analogously for the other matrix elements.

In any case, the total cross section is expected to be dominated by regions, in which at least one of the Mandelstam variables is small [of $\mathcal{O}(M_W^2)$]. Therefore, we do not discuss the influence of the resummation on integrated cross sections and focus on differential distributions in energy-like observables and study the behaviour in the tails only. In order to analyse the quality of this approximation, we first consider unresummed SCET_{EW}, meaning that the exponentiated amplitude is expanded to first order in α . In this approximation the SCET_{EW} results agree with the fixed-order one-loop results up to powers of M^2/s_{ij} with M being any of the EW mass scales and $s_{ij} \in \{s, t, u\}$.

Therefore we organise the plots as follows:

- The upper panels show the LO differential cross section both in fixed order and using SCET_{EW} on the HEPS (6.13). Moreover, the sum of LO and IR-finite virtual corrections is displayed in fixed order.
- The middle panels demonstrate the quality of the high-energy approximation, showing the quantities

$$\begin{aligned} \Delta_{\text{SCET}} &= 1 - \frac{d\sigma^{\text{Born, SCET}}/d\mathcal{O}}{d\sigma^{\text{Born, FO}}/d\mathcal{O}}, \\ \delta_{\text{FO}}^{\text{virt}} - \delta_{\text{SCET}}^{\text{virt}} &= \frac{d\sigma^{\text{virt, FO, fac}}/d\mathcal{O}}{d\sigma^{\text{Born, FO}}/d\mathcal{O}} - \frac{d\sigma^{\text{virt, SCET}}/d\mathcal{O}}{d\sigma^{\text{Born, SCET}}/d\mathcal{O}}, \end{aligned} \quad (6.47)$$

with $d\sigma^{\text{virt, FO, fac}}$ denoting the factorisable virtual corrections in DPA. The quantities in (6.47) quantify the validity of the SCET_{EW} approximation at tree level and one-loop level, respectively. Note that both $d\sigma^{\text{Born, SCET}}$ and $d\sigma^{\text{virt, SCET}}$ are evaluated on the HEPS defined by (6.13).

- The lower panels show the relative virtual corrections calculated in fixed order, and using SCET_{EW} on the HEPS.

Results

In Figs. 6.17, 6.18, 6.19, and 6.20 we show differential distributions in the four-lepton invariant masses, the $M_{e-\mu^+}$ invariant mass, and the lepton transverse momenta for the four diboson processes under consideration.

In the first few bins, that dominate the cross section, the SCET_{EW} results are smaller by a factor of 2–5 than the fixed-order ones because of the technical cut (6.11): The SCET_{EW} matrix elements are thus not appropriate. Towards the high-energy tails the results converge against each other, up to sub-percent accuracy from $M_{4\ell} \approx 1000$ GeV and $p_{T,\ell} \approx 500$ GeV depending on the process and the polarisation state.⁴ In the tails, i.e. at energy scales of several TeV, the deviation becomes of $\mathcal{O}(10^{-4})$, which is the expected order of magnitude for power corrections.

⁴Note that the plots have different ranges: For larger cross sections a longer high-energy tail is shown. Thus, $M_{4\ell} \approx 1000$ GeV is not at the same point in each plot!

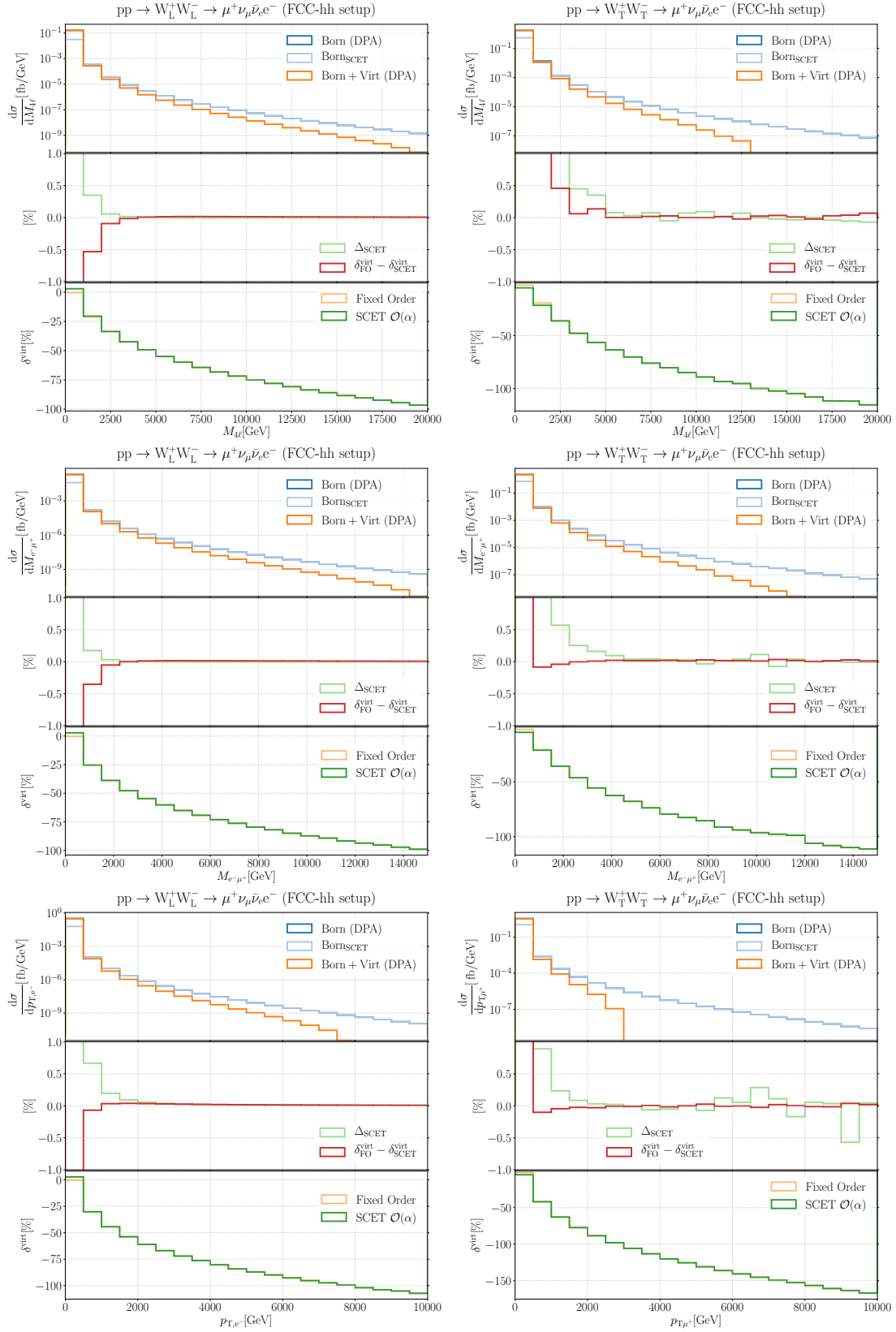


Figure 6.17.: Validation of the setup: Virtual corrections to longitudinal (left) and transverse (right) W^+W^- production calculated in conventional fixed-order perturbation theory compared to the first-order expansion of the SCET results in α . Δ_{SCET} is defined in (6.47).

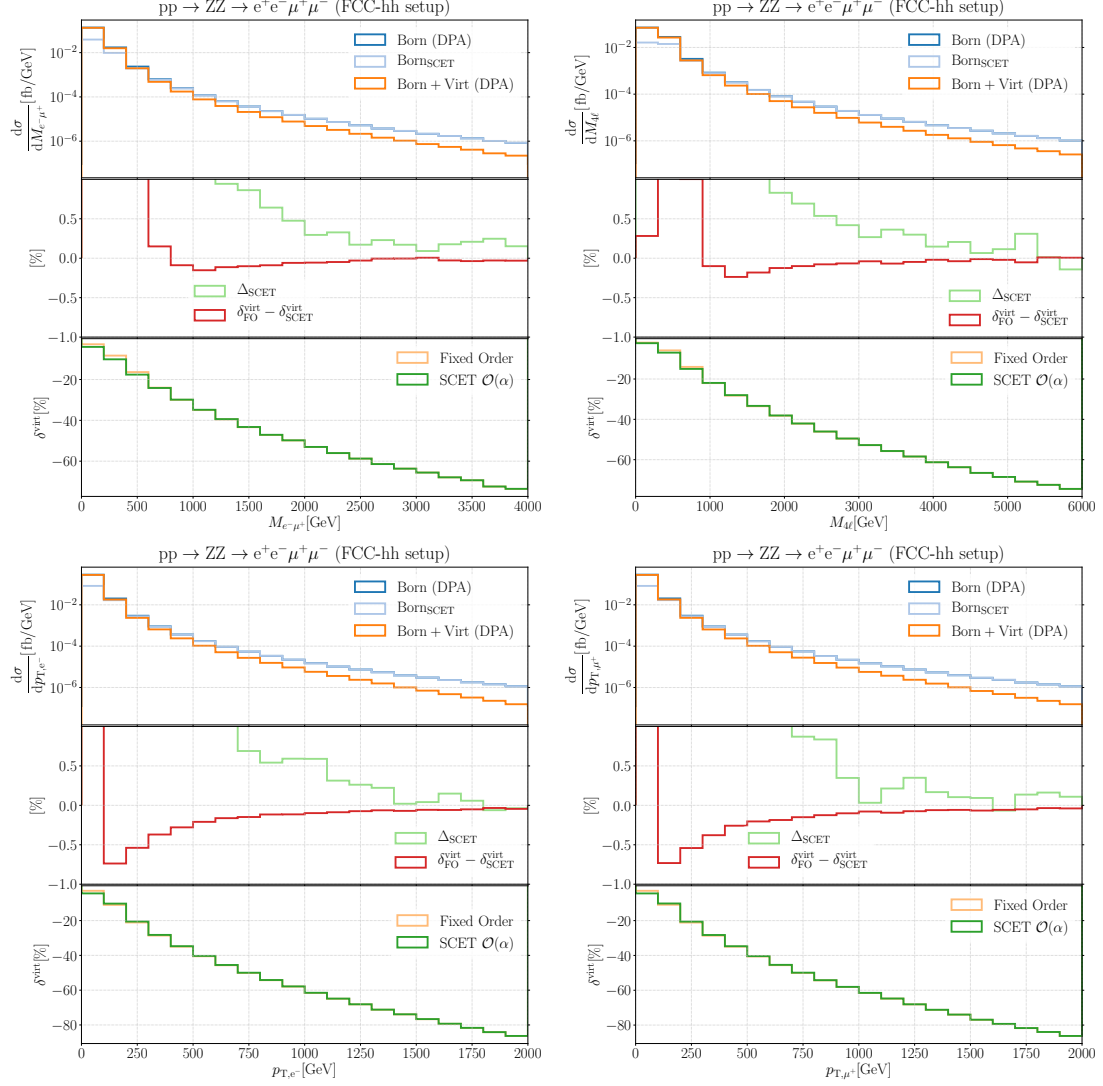


Figure 6.18.: Validation of the setup: Virtual corrections to $pp \rightarrow ZZ \rightarrow e^+e^-\mu^+\mu^-$ calculated in conventional fixed-order perturbation theory compared to the first-order expansion of the SCET results in α . Δ_{SCET} is defined in (6.47).

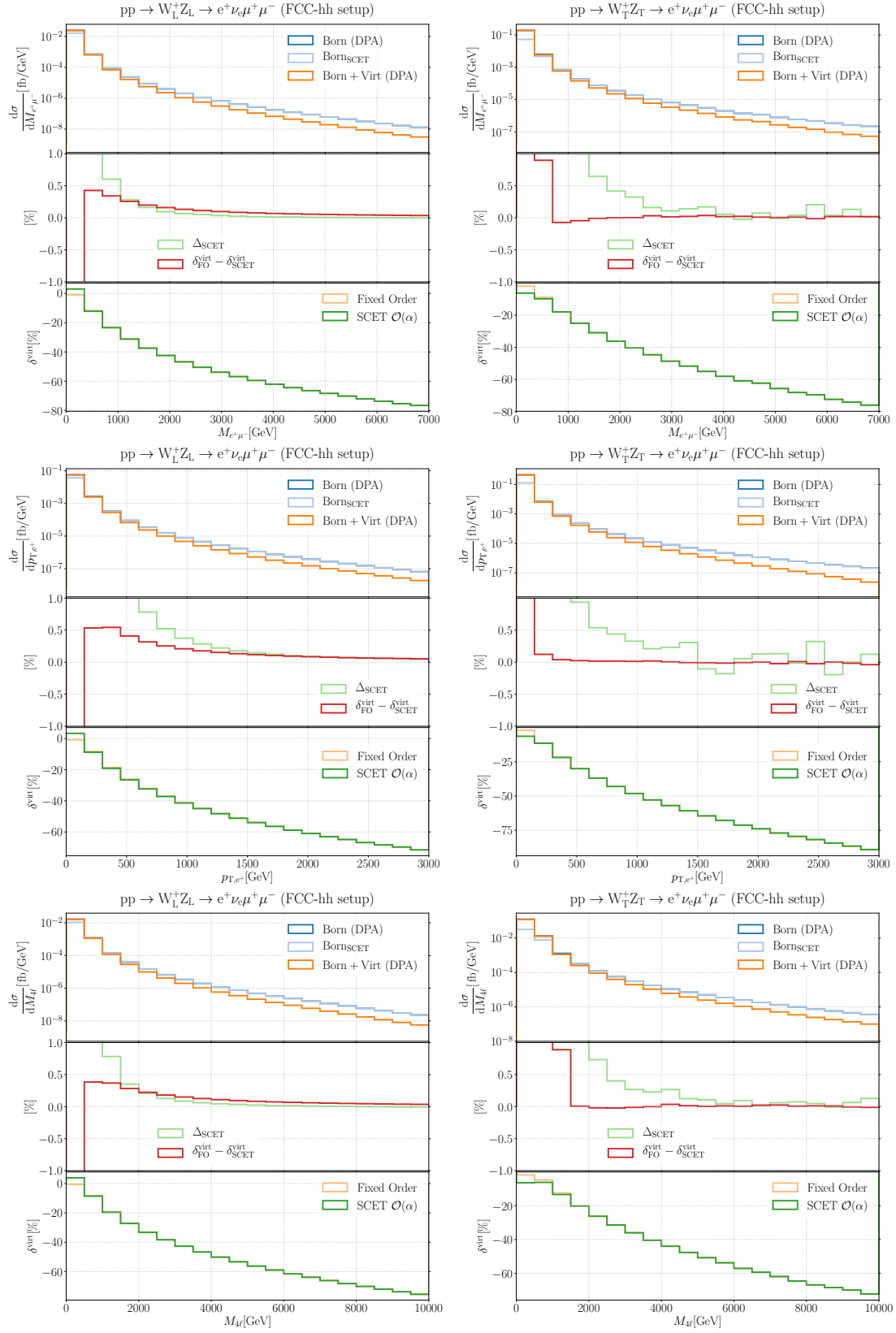


Figure 6.19.: Validation of the setup: Virtual corrections to longitudinal (left) and transverse (right) W^+Z production calculated in conventional fixed-order perturbation theory compared to the first-order expansion of the SCET results in α . Δ_{SCET} is defined in (6.47).

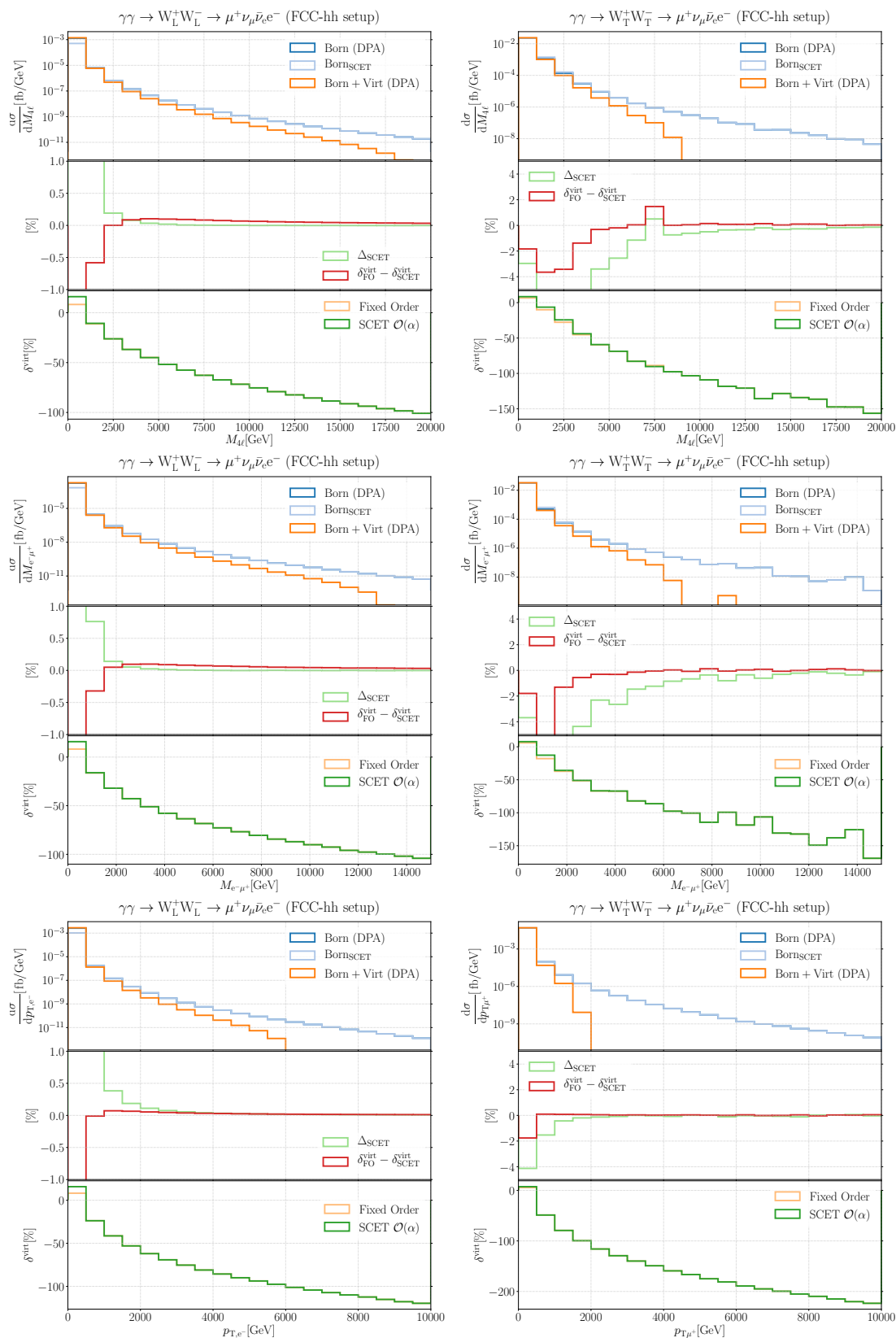


Figure 6.20.: Validation of the setup: Virtual corrections to longitudinal (left) and transverse (right) $\gamma\gamma \rightarrow W^+W^- \rightarrow \mu^+\nu_\mu\bar{\nu}_e e^-$ production calculated in conventional fixed-order perturbation theory compared to the first-order expansion of the SCET results in α . Δ_{SCET} is defined in (6.47).

In general, in the results for the transverse polarisations the agreement is worse since they are dominated by the small- $|t|$ or small- $|u|$ regime, as described above. We also recognise that the results for $\gamma\gamma \rightarrow W^+W^-$, shown on the r.h.s. of Fig. 6.20, exhibit a slower convergence in the high-energy tails. This is due to the quadratic t dependence of the tree-level amplitudes, see (6.46). We note, however, that even in regions where the Born results differ by a few percent (where the green curve is outside the range of the middle panels), the difference in the relative corrections is already of the order of 0.1% (see for instance $\gamma\gamma$ -induced transverse WW production in Fig. 6.20). This indicates that the error owing to small- $|t|$ or small- $|u|$ events is strongly reduced for the relative virtual corrections.

For $\gamma\gamma \rightarrow W_T W_T$, which is dominated by W production in the forward/backward direction, Δ_{SCET} reaches the subpercent level at $M_{4\ell} \approx 8$ TeV, and $\delta_{\text{FO}}^{\text{virt}} - \delta_{\text{SCET}}^{\text{virt}}$ at about $M_{4\ell} \approx 5$ TeV. In these regions, however, almost no statistics is to be expected since the differential cross section is already below 10^{-6} fb/GeV. Even if one would consider an overflow bin from $M_{4\ell} = 10$ TeV to infinity, the cross section in that bin would not exceed 1 ab. In the high- $p_{T,\ell}$ tails, events with low $|t|$ or $|u|$ are suppressed: because the gauge bosons are produced with high energy, their decay products are preferentially radiated in the forward direction. A high lepton p_T is thus likely to result from the decay of a gauge boson with high p_T . Thus in the high- $p_{T,\ell}$ tails the convergence looks better, reaching the subpercent level between 1 and 2 TeV. However, for the same reason the cross section falls off very fast in these distributions, and only for $p_{T,\ell} \lesssim 2$ TeV a measurable cross section is to be expected (remember that the expected luminosity is $\mathcal{L}_{\text{FCC-hh}} = 20 \text{ ab}^{-1}$). Thus, the window in which SCET_{EW} can be applied and at the same time sufficient statistics can be expected is rather narrow for this process.

In the other cases, however, the cross section is still measurable in the phase-space regions, in which SCET_{EW} is about to work, which is demonstrated more explicitly in section 6.4.2.

Influence of the phase-space cut

One should note that the discrepancy has in principle two causes: The fact that the SCET_{EW} cross section is subjected to the cut (6.11) and the impact of the mass-suppressed terms in the matrix elements. In Fig. 6.21 we compare the effect of the cut (6.11) by relating the SCET_{EW} results to the SM results in the same way as in (6.22), but with the $d\sigma^{\text{full}}$ evaluated on the HEPS only. We do that exemplarily for $\gamma\gamma \rightarrow W^+W^- \rightarrow \mu^+\nu_\mu\bar{\nu}_e e^-$ because Δ_{DPA} has particularly large values for transversely polarised Ws and particularly small values for longitudinally polarised Ws.

The difference between the purple and the green curve in Fig. 6.21, which quantifies the effect of the cut, is clearly smaller than the absolute value of both curves: In the transverse case where the difference due to the mass-suppressed terms is of the order of several percent in the regions of $M_{4\ell} \approx 3 - 7$ TeV or $p_T \approx 1$ TeV, the effect of the cut is already at the subpercent level in the same phase-space region. In the tails of the distributions it is actually exactly zero, as the cut (6.11) does not cut a single event during the integration (with each bin containing 5,000-10,000 events). In the longitudinal case the difference is $< 10^{-5}$ everywhere but in the first bin of the distribution. In addition, since the cut can only make the FO cross section smaller, its effect on Δ_{SCET} can only be negative. The dominant contributions from the matrix element are also negative, the deviations are thus slightly larger if the SCET_{EW} cut is applied to the result.

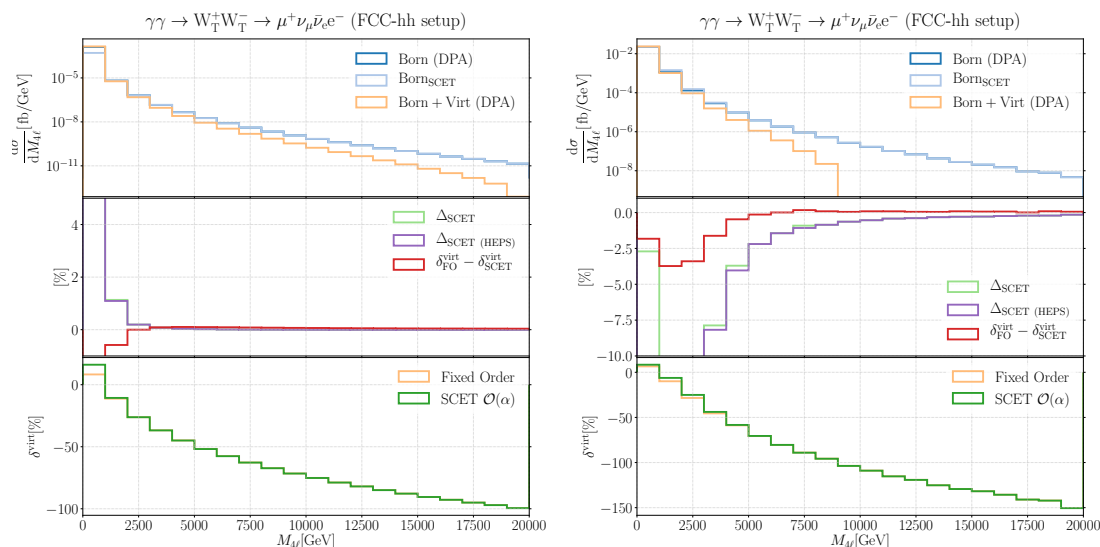


Figure 6.21.: Distribution in the four-lepton invariant mass in $\gamma\gamma \rightarrow W_L W_L \rightarrow \mu^+ \nu_\mu \bar{\nu}_e e^-$ (left) and $\gamma\gamma \rightarrow W_T W_T \rightarrow \mu^+ \nu_\mu \bar{\nu}_e e^-$ (right). The green and red curves show Δ_{SCET} as defined in (6.47), while the purple (HEPS) curves show the same quantity with the SM matrix elements being computed on the HEPS. In the longitudinal case the curves for Δ_{SCET} and $\Delta_{\text{SCET,HEPS}}$ are not to distinguish.

6.3.5. The individual SCET_{EW} ingredients

In Figs. 6.22 and 6.23 we demonstrate exemplarily the role of the individual contributions entering the curves in the previous section. We choose two somewhat representative partonic sample processes, $d\bar{d} \rightarrow W_L W_L \rightarrow \mu^+ \nu_\mu \bar{\nu}_e e^-$ and $\bar{u}u \rightarrow Z_T Z_T e^+ e^- \mu^+ \mu^-$, for illustration. The different curves are labelled as follows:

- DL: Double-logarithmic contributions from the collinear anomalous dimension γ_C .
- SL: Single-logarithmic contributions from γ_C .
- PR: Corrections associated with the renormalisation of α and θ_w . Both logarithmic and finite contributions are included.
- Soft: Angular-dependent single logarithms from γ_S .
- HSM: High-scale matching coefficient: The $\mathcal{O}(\alpha)$ corrections evaluated in the SySM.
- LSM: Low-scale corrections: The logarithmic and the finite part of D_C to $\mathcal{O}(\alpha)$.
- Decay: Corrections associated with the W- or Z-boson decay.
- The sum of all is denoted as $\text{SCET } \mathcal{O}(\alpha)$.

For the definitions of the quantities D_C , γ_C , and γ_S , we refer to Sec. 5.2. It should be stressed that the distinction of these contributions is only possible if the SCET_{EW} amplitude is expanded in α . Otherwise the matrix structure of the anomalous dimension mixes with the high-scale matching coefficients producing terms that can not unambiguously be identified with one of the

above categories. We present these results in order to give a rough estimate of the respective effects.

In transversal Z-pair production (Fig. 6.22) the dominant DL contributions reach -100% at $M_{4\ell} \approx 4.5$ TeV and $p_{T,e^-} \approx 1.5$ TeV. The SL contributions account for $\sim +25\%$ and the PR contributions for $\sim -20\%$ in this regions. The soft contributions behave differently in the two distributions: in the high-lepton- p_T region they are partially shielded and do not exceed 10% , because small values of $-t/s$ (in the ZZ production process) are not allowed in this region. On the other hand, in the high- $M_{4\ell}$ region they can reach up to $+30\%$. We further note that the logarithmic part of the LSM contributions (see (3.124), (3.125)) is small, such that the total LSM corrections are $< 10\%$ and its curve looks almost constant. It is thus not necessary to resum these logarithmic corrections, which are associated with the collinear anomaly. The other contributions, which are not logarithmically enhanced, yield contributions of few percent. Note that the qualitative behaviour of the various curves may be expected to be similar, as it is determined by the W^3W^3 subprocess in the ZZ-production case.

For the production of longitudinal W^\pm bosons, which have smaller Casimir invariants, the DL contributions are genuinely smaller, reaching -100% at $M_{4\ell} \approx 20$ TeV and $p_{T,e^-} \approx 7$ TeV, respectively (see Fig. 6.23). Owing the Yukawa-coupling term in (5.41), the SL contributions are also negative ($\sim -10\%$ in the tails). As in the transverse case, the PR contributions are at about -20% . The Soft contributions are always positive and account for up to 20% in both the high- $M_{4\ell}$ and the high- p_{T,e^-} tails. The other contributions are on the level of few percent. This implies that the full results are in incidently well approximated by the DL corrections alone.

6.4. Resummed results

In this section we present the main results, the resummed differential cross sections calculated in SCET_{EW}. The relative corrections of the resummed results are defined in analogy to fixed order:

$$\delta^{\text{res}} = \frac{d\sigma^{\text{res}}/d\mathcal{O} - d\sigma^{\text{Born, SCET}}/d\mathcal{O}}{d\sigma^{\text{Born, SCET}}/d\mathcal{O}}, \quad (6.48)$$

with $\sigma^{\text{Born, SCET}}$ denoting the Born cross section evaluated on the high-energy phase space only. Note that within the SCET_{EW} framework this definition of a relative correction is not the only plausible one. It is chosen in order to enable a direct comparison against the FO result. We consider three out of the four sets of terms given in (5.95):

- LL+NLO: The double logarithms are exponentiated and the single logarithms are added perturbatively. This implies that the exponential of the integrated anomalous dimension master formula (5.14) is expanded according to (5.94).
- NLL_{FO}+NLO: The exponential in (5.14) is approximated according to (5.93).
- NLL+NLO: The matrix exponential in (5.14) is taken to all orders. Note that the anomalous dimension is calculated only up to first order in α . The $\mathcal{O}(\alpha^2L^2)$ contributions from the two-loop cusp anomalous dimension are thus neglected.

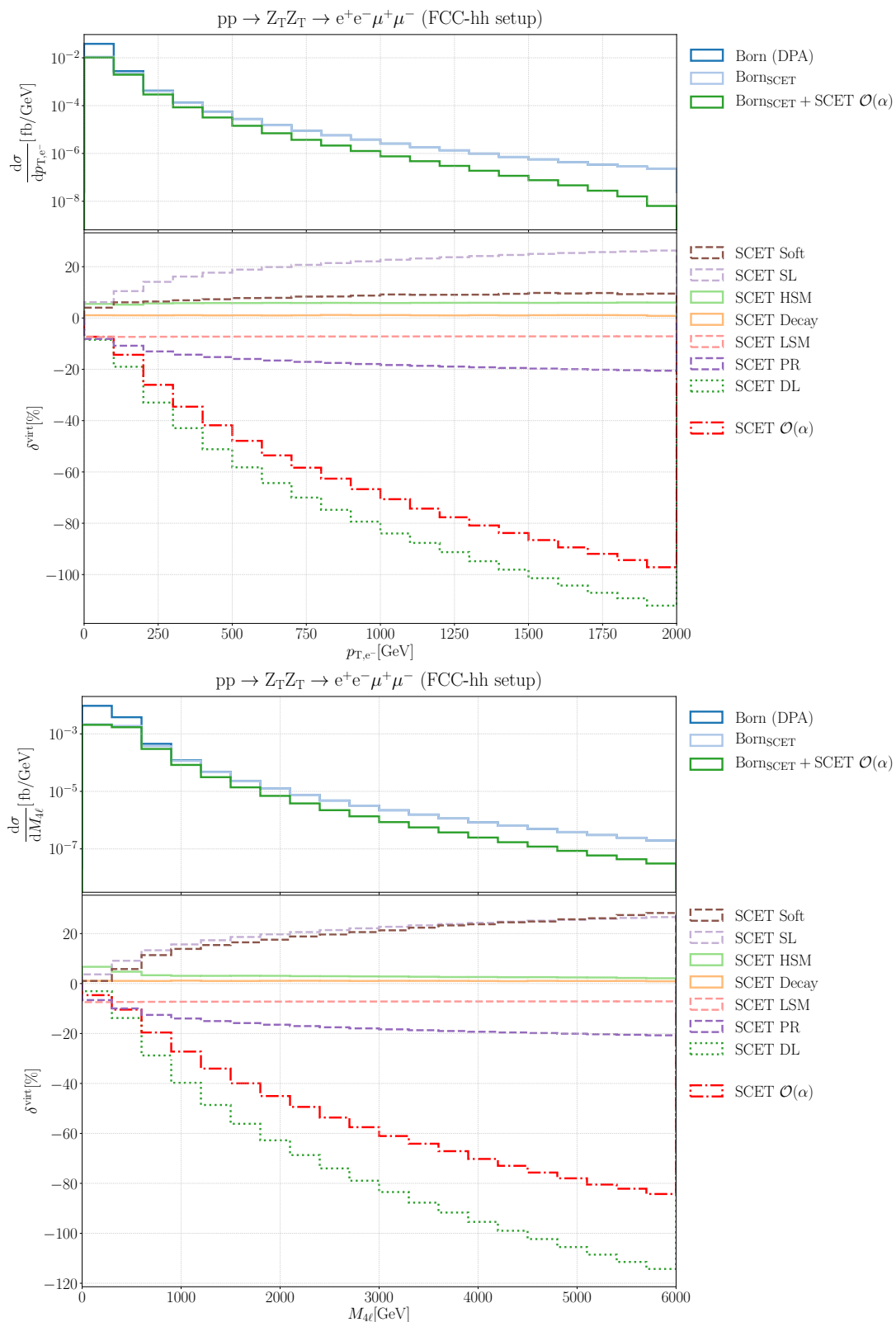


Figure 6.22.: Individual SCET contributions in the partonic process $\bar{u}u \rightarrow Z_T Z_T \rightarrow e^+ e^- \mu^+ \mu^-$ differential in the electron p_T and the four-lepton invariant mass. The meaning of the abbreviations is explained in the text.

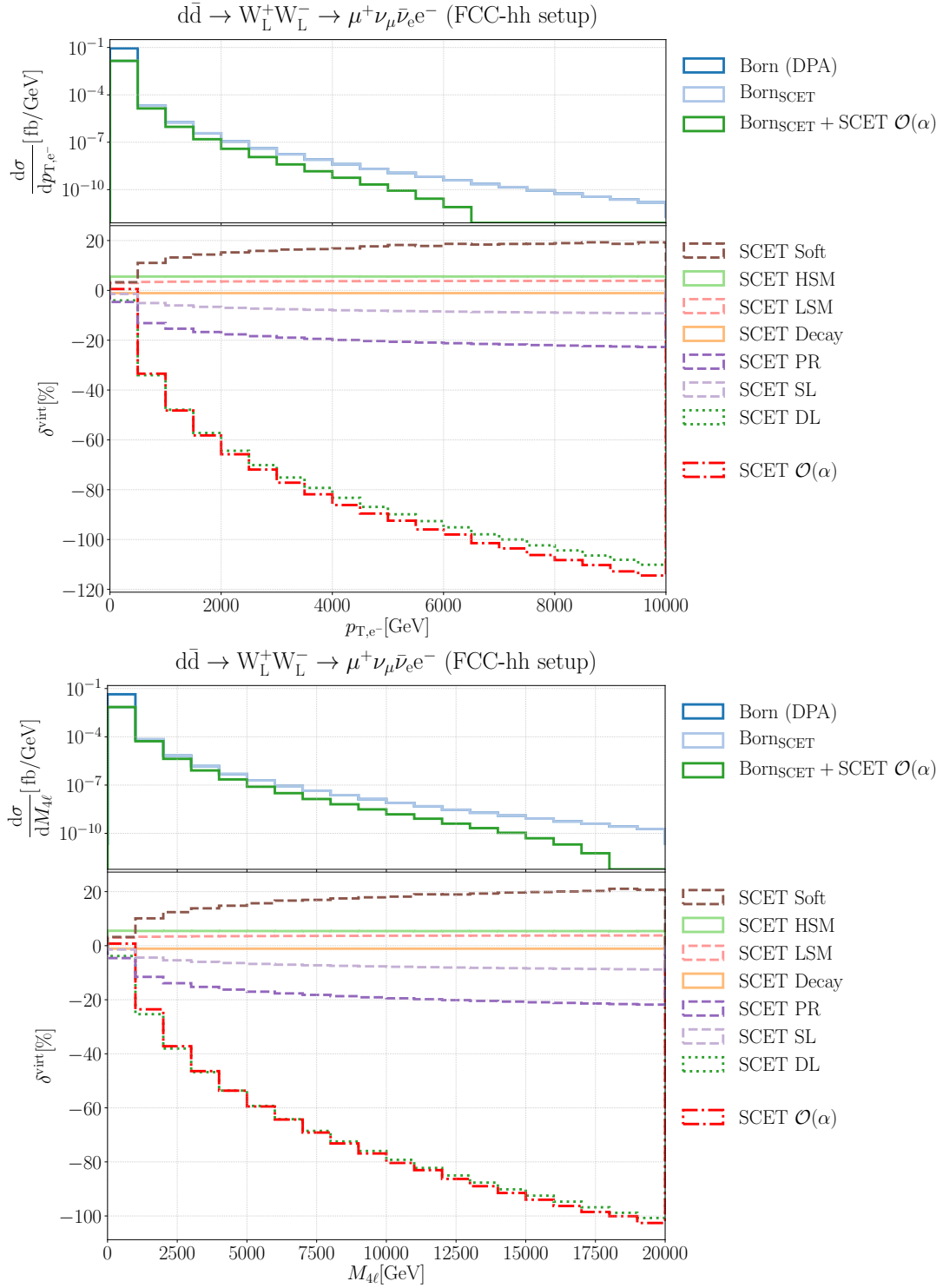


Figure 6.23.: Individual SCET contributions in the partonic process $d\bar{d} \rightarrow W_L W_L \rightarrow \mu^+ \nu_\mu \bar{\nu}_e e^-$ differential in the electron p_T and the four-lepton invariant mass. The meaning of the abbreviations is explained in the text.

6.4.1. Virtual corrections only

The effect of the resummation on polarised results is shown in Fig. 6.24 for $pp \rightarrow W^+W^- \rightarrow \mu^+\nu_\mu\bar{\nu}_e e^-$, in Fig. 6.25 for $pp \rightarrow W^+Z \rightarrow e^+\nu_e\mu^+\mu^-$, in Fig. 6.26 for $pp \rightarrow ZZ \rightarrow e^+e^-\mu^+\mu^-$, and in Fig. 6.27 for $\gamma\gamma \rightarrow W^+W^- \rightarrow \mu^+\nu_\mu\bar{\nu}_e e^-$. We show distributions differential in the same quantities as in Figs. 6.17, 6.18, 6.19, and 6.20. All partonic production channels are included. The polarised contributions are presented separately in order to demonstrate the different behaviour of the resummed curves. In order to take the effects of the DPA into account, we rescale the virtual corrections via Eq. (6.27), as we did already for the unresummed results in section 6.3.3. The effects of the resummation can be read off the plots as follows:

- The shift between the dark green curves (LL) and the orange curves (fixed order) show the effect of the LL resummation (see (5.94) and the explanation below).
- The difference between the dark green (LL) and the pale green curves (NLL_{FO}) is given by the product of the exponentiated leading logs and the perturbative single logarithms, see (5.93), (5.94). The dominant terms are of $\mathcal{O}(\alpha^2 L^3)$. Because the double logarithms are negative and the single logarithms are typically positive, these terms are negative.
- The effect of the exponentiated single-logarithmic contributions can be obtained from difference between the pale green and the red curve.

The resummation and matching affect the longitudinally and transversely polarised cross sections in a rather different way. In transverse W^\pm -pair production (r.h.s. of Fig. 6.24) the effect of the LL resummation, which is in this case obtained from substituting the DL corrections by their exponential on the level of the matrix elements, accounts for slightly more than 100% in the high- $p_{T\ell}$ tail and slightly below 100% in the high- $M_{4\ell}$ -tail. Including the negative $\mathcal{O}(\alpha^2 L^3)$ terms has a similarly large effect: In the high- $M_{4\ell}$ tail the NLL_{FO} resummed cross section is shifted with respect to the LL resummed one by $\sim -70\%$ in the high- $M_{4\ell}$ tail, by $\sim -60\%$ in the high- $M_{e^-\mu^+}$ tail, and by -40% in the high- p_{T,e^-} tail. For transverse W bosons the effect of NLL resummation is about $+10\%$ in both invariant-mass distribution tails. In the region of high lepton p_T , it is much lower because of the suppression of the angular-dependent logarithms, see Fig. 6.22 and its discussion.

In longitudinal W^+W^- production (l.h.s. of Fig. 6.24) we observe that, while the effect of the LL resummation accounts for $\sim 40\%$, the cancellation of single-logarithmic contributions mentioned in Sec. 6.3.5 suppresses the effects of resummation beyond LO: The angular logarithms are positive, while the collinear SL contribution is negative due to the Yukawa coupling term. The sum is small and hence exponentiating it has little effect: The NLL_{FO} resummation accounts for a -10% shift in all tails and the effect of the NLL resummation is only few percent.

In W^+Z production (Fig. 6.25) some general features of the W^\pm results are reproduced including the different resummation effects depending on the polarisations: In the transverse case (plots on the r.h.s.) the effect of the LL resummation is about 60% at $M_{4\ell} \approx 10\text{TeV}$, which is similar to what can be read off the lower left plot in Fig. 6.24 (note the different plot ranges). In the high- p_{T,e^-} tail this effect is slightly below 60%, while in the high- $M_{e^+\mu^-}$ tail it reaches almost 70%. The effects of the NLL_{FO} resummation is similar, at $M_{4\ell} \approx 10\text{TeV}$ and $M_{e^+\mu^-} \approx 7\text{TeV}$ it compensates the LL effect up to $\sim 15\%$. The NLL resummation accounts for at most 10% for large invariant masses ($M_{4\ell} \gtrsim 4\text{TeV}$, $M_{e^+\mu^-} \gtrsim 2\text{TeV}$).

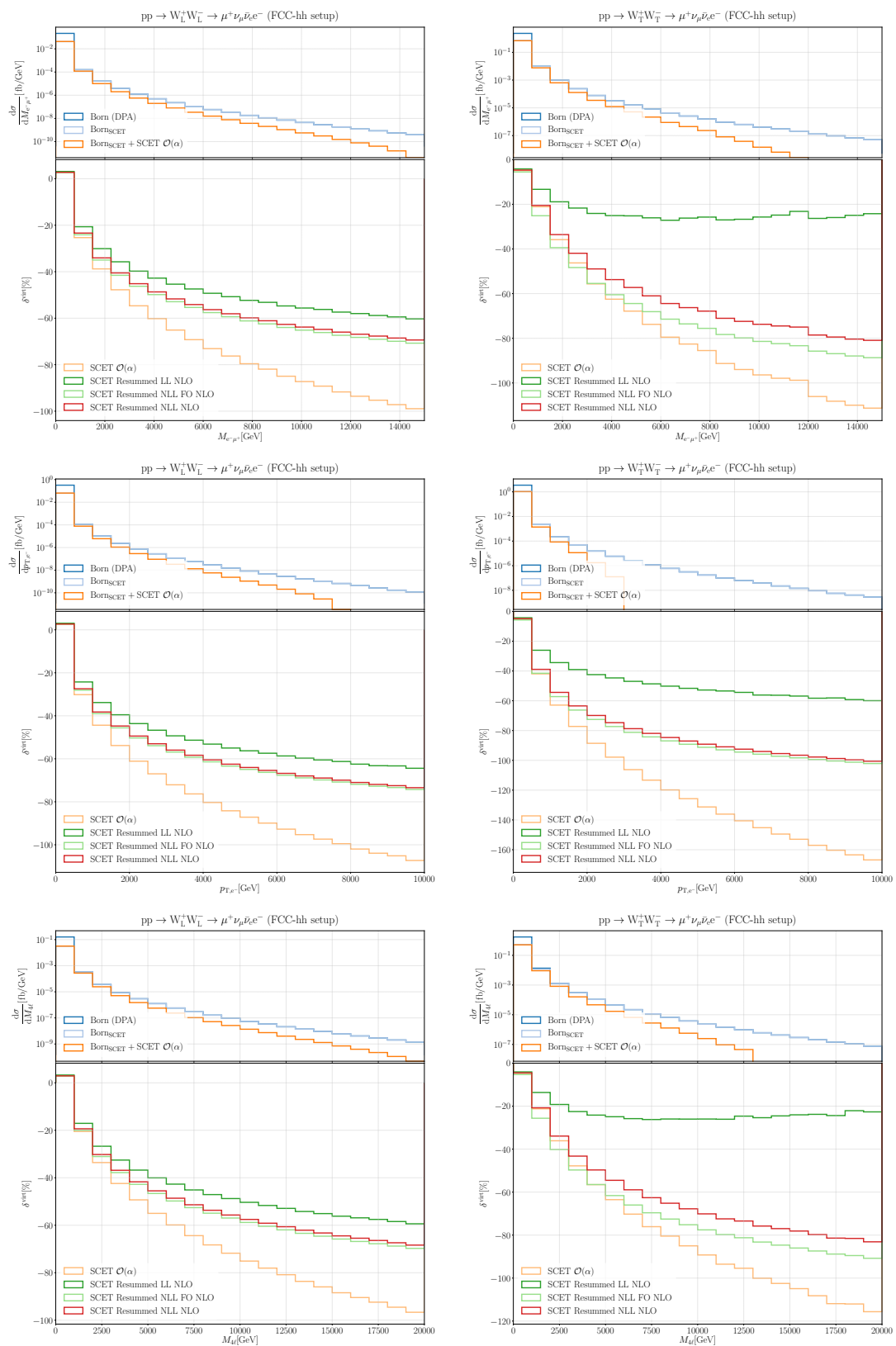


Figure 6.24.: Effect of the SCET resummation on distributions of virtual corrections to $pp \rightarrow W^+W^- \rightarrow \mu^+\nu_\mu\bar{\nu}_e e^-$ with longitudinal (left) and transverse (right) polarisations differential in the $e^-\mu^+$ invariant mass, the electron p_T , and the four-lepton invariant mass.

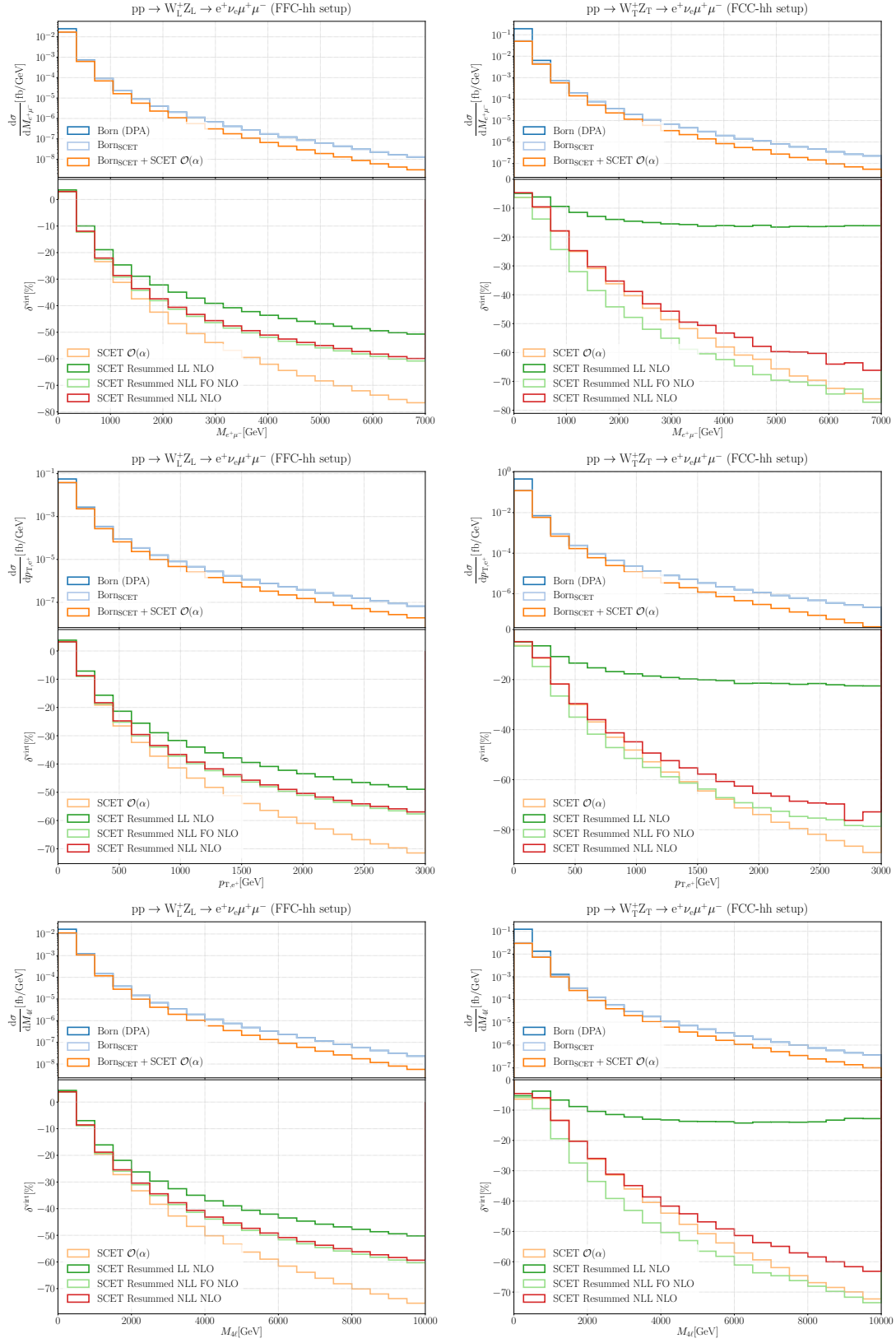


Figure 6.25.: Effect of the SCET resummation on differential distributions of virtual corrections to $pp \rightarrow W^+Z \rightarrow e^+\nu_e\mu^+\mu^-$ with longitudinal (left) and transverse (right) polarisations differential in the $e^+\mu^-$ invariant mass, the positron p_T , and the four-lepton invariant mass.

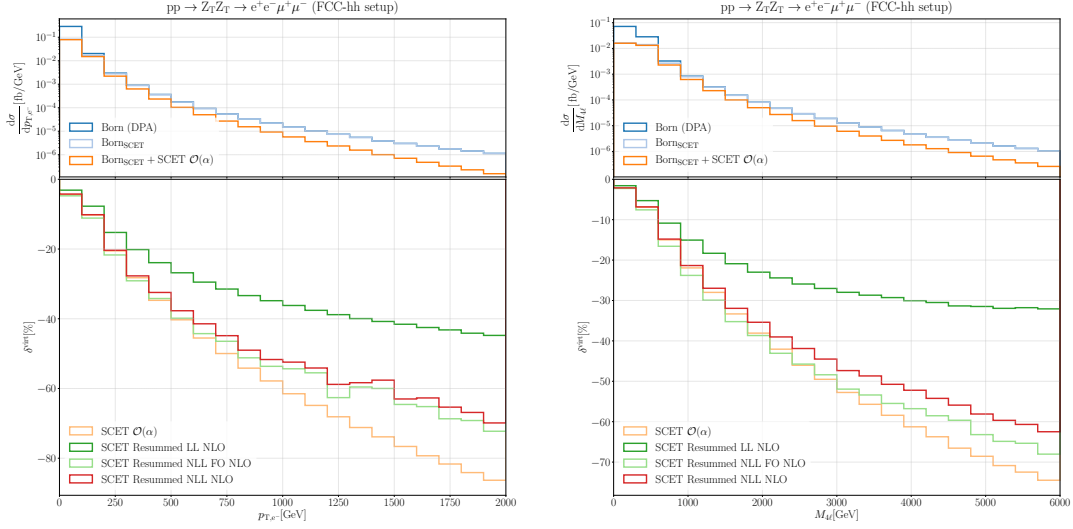


Figure 6.26.: Effect of the SCET resummation on differential distributions of virtual corrections to $pp \rightarrow ZZ \rightarrow e^+e^- \mu^+ \mu^-$ differential in the electron p_T and the four-lepton invariant mass.

For longitudinally polarised bosons (see the plots on the l.h.s.) the effects of the various terms are again smaller. The LL resummation accounts for 25% – 30% in the tails, the effect of the NLL_{FO} terms is about -10% , and the NLL contributions are only at the percent level.

In Fig. 6.26 we show differential results in the electron p_T and the four-lepton invariant mass for $e^+e^- \rightarrow ZZ \rightarrow \tau^+\tau^-\mu^+\mu^-$. At $M_{4\ell} \approx 5$ TeV the LL resummation shifts the cross section by 35%, which is slightly less than in the value in the corresponding transverse W^\pm distribution. This can be explained by the fact that the Abelian subprocesses of the ZZ -production process (remember that the matrix element is decomposed according to (5.67)) receive smaller DL corrections. Including the NLL_{FO} terms again undoes that effect to a large extent, and the NLL terms provide a shift of $\sim 5\%$ in the $M_{4\ell}$ tail and even less in the p_{T,e^+} tail.

The photon-induced case (Fig. 6.27) features the largest resummation effects, especially for transversely polarised W bosons (plots on the r.h.s.): In this case the effect of the LL resummation exceeds 100% already at $M_{4\ell} \approx 10$ TeV, $p_{T,e^-} \approx 3$ TeV, and $M_{e^-\mu^+} \approx 6$ TeV, making resummation definitely mandatory. The cancellation of the LL resummation effect owing to the NLL_{FO} terms is again stronger for transverse W bosons than for longitudinal ones. For $M_{4\ell} \gtrsim 13$ TeV, $M_{e^-\mu^+} \gtrsim 11$ TeV, and $p_{T,e^-} \gtrsim 6$ TeV the NLL resummed results still exceed -100% relative corrections.

We close this discussion with a few general remarks. If the FO result is dominated by the DL corrections, one can use the approximate formula

$$\delta_{\text{LL}} \approx \exp(\delta_{\text{FO}}^{\text{virt}}) - 1, \quad (6.49)$$

that has for instance been employed in Ref. [76]. This rule applies to some extent for instance in the processes $pp \rightarrow W_L^+ Z_L$ and $pp \rightarrow W_L^+ W_L^-$ (on the l.h.s. of Figs. 6.24, 6.25), where the SL and soft contributions partly cancel, see Fig. 6.23 in Sec. 6.3.5. In all other cases the situation is actually more involved, even though (6.49) gives a rough estimation of the resummation effect.

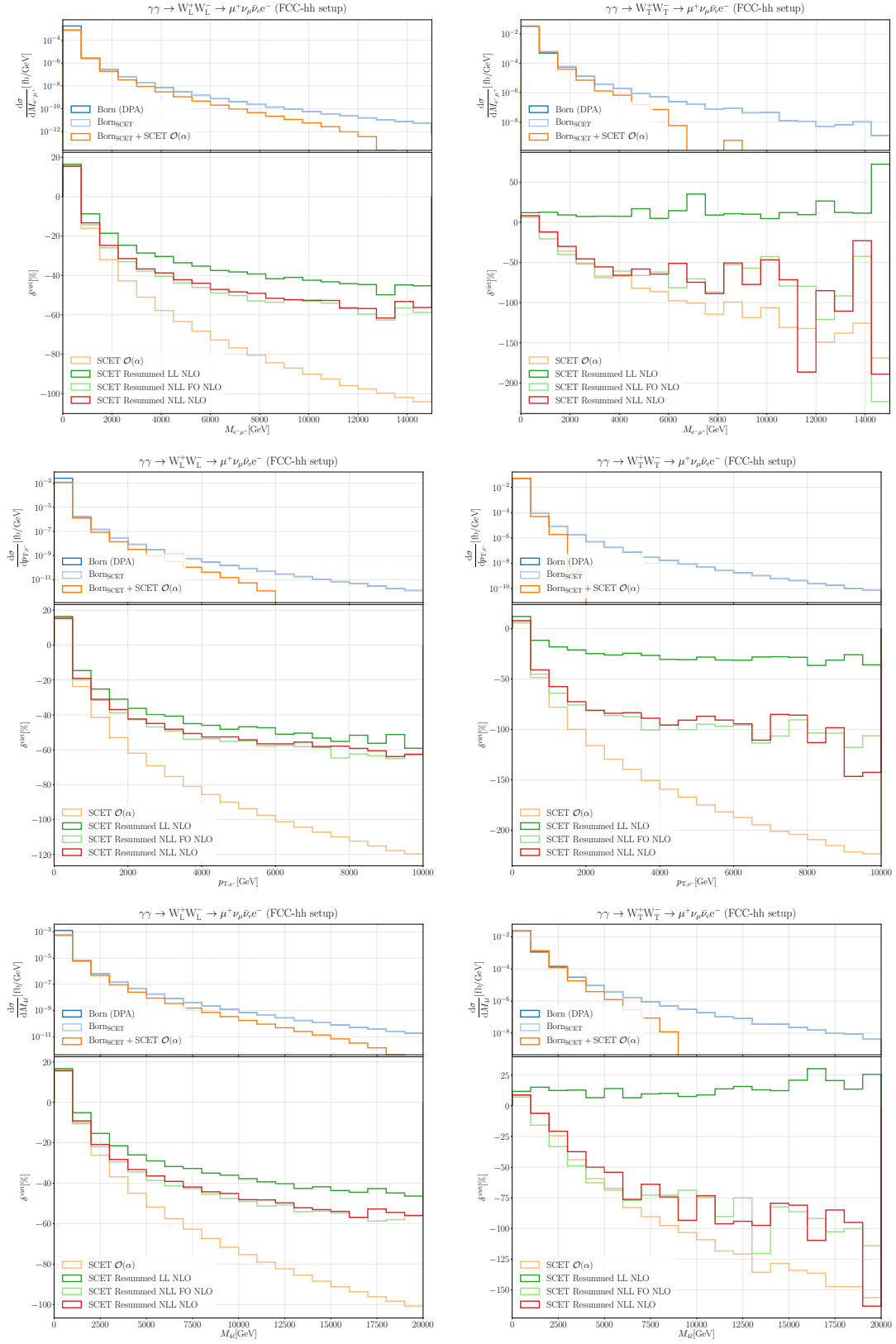


Figure 6.27.: Effect of the SCET resummation on differential distributions of virtual corrections to longitudinal (left) and transverse (right) W^+W^- production in $\gamma\gamma \rightarrow W^+W^- \rightarrow \mu^+\nu_\mu\bar{\nu}_\mu e^-$ differential in the $e^-\mu^+$ invariant mass, the electron p_T , and the four-lepton invariant mass.

One should not be worried by the large relative corrections in the resummed distributions with respect to the unresummed Born: As also mentioned in Sec. III of [45], once the correction factor αL^2 becomes of order one, any resummed results deviates from the fixed-order Born result by a finite amount:

$$\sigma_{\text{LL}}^{\text{resummed}} = \sigma^{\text{Born}} \times \exp\left(-\frac{1}{2}\alpha \log^2 \frac{\mu_h^2}{\mu_l^2}\right). \quad (6.50)$$

The quality of the perturbation series can instead be read off the magnitude of the matching and $N^{(n)}$ LL corrections, i.e. from the difference between the green and red curves in Figs. 6.24, 6.25, 6.26, and 6.27.⁵

6.4.2. Full resummed differential cross sections

At this point we can discuss the impact of the resummation, taking into account the expected counting rates at the FCC–hh. In Fig. 6.28 we show some high-energy tails with the respective counting rates instead of cross sections, including the statistical error on the fixed-order rate as a band for demonstration. The counting rates are obtained from the differential cross sections and the assumed FCC–hh luminosity of $\mathcal{L}_{\text{FCC-hh}} = 20 \text{ ab}^{-1}$ via (6.15). The results are summed over the polarisations and include, besides the factorisable virtual corrections, also real corrections, integrated-dipole contributions and non-factorisable virtual corrections.

For ZZ production (upper left plot in Fig. 6.28) we see that in the window of $1.5 \text{ TeV} < M_{4\ell} < 3 \text{ TeV}$ the impact of the LL resummation exceeds the statistical error on the counting rate within the given binning, indicating that a resummation of the leading logarithms is indeed necessary at these energies. Remember that the error due to the SCET_{EW} assumption in this phase-space region amounts to $\delta_{\text{FO}}^{\text{virt}} - \delta_{\text{SCET}}^{\text{virt}} < 0.5\%$, see Fig. 6.18. The effect of the LL resummation varies between 15% and 30% in this range, the NLL effect is of the same order of magnitude, but with a different sign, such that the NLL+NLO results do not differ by more than 10% from the fixed-order result in the displayed range, which is not significant in view of the experimental error, which reaches 10% ($N_{\text{ev}} = 100$ events) at $M_{4\ell} \approx 2 \text{ TeV}$ already. One should again note that this cancellation is accidental and should not lead to the conclusion that the resummation effects in general are small or even negligible.

In W^+Z and W^+W^- production (upper right and lower left plot in Fig. 6.28), which has by far the highest cross section of the diboson processes, the significance of the LL resummation, which shifts the cross section by more than 50% in the tails, is clearer. The effect of the LL resummation significantly exceeds the statistical uncertainty on the counting rates up to an invariant mass of $M_{4\ell} \approx 6 \text{ TeV}$ and $M_{4\ell} \approx 12 \text{ TeV}$ for W^+Z and W^+W^- production, respectively. Including the NLL_{FO} resummation again has a similarly large effect with an opposite sign. The NLL-resummed result shifts the differential cross section by 5–10% and differs from the fixed-order result by a few percent with respect to LO. Therefore, SCET_{EW} resummation of both the LL and NLL contributions should be included if a precise comparison is aimed for.

In the photon-induced case (lower right plot in Fig. 6.28) the effect of the resummation, normalised to the LO cross section, is largest because of the large Casimir invariant of the

⁵Eventually, for the resummed cross section to be finite in the high-energy limit, the corrections have to be suppressed, such that the NLL-resummed curves saturate at about -100% . However, depending on the coefficients of the double- and single-logs, this may happen many orders of magnitude above the shown energy range.

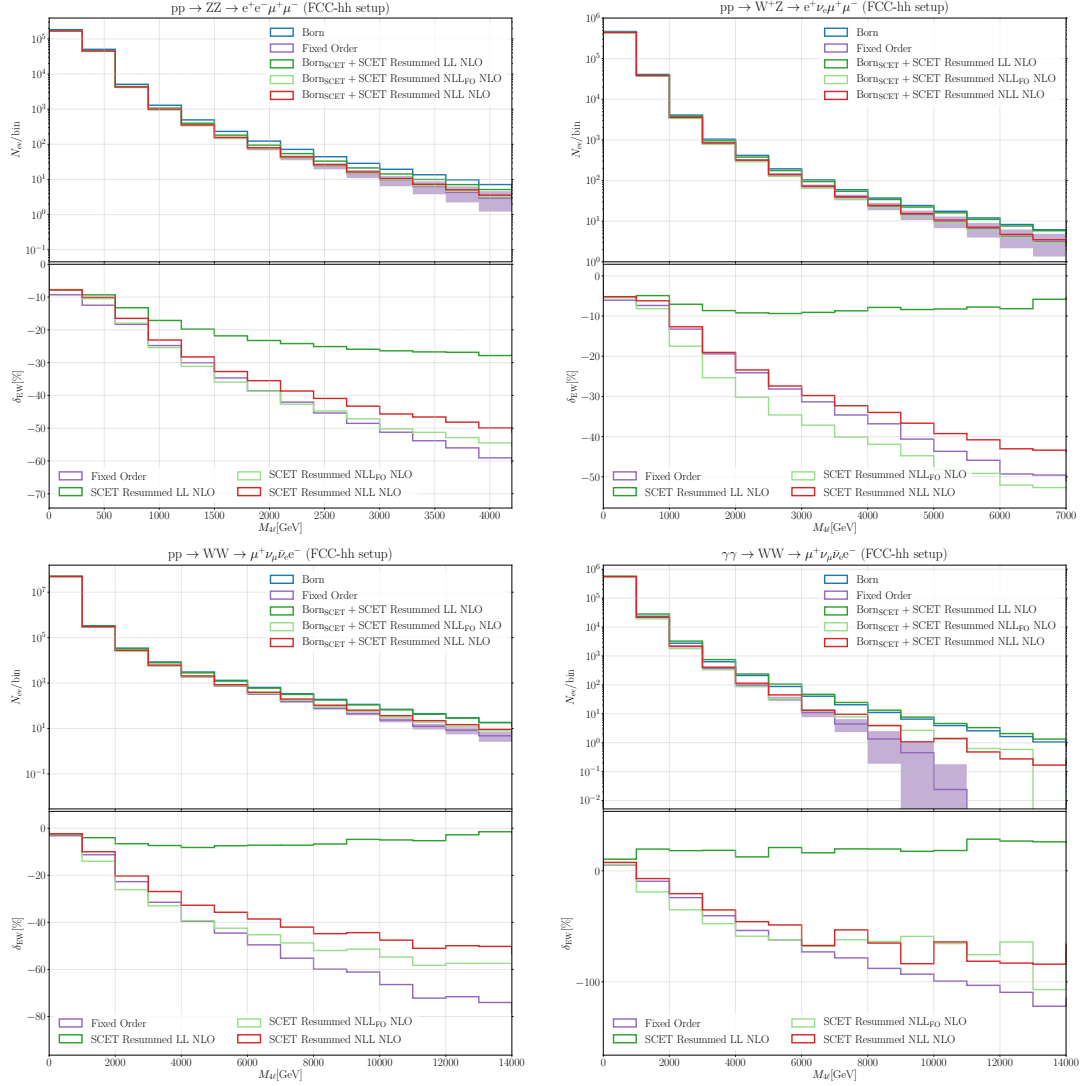


Figure 6.28.: Differential distributions in the four-lepton invariant masses for unpolarised $pp \rightarrow ZZ \rightarrow e^+e^-\mu^+\mu^-$, $pp \rightarrow W^+Z \rightarrow e^+\nu_e\mu^+\mu^-$, $pp \rightarrow W^+W^- \rightarrow \mu^+\nu_\mu\bar{\nu}_e e^-$, production with the error on the counting rates shaded around the purple curves.

W boson. The expected event rate is, similar to the W^+Z and ZZ case, only significant up to $M_{4\ell} \sim 6$ TeV (note further that the photon PDFs also introduce higher uncertainties in particular at large momentum fractions). The qualitative behaviour of the resummed curves is similar to the quark-induced cases: for $M_{4\ell} \sim 6$ TeV the LL resummation increases the cross section by almost 100%, but the inclusion of the NLL_{FO} and NLL undoes the bulk of the effect such that the difference between the fixed-order and NLL-resummed results is at the level of 10%.

7. Results for the CLIC setup

The Compact Linear Collider (CLIC) project aims at a new level of experimental precision in high-energy e^+e^- collisions [16, 231, 232]. In several stages it is planned to operate at collision energies up to

$$\sqrt{s} = 3 \text{ TeV}, \quad (7.1)$$

which we consider in the following. Even though if it operates at energies two orders of magnitude smaller than the FCC-hh, it may be expected to yield more statistics in the interesting high-energy regime because most partonic interactions involve only small energy fractions at pp collisions. In addition all experimental signatures can be expected to be much cleaner than at a hadron collider because of less QCD radiation.

The fact that the bulk of interactions takes place at very high energies makes a high-energy lepton collider a particularly well-suited case of application for SCET_{EW}. There is, however, a number of questions related to how observables have to be defined when leptons with such a large energy interact. In order to demonstrate the effect of SCET_{EW} we have to make some assumptions, of which a detailed discussion is beyond the scope of this work.

- The effects of initial-state radiation, which appear to be challenging for future lepton colliders (see for instance Ref. [233] for details) are treated perturbatively. Thus, we do not use lepton PDFs but assume that only e^+e^- pairs of exactly 3 TeV contribute at LO. The occurring collinear singularities are regulated by the electron mass, leading to logarithmic contributions of the form

$$\delta_{\text{coll}} = \frac{\alpha}{\pi} \left(\log \frac{s}{m_e^2} - 1 \right) \approx 7\%, \quad (7.2)$$

assuming an electron mass of

$$m_e = 5.11 \cdot 10^{-4} \text{ GeV}. \quad (7.3)$$

These logarithms remain unresummed within our framework. However, resummation techniques for these collinear logarithms have been available for a long time [180, 234–236]. For precise predictions in lepton collisions at very high energies the inclusion of lepton-PDF effects is necessary. Recently, results for high-energy lepton PDFs including initial-state radiation of all SM particles have been published [237].

- We assume all leptons to be distinguishable if their pair invariant mass is above 10 GeV (the numerical value is inspired by LHC analyses). In particular we do not include corrections associated with real emission of massive gauge bosons or their decay products.

The CLIC integrated luminosity is assumed as [232]

$$\mathcal{L}_{\text{int}}^{\text{CLIC}} = 5 \text{ ab}^{-1}. \quad (7.4)$$

This value is used to convert cross sections to event rates using (6.15).

7.1. Processes, input, and setup

We consider vector-boson pair production at the highest energy aimed within the CLIC project. In particular we consider the processes

$$e^+e^- \rightarrow W^+W^- \rightarrow \mu^+\nu_\mu\bar{\nu}_\tau\tau^-, \quad (7.5)$$

$$e^+e^- \rightarrow ZZ \rightarrow \tau^+\tau^-\mu^+\mu^-, \quad (7.6)$$

at $\sqrt{s} = 3 \text{ TeV}$. Compared to (6.17), (6.20) we have introduced τ leptons in the final state. We are aware that both these final states are not the phenomenologically most interesting ones:

- (7.5) is usually not considered in experimental analyses of W^+W^- production because the τ has to be reconstructed via its decay products, which involve another W boson.
- (7.6) suffers from low statistics: As the branching fraction of a Z boson into two charged leptons is about 10% [238], final states similar to (7.6) account for only 1% of all ZZ events. Without the overwhelming QCD background of a hadron collider, experimental analyses will very likely be dominated by (semi-)hadronic and invisible decay channels.

We stick to this choice anyway for several reasons:

- We avoid final-state electrons in order to suppress non-doubly-resonant background contributions. We choose different lepton flavours to minimize interference contributions, which can not be calculated within the DPA.
- The processes do not obtain QCD corrections at NLO. This is merely a matter of simplicity, as we are only considering EW corrections within this work.
- When decaying into quarks, the gauge bosons are very likely to produce single (fat) jets, complicating the signal/background relation even more. In particular, assuming fully hadronic final states, the two processes develop a very similar signal and can only be distinguished by the respective jet invariant masses. However, if an efficient tagging of these jets can be achieved, the gauge bosons are in fact detected directly and one can simply apply SCET_{EW} to the production process: Everything besides the gauge-boson production process would in that case be part of the jet algorithm.

In the following we choose the z -axis such that the incoming positron travels in positive z -direction, see Fig. 7.1.

For W^+W^- production all angular differential distributions have asymmetric properties. According to the charge flow we define the *forward region* such that an outgoing W^+ (or its decay product) travels in positive z -direction and a W^- travels in negative z -direction. Thus, in the forward direction the μ^+ has small scattering angles and the τ^- has large scattering angles.

Input parameters

We use the SM input parameters (6.1)–(6.3), supplemented by a numerical value for the electron mass,

$$m_e = 5.11 \cdot 10^{-4} \text{ GeV}. \quad (7.7)$$

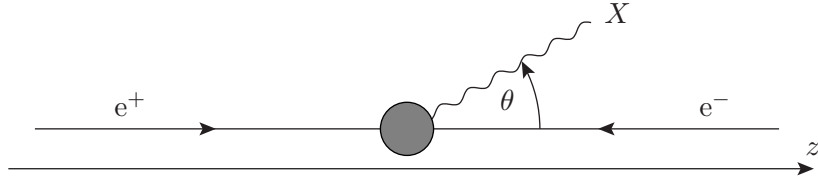


Figure 7.1.: Definition of the scattering kinematics in e^+e^- collisions. X denotes an arbitrary final-state particle.

This is needed in order to regularize the collinear singularities, as explained above.

Event selection

We use the following charged-lepton acceptance cuts:

$$\begin{aligned} p_{T,\ell} &> 20 \text{ GeV}, & 10^\circ < \theta_\ell < 170^\circ, \\ m_{\text{inv},\ell\ell'} &> 10 \text{ GeV}, \end{aligned} \quad (7.8)$$

with θ_ℓ denoting the angle of the lepton with the positron-beam axis. In the ZZ case we impose an additional invariant-mass cut in analogy to (6.8):

$$81 \text{ GeV} < M_{\mu^+\mu^-} < 101 \text{ GeV}, \quad 81 \text{ GeV} < M_{\tau^+\tau^-} < 101 \text{ GeV}. \quad (7.9)$$

The photon-lepton recombination condition is given by (6.10) as in the FCC-hh setup. Furthermore, the condition (6.11) is enforced in all SCET_{EW} calculations.

7.2. Validation

7.2.1. Double-pole approximation

As already mentioned in the previous section, the non-doubly resonant background can be quite sizeable for diboson processes at high-energy lepton colliders. Nevertheless we have to rely on the DPA in order to apply SCET_{EW} to the production process. In the following we analyse the quality of the DPA in the same manner as in the FCC-hh setup.

For the validation of the DPA we use the same quantities as in Sec. 6.3.1 [See (6.22), (6.26)]. The deviation between DPA and off-shell result appears approximately constant over most of the phase space, with Δ_{DPA} fluctuating around 5% and $\delta_{\text{full}}^{\text{virt}} - \delta_{\text{DPA}}^{\text{virt}}$ around 1.5 – 2%, respectively.

Z-pair production

The fiducial cross section for ZZ production reads

$$\sigma_{\text{full}} = 0.013047(3) \text{ fb}, \quad \sigma_{\text{DPA}} = 0.012274(3) \text{ fb}, \quad \Delta_{\text{DPA}} = 5.93(2)\%. \quad (7.10)$$

All errors are MC integration errors. For the relative virtual corrections we obtain

$$\delta_{\text{full}}^{\text{virt}} = -44.58(2)\%, \quad \delta_{\text{DPA}}^{\text{virt}} = -46.21(4)\%, \quad \delta_{\text{full}}^{\text{virt}} - \delta_{\text{DPA}}^{\text{virt}} = 1.63(2)\%, \quad (7.11)$$

with the virtual corrections defined as in (6.25).

Fig. 7.2 shows the differential distributions of the ZZ-production cross section as well as the deviation between DPA and full result differential in the μ^+ angle, the τ^- angle, the μ^+ energy, and the $\tau^-\mu^-$ invariant mass. The scattering-angle distributions have a double-peak structure with maxima at $\theta_{\mu^+} = \theta_{\tau^-} \approx 25^\circ$, $\theta_{\mu^+} = \theta_{\tau^-} \approx 155^\circ$, corresponding to the t - and u -channel enhancements, respectively. In the central region the cross section is suppressed by one order of magnitude. The virtual EW corrections vary between -75% in the central region and -20% in the tails.

The energy distribution is peaked at very low and very high energies with the first and last bin ($E < 75$ GeV, $E > 1425$ GeV) being suppressed owing to the phase-space cuts. The relative virtual corrections are approximately constant over energy both in DPA and off-shell.

Finally we include a distribution over the invariant mass of the $\tau^-\mu^-$ system, which is peaked around $M_{\tau^-\mu^-} \approx 800$ GeV. The virtual EW corrections are rather constant over this distribution, varying around the -45% obtained for the integrated result.

W-pair production

For W^+W^- production we obtain the fiducial cross section

$$\sigma_{\text{full}} = 1.760(7) \text{ fb}, \quad \sigma_{\text{DPA}} = 1.456(3) \text{ fb}, \quad \Delta_{\text{DPA}} = 17.3(4)\%. \quad (7.12)$$

The relative virtual corrections read

$$\delta_{\text{full}}^{\text{virt}} = -33.9(2)\%, \quad \delta_{\text{DPA}}^{\text{virt}} = -34.6(1)\%, \quad \delta_{\text{full}}^{\text{virt}} - \delta_{\text{DPA}}^{\text{virt}} = 0.7(2)\%. \quad (7.13)$$

Compared to the ZZ-production results, Δ_{DPA} is larger because the Z-window cuts isolate the doubly-resonant contributions. The difference $\delta_{\text{full}}^{\text{virt}} - \delta_{\text{DPA}}^{\text{virt}}$ is smaller than one percent, indicating that treating the virtual corrections with the DPA does not introduce tremendous errors if the rescaling (6.27) is applied.

Figure 7.3 shows a comparison between fully off-shell results and the DPA on the differential level in the μ^+ and τ^- production angle, the τ^- energy, and the $\tau^-\mu^+$ invariant mass in analogy to Fig. 7.2. The energy distribution is peaked at high charged-lepton energies for helicity-conservation reasons: Because in the forward region, where the cross section is large, the W^+W^- has a preferred polarisation configuration of $(-, +)$ and preferably decays into a high-energy lepton and a low-energy neutrino. In the high-energy tails the quality of the DPA is satisfactory (Δ_{DPA} is about 15%, but the difference of the relative corrections is $< 1\%$), while towards the low-energy regime $\delta_{\text{full}}^{\text{virt}} - \delta_{\text{DPA}}^{\text{virt}}$ grows up to 25%.

The angular distribution is clearly dominated by the forward region owing to the dominant contribution from the t -channel diagram. Towards the backward region the cross section decreases by up to four orders of magnitude. The off-shell virtual EW corrections are between -20% and -40% in the forward region, grow towards the central region and decrease again to -30% in the backward region. Note that the virtual corrections in DPA reach -80% in the backward region. The difference Δ_{DPA} between full calculation and DPA increases from 10% in the forward direction to 80% in the backward direction. The corresponding difference of the relative corrections remains below 5% in the forward hemisphere and increases where the cross section is small.

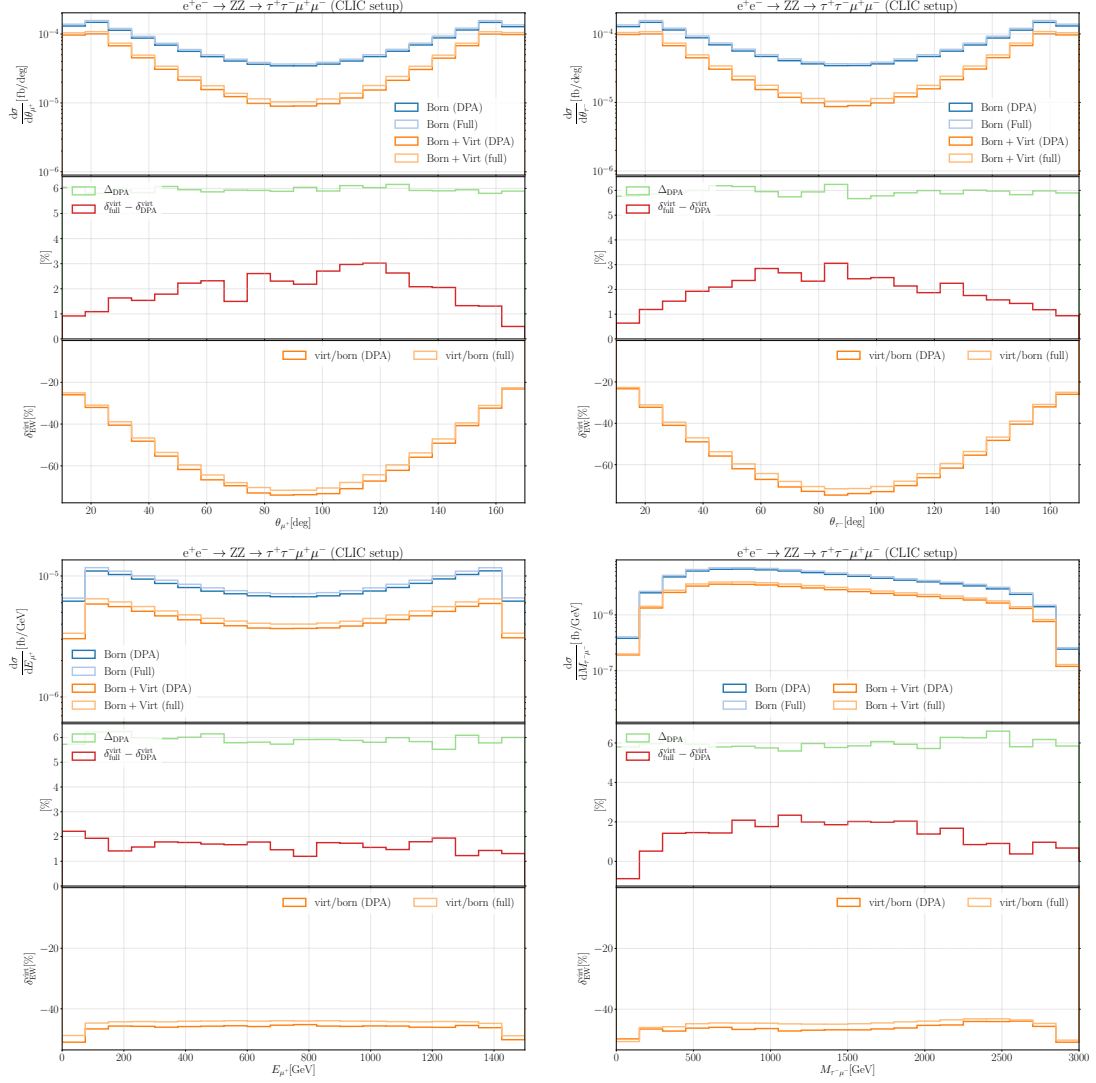


Figure 7.2.: Comparison between DPA and fully off-shell calculation for $e^+e^- \rightarrow ZZ \rightarrow \tau^+\tau^-\mu^+\mu^-$: Differential distributions in the μ^+ and τ^- production angle, the antimuon energy, and the $\tau^-\mu^-$ invariant mass. The upper panels show the differential cross sections, the middle ones the deviations owing to the DPA with Δ_{DPA} as defined in (6.22), while the lower ones show the relative virtual EW corrections.

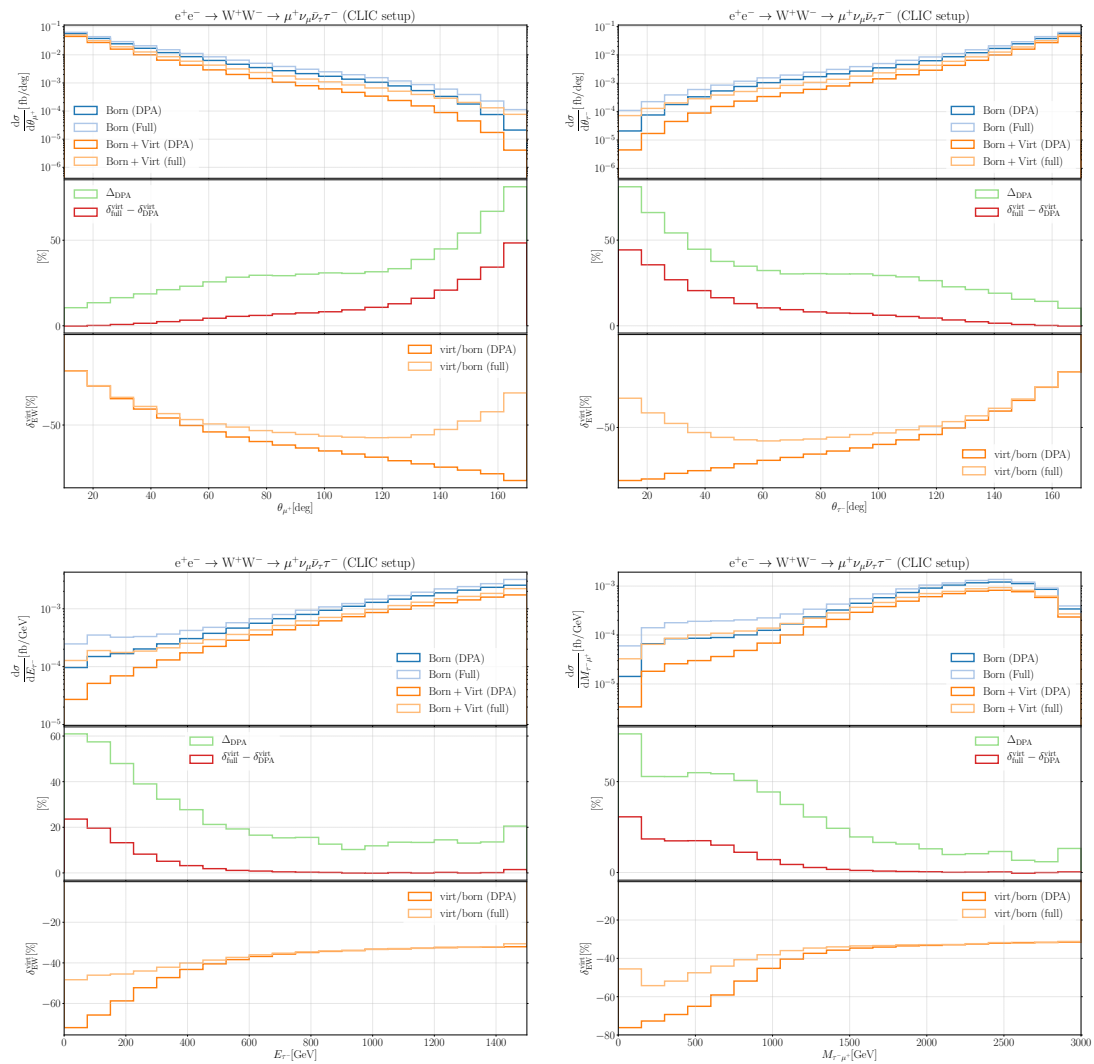


Figure 7.3.: Comparison between DPA and fully off-shell calculation for $e^+e^- \rightarrow W^+W^- \rightarrow \mu^+\nu_\mu\bar{\nu}_\tau\tau^-$: Differential distributions in the μ^+ and τ^- production angle, the tau energy, and the $\tau^-\mu^+$ invariant mass. The plots are structured as in Fig. 7.2.

Pol.	σ^{ZZ}/fb	δ	Pol.	σ^{WW}/fb	δ
UU	$1.2274(3) \cdot 10^{-2}$	100%	UU	1.456(4)	100%
TT	$1.2249(11) \cdot 10^{-2}$	99.8%	TT	1.418(4)	97.4%
TL+LT	$1.419(3) \cdot 10^{-5}$	0.11%	TL+LT	$1.5013(10) \cdot 10^{-3}$	0.1%
LL	$3.533(4) \cdot 10^{-8}$	$\mathcal{O}(10^{-4})\%$	LL	$3.757(3) \cdot 10^{-2}$	2.5%
Σ	$1.2264(11) \cdot 10^{-2}$	99.9%	Σ	1.457(4)	100.1%

Table 7.1.: Integrated fiducial cross sections for $e^+e^- \rightarrow ZZ \rightarrow \tau^+\tau^-\mu^+\mu^-$ (left) and $e^+e^- \rightarrow W^+W^- \rightarrow \mu^+\nu_\mu\bar{\nu}_\tau\tau^-$ (right) with definite polarisation states. The sum Σ includes TT, TL+LT, and LL. All percentages δ are given with respect to the unpolarised result.

Pol.	σ^{ZZ}/fb	δ	Pol.	σ^{WW}/fb	δ
TT	$1.2249(11) \cdot 10^{-2}$	100%	TT	1.418(3)	100%
++	$7.430(8) \cdot 10^{-9}$	$\mathcal{O}(10^{-5})\%$	++	$\sim 5 \cdot 10^{-7}$	$\mathcal{O}(10^{-5})\%$
+-	$6.172(6) \cdot 10^{-3}$	50.4%	+-	0.06933(10)	4.9%
-+	$6.171(6) \cdot 10^{-3}$	50.4%	-+	1.349(3)	95.1%
--	$7.435(8) \cdot 10^{-9}$	$\mathcal{O}(10^{-5})\%$	--	$\sim 5 \cdot 10^{-7}$	$\mathcal{O}(10^{-5})\%$
Σ	$1.2343(8) \cdot 10^{-2}$	100.8%	Σ	1.418(4)	100%

Table 7.2.: Integrated fiducial cross sections for $e^+e^- \rightarrow ZZ \rightarrow \tau^+\tau^-\mu^+\mu^-$ (left) and $e^+e^- \rightarrow W^+W^- \rightarrow \mu^+\nu_\mu\bar{\nu}_\tau\tau^-$ (right) with definite polarisation states. The sum Σ includes ++, +-, -+, and --. All percentages δ are given with respect to the TT value.

All in all, the DPA result at LO is never really appropriate. As discussed already in the previous section, that does not imply that the DPA is worthless because it is still possible to compute only the relative virtual corrections in DPA and use (6.26) as a measure of accuracy. In this respect the DPA works best in the regions of phase space, where the cross section is largest: In the forward region, in the region of large dilepton invariant masses, and for large lepton energies, $\delta_{\text{full}}^{\text{virt}} - \delta_{\text{DPA}}^{\text{virt}}$ is at the subpercent level. Because these regions dominate the cross section, the small value in (7.13) is obtained. In some regions with small cross sections the DPA happens to fail completely. For instance, $\delta_{\text{full}}^{\text{virt}} - \delta_{\text{DPA}}^{\text{virt}}$ grows up to $\sim 50\%$ in the backward region, where the cross section is dominated by singly-resonant contributions.

7.2.2. Polarised leading-order results

The integrated fiducial cross sections for all possible polarisation states are collected in Tabs. 7.1 and 7.2. The mass-suppressed contributions (mixed and longitudinal for ZZ production and mixed polarisations for W^+W^- production) can safely be neglected. The same holds for the interference terms since the sum of the polarisation states reproduces the unpolarised cross section up to 0.1%. The transversal polarisation states with parallel polarisations, ++ and --, are suppressed by M_W^4/s_{ij}^2 in the high-energy limit and therefore definitely negligible (of $\mathcal{O}(10^{-7})$ of the fiducial cross section).

The ZZ cross section receives a shift of about -0.8% owing to interference contributions between the $+-$ and the $-+$ polarisation state, see Tab. 7.2. In the W^+W^- case the transverse interference contributions are zero within the numerical accuracy of the MC integration error.

In Figs. 7.4, 7.5 we show the differential distributions in the same variables as in Figs. 7.2, 7.3 for ZZ and W^+W^- production, respectively. The plots are organised as in Sec. 6.3.2, the definitions of the variables $\Delta_{\text{pol/int}}$ can be found in (6.36), (6.37), and (6.38).

In the ZZ case the mixed polarisation configurations exhibit a maximum in the central region (see the μ^+/τ^- angle distributions in the upper row of Fig. 7.4), but do not exceed 0.5% even in this region. In the distributions of the τ^- energy and the dilepton invariant mass the interference fluctuates on a slightly lower level, between 0.1% and 0.3% .

In the μ^+ and τ^- production-angle distributions in W^+W^- production (upper plots in Fig. 7.5) there is an increase of the mixed-polarised contributions in the backward-scattering region (large antimuon production angle, small tau production angle). Here the interference and mixed contributions account for up to 6% , of which the major part is given by the mixed-polarisation contributions (difference between the red and green curve). Since the cross section is small in this region, the influence on the fiducial cross section is still small. In the $M_{\tau-\mu^+}$ distribution $\Delta_{\text{pol/int}}$ fluctuate in the range of $\pm 0.5\%$ except for the last bin in the $M_{\tau-\mu^+}$, which is likely a numerical artefact.

In Fig. 7.6 we show corresponding results for the interference contributions among the transverse polarisation states differential in the μ^+ production angle and the τ^- energy. We can see that the interference contributions are distributed rather constant over both variables in both processes. In the ZZ case (plots on the l.h.s.) both contributions account for around 0.8% . For $e^+e^- \rightarrow W^+W^- \rightarrow \mu^+\nu_\mu\bar{\nu}_\tau\tau^-$ (plots on the r.h.s.) one can merely observe numerical fluctuations around 0 in regions with small cross section (small τ^- energy and large μ^+ angles).

The error owing to the incoherent polarisation sum can thus concluded to be at the sub-percent level for both processes (7.5), (7.6). In contrast to the hadron-collider setup both the contributions from mixed transverse/longitudinal configurations and the interference contributions between transverse and longitudinal polarisation states account for less than 1% of the unpolarised cross section almost on the whole phase space and can hence be neglected to a good approximation.

7.2.3. Real and virtual corrections

In analogy to the results of Sec. 6.3.3 in the FCC-hh setup we present the role of virtual and real corrections as well as the integrated dipoles within the Catani–Seymour subtraction framework. In Tab. 7.3 we show the respective contributions to the integrated fiducial cross section for both processes under consideration. The large negative virtual corrections determine the negative sign of the total NLO EW corrections, even though the inclusion of positive real-radiation effects reduces the effect to $\sim -12\%$ and $\sim -25\%$ for W^+W^- and ZZ production, respectively. In Fig. 7.7 we show the subtracted real, virtual, and integrated dipole corrections (the latter two defined via their infrared finite parts) for W^+W^- production. We see that both the real and the idip contributions also develop large corrections, at least in some regions of phase space:

- In the backward-scattering region the corrections related to real radiation and the idip corrections are large. While the tree-level cross section of the dominating doubly-resonant transverse polarisation state is suppressed, the additional photon opens up new phase-space

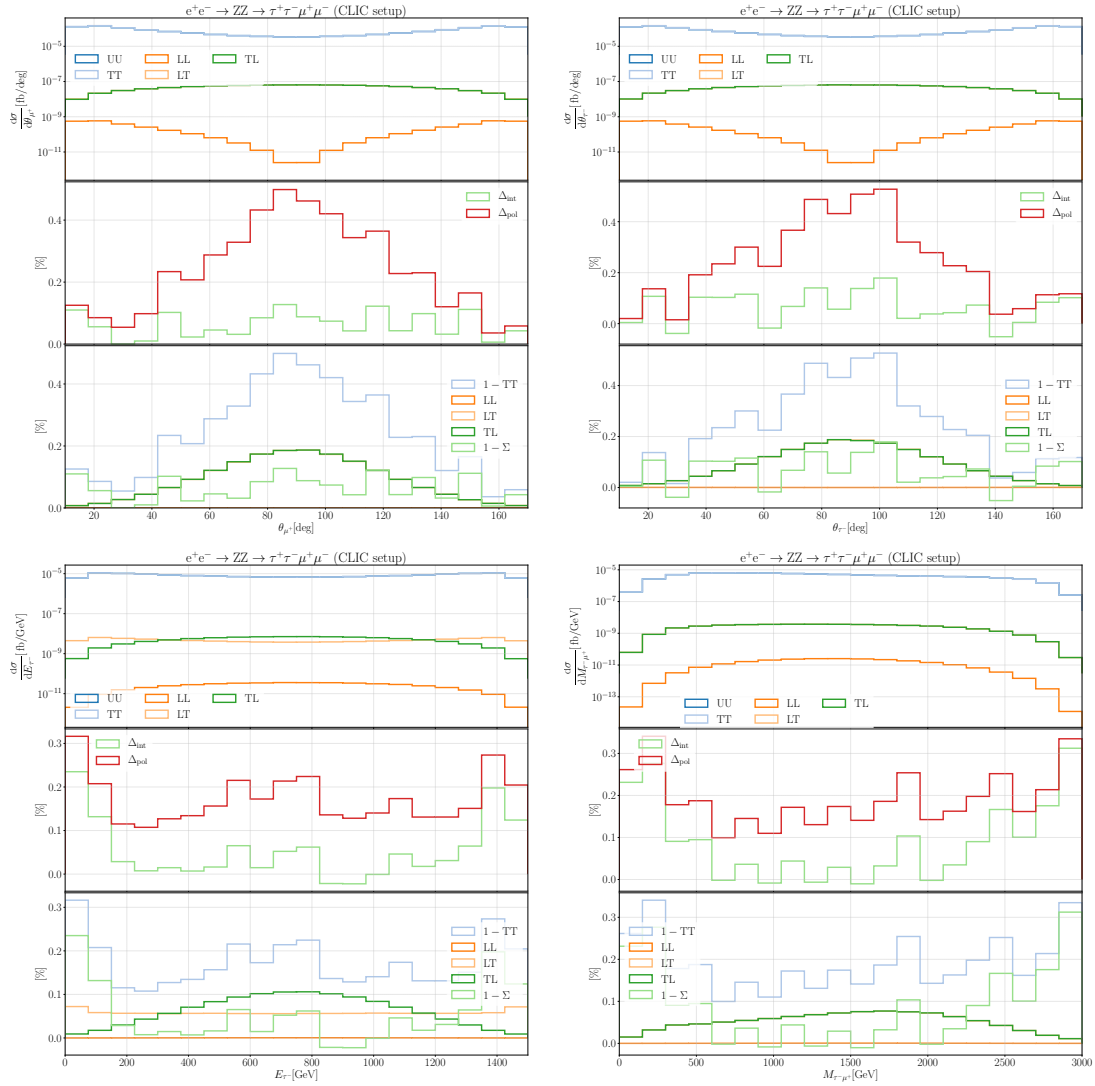


Figure 7.4.: Polarised cross sections for $e^+e^- \rightarrow ZZ \rightarrow \tau^+\tau^-\mu^+\mu^-$ differential in the μ^+ and τ^- production angle, the tau energy, and the $\tau^-\mu^+$ invariant mass. The curves TL and LT are sometimes not to distinguish, the same holds for the TT, UU, and the sum Σ . More details on the curves can be found in Sec. 6.3.2.

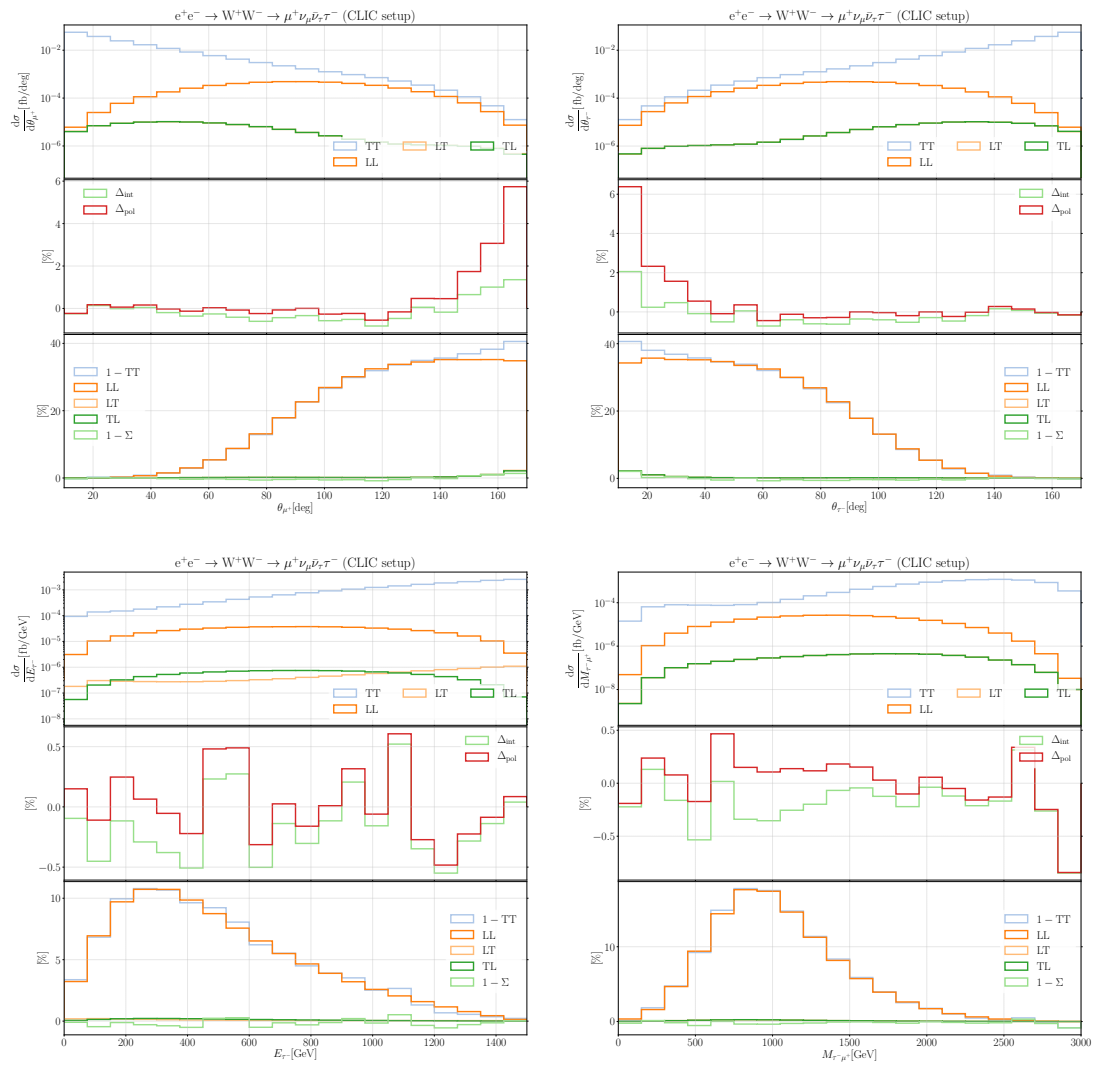


Figure 7.5.: Polarised cross sections for $e^+e^- \rightarrow W^+W^- \rightarrow \mu^+\nu_\mu\bar{\nu}_\tau\tau^-$ differential in the μ^+ and τ^- production angle, the tau energy, and the $\tau^-\mu^+$ invariant mass. The curves TL and LT are sometimes not to distinguish, the same holds for the TT, UU, and the sum Σ . More details on the curves can be found in Sec. 6.3.2.

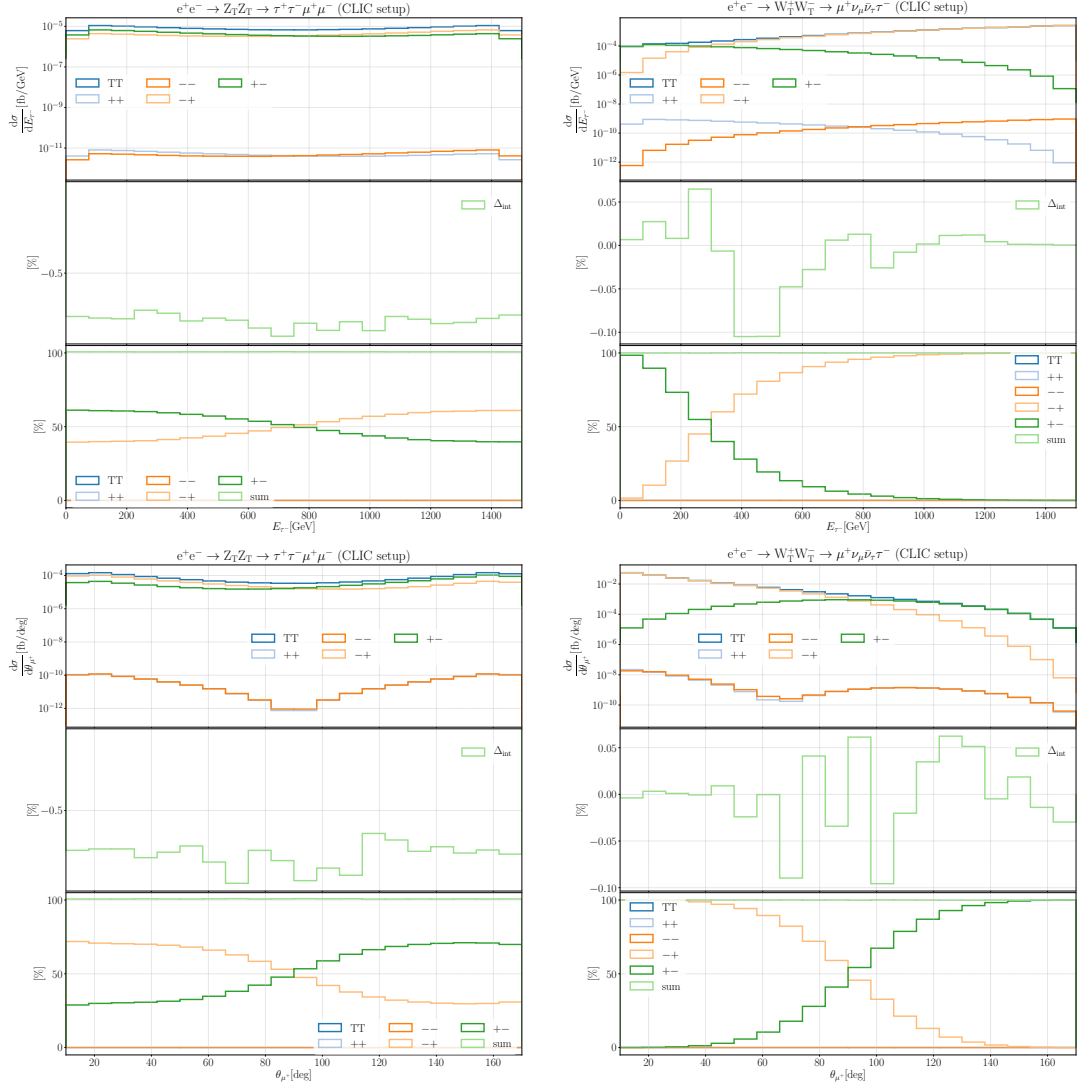


Figure 7.6.: Polarised differential cross sections in the μ^+ production angle and the τ^- energy for $e^+e^- \rightarrow Z_T Z_T \rightarrow \tau^+ \tau^- \mu^+ \mu^-$ (left) and $e^+e^- \rightarrow W_T^+ W_T^- \rightarrow \mu^+ \nu_\mu \bar{\nu}_\tau \tau^-$ (right) broken down to the left (+) and right-handed (-) polarisation states. More details on the curves can be found in Sec. 6.3.2. All curves in the lower panels are normalised to the TT cross section. The -- and ++ curves are not always to distinguish.

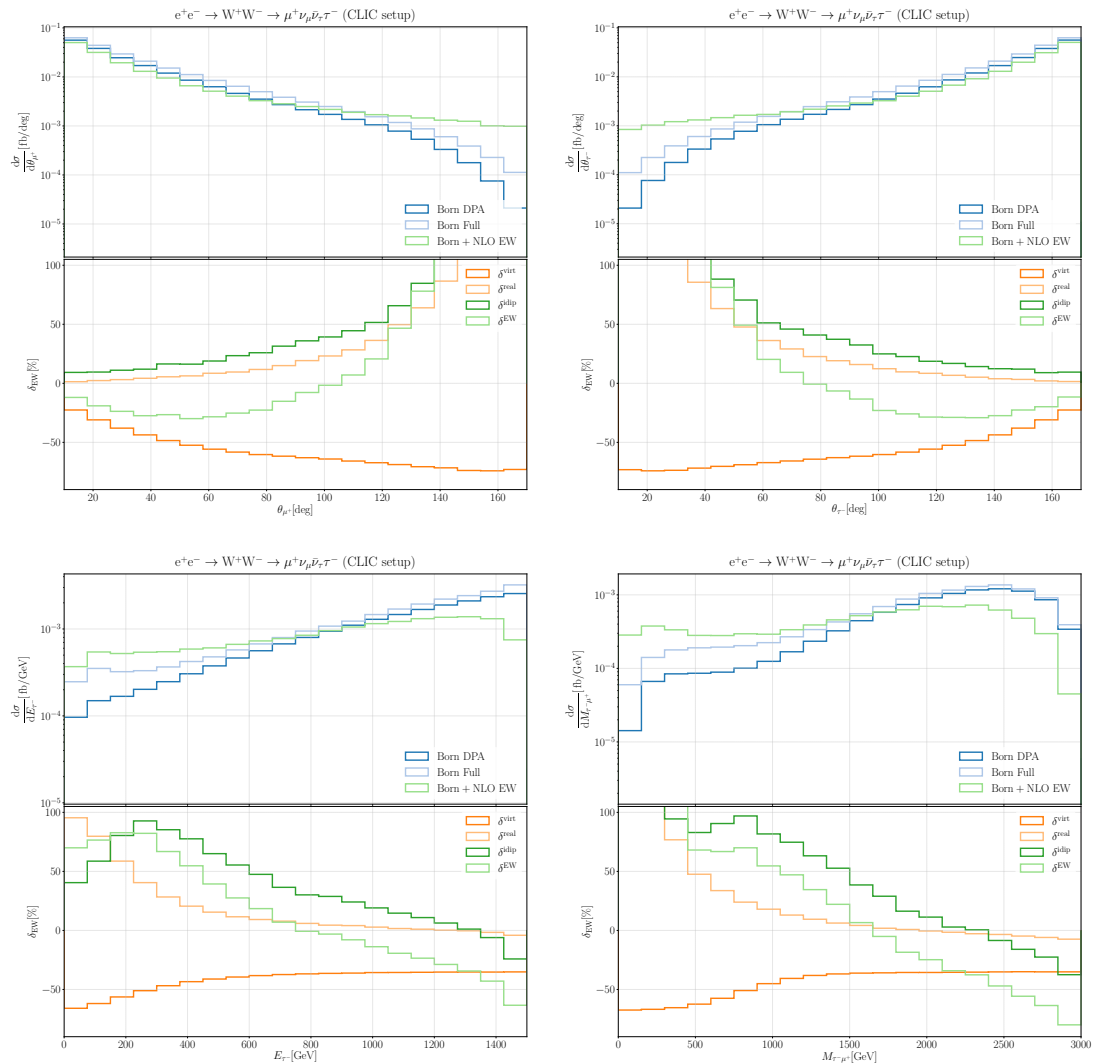


Figure 7.7.: Real, virtual, and integrated dipole (idip) NLO EW corrections for $e^+e^- \rightarrow W^+W^- \rightarrow \mu^+\nu_\mu\bar{\nu}_\tau\tau^-$ differential in the μ^+ and τ^- production angle, the tau energy, and the $\mu^+\tau^-$ invariant mass. The real and idip corrections are normalised by the fully off-shell LO cross section, while the virtual corrections are computed in the DPA. The definition of δ^{EW} is given in eq. (6.39). To obtain the green curve in the upper panel the rescaling (6.27) is applied for the virtuals.

Contribution	$\sigma^{ZZ}/(10^{-2} \text{ fb})$	δ	Contribution	σ^{WW}/fb	δ
LO	1.3047(3)	-	LO	1.760(7)	-
LO (DPA)	1.2274(3)	-	LO (DPA)	1.456(4)	-
NLO virt	-0.5816(2)	-44.6%	NLO virt	-0.5975(18)	-33.9%
NLO virt (DPA)	-0.5668(5)	-46.2%	NLO virt (DPA)	-0.5032(2)	-34.6%
NLO real	0.032(5)	2.5%	NLO real	0.1020(9)	5.8%
NLO idip	0.2237(8)	17.1%	NLO idip	0.271(3)	15.4%
NLO tot	-0.3029	-24.9%	NLO tot	-0.222	-12.6%
NLO tot (DPA)	-0.3046	-26.6%	NLO tot (DPA)	-0.234	-13.7%

Table 7.3.: Integrated fiducial cross sections for $e^+e^- \rightarrow ZZ \rightarrow \tau^+\tau^-\mu^+\mu^-$ (left) and $e^+e^- \rightarrow W^+W^- \rightarrow \mu^+\nu_\mu\bar{\nu}_\tau\tau^-$ (right) with NLO EW corrections in fixed order. The relative corrections δ are defined according to (6.39). To obtain the absolute values of the NLO corrections, the virtuals are rescaled according to (6.27).

configurations, leading to large positive relative corrections of over 100%. In the integrated dipole formulae the convolution of the integrated splitting kernels with the reduced LO matrix elements yields the additional unsuppressed contributions (see the $x, z \neq 1$ terms in the formulae in Sec. 4.1).

- A similar mechanism holds for the small- $M_{\tau^-\mu^+}$ region, for which the tree-level cross section is suppressed by the requirement that the W^+W^- -pair is produced back-to-back. If an additional photon is radiated, configurations with the charged leptons being parallel are more likely to occur leading to large real corrections.

On the other hand the EW corrections are dominated by the virtuals in the high-energy and high-dilepton-invariant-mass regimes as well as in the forward region, where the cross section is largest.

In the case of ZZ production, as displayed Fig. 7.8, a similar mechanism drives the relative real and integrated dipole corrections up in the region of small $M_{\tau^-\mu^+}$ (see lower right plot) and, to some extent, also in the region of small τ^- energy. Here the total EW corrections are positive because of the large real-radiation effects. For large values of E_{τ^-} and $M_{\mu^+\tau^-}$ the negative Sudakov corrections in the virtuals, that are about -50%, dominate the NLO corrections. Over the production-angle distributions, the real and idip corrections behave more “regular” (plots in the upper row), with the idip corrections ranging between 15% and 25% and the real corrections smaller than 10%. The virtuals give negative corrections of between -25% in the region of small or large production angles and -70% in the central region.

Resumming the large Sudakov logarithms of virtual origin is thus clearly needed for a meaningful prediction, but in fact they are not the only large contribution to the EW corrections: The real-radiation effects, which in our setup are manifest by large integrated-dipole corrections, are large mainly for two reasons:

- the electron-mass dependence, see (7.2), for which resummation techniques are known, and

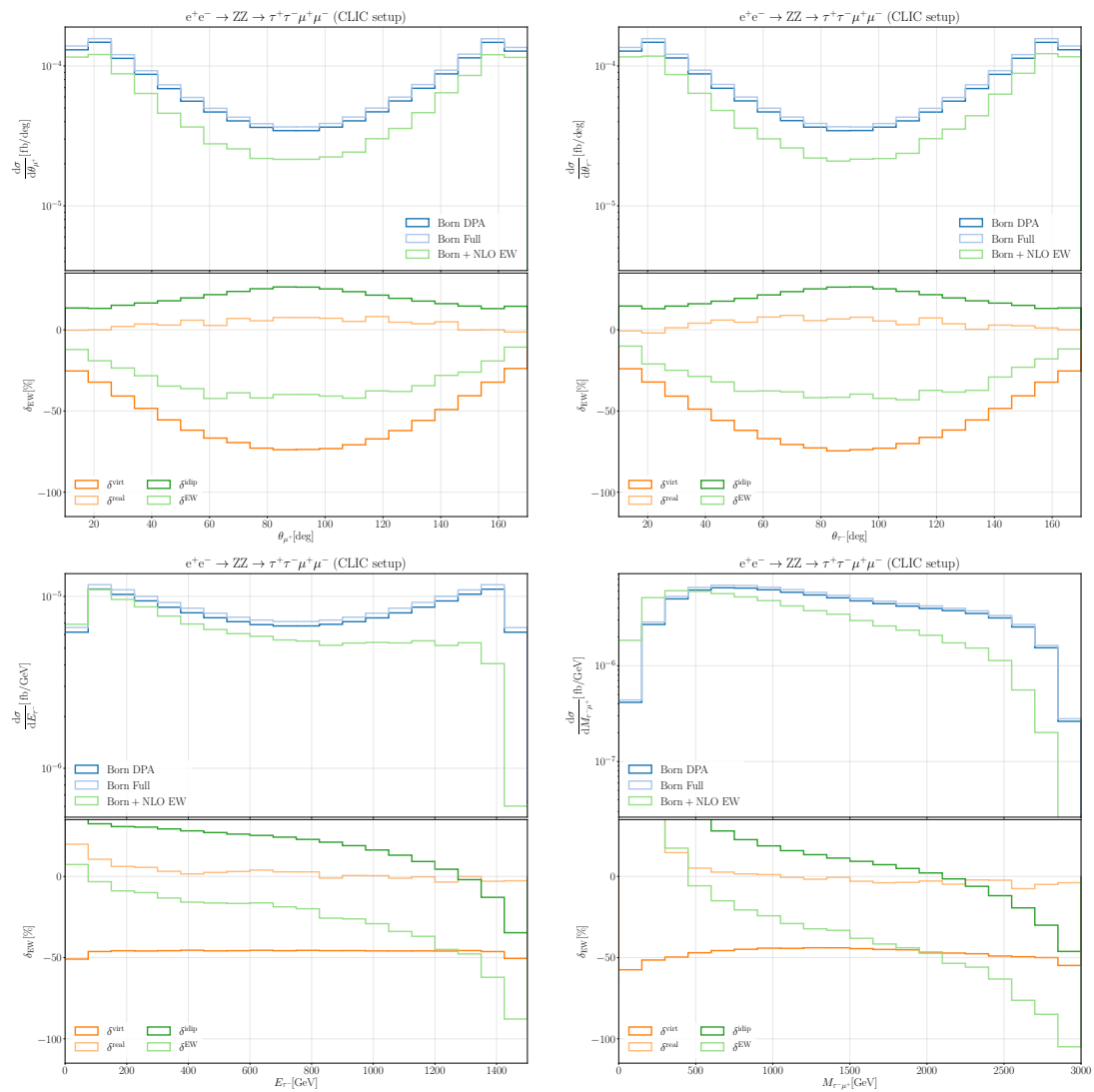


Figure 7.8.: Real, virtual, and integrated dipole (idip) NLO EW corrections for $e^+e^- \rightarrow ZZ \rightarrow \tau^+\tau^-\mu^+\mu^-$ differential in the μ^+ and τ^- production angle, the tau energy, and the $\tau^-\mu^+$ invariant mass. The plots are structured as in Fig. 7.7.

- the terms of the form $\log \frac{s_{ij}}{\mu_{\text{IR}}^2}$ in the dipole formulae, see Sec. 4.1.

The shape of the τ^- -energy and $M_{\tau-\mu^+}$ -invariant-mass distributions in Figs. 7.7 and 7.8 is mainly determined by the real-radiation correction effects.

7.2.4. SCET_{EW} vs. Fixed-order

The next step is again to check the validity of the SCET_{EW} approximation $s, t, u \gg M_W^2$. To estimate the order of magnitude of power-suppressed terms we calculate

$$\frac{M_W^2}{(3 \text{ TeV})^2} \approx 7 \cdot 10^{-4}, \quad \frac{M_Z^2}{(3 \text{ TeV})^2} \approx 9 \cdot 10^{-4}. \quad (7.14)$$

These values are a lower boundary, as power corrections with t and u in the denominator can be expected to be larger by up to one order of magnitude.

The plots are organised as described in Sec. 6.3.4, but for each plot we added a curve showing the logarithmic approximation (LA), which is defined by neglecting all constant contributions and keeping only logarithmic corrections [19]. This has been put to use in some setups in which complete EW corrections are not available in order to include the dominant contributions, see for instance Ref. [71].

In the τ -energy and τ -production-angle distributions as well as the distributions in the $M_{\tau-\mu^+}$ and $M_{\tau-\mu^-}$ invariant masses in ZZ production (Fig. 7.9), the deviation between the fixed-order result and SCET_{EW} approximation, parameterised as in (6.47), is about 0.4% at Born level and roughly constant over all distributions. The accuracy of the relative virtual corrections is even better: $\delta_{\text{FO}}^{\text{virt}} - \delta_{\text{SCET}}^{\text{virt}}$ is $\lesssim 0.1\%$ on the whole fiducial phase space. The LA describes the full result well only in the central region $50^\circ \leq \theta_\tau \leq 140^\circ$. Outside this region, the omitted $\mathcal{O}(\alpha)$ terms contribute by up to 15% with respect to LO. In the invariant-mass distributions, Δ_{DPA} as well as the difference between the virtual corrections is more or less uniformly distributed. Like in the lepton-energy distribution, the LA is nowhere really appropriate.

The results for the distribution in the antimuon production angle in W^+W^- production are displayed in Fig. 7.10 for longitudinal and transverse polarisations separately, both as a consistency check and in order to spot possible differences: The unpolarised results are qualitatively well described by the purely transverse contributions in all cases. In the longitudinal case, Δ_{SCET} shows an asymmetric behaviour, ranging from $\sim +0.7\%$ in the forward to -5% in backward region (not visible in the plot). The deviation in the virtual corrections, $\delta_{\text{FO}}^{\text{virt}} - \delta_{\text{SCET}}^{\text{virt}}$ grows from -0.2% in the forward region to only 0.8% in the backward region. In the central region, which dominates the cross section, both quantities are close to 0. Together with the cancellation of positive and negative deviations, this yields a value below 0.1% for the fiducial cross section. In the transverse case both Δ_{SCET} and $\delta_{\text{FO}}^{\text{virt}} - \delta_{\text{SCET}}^{\text{virt}}$ vary between -0.5% and $+0.5\%$, except for the last bin in the backward region, where the cross section is suppressed. For transverse W-pair production the LA is a reasonable approximation in the central region (similar as in the ZZ case), while for longitudinal W-boson production the non-logarithmic $\mathcal{O}(\alpha)$ terms contribute more than ten percent over most of the distribution.

All in all, the deviations between fixed-order and SCET results are at the level of one percent and hence in the range expected for power-suppressed corrections, which can safely be neglected in the considered setups. An exception is given by the purely longitudinally polarised W^+W^- production in the backward region, which is, however, phenomenologically not relevant.

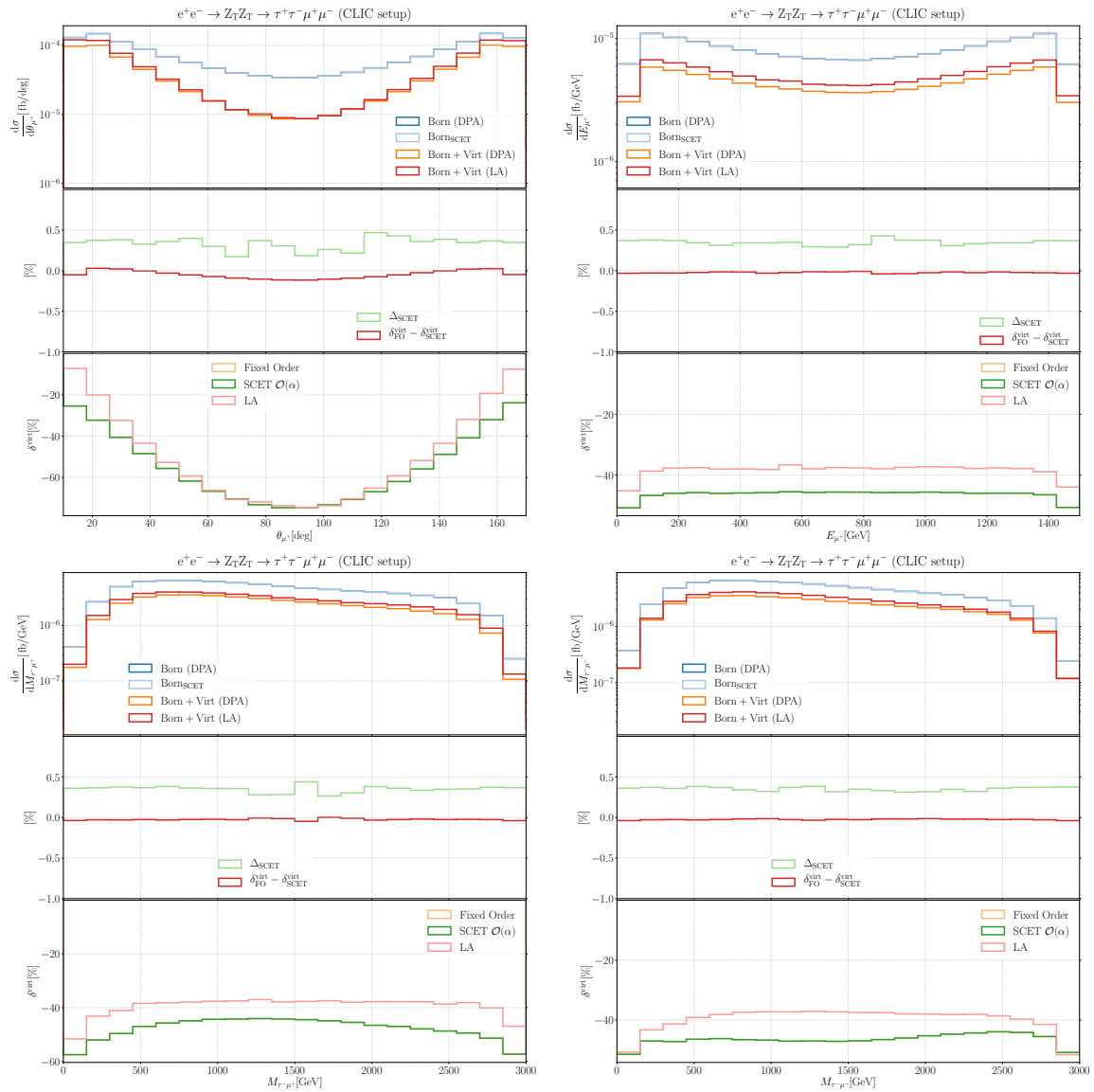


Figure 7.9.: Virtual corrections to $e^+e^- \rightarrow ZZ \rightarrow \tau^+\tau^-\mu^+\mu^-$ differential in the μ^+ and energy, and the $\tau^-\mu^+$ and $\mu^-\tau^-$ invariant masses, calculated in conventional fixed-order perturbation theory compared to the first-order expansion of the SCET results in α .

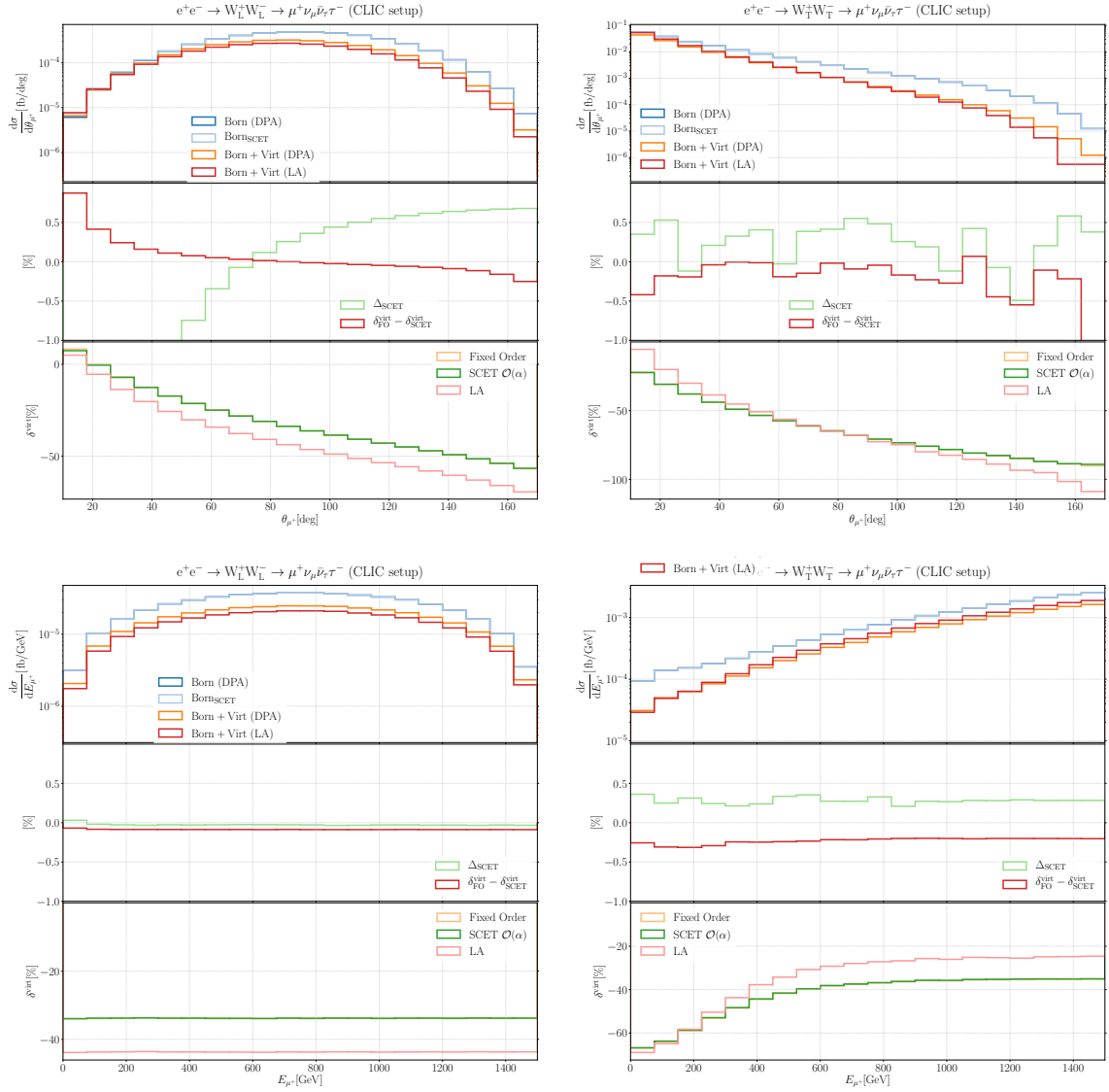


Figure 7.10.: Virtual corrections to $e^+e^- \rightarrow W^+W^- \rightarrow \mu^+\nu_\mu\bar{\nu}_\tau\tau^-$ differential in the antimuon production angle and energy with longitudinally (left) and transversely (right) polarised W bosons calculated in conventional fixed-order perturbation theory compared to the first order expansion of the SCET results in α .

7.2.5. Individual SCET contributions

The individual contributions within the SCET_{EW} calculation expanded to $\mathcal{O}(\alpha)$ are displayed in Figs. 7.11, 7.12, and 7.13. The descriptions of the contributions can be found in Sec. 6.3.4.

Conceivably the DL contributions are by far the dominant ones, followed by the SL, Soft, and PR ones. The most important qualitative difference between the two sample processes is the sign of the SL contribution, which is positive for transverse gauge bosons and fermions. When longitudinal gauge bosons are involved, the top-mass enhanced last term in (5.41), which comes with a different sign, dominates the SL contribution and renders it negative (see Fig. 7.13).

As is to be expected, the main difference with respect to the hadronic case is that many quantities are constant or almost constant over the whole phase space: The phase-space dependence, i.e. the shape of the distributions is mostly determined by the soft and the high-scale matching contributions. For W^+W^- production all other contributions are completely flat for both polarisation states. In the ZZ plots the other contributions have a slight angular dependence owing to the different corrections to the subamplitudes associated with left- and right-handed electrons in the initial state. In this context it is worth mentioning that one can observe a partial cancellation between the HSM and Soft contributions, which can be explained by the fact that within the SCET_{EW} formalism the angular dependent logarithms in the total correction are split according to (we pick the Mandelstam variable t for definiteness)

$$\frac{1}{2} \log^2 \left(\frac{-t}{M_{W/Z}^2} \right) \rightarrow \underbrace{\frac{1}{2} \log^2 \left(\frac{-t}{s} \right)}_{\in \text{HSM}} + \underbrace{\log \left(\frac{-t}{s} \right) \log \left(\frac{s}{M_{W/Z}^2} \right)}_{\in \gamma_S} + \underbrace{\frac{1}{2} \log^2 \left(\frac{s}{M_{W/Z}^2} \right)}_{\in \gamma_C}. \quad (7.15)$$

The l.h.s. is proportional to a single contribution obtained in LA in fixed-order, even though in the strict LA expansion the first term on the r.h.s. is neglected (see Ref. [19]). The first term on the r.h.s. contains no low-energy information and is hence part of the high-scale matching coefficients, while the second and third terms are part of the anomalous dimension. If $-t$ becomes small with respect to s , the first term will be the dominant one in the HSM and gives a positive contribution, while the second one gives a negative contribution (up to prefactors that might yield another global sign). Therefore in the small- $|t|$ tails the HSM- and γ_S -related contributions are always of opposite sign.

Finally we remark that recent implementation of EW corrections in LA have in some occasions included also the universal first terms on the r.h.s., see Refs. [71–73].

7.3. Resummed results

In this section we discuss the influence of the resummation of the observables discussed before. In contrast to the FCC–hh setup the validity of the SCET_{EW} assumption is not restricted to certain high-energy tails. It is therefore worthwhile to consider also fiducial cross sections as well as the shape of normalised distributions. We consider the same grades of resummation as in the FCC–hh setup (a list of included contributions in the respective calculations can be found in Sec. 6.4). All relative corrections are defined as in (6.48),

$$\delta^{\text{res}} = \frac{d\sigma^{\text{SCET}} - d\sigma^{\text{Born, SCET}}}{d\sigma^{\text{Born, SCET}}}, \quad (7.16)$$

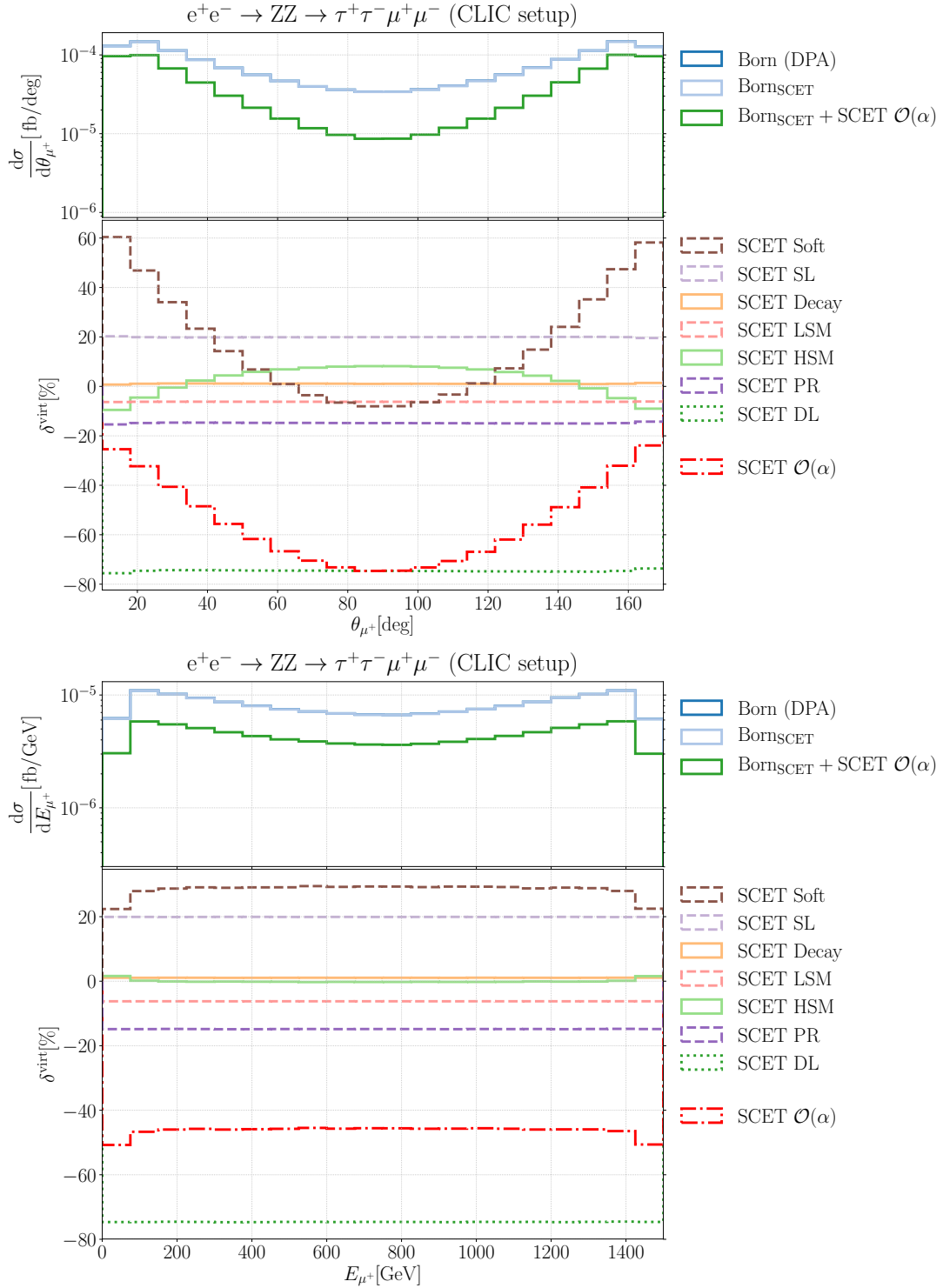


Figure 7.11.: Individual SCET contributions in differential distributions in the antimuon production angle and energy in $e^+e^- \rightarrow ZZ \rightarrow \tau^+\tau^-\mu^+\mu^-$. The meaning of the abbreviations is explained in the text in Sec. 6.3.4.

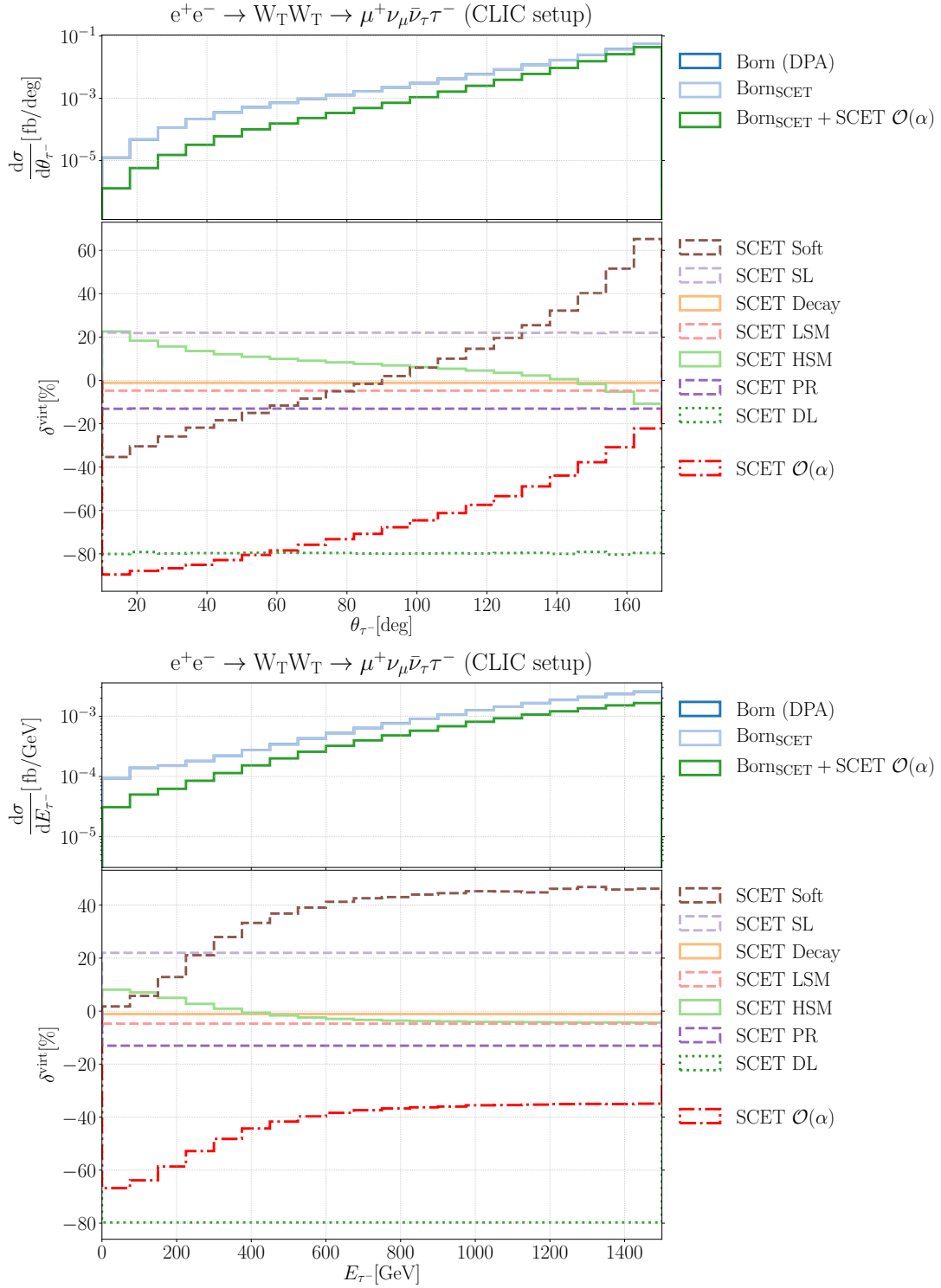


Figure 7.12.: Individual SCET contributions in differential distributions in the tau production angle and energy in $e^+e^- \rightarrow W^+W^- \rightarrow \mu^+\nu_\mu\bar{\nu}_\tau\tau^-$ with transversely polarised W bosons. The meaning of the abbreviations is explained in the text in Sec. 6.3.4.

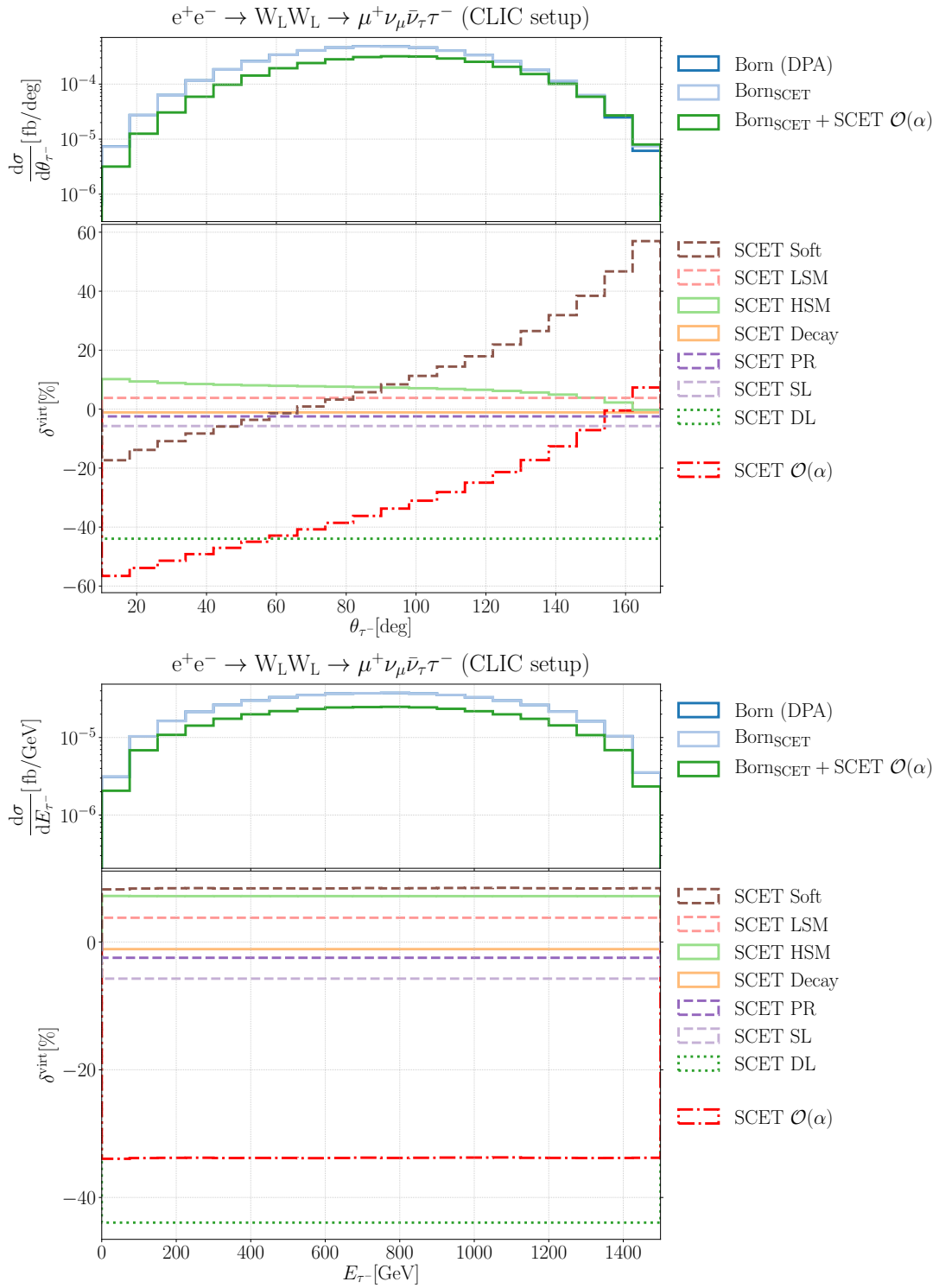


Figure 7.13.: Individual SCET contributions in differential distributions in the tau production angle and energy in $e^+e^- \rightarrow W^+W^- \rightarrow \mu^+\nu_\mu\bar{\nu}_\tau\tau^-$ with longitudinally polarised W bosons. The meaning of the abbreviations is explained in the text in Sec. 6.3.4.

Accuracy	$\sigma^{\text{WW}}/\text{fb}$	δ^{EW}
Fixed order	1.519(9)	-13.7%
SCET $\mathcal{O}(\alpha)$	1.524(9)	-13.4%
LL+NLO	1.901(9)	8.0%
NLL _{FO} +NLO	1.415(9)	-19.6%
NLL+NLO	1.563(9)	-11.2%
LL+NLO+running	2.044(9)	16.1%

Accuracy	$\sigma^{\text{ZZ}}/\text{fb}$	δ^{EW}
Fixed order	0.00958(5)	-26.6%
SCET $\mathcal{O}(\alpha)$	0.00960(5)	-26.4%
LL+NLO	0.01262(5)	-3.3%
NLL _{FO} +NLO	0.00952(5)	-27.0%
NLL+NLO	0.01127(5)	-13.6%

Table 7.4.: Integrated fiducial cross sections for $e^+e^- \rightarrow W^+W^- \rightarrow \mu^+\nu_\mu\bar{\nu}_\tau\tau^-$ (left) and $e^+e^- \rightarrow ZZ \rightarrow \tau^+\tau^-\mu^+\mu^-$ (right) with the virtual corrections replaced by the respective SCET_{EW}-resummed results. The contributions included in the (N)LL+NLO calculations are given in Sec. 5.3.

in the following.

7.3.1. Integrated cross sections

In the case of W^+W^- production (l.h.s. of Tab. 7.4) the LL resummation shifts the NLO FO cross section by 21.4% of the the LO cross section. From Tab. 7.4 this is obtained as the difference between SCET $\mathcal{O}(\alpha)$ and LL+NLO. The magnitude of this effect can be estimated from the size of the DL corrections to the transverse polarisations (80%) as $\exp(-0.8) - 1 + 0.8 \approx 25\%$. The difference between LL+NLO and NLL+NLO is about -19% with respect to Born. This quantity serves as a measure for the effect of the NLL resummation alone (without the effect of the LL resummation). To determine the effect of the most important terms of the NLL resummation, we can consider the difference between LL+NLO and NLL_{FO}+NLO, which is about -28% . These schemes differ by the terms given in the second column of (5.87) (excluding the uppermost one of course), of which the dominant one is the α^2L^3 term. It turns out that these terms have an even larger impact than the ones in the first column (again excluding the first one). The remaining 9% are then given by the resummed single logarithms, i.e. the second column of (5.89).

For ZZ-pair production one has a similar picture: The LL resummation accounts for a $\sim 23\%$ shift. Going to NLL_{FO} slightly overcompensates this effect: The cross section is shifted by -24% . And the remaining NLL terms produce another positive shift of $\sim 14.5\%$.

It can therefore be concluded that an accurate theoretical prediction for this collider setup should include at least NLL-resummed EW corrections. Also the influence of higher-order terms in the log-counting as well as a resummation of the logarithms associated with coupling renormalisation should be analysed.

7.3.2. Differential distributions

Virtual corrections only

In the following we discuss how the resummation affects the differential distributions. In analogy to Sec. 6.4 we start by comparing the virtual corrections in the resummed and unresummed case.

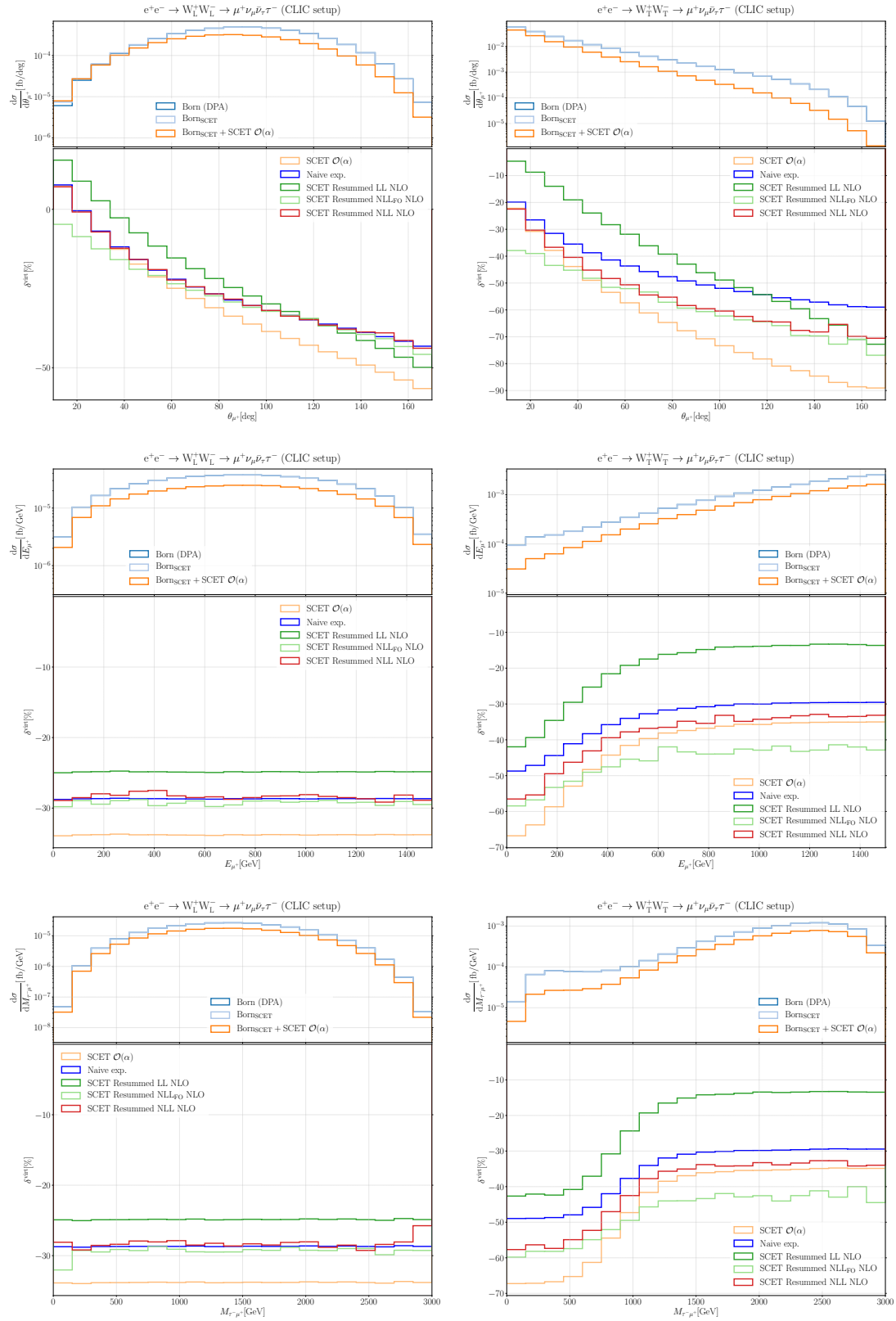


Figure 7.14.: Effect of the SCET resummation on distributions in the antimuon production angle and energy of the virtual EW corrections to $e^+e^- \rightarrow W^+W^- \rightarrow \mu^+\nu_\mu\bar{\nu}_\tau\tau^-$ with longitudinal (left) and transverse (right) W bosons.

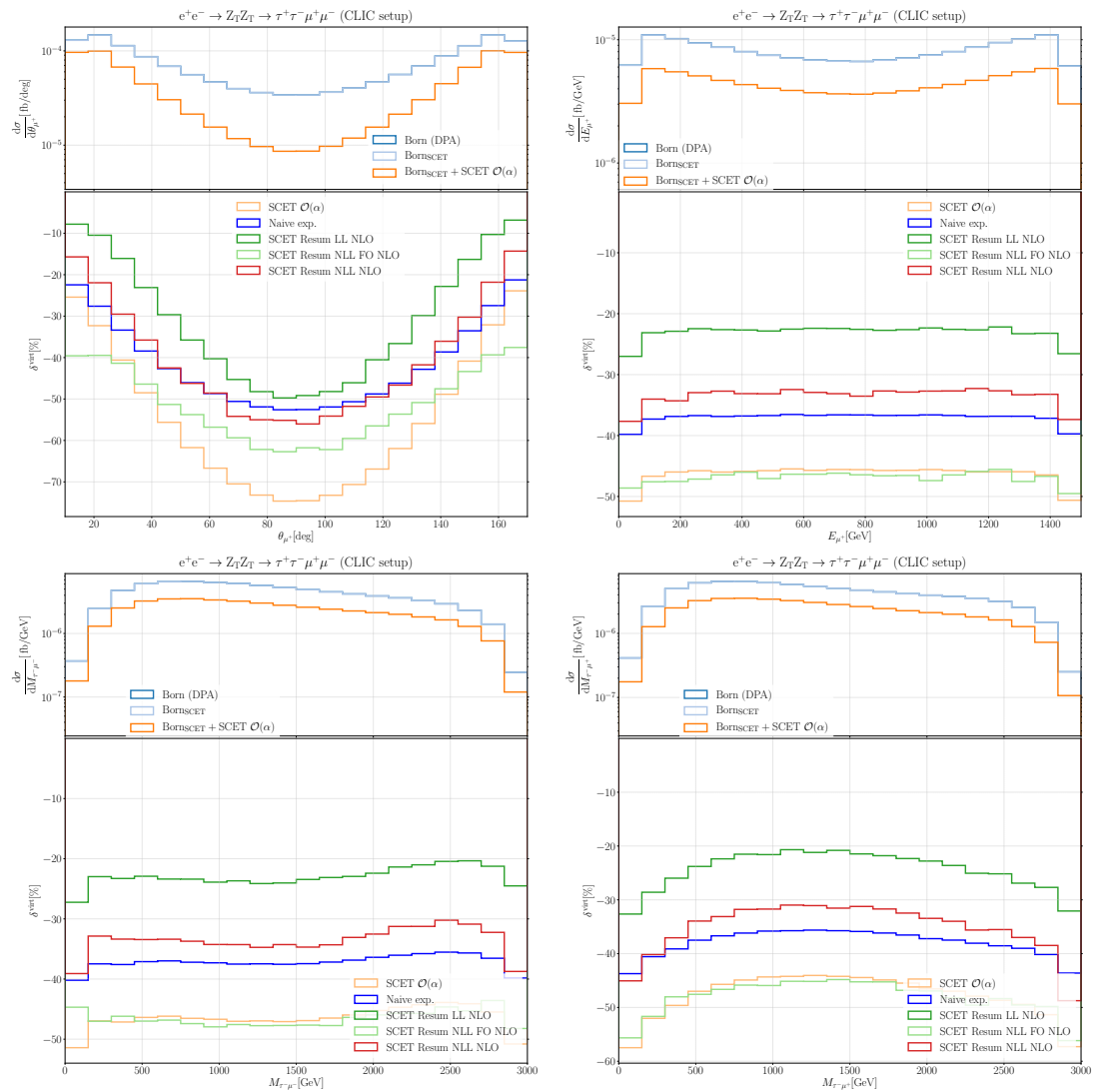


Figure 7.15.: Effect of the SCET resummation on distributions of virtual corrections to $e^+e^- \rightarrow ZZ \rightarrow \tau^+\tau^-\mu^+\mu^-$ differential in the antimuon production angle and energy, as well as the $\tau^-\mu^-$ and $\tau^-\mu^+$ invariant mass.

The result can be found in Figs. 7.14, 7.15 for several differential distributions in W^+W^- - and ZZ -pair production, respectively.

Compared to the analogous discussion in Sec. 6.4, we show in addition the curves from the “naive” exponentiation,

$$\delta_{\text{FO}}^{\text{virt}} \rightarrow \exp(\delta_{\text{FO}}^{\text{virt}}), \quad (7.17)$$

which has occasionally be employed, see for instance Ref. [76].

The effect of the LL resummation is (almost) constant over phase space. This is (roughly) the deviation between the $\mathcal{O}(\alpha)$ (orange) curve and the dark green curve, up to $\mathcal{O}(\alpha^2\text{L})$ -contributions from the product of one-loop matching and $\mathcal{O}(\alpha)$ soft anomalous dimension, see (5.95) and the footnote underneath. The effects of the NLL and NLL_{FO} terms are strongest in the forward region, where the angular-dependent logarithms are large (see the “SCET Soft” curves in Fig. 7.12). Here the total negative shift due to the NLL_{FO} terms (the difference between the dark green and the pale green curve, $\mathcal{O}(\alpha^2\text{L}^3)$) grows up to $\sim 20\%$ in the longitudinal case and exceeds 30% in the transverse case. The larger impact in the transverse case is explained both by the larger values of the double logarithms (owing to larger EW Casimir for transverse W bosons) and by the fact that the Yukawa-coupling term in the Goldstone-boson anomalous dimension (5.41) contributes with a negative sign to the SL corrections, leading to a smaller value for the SL corrections in the longitudinal case. Towards the backward region the magnitude of the shifts shrinks until it eventually changes the sign and becomes positive for small scattering angles ($\theta_{\mu^+} \gtrsim 150^\circ$). This region, however, contributes little to the total cross section. The NLL terms (difference between pale green and red curve) show a similar behaviour and range between +15% and about 0% for both polarisation states. Since these terms are dominated by the exponential of the soft anomalous dimension, their dependence on the polarisation state is weaker: the angular-dependent logarithms have a similar magnitude ($\sim 60\%$) for both polarisation states (see Figs. 7.12, 7.13). In the muon-energy distribution all resummation effects are more or less flat in the longitudinal case. In the transverse case the effects of both the NLL_{FO} and NLL terms are largest in the high-energy region and decrease towards lower energies.

The quality of the naive exponentiation prescription is different for the polarisation states: Because of the small single-logarithmic corrections, the corrections in the longitudinal case are strongly dominated by the DL corrections and the naive exponentiation prescription works well in the sense that it reproduces the NLL+NLO result up to $\lesssim 1\%$. In the dominating transverse case the difference between the NLL+NLO result and the naive prescription is significant, reaching more than 10% with respect to Born in the backward region. In the small-energy regime and in the forward region, where the cross section is large, the difference accounts for $\lesssim 5\%$.

In Fig. 7.15 we show the analogous distributions for ZZ production. For the antimuon-energy distribution the curves for the relative corrections are approximately parallel, which implies that the resummation effects are more or less constant. In the angular distribution for the antimuon the NLL_{FO} and NLL terms have larger effects in the forward and backward region: The shift between the green curves reaches 30% in the first and last bin, while in the central region it is about 12%. The shift between pale green and red curve is about 25% in the forward and backward region and about 7% in the central region. At the end this implies that going from LL to NLL (from dark green to red) yields a roughly constant shift of about 5%.

The naive exponentiation describes the exponentiation well for moderate lepton production angles ($40^\circ \lesssim \theta_{\mu^+} \lesssim 70^\circ$), while both in the central region and in the forward and backward

regimes it introduces an error of 3% – 5%. Over the lepton energy, the error is more or less uniformly distributed, accounting for $\sim 3\%$.

Full resummed differential cross sections

Figures 7.16 and 7.17 show the same differential distributions as Figs. 7.14 and 7.15, but with the full NLO cross sections summed over the polarisations and including contributions of real corrections, virtual (factorisable and non-factorisable) corrections, and integrated dipoles. All cross sections have been converted to expected event rates at CLIC using (6.15) and (7.4).

Figure 7.16 confirms that the anticipated statistics of the considered ZZ decay channel is rather low, owing to the purely leptonic final state: The cross section of ~ 10 ab is expected to yield around 50 events in total, rendering a measurement at the differential level impossible. One should, however, notice that the SCET_{EW} results can be used in the same way for the more prominent decay channels with expected event rates being larger by a factor 10–100. Besides that the radiative corrections are dominated by real-radiation effects in the low lepton-energy regime (see upper right plot), where including the real corrections renders the total NLO EW corrections positive. In the angular distribution (upper left plot) the effects of the real corrections appear to be strongest in the central region, thus flattening the curves of the relative corrections compared to Fig. 7.15. The invariant-mass distributions receive huge corrections in the small-invariant-mass region, which is suppressed for Born-like kinematics.

In the W^+W^- case (Fig. 7.17), in contrast, the expected statistics is sufficient on a wide range of phase space. In regions with particularly large cross sections, such as the forward direction or the high-energy and high-invariant-mass regions both the effects of the LL and NLL_{FO} contributions clearly exceed the numerical uncertainties, suggesting that the NLL- and NLO-effects may be visible within this experimental setup. At the end the NLL results incidentally lie within the shaded bands again. In the backward region (large θ_{μ^+}) as well as in the region of small dilepton invariant masses, we observe that, while the total cross section is suppressed, the relative EW corrections reach high positive values because they are, like in the ZZ case dominated by real-radiation effects. This can be explained by the fact that the additional photon opens up kinematically suppressed phase-space regions. A similar effect can be observed in the region of small antimuon energies and small dilepton invariant masses.

Normalised distributions

Finally we investigate some of the distributions normalised on the respective total cross sections, which is a common technique to analyse the shapes of curves with different normalisation.

In Fig. 7.18 this is done for distributions from Fig. 7.16 in ZZ-production. Each plot contains the LO result and the both the fixed-order NLO result and the resummed SCET_{EW} predictions as defined in (5.95). Because of the low statistics, we do not include the uncertainties in this plot: obviously the uncertainties are larger than the differences between the curves. The curves in the production-angle plot are slightly stretched towards the forward and backward regions by the EW corrections because the impact of the corrections is largest near the minimum in the central region. Near the maxima the corrections are smaller and the peak of the normalised distribution gets higher. The large corrections in low-energy tail lead to a distortion of the curve towards the low-energy region, when the NLO EW corrections are included. In all distributions the inclusion of the SCET_{EW} resummation partially reverses the effects of the NLO corrections. While the inclusion of NLO EW corrections appears mandatory to obtain a qualitatively accurate

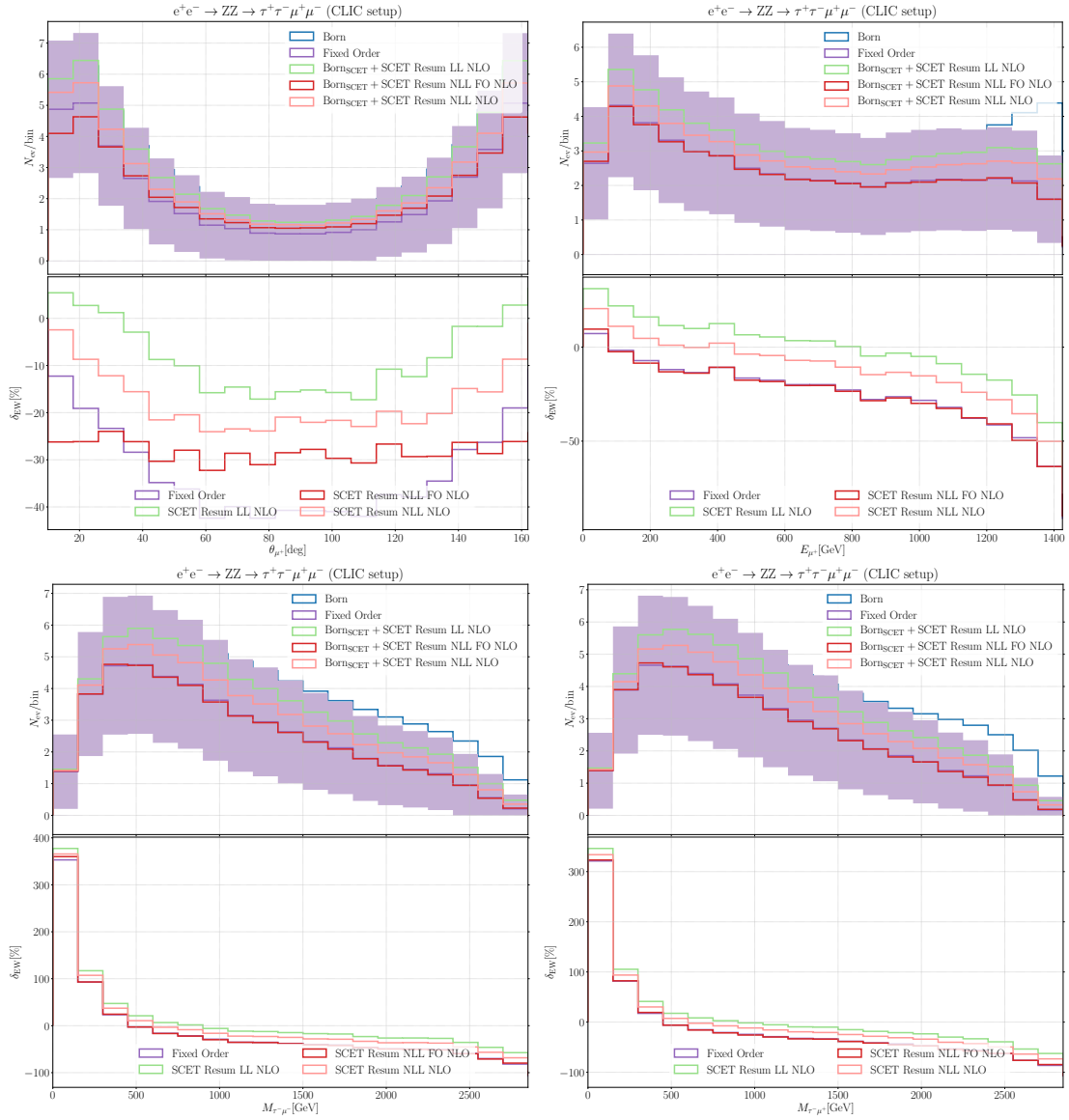


Figure 7.16.: Differential distributions in the μ^+ production angle and energy, as well as the $\tau^-\mu^-$ and the $\tau^-\mu^+$ invariant masses for $e^+e^- \rightarrow ZZ \rightarrow \tau^+\tau^-\mu^+\mu^-$ with the error on the counting rates shaded around the purple curves.

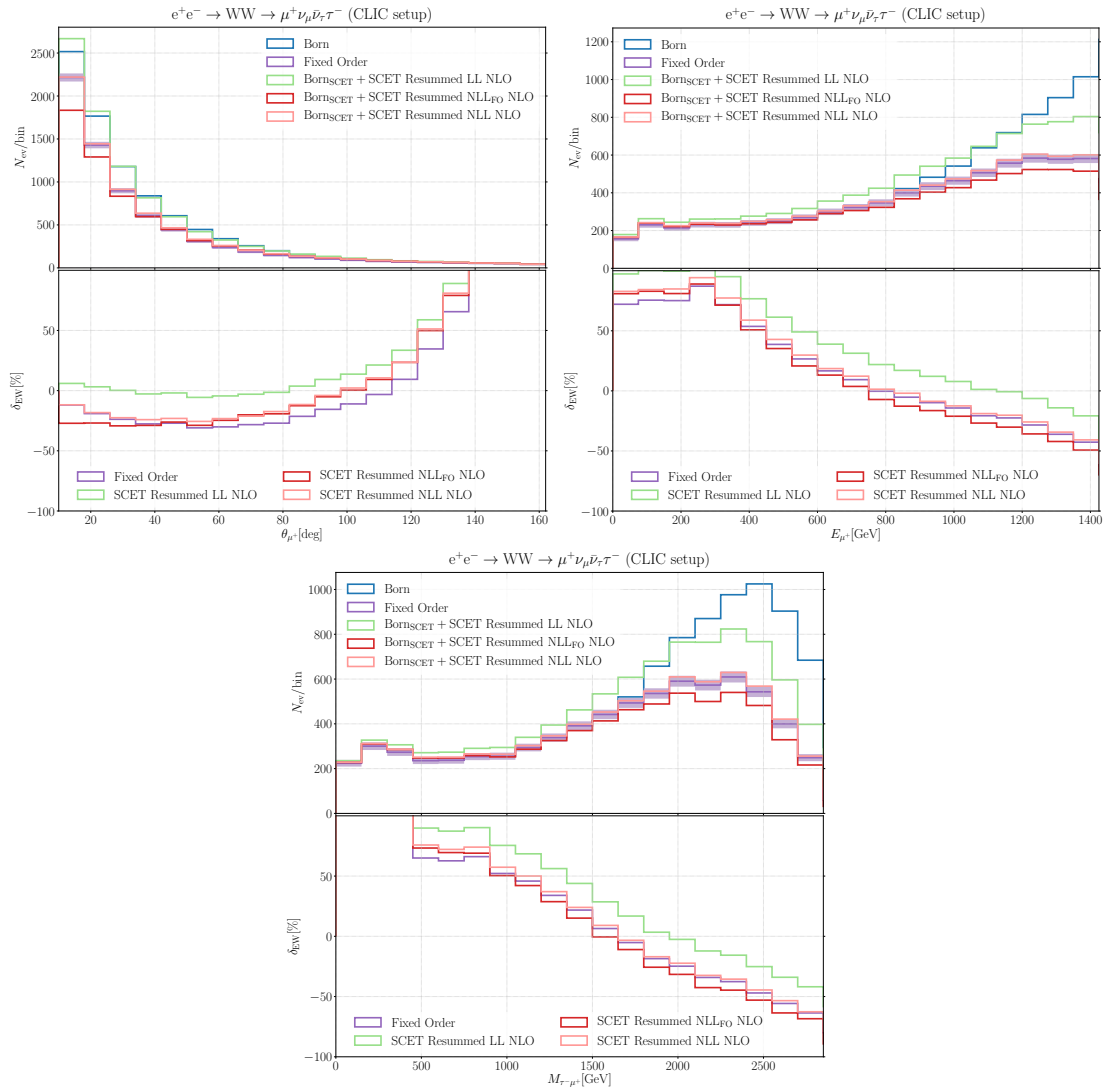


Figure 7.17.: Differential distributions in θ_{μ^+} , E_{μ^+} , and $M_{\tau^-\mu^+}$ for $e^+e^- \rightarrow W^+W^- \rightarrow \mu^+\nu_\mu\bar{\nu}_\tau\tau^-$ with the error on the counting rates shaded around the purple curves.

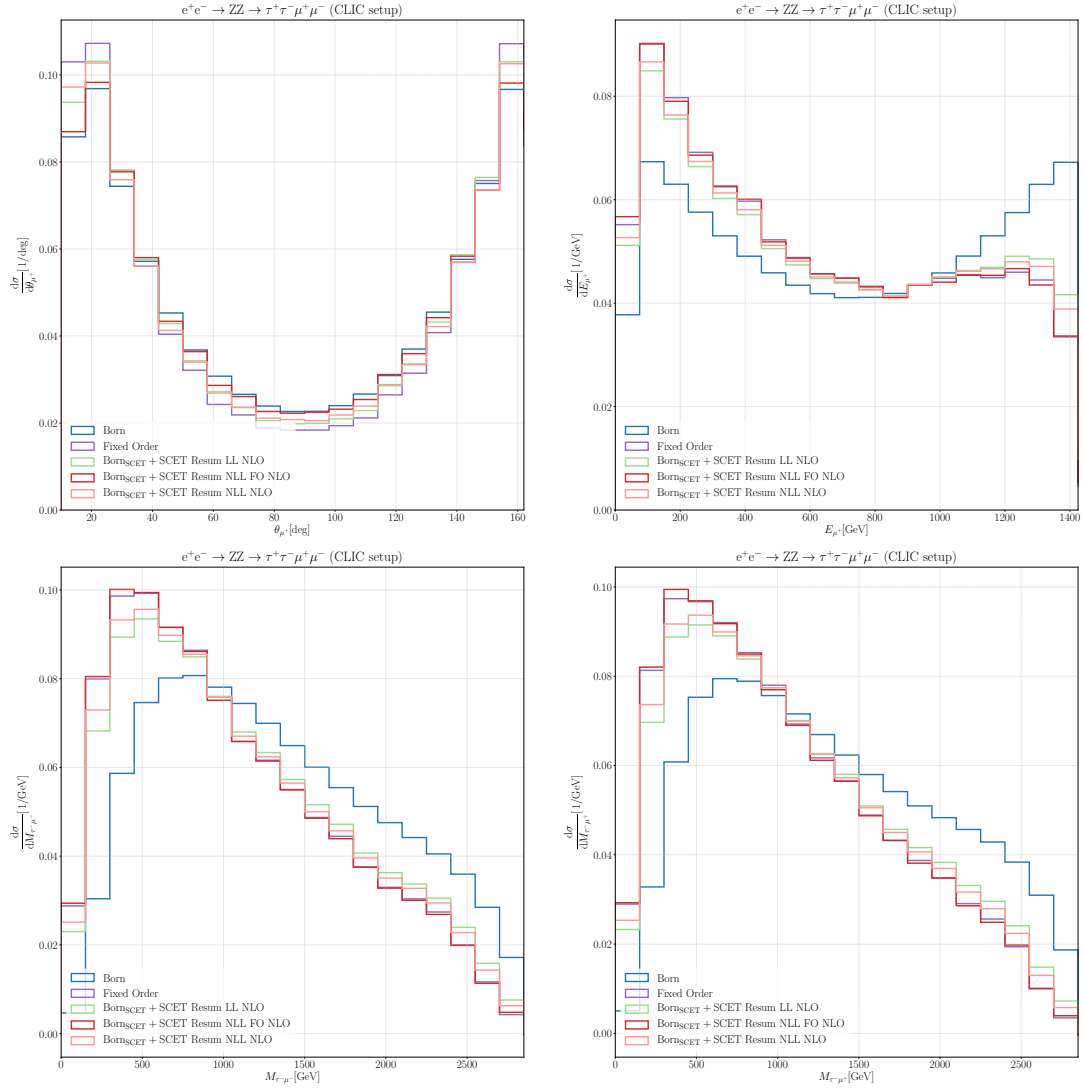


Figure 7.18.: Normalised distributions for $e^+e^- \rightarrow ZZ \rightarrow \tau^+\tau^-\mu^+\mu^-$ differential in the antimuon production angle and energy, as well as the invariant masses of the $\tau^-\mu^-$ and the $\tau^-\mu^+$ systems.

prediction, the influence of the resummation does not change the curves in a measurable way even if higher statistics is assumed.

For W^+W^- production the results are shown in Fig. 7.19. The distributions are same as in Fig. 7.17 and we also included the statistical uncertainties from the previous plots. The angular distribution is peaked in the forward region. The peak is slightly lowered by including the NLO corrections, which is again partly undone if SCET_{EW} is applied. On the other hand the muon-energy and the $M_{\tau-\mu^+}$ distributions are flattened towards smaller values, which is mostly an effect of real radiation. In both cases including the resummation partly removes the effect of the virtual corrections. The effects do exceed the statistical uncertainties, but they are of the same order of magnitude. Note that the approximately constant shift owing to the LL resummation implies that the shape of the curve is not changed with respect to the FO result, which is indeed what can be seen in the results.

All in all, we conclude that a measurable effect of the SCET_{EW} on normalised diboson distributions at the CLIC collider is unlikely. If at all, distortions in the regions of high- and low-energy tails may exceed the experimental errors.

7.3.3. Effect of the running couplings

In this section, we investigate the impact of the parameter-logarithm resummation, as compared to the LL+NLO scheme (see Sec. 5.3). Recapitulate that the included terms are given by (5.95). In addition we fix α by its value in the $\overline{\text{MS}}$ scheme at M_Z (see Sec. 10 of Ref. [238])

$$\alpha(M_Z) = \frac{1}{127.952} \quad (7.18)$$

at the low scale. From the input for c_w and s_w ,

$$c_w^2(M_Z) = \frac{M_W^2}{M_Z^2}, \quad s_w^2(M_Z) = 1 - c_w^2(M_Z), \quad (7.19)$$

we infer the values for the U(1) and SU(2) gauge couplings at M_Z :

$$g_1(M_Z) = \frac{\sqrt{4\pi\alpha(M_Z)}}{c_w(M_Z)}, \quad g_2(M_Z) = \frac{\sqrt{4\pi\alpha(M_Z)}}{s_w(M_Z)}. \quad (7.20)$$

For the high-scale contributions the one-loop RGE solutions for the EW gauge couplings,

$$g_{1/2}^2(\mu_h) = \frac{g_{1/2}^2(M_Z)}{1 - \beta_{0,1/2} \frac{g_{1/2}^2(M_Z)}{8\pi^2} \log \frac{\mu_h}{M_Z}}, \quad (7.21)$$

with $\beta_{0,1/2}$ defined in (3.120), are used as input parameters.

The difference between the two setups at the integrated level is about 8% with respect to the Born for W^+W^- production, see rows 4 and 7 on the left of Table 7.4. The major part of this effect is explained by the $\alpha^2\text{L}^3$ contributions associated with the running of the couplings, which are not present in our definition of LL+NLO. While this effect is conceivably smaller than the difference between LL and NLL_{FO} , which is also caused by $\alpha^2\text{L}^3$ effects, it is not negligible and a should be taken into account.

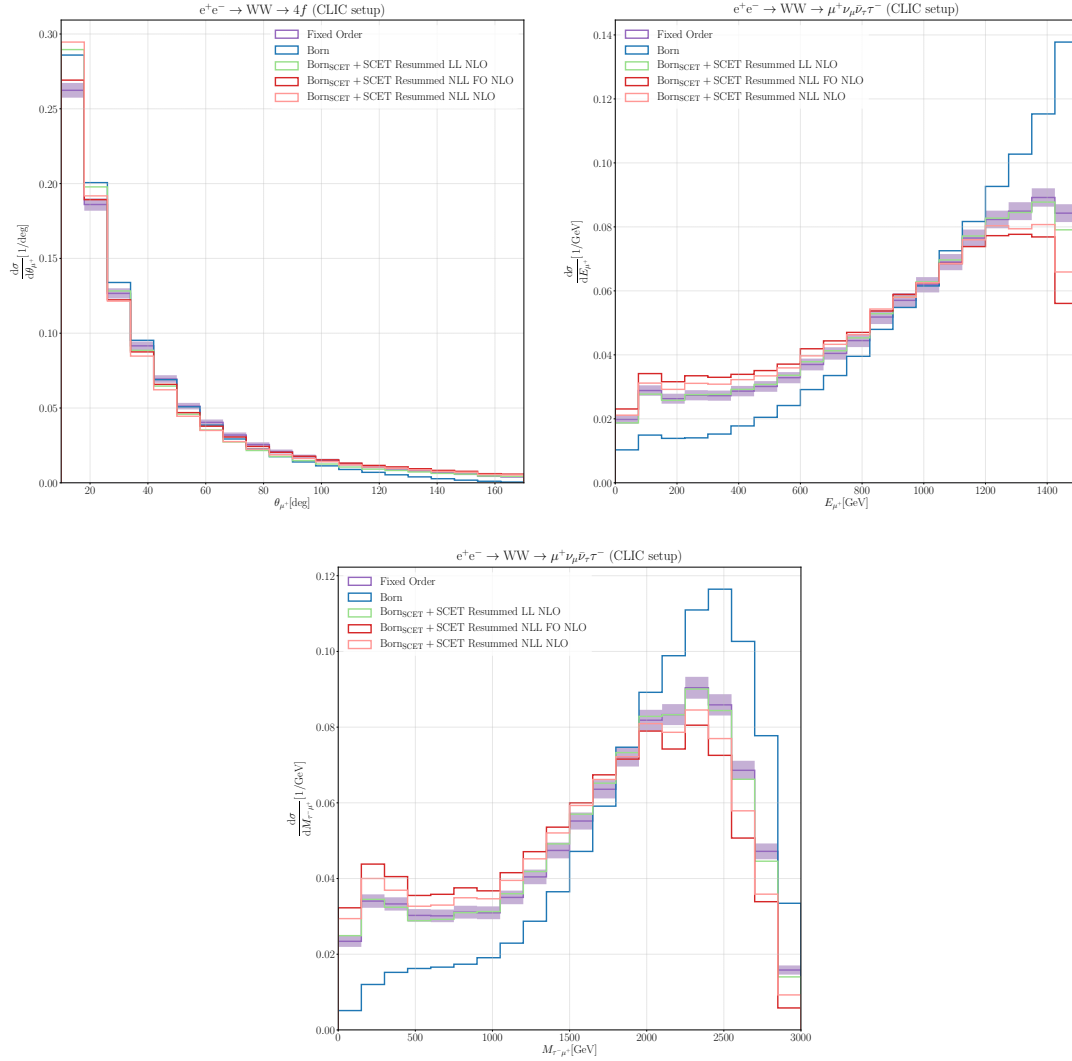


Figure 7.19.: Normalised distributions for $e^+e^- \rightarrow W^+W^- \rightarrow \mu^+\nu_{\mu}\bar{\nu}_{\tau}\tau^-$ differential in the antimuon production angle and energy and the $\tau^-\mu^+$ invariant mass with the error on the counting rates shaded around the purple curves.

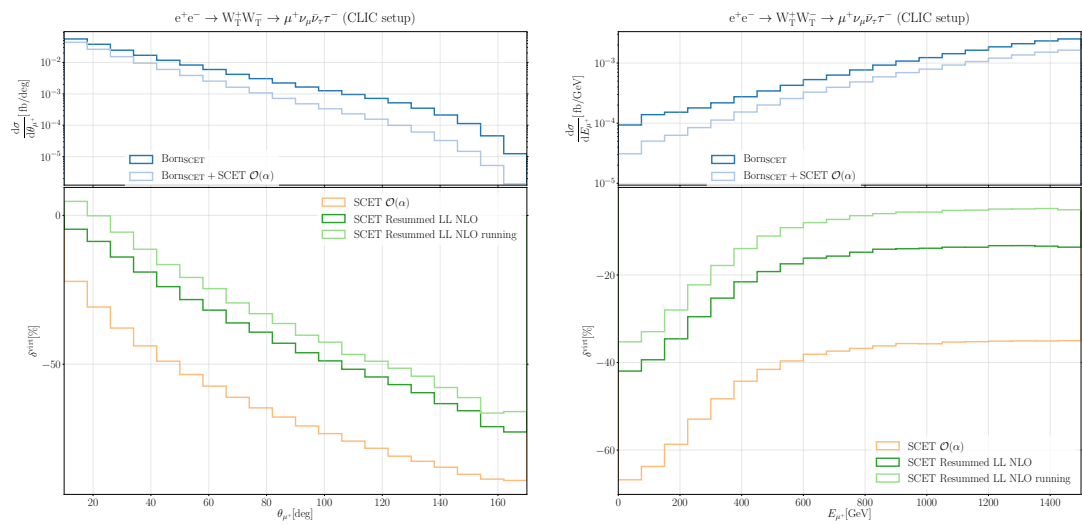


Figure 7.20.: Effect of the running EW gauge couplings in $e^+e^- \rightarrow W_T^+W_T^- \rightarrow \mu^+\nu_\mu\bar{\nu}_\tau\tau^-$ differential in the muon production angle and energy.

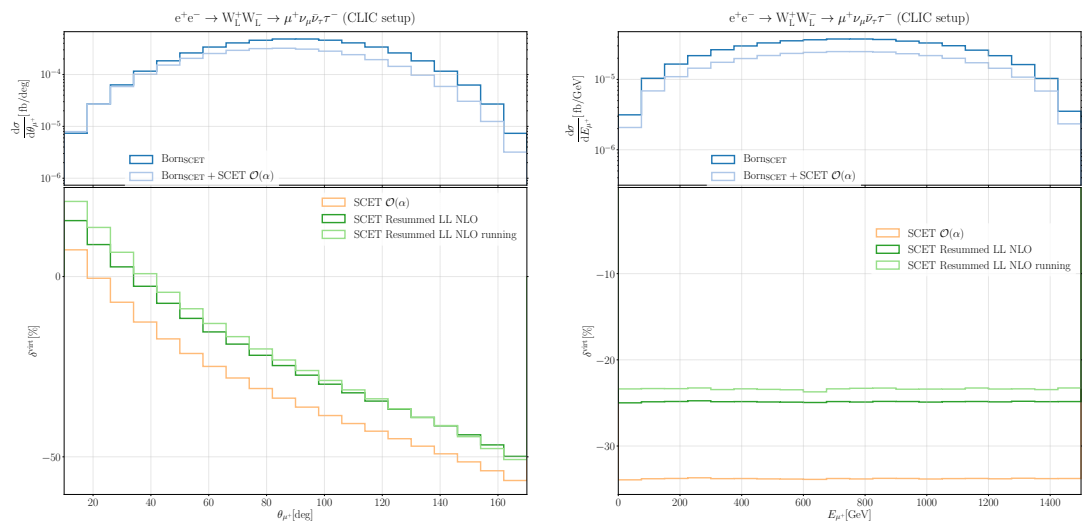


Figure 7.21.: Effect of the running EW gauge couplings in $e^+e^- \rightarrow W_L^+W_L^- \rightarrow \mu^+\nu_\mu\bar{\nu}_\tau\tau^-$ differential in the muon production angle and energy.

The differential results are shown in Figs. 7.20 and 7.21 for the production of transverse and longitudinal W bosons, respectively. The phase-space variation of the difference is at the level of few percent. While the aforementioned $\alpha^2 L^3$ terms are constant, a small dependence is explained by the fact that the dominant phase-space dependent contributions, namely the angular-dependent logarithms, are calculated with a different value of α .

8. Conclusion and outlook

For a long time it has been known that Sudakov logarithms can potentially spoil the convergence of the perturbation series in the weak coupling constant, which poses limitations for the accuracy of theoretical predictions especially at future colliders. Soft-collinear effective theory for electroweak corrections (SCET_{EW}) has been shown to be an appropriate framework to resum these large logarithms to all orders in the coupling constant.

In this thesis, we presented an automation framework for the computation of resummed EW Sudakov corrections to collider processes. Complicated processes with internal unstable vector bosons are factorised into simpler subprocesses using the double-pole approximation (DPA) and the matrix elements for the vector-boson-production subprocess are calculated using a SCET_{EW} factorisation formula. This formula is valid to leading power, thus neglecting all terms of $\mathcal{O}(M_W^2/s_{ij})$ with s_{ij} being a kinematic invariant of the production subprocess. The longitudinal degrees of freedom of the massive EW vector bosons are treated using the Goldstone-boson equivalence theorem (GBET). Using an operator basis with charge and flavour eigenstates allows for the evaluation of the tree-level and one-loop Wilson coefficients and operator matrix elements in the symmetric phase of the Standard Model (SySM) using RECOLA2. All other ingredients of the factorisation formula are process independent and have been directly implemented into the MC-integration program MOCANLO, which is used for the numerical evaluation of cross-sections on the integrated and fully-differential level.

We applied the setup to pair production of massive EW gauge bosons within two different collider setups. In the hadron-hadron Future Circular Collider (FCC-hh) setup, even though a beam energy of $\sqrt{s} = 100$ TeV is assumed, the bulk of the diboson cross-section is found to originate from interactions, which do not allow the application of SCET_{EW} because at least one kinematic invariant is not large compared to the EW scale. In the high-energy tails of differential distributions, however, we find the SCET_{EW} assumption to be increasingly well working, reaching subpercent accuracy in experimentally accessible regions for all quark-induced diboson-production channels, given the assumed FCC-hh luminosity. In these regions, which are typically within an energy range of 3–12 TeV, the Sudakov logarithms render the EW corrections of $\mathcal{O}(1)$, such that a resummation is inevitable.

The DPA introduces large errors in some tails, indicating a strong influence from non-doubly resonant contributions. This is particularly relevant in the high- $p_{T,\ell}$ tails of distributions for processes involving W bosons, which do not allow a direct invariant-mass phase-space cut on their decay products. In these processes the DPA-approximated results are off the off-shell results by up to 50%. The suppression of non-resonant background can thus be expected to be a general issue for both experimental and theoretical investigations of diboson processes at these energy scales. For ZZ production, the DPA works within the expected accuracy.

We investigated the effect of the SCET_{EW} resummation in several steps, studying the influence of the individual terms in the logarithm counting. The leading-logarithm (LL) resummation has a huge effect in the high-energy tails, shifting the differential cross sections by 60% – 100%, depending on the process and the polarisation state under consideration. The dominant

transverse polarisation states are affected stronger than the longitudinal ones. The terms that are next-to-leading-logarithmic in the fixed-order counting scheme (NLL_{FO}) give large negative contributions, leading to a strong cancellation with the LL terms. At the end, we find that the next-to-leading-logarithmic (NLL) results, which include also terms of $\mathcal{O}(\alpha^2 L^2)$ differ from the fixed-order results by about 10% at several TeV, which is certainly a non-negligible effect, given the high desired accuracy.

In the second part we investigated W^\pm and Z-boson pair production in e^+e^- collisions at $\sqrt{s} = 3 \text{ TeV}$, inspired by the Compact Linear Collider (CLIC) project. In contrast to the first setup, the SCET_{EW} assumption is reasonable on the whole phase space in this case. In some regions, such as for small lepton production angles or energies, the electroweak corrections are, however, dominated by real-radiation effects, which can not be treated using SCET_{EW} .

In the case of W^\pm pair production, there are again large deviations between the off-shell and the DPA results. They are, however, strongest in phase-space regions with small cross sections, such as the backward region. In the regions that dominate the cross section, the DPA is found to work well if only the relative virtual corrections are computed in the DPA.

In fixed order we find relative next-to-leading order (NLO) EW corrections to amount for -13.5% and -24.8% at the integrated level for W^\pm and Z-boson pair production, respectively. The $\text{NLL}+\text{NLO}$ SCET_{EW} corrections correspond to corrections of -11.1% in the W-pair production and -11.8% in the Z-pair production with respect to the Born cross section. These relatively small shifts arise again from cancellations between positive LL and negative NLL_{FO} terms. While these effects exceeding the expected statistical uncertainties on a wide range of phase space at least for W^\pm -pair production, the shape of normalised distributions remains more or less unaffected.

In addition we investigated the impact of the running EW couplings in W^\pm pair production. The fact that the effect of the resummation of the associated logarithmic corrections accounts for a $+8\%$ shift on the integrated cross section at LL accuracy indicates that a closer investigation of the associated higher-order terms would also be worthwhile in the future.

The resummation of EW Sudakov logarithms will undoubtedly be a topic of concern in the era of next-generation colliders. While we demonstrated some important phenomenological effects of the SCET_{EW} resummation in high-energy collisions, there are some complications with the consistent application of SCET_{EW} to complicated processes, which are in particular associated with the treatment of non-resonant contributions and the interplay with real-radiation effects. A complete NLL resummation requires also the inclusion of the two-loop cusp anomalous dimensions as well as the complete running of the SM gauge couplings.

A. One-loop Feynman integral calculus

In this appendix we collect some basic tools for the calculation of one-loop integrals.

A.1. Dimensional Regularisation

In this appendix we review the concept of Dimensional regularisation (DimReg) and collect some basic conventions and notations. The Feynman rules of quantum field theory require integration over each loop momentum k when calculating S-matrix elements. When written in four space-time dimensions, these integrals may show singularities

- as $|k| \rightarrow 0$ or $k \parallel p$ for p external (IR), or
- or as $|k| \rightarrow \infty$ (ultraviolet, UV).

In order to assign values to these integrals cut-off quantities are introduced which parameterise the infinite behaviour. This is referred to as *regularisation*. Of course any physical quantity has to be independent of the cut-off parameters, which happens in different ways for UV- and IR-related divergences, respectively: UV divergences are removed by applying a renormalisation transformation with suitable counterterms (see Sec. 2.2), while IR divergences cancel between virtual and real corrections via the KLN theorem.

Dimensional regularisation [148, 149] provides a way to regularise both types of divergences by shifting the number of space-time dimensions occurring in the integration measure away from $D = 4$:

$$\int d^4k \rightarrow (2\pi\mu)^{4-D} \int d^Dk, \quad D \in \mathbb{C}, \quad (\text{A.1})$$

where the scale variable μ is introduced to retain the mass dimension of the integral. Note that D is assumed to be complex in order to use analytic properties of the resulting integrals interpreted as functions of D . The defining properties of dimensionally regulated integrals are linearity and a proper scaling behaviour. One result which follows from these requests is the fact that scaleless integrals are zero, i.e.

$$\int d^Dk (k^2)^\alpha = 0 \quad (\text{A.2})$$

for all $\alpha \in \mathbb{C}$ [239]. This seemingly paradox result has important consequences, as it implies that all integrals without a dependence on any scale evaluate to zero. Furthermore, any scaleless integral I can be written as a (vanishing) sum of UV and IR poles:

$$I = \sum_k \left(\frac{C_k}{\varepsilon_{\text{UV}}^k} - \frac{C_k}{\varepsilon_{\text{IR}}^k} \right), \quad (\text{A.3})$$

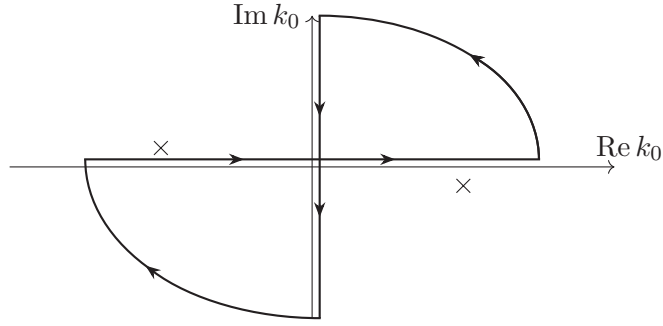


Figure A.1.: Wick rotation for the one-point integral. The pole positions are marked with crosses, and the contour is closed in a way that the contour integral vanishes.

with some coefficients C_k and $\varepsilon_{\text{UV/IR}}$ defined via

$$D = 4 - 2\varepsilon_{\text{UV/IR}}. \quad (\text{A.4})$$

The coefficients in (A.3) can be extracted by regularising either the UV or the IR divergences with a scheme different from DimReg.

A.2. The scalar one-point integral

As an example, and because the result will be used in a later calculation, we demonstrate the calculation of the D -dimensional one-point integral defined as

$$A_0(M^2) = \frac{\mu^{4-D}}{i\pi^2} \int \frac{d^D k}{k^2 - M^2 + i0} = \frac{\mu^{4-D}}{i\pi^2} \int_{-\infty}^{\infty} dk_0 \int \frac{d^{D-1} \mathbf{k}}{k_0^2 - \mathbf{k}^2 - M^2 + i0}. \quad (\text{A.5})$$

The scalar one-point integral is the simplest Feynman integral and is therefore a natural candidate to exemplify some important techniques of Feynman-integral calculus. It is sometimes referred to as the tadpole integral because of the shape of the associated Feynman diagrams.

In the last step of (A.5), the time component of the loop-momentum Minkowski four vector k . In order to obtain a volume integral, the integration over the real k_0 axis is rotated to the imaginary axis as sketched in Fig. A.1. The locations of the poles in k_0 are obtained from the infinitesimal imaginary part denoted by $i0$:

$$k_0 = \pm \sqrt{\mathbf{k}^2 + M^2} \left(1 - \frac{i0}{2(\mathbf{k}^2 + M^2)} + \dots \right) \quad (\text{A.6})$$

with the ellipsis denoting higher-order terms in $i0$. It can therefore be seen that the poles are in the upper left and in the lower right quarter of the complex k_0 plane. Closing the contour as shown in Fig. A.1 avoids enclosing any poles and thus allows for substituting the integral along the real axis by an integral along the imaginary axis. Subsequently substituting $k_0 \rightarrow ik_0$

renders the integration bounds real and one obtains

$$\begin{aligned}
 A_0(M^2) &= \frac{\mu^{4-D}}{i\pi^2} \int_{i\infty}^{-i\infty} dk_0 \int \frac{d^{D-1}\mathbf{k}}{k_0^2 + \mathbf{k}^2 + M^2 - i0} = \frac{\mu^{4-D}}{\pi^2} \int_{-\infty}^{\infty} dk_0 \int \frac{d^{D-1}\mathbf{k}}{k_0^2 + \mathbf{k}^2 + M^2 - i0} \\
 &= -\frac{\mu^{4-D}}{\pi^2} \int \frac{d^D k_E}{k_E^2 + M^2 - i0} = -\frac{\mu^{4-D}}{\pi^2} \int_0^\infty d|k_E| \int \frac{d^{D-1}\Omega |k_E|^{D-1}}{|k_E|^2 + M^2 - i0}, \tag{A.7}
 \end{aligned}$$

with the Euclidean four momentum k_E . In the last step we have introduced D -dimensional spherical coordinates. To proceed, we use the analytic continuation of the surface of an n -sphere (with n being a natural number),

$$\int d^{D-1}\Omega = \frac{2\pi^{(D-1)/2}}{\Gamma\left(\frac{D-1}{2}\right)}, \tag{A.8}$$

to non-integer values D . In the above formula $\Gamma(z)$ denotes Euler's Γ function, defined as

$$\Gamma(z) = \int_0^\infty dt t^{z-1} e^{-t}. \tag{A.9}$$

Using these definitions, the radial integral in (A.7) can be performed to obtain

$$A_0(M^2) = -(4\pi\mu)^{(4-D)/2} \Gamma\left(1 - \frac{D-2}{2}\right) (M^2 - i0)^{(D/2-1)}. \tag{A.10}$$

In the special case of D being close to four, one conveniently parameterises the space-time dimension as $D = 4 - 2\varepsilon$ and (A.10) becomes

$$A_0(M^2) = M^2 \left(\frac{1}{\varepsilon} - \log \frac{M^2}{\mu^2} + 1 \right) + \mathcal{O}(\varepsilon). \tag{A.11}$$

The divergence associated with the limit $\varepsilon \rightarrow 0$ arises as $|k_E|$ goes to infinity and is therefore of UV origin.

B. Calculation of the SCET anomalous dimension and low-scale corrections

In this appendix we calculate the one-loop SCET corrections, from which the anomalous dimension and the low-scale corrections can be extracted. Starting from the massless case, which has been discussed in Ref. [159] and whose results we gave in Sec. 3.2.6, we proceed to the case of the EW standard model. The case of exchanging a massive gauge boson between external massless fermions has been discussed in Ref. [46] using the Δ -regulator. We also discussed the regularisation in Sec. 3.3.2 and gave some qualitative results. A more detailed calculation of these results is given in Sec. B.2 for the collinear functions of external fermions, gauge bosons, and scalars, as well as for the universal soft function. The final results in the form of Ref. [48] are provided in Sec. B.3.

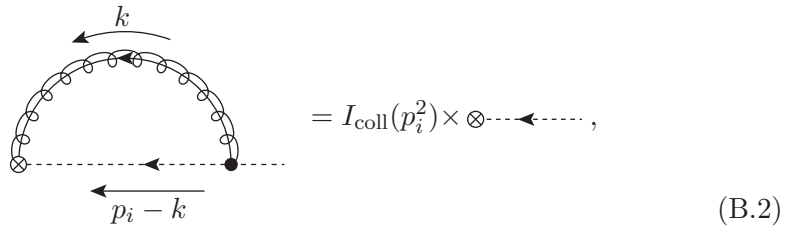
B.1. Massless case

Quark jet function

The quark jet function is obtained from the p_i -collinear radiative corrections to operators involving the gauge-invariant building block

$$\chi_{p_i} = W^\dagger(x)\xi_{p_i}. \quad (\text{B.1})$$

Apart from wavefunction corrections they are obtained from the diagram



$$= I_{\text{coll}}(p_i^2) \times \otimes \text{---} \leftarrow \text{---} \text{---} \text{---} , \quad (\text{B.2})$$

implicitly defining the collinear integral $I_{\text{coll}}(p_i^2)$. Using the Feynman rules given in Fig. 3.1 and, in addition, the Feynman rule for the emission of a collinear gluon with momentum k from the operator in Eq. (B.1),



$$\begin{array}{c} \mu, a, k \\ \otimes \text{---} \text{---} \text{---} \text{---} \end{array} = g_s \frac{\bar{n}^\mu T^a}{\bar{n} \cdot k}, \quad (\text{B.3})$$

the collinear integral reads

$$\begin{aligned}
 I_{\text{coll}} &= 2ig_s^2 C_F(\mu)^{4-D} \int \frac{d^D k}{(2\pi)^D} \frac{1}{\bar{n} \cdot k} \frac{\bar{n}(p_i - k)}{(p_i - k)^2 + i0} \frac{1}{k^2 + i0} \\
 &= ig_s^2 C_F(\mu)^{4-D} \int \frac{dk^- d\mathbf{k}_\perp^{D-2} dk^+}{(2\pi)^D} \frac{1}{k^-} \\
 &\quad \times \frac{(p_i^- - k^-)}{p_i^2 + k^+ k^- + \mathbf{k}_\perp^2 - (p_i^- k^+ + p_i^+ k^- + 2\mathbf{k}_\perp \cdot \mathbf{p}_{i,\perp}) + i0} \frac{1}{k^+ k^- + \mathbf{k}_\perp^2 + i0}, \tag{B.4}
 \end{aligned}$$

where we kept p_i^2 finite in order to regularise the IR singularities. Note that there is a Jacobian factor of 1/2 when transforming from $dk_0 dk_3$ to $dk^+ dk^-$. The basic steps (also concerning the bosonic and the massive case) are the following:

- Integrate over k^+ using contour integration. This constrains the integration boundary for k^- .
- Integrate over \mathbf{k}_\perp . This gives a tadpole integral in $D = 2 - 2\varepsilon$ dimensions.
- The remaining k^- integration can be performed analytically or reduced to the scalar integral f_S defined as

$$f_S(w, x) = \int_0^1 dz \frac{2-z}{z} \log \frac{1-z+xz-wz(1-z)}{1-z}. \tag{B.5}$$

The poles in k^+ are located at

$$k^+ = \frac{-\mathbf{k}_\perp^2 - i0}{k^-}, \quad k^+ = \frac{-\mathbf{k}_\perp^2 - p_i^2 + k^- p_i^+ + 2\mathbf{k}_\perp \cdot \mathbf{p}_{i,\perp} - i0}{(k^- - p_i^-)}. \tag{B.6}$$

If k^- and $k^- - p_i^-$ have the same sign, both poles are on the same side of the real axis. The contour can be closed containing no poles and I_{coll} vanishes. Because p_i^- has to be non-negative for a physical momentum, the k^- integration runs from 0 to p_i^- . Using the residue theorem yields

$$I_{\text{coll}} = -2\pi g_s^2 C_F(\mu)^{4-D} \int_0^{p_i^-} dk^- \int \frac{d\mathbf{k}_\perp^{D-2}}{(2\pi)^D} \frac{1}{k^-} \frac{(p_i^- - k^-)}{k^- (p_i^2 - k^- p_i^+ - 2\mathbf{k}_\perp \cdot \mathbf{p}_{i,\perp}) + p_i^- \mathbf{k}_\perp^2 + i0}. \tag{B.7}$$

Next we substitute $z = k^-/p_i^-$ and shift $\mathbf{k}_\perp \rightarrow \mathbf{k}_\perp + 2z\mathbf{p}_{i,\perp}$ to obtain the standard integral in \mathbf{k}_\perp ,

$$I_{\text{coll}} = -2\pi g_s^2 C_F(\mu)^{4-D} \int_0^1 dz \int \frac{d\mathbf{k}_\perp^{(2-2\varepsilon)}}{(2\pi)^{(4-2\varepsilon)}} \frac{1-z}{z} \frac{1}{\mathbf{k}_\perp^2 - \underbrace{z^2 \mathbf{p}_{i,\perp}^2 - z^2 p_i^+ p_i^- + z p_i^2}_{=-z^2 p_i^2} + i0}. \tag{B.8}$$

After writing $\mathbf{k}_\perp^2 = -\mathbf{k}_E^2$, (B.8) is a special case of the D -dimensional Euclidean tadpole integral (A.7)/(A.10):

$$A_0(m^2) = -\frac{(2\pi\mu)^{(4-D)}}{\pi^2} \int dk_E^D \frac{1}{k_E^2 + m^2 - i0} = -(4\pi\mu^2)^{(4-D)/2} \Gamma(1 - D/2) (m^2 - i0)^{(D/2-1)}. \quad (\text{B.9})$$

Using (B.9) with $D = 2 - 2\varepsilon$ and $m^2 = -p_i^2 z(1-z)$ yields

$$\begin{aligned} I_{\text{coll}} &= -\frac{\alpha_s}{2\pi} C_F \left(\frac{\mu^2}{-p_i^2} \right)^\varepsilon \Gamma(\varepsilon) \int_0^1 dz \frac{(1-z)^{(1-\varepsilon)}}{z^{(1+\varepsilon)}} \\ &= -\frac{\alpha_s}{2\pi} C_F \left(\frac{\mu^2}{-p_i^2} \right)^\varepsilon \Gamma(\varepsilon) \frac{\Gamma(-\varepsilon)\Gamma(2-\varepsilon)}{\Gamma(2-2\varepsilon)} \\ &= \frac{\alpha_s C_F \Gamma(1+\varepsilon)}{4\pi} \left(\frac{2}{\varepsilon^2} + \frac{2}{\varepsilon} \left(1 + \log \frac{\mu^2}{-p_i^2} \right) - \frac{\pi^2}{3} + 4 + \log^2 \frac{\mu^2}{-p_i^2} + 2 \log \frac{\mu^2}{-p_i^2} \right). \end{aligned} \quad (\text{B.10})$$

The wavefunction graphs are unchanged with respect to QCD and one has the usual quark field-renormalisation constant

$$\delta Z_q = -\frac{\alpha_s \Gamma(1+\varepsilon)}{4\pi} \left(\frac{1}{\varepsilon} + 1 + \log \frac{\mu^2}{-p_i^2} \right), \quad (\text{B.11})$$

leading to the quark jet function

$$\mathcal{J}_q = I_{\text{coll}} + \frac{1}{2} \delta Z_q = \frac{\alpha_s}{4\pi} C_F \left(\frac{2}{\varepsilon^2} + \frac{2}{\varepsilon} \log \frac{\mu^2}{-p^2} + \frac{3}{2\varepsilon} - \frac{\pi^2}{3} + \frac{7}{2} + \log^2 \frac{\mu^2}{-p_i^2} + \frac{3}{2} \log \frac{\mu^2}{-p_i^2} \right). \quad (\text{B.12})$$

Gluon jet function

The gluon jet function is obtained from a similar diagram as the quark jet function. The external gluon is described by the gauge-invariant building block in (3.57),

$$\hat{\mathcal{A}}_p^\mu = \frac{1}{g} \hat{W}^\dagger(x) \left(i \hat{D}_c^\mu \hat{W}(x) \right) = \frac{1}{g} \exp \left(\frac{g_s \bar{n} \cdot A_p^a \hat{T}^a}{\bar{n} \cdot p} \right) \left[p^\mu \hat{1} + g_s A_p^{\mu,a} \hat{T}^a \right] \exp \left(-\frac{g \bar{n} \cdot A_p^a \hat{T}^a}{\bar{n} \cdot p} \right). \quad (\text{B.13})$$

Here $\hat{\mathcal{A}}_p^\mu$ acts as a matrix in the fundamental representation, while the adjoint indices are contracted. All quantities that are matrices in the fundamental space are denoted with a hat in the following. A single gluon with colour index a is produced by the projection of $\hat{\mathcal{A}}_p^\mu$ onto a single adjoint component, (cf. eq. (2) of Ref. [240])

$$\hat{\mathcal{A}}_p^\mu = \mathcal{A}_p^{\mu,a} \hat{T}^a \quad \rightarrow \quad \mathcal{A}_p^{\mu,a} = 2 \text{Tr} \{ \hat{T}^a \hat{\mathcal{A}}_p^\mu \}. \quad (\text{B.14})$$

At leading power only the transverse part of $\mathcal{A}^{\mu,a}$ contributes because the polarisation vectors have to be transverse.

We decompose the gluon field into its polarisation states:

$$\mathcal{A}^{\mu,a} = \mathcal{A}^{\mu,\lambda,a} + \mathcal{A}^{\mu,\bar{\lambda},a} = (\bar{\varepsilon}_p^\lambda \cdot A_p^a) \varepsilon_p^{\lambda,\mu} + (\varepsilon_p^\lambda \cdot A_p^a) \bar{\varepsilon}_p^{\lambda,\mu} \quad (\text{B.15})$$

with $\varepsilon_p^{\lambda,\mu}$ being the polarisation vector of the polarisation state λ and momentum p , and $\bar{\varepsilon}_p^{\lambda,\mu}$ being its transverse complement:

$$\begin{aligned}\bar{n}_p \cdot \bar{\varepsilon}_p^\lambda &= n_p \cdot \bar{\varepsilon}_p^\lambda = (\bar{\varepsilon}_p^\lambda)^2 = 0, \\ \bar{\varepsilon}_p^\lambda \cdot \varepsilon_p^\lambda &= 1.\end{aligned}\tag{B.16}$$

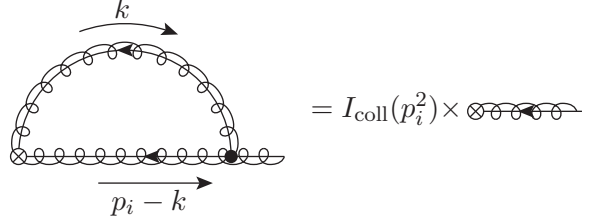
In fact this is fulfilled by $\bar{\varepsilon}^{\mu,\lambda} = -(\varepsilon^{\mu,\lambda})^*$. If we assume the gluons to have definite helicities λ, λ' , an exemplary SCET operator contributing to the process $\bar{q}q \rightarrow gg$ takes the form

$$\mathcal{O} = \bar{\chi}_{k_1} \gamma^\mu \hat{T}^a \gamma^\nu \hat{T}^b \chi_{k_2} \mathcal{A}_{\mu,p_1}^{a,\lambda} \mathcal{A}_{\nu,p_2}^{b,\lambda'} = \bar{\chi}_{k_1} \gamma^\mu \hat{T}^a \gamma^\nu \hat{T}^b \chi_{k_2} (\bar{\varepsilon}_{p_1}^\lambda \cdot \mathcal{A}_{p_1}^{a,\lambda}) \varepsilon_{p_1,\lambda}^{\nu,\lambda'} (\bar{\varepsilon}_{p_2}^{\lambda'} \cdot \mathcal{A}_{p_2}^{b,\lambda'}) \varepsilon_{p_2,\nu}^{\lambda'}.\tag{B.17}$$

Just like the χ_{k_i} fields the $\mathcal{A}_{\mu,k_i}^{a,\lambda}$ fields contain arbitrary many n_i -collinear gluons at leading power via the Wilson lines. The one-loop p_i -collinear jet function can be defined as the correction factor arising from the exchange of p_i -collinear gluons.¹ It can be written as

$$\mathcal{O} \rightarrow (1 + J(p_i^2)) \mathcal{O} = \left(1 + I_{\text{coll}}(p_i^2) + \frac{\delta Z_A}{2}\right) \mathcal{O},\tag{B.18}$$

with the gluon field-renormalisation constant δZ_A . The jet function $J(p_i^2)$ is independent of the fields other than $\mathcal{A}_{p_i}^\mu$. It is a scalar because the collinear SCET graphs do not mix Lorentz and colour structures into each other. In the following we write $\varepsilon^\mu, \bar{\varepsilon}^\mu$ instead of $\varepsilon_{p_i}^{\lambda,\mu}, \bar{\varepsilon}_{p_i}^{\lambda,\mu}$. Parameterising the loop momenta as follows,²



$$= I_{\text{coll}}(p_i^2) \times \text{diagram of two collinear gluons connected by a loop},\tag{B.19}$$

the one-loop jet function is obtained from the integral

$$I_{\text{coll}}^a(p_i^2) = \frac{1}{2} \bar{\varepsilon}^\mu \cdot \left\{ \int d^D k V_{\mu\nu\rho}^{abc}(k, -p_i, p_i - k) \frac{i}{k^2 + i0} \frac{i}{(k - p_i)^2 + i0} \hat{U}^{\nu\rho,bc}(k - p_i, -k) \right\}\tag{B.20}$$

with the $1/2$ being the symmetry factor, $V_{\mu\nu\rho}^{abc}(k, -p_i, p_i - k)$ being the usual three-gluon-vertex tensor,

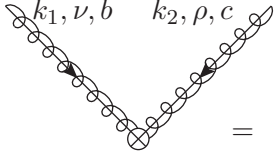
$$V_{\mu\nu\rho}^{abc}(k, -p_i, p_i - k) = g f^{abc} (g_{\mu\nu}(k - 2p_i)_\rho + g_{\nu\rho}(p_i - 2k)_\mu + g_{\rho\mu}(k + p_i)_\nu),\tag{B.21}$$

and $U^{\nu\rho,bc}(k_1, k_2)$ being the Feynman rule for the emission of two collinear gluons with momenta k_1, k_2 , colour indices b, c , and Lorentz indices ν, ρ from the transverse component of the operator

¹Usually the jet function is defined via the gluon two-point function [36]. This definition is, however, equivalent because it is computed from the same diagrams.

²In the following the external gluon is assumed to be outgoing. However, since the jet functions depend only on p_i^2 , it has to be the same for the incoming case.

in Eq. (B.13):



$$= \hat{U}^{\nu\rho,bc}(k_1, k_2) = \frac{\delta^2(\bar{\varepsilon} \cdot \hat{A})}{\delta A_{\nu, k_1}^b \delta A_{\rho, k_2}^c}. \quad (\text{B.22})$$

Expanding (B.13) leads to 10 terms with two gluons. To see which terms contribute, we first calculate the transverse component of the vertex tensor

$$\bar{\varepsilon}^\mu V_{\mu\nu\rho}^{abc}(-k, k - p_i) = g f^{abc} (g_{\nu\rho} \varepsilon \cdot (p_i - 2k) + \varepsilon_\nu (k - 2p_i)_\rho + \varepsilon_\rho (k + p_i)_\nu). \quad (\text{B.23})$$

Because $\bar{\varepsilon} \cdot \bar{n} = \varepsilon \cdot \bar{n} = \bar{n}^2 = 0$, we can restrict ourselves to the contributions of $\hat{U}_{bc}^{\nu\rho}$ that have at least one component proportional to $\bar{\varepsilon}$:

$$\begin{aligned} \hat{U}^{\nu\rho}(-k, k - p_i) &= g \left(-\frac{\bar{\varepsilon}^\nu \bar{n}^\rho}{-\bar{n} \cdot k} + \frac{\bar{n}^\nu \bar{\varepsilon}^\rho}{\bar{n} \cdot (k - p_i)} \right) (\hat{T}^b \hat{T}^c - \hat{T}^c \hat{T}^b) + \dots \\ &= ig \left(-\frac{\bar{\varepsilon}^\nu \bar{n}^\rho}{-\bar{n} \cdot k} + \frac{\bar{n}^\nu \bar{\varepsilon}^\rho}{\bar{n} \cdot (k - p_i)} \right) f^{bcd} \hat{T}^d + \dots \end{aligned} \quad (\text{B.24})$$

with the ellipsis denoting terms proportional to $\bar{n}^\nu \bar{n}^\rho$, $\bar{n}^\nu \bar{n}^\rho$, which vanish when projected onto (B.23). The colour algebra yields a factor of

$$f^{abc} f^{bcd} \hat{T}^d = C_A \hat{T}^a \mathbb{1} \quad (\text{B.25})$$

and the collinear integral is defined as the prefactor in front the colour matrix,

$$I_{\text{coll}}^a(p_i^2) = I_{\text{coll}}(p_i^2) \hat{T}^a, \quad (\text{B.26})$$

in order to fulfill (B.19). The Lorentz algebra produces two terms, one for each in the brackets in (B.24). The first one reads

$$I_1(p_i^2) = -\frac{1}{2} i C_A g^2 \int d^D k \frac{\bar{n} \cdot (2p_i - k)}{(k^2 + i0)[(p_i - k)^2 + i0](-\bar{n} \cdot k + i0)} \quad (\text{B.27})$$

and the second one

$$\begin{aligned} I_2(p_i^2) &= -\frac{1}{2} i C_A g^2 \int d^D k \frac{\bar{n} \cdot (k + p_i)}{(k^2 + i0)[(k - p_i)^2 + i0](\bar{n} \cdot (k - p_i) + i0)} \\ &= -\frac{1}{2} i C_A g^2 \int d^D k \frac{\bar{n} \cdot (-k + 2p_i)}{[(-k + p_i)^2 + i0](k^2 + i0)(-\bar{n} \cdot k + i0)} = I_1(p_i^2), \end{aligned} \quad (\text{B.28})$$

where the second form is obtained by shifting $k \rightarrow k + p_i$ and subsequently substituting $k \rightarrow -k$. We thus obtain the final result

$$I_{\text{coll}}(p_i^2) = -i C_A g^2 \int d^D k \frac{\bar{n} \cdot (2p_i - k)}{(k^2 + i0)[(p_i - k)^2 + i0](-\bar{n} \cdot k + i0)}, \quad (\text{B.29})$$

which is the same integral as in the quark case, except for the factor 2 in the numerator and a global factor of $1/2$. This does, however not affect the integrations over k^+ and \mathbf{k}_\perp , which can be performed in complete analogy to Eqs. (B.7)–(B.8). The z integration yields

$$\begin{aligned} I_{\text{coll}}(p_i^2) &= -\frac{\alpha_s}{4\pi} C_A \left(\frac{\mu^2}{-p_i^2} \right)^\varepsilon \Gamma(\varepsilon) \int_0^1 dz \frac{(2-z)(1-z)^{-\varepsilon}}{z^{1+\varepsilon}} \\ &= -\frac{\alpha_s}{4\pi} C_A \left(\frac{\mu^2}{-p_i^2} \right)^\varepsilon \Gamma(\varepsilon) \Gamma(1-\varepsilon) \frac{2(1-2\varepsilon)\Gamma(-\varepsilon) - \Gamma(1-\varepsilon)}{\Gamma(2-2\varepsilon)} \\ &= \frac{\alpha_s}{4\pi} C_A \Gamma(1+\varepsilon) \left(\frac{\mu^2}{-p_i^2} \right)^\varepsilon \left[\frac{2}{\varepsilon^2} + \frac{1}{\varepsilon} + 2 - \frac{\pi^2}{6} \right]. \end{aligned} \quad (\text{B.30})$$

Adding the field-renormalisation-constant contributions

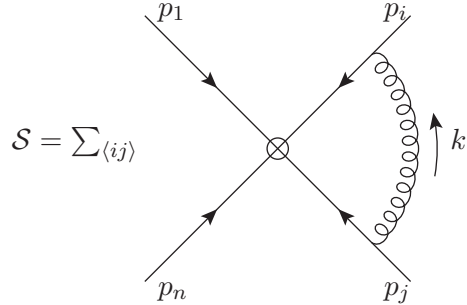
$$\frac{\delta Z_A}{2} = \frac{\alpha_s \Gamma(1+\varepsilon)}{4\pi} \left[\left(\frac{5}{6} C_A - \frac{2}{3} T_F n_f \right) \frac{1}{\varepsilon} \right] + \frac{\delta Z_A}{2} \Big|_{\text{finite}} \quad (\text{B.31})$$

we obtain the final result

$$J(p_i^2) = \frac{\alpha_s C_A \Gamma(1+\varepsilon)}{4\pi} \left(\frac{2}{\varepsilon^2} + \frac{1}{\varepsilon} \left[\log \left(\frac{\mu^2}{-p_i^2} \right) + \frac{\beta_0}{2} \right] + 2 - \frac{\pi^2}{6} \right) + \frac{\delta Z_A}{2} \Big|_{\text{finite}}. \quad (\text{B.32})$$

Soft function

The one-loop soft function is obtained from diagrams with soft-gluon exchange between collinear external legs [159],



$$\mathcal{S} = \sum_{(ij)} \quad (\text{B.33})$$

with the arrow lines indicating either collinear quarks or collinear gluons.

To calculate these diagrams one should first recapitulate the scaling of the soft gluon: $k \sim (\lambda^2, \lambda^2, \lambda^2)$. Applying the Feynman rules in Fig. 3.1 and putting $k^2 \ll 2p_i k$, $\bar{n}_i \cdot k \ll \bar{n}_i \cdot p_i$ in the propagators of the collinear particles³ leads to (we assume all momenta to be incoming!)

$$\mathcal{S} = -ig_s^2 \sum_{i \neq j} \frac{\mathbf{T}_i \cdot \mathbf{T}_j}{2} \int \frac{d^D k}{(2\pi)^D} \frac{\bar{n}_i \cdot p_i}{p_i^2 + 2p_i k + i0} \frac{\bar{n}_j \cdot p_j}{p_j^2 - 2p_j k + i0} \frac{n_i \cdot n_j}{k^2 + i0}. \quad (\text{B.34})$$

³This corresponds to an expansion by regions. If the multipole-expanded SCET Lagrangian is used, a “manual” expansion by regions is not necessary anymore. This is however not possible for off-shell quantities, see [159].

The numerators in Eq. (B.34) can be combined to give

$$(n_i \cdot n_j)(\bar{n}_i \cdot p_i)(\bar{n}_j \cdot p_j) = 4p_i \cdot p_j \equiv 2s_{ij}. \quad (\text{B.35})$$

We parametrise the loop momentum according to the direction of p_i , which scales like

$$p_i^+ = \mathcal{O}(\lambda^2), \quad p_i^- = \mathcal{O}(1), \quad \mathbf{p}_{i,\perp} = \mathcal{O}(\lambda). \quad (\text{B.36})$$

Because p_i and p_j enclose a finite angle, all components of p_j are finite,

$$p_j^+ = \mathcal{O}(1), \quad p_j^- = \mathcal{O}(1), \quad \mathbf{p}_{j,\perp} = \mathcal{O}(1), \quad p_j^2 = \mathcal{O}(\lambda^2). \quad (\text{B.37})$$

All components of the soft loop momentum scale like λ^2 . Parameterising the soft integral (B.34) in light-cone coordinates of p_i leads to

$$\begin{aligned} \mathcal{S} = & -2ig_s^2 \sum_{i \neq j} s_{ij} \frac{\mathbf{T}_i \cdot \mathbf{T}_j}{2} \\ & \times \int \frac{d^D k}{(2\pi)^D} \frac{1}{p_i^2 + p_i^- + k^+ + i0} \frac{1}{p_j^2 - p_j^+ k^- - p_j^- k^+ - 2\mathbf{p}_{j,\perp} \cdot \mathbf{k}_\perp + i0} \frac{1}{k^+ k^- + \mathbf{k}_\perp^2 + i0}. \end{aligned} \quad (\text{B.38})$$

Following the same strategy as for the jet functions, we obtain for the pole positions in k^-

$$k^- = \frac{-\mathbf{k}_\perp^2 - i0}{k^+}, \quad k^- = \frac{p_j^2 - k^+ p_j^- - 2\mathbf{k}_\perp \cdot \mathbf{p}_{j,\perp} + i0}{p_j^+}. \quad (\text{B.39})$$

Because of the $i0$ -prescription, k^+ and p_j^+ need to have the same sign. Because p_j^+ is always positive, we thus restrict k^+ to positive values. Applying the residue theorem yields

$$\begin{aligned} \mathcal{S} = & \frac{2g_s^2}{\pi} \sum_{i \neq j} s_{ij} \frac{\mathbf{T}_i \cdot \mathbf{T}_j}{2} \\ & \times \int_0^\infty \frac{dk^+}{2\pi} \int \frac{d^{(D-2)} \mathbf{k}_\perp}{(2\pi)^{(D-2)}} \frac{1}{p_i^2 + p_i^- k^+ + i0} \frac{1/k^+}{p_j^2 - p_j^- k^+ + p_j^+ / k^+ \mathbf{k}_\perp^2 - 2\mathbf{p}_{j,\perp} \cdot \mathbf{k}_\perp + i0}. \end{aligned} \quad (\text{B.40})$$

Using the substitution $z = k^+ / p_j^+$ and shifting $\mathbf{k}_\perp \rightarrow \mathbf{k}_\perp - 2z\mathbf{p}_{j,\perp}$, we obtain again a two-dimensional tadpole integral. One should note that the integration variable z scales like λ^2 . It

should thus consistently be neglected whenever possible:

$$\begin{aligned}
 \mathcal{S} &= 2\alpha_s \sum_{i \neq j} s_{ij} \frac{\mathbf{T}_i \cdot \mathbf{T}_j}{2} \\
 &\times \int_0^\infty dz \int \frac{d^{(D-2)} \mathbf{k}_\perp}{(2\pi)^{(D-2)}} \frac{1}{p_i^2 + zp_i^+ p_j^- + i0} \frac{1}{\mathbf{k}_\perp^2 \underbrace{-z^2 \mathbf{p}_{j,\perp}^2 - 2z^2 p_j^+ p_j^-}_{=-z^2 p_j^2 = \mathcal{O}(\lambda^6)} + zp_j^2 + i0} \\
 &= 2\alpha_s \sum_{i \neq j} s_{ij} \frac{\mathbf{T}_i \cdot \mathbf{T}_j}{2} \int_0^\infty dz \int \frac{d^{(D-2)} \mathbf{k}_\perp}{(2\pi)^{(D-2)}} \frac{1}{p_i^2 + zp_i^+ p_j^- + i0} \frac{1}{\mathbf{k}_\perp^2 + zp_j^2 + i0}. \tag{B.41}
 \end{aligned}$$

The \mathbf{k}_\perp -integral can again be evaluated using the tadpole formula (B.9):

$$\begin{aligned}
 \mathcal{S} &= \frac{\alpha_s}{2\pi} \left(\frac{\mu^2}{-p_j^2} \right)^\varepsilon \Gamma(\varepsilon) \sum_{i \neq j} \frac{\mathbf{T}_i \cdot \mathbf{T}_j}{2} \int_0^\infty dz \frac{z^{-\varepsilon}}{\frac{p_i^2}{s_{ij}} + z} \\
 &= \frac{\alpha_s}{2\pi} \sum_{i \neq j} \left(\frac{\mu^2(-s_{ij})}{(-p_j^2)(-p_i^2)} \right)^\varepsilon \frac{\Gamma(\varepsilon)\pi}{\sin(\varepsilon\pi)} \frac{\mathbf{T}_i \cdot \mathbf{T}_j}{2} \\
 &= \frac{\alpha_s}{4\pi} \Gamma(1 + \varepsilon) \sum_{i \neq j} \frac{\mathbf{T}_i \cdot \mathbf{T}_j}{2} \left(\frac{2}{\varepsilon^2} + \frac{2}{\varepsilon} \log \left(\frac{\mu^2(-s_{ij})}{(-p_i^2)(-p_j^2)} \right) + \log^2 \left(\frac{\mu^2(-s_{ij})}{(-p_i^2)(-p_j^2)} \right) + \frac{\pi^2}{6} \right). \tag{B.42}
 \end{aligned}$$

The combination of the jet and soft functions is obtained by rewriting

$$\log \left(\frac{\mu^2(-s_{ij})}{(-p_i^2)(-p_j^2)} \right) = \log \left(\frac{-s_{ij}}{\mu^2} \right) + \log \left(\frac{\mu^2}{-p_i^2} \right) + \log \left(\frac{\mu^2}{-p_j^2} \right) \tag{B.43}$$

and performing the colour sum for the latter two terms. Note that we do this only for the UV-divergent terms, as we can infer from these the form of the IR-divergent terms in the photonic corrections to the fermion jet functions, see below. The UV-finite terms are IR divergent and hence remain dependent on the regulators p_i^2, p_j^2 . Using (B.43) as well as $\sum_i \mathbf{T}_i \cdot \mathbf{T}_i = C_i$, we find

$$\begin{aligned}
 &\mathcal{S}(\{p^2\}) + \sum_i \mathcal{J}(p_i^2) = \\
 &= \frac{\alpha_s \Gamma(1 + \varepsilon)}{4\pi} \left(\sum_i \frac{C_i}{\varepsilon^2} + \sum_{i \neq j} \mathbf{T}_i \cdot \mathbf{T}_j \left[\frac{1}{\varepsilon} \log \left(\frac{-s_{ij}}{\mu^2} \right) + \frac{1}{2} \log^2 \left(\frac{-s_{ij}}{\mu^2} \right) \right] + \frac{1}{\varepsilon} \sum_i \gamma_i \right) + \mathcal{O}(\varepsilon^0) \tag{B.44}
 \end{aligned}$$

with

$$\gamma_q = 3C_F, \quad \gamma_A = \beta_0. \tag{B.45}$$

We have seen that in the UV poles the regulator dependence has cancelled. The anomalous dimension can be calculated as the coefficient in front of the $1/\varepsilon$ -pole times -2 :

$$\Gamma = -\frac{\alpha_s}{\pi} \left(\sum_{i \neq j} \frac{\mathbf{T}_i \cdot \mathbf{T}_j}{2} \log \left(\frac{-s_{ij}}{\mu^2} \right) + \sum_i \gamma_i \right), \quad (\text{B.46})$$

in accordance with Ref. [159].

B.2. Massive case

B.2.1. Fermion jet function

In the following we generalise the obtained results to the case of massive gauge-boson exchange. We describe this for the collinear integral of a massless fermion. We denote with g the coupling between the fermion and the gauge boson.

Δ -regulator

When the gauge bosons are taken to be massive, the collinear and soft integrals are separately divergent, requiring an additional regulator. We choose the Δ regulator, which has the advantage to enable a jet-function definition employing a single Wilson line in each direction [46]. If we consider the collinear integral (B.4) and give the gauge boson a mass M , the first pole position in k^+ moves to

$$k^+ = \frac{-\mathbf{k}_\perp^2 + M^2 - i0}{k^-} \quad (\text{B.47})$$

After contour integration one obtains

$$\begin{aligned} I_{\text{coll}} &= -2\pi g^2 (\mu^2)^\varepsilon \\ &\times \int_0^{p_i^-} dk^- \int \frac{d\mathbf{k}_\perp^{D-2}}{(2\pi)^D} \frac{1}{k^-} \frac{(p_i^- - k^-)}{k^- (M^2 + p_i^2 - k^- p_i^+ - 2\mathbf{k}_\perp \mathbf{p}_{i,\perp}) + p_i^- (\mathbf{k}_\perp^2 - M^2) + i0}, \end{aligned} \quad (\text{B.48})$$

which yields a tadpole integral with mass $M^2(1-z) - p_i^2 z(1-z)$. Performing the same substitution as in the massless case produces the following z -integral:

$$I_{\text{coll}} = -\frac{\alpha}{2\pi} (\mu^2)^\varepsilon \Gamma(\varepsilon) \int_0^1 dz \frac{(1-z)}{z} (M^2(1-z) - p_i^2 z(1-z))^{-\varepsilon}, \quad (\text{B.49})$$

which diverges as $z \rightarrow 0$, thus necessitating a regularisation of the Wilson line propagator $\frac{1}{k^-}$. This is achieved by shifting all particles' masses according to

$$\frac{1}{(p_i + k)^2 - m_i^2} \rightarrow \frac{1}{(p_i + k)^2 - m_i^2 - \Delta_i} \quad (\text{B.50})$$

while keeping the on-shell conditions $p_i^2 = m_i^2$ unchanged. After this shift the final factor reads

$$\frac{\varepsilon \cdot \bar{n}_i}{\bar{n}_i \cdot k - \delta_{i,n_j} + i0} \quad (\text{B.51})$$

with δ_{i,n_j} defined according to

$$\delta_{i,n_j} = \frac{2\Delta_i}{(n_i \cdot n_j)(\bar{n}_i \cdot p_i)}. \quad (\text{B.52})$$

After substituting this into (3.102), the sum over j can not be performed anymore because of the j -dependence of the prefactor beyond the colour operator.

Thus we obtain for (B.49) the regularised form

$$\begin{aligned} I_{\text{coll}} &= -\frac{\alpha}{2\pi} \Gamma(\varepsilon) \left(\frac{\mu^2}{M^2 - \Delta_i} \right)^\varepsilon \int_0^1 dz \frac{(1-z)^{1-\varepsilon}}{z + \frac{\delta_{i,n_j}}{p_i^-}}, \\ &= -\frac{\alpha}{2\pi} \Gamma(\varepsilon) \left(\frac{\mu^2}{M^2 - \Delta_i} \right)^\varepsilon \left(\int_0^1 dz \frac{1-z}{z + \frac{\delta_{i,n_j}}{p_i^-}} - \varepsilon \int_0^1 dz \frac{(1-z) \log(1-z)}{z} + \mathcal{O}(\varepsilon^2) \right) \\ &= \frac{\alpha}{4\pi} \Gamma(1+\varepsilon) \left(\frac{\mu^2}{M^2} \right)^\varepsilon \left(\frac{2}{\varepsilon} + \frac{2}{\varepsilon} \log \frac{\delta_{i,n_j}}{p_i^-} + 2 - \frac{\pi^2}{3} \right), \end{aligned} \quad (\text{B.53})$$

where we have set p_i^2 to 0 because with a finite gauge-boson mass there is no need to regularise IR divergences. In addition we have expanded the integrand in ε before performing the integration, because the second term can be evaluated with $\delta_{i,n_j} = 0$.

Zero-bin subtraction

While (B.53) is a well-defined integral, it is not independent of j , which questions, why it is reasonable to write the operators in terms of single n_i -collinear Wilson lines. The point is that the Δ -regulators induce a non-vanishing double-counting of the soft-collinear region. The n_i soft-collinear region is contained both in the soft and the n_i -collinear region and is hence counted twice if the contributions of jet and soft functions are added. While without regulators its contribution vanishes, in terms of the Δ regulators it is most easily obtained by considering the soft limit of collinear loop integral, (B.48), dropping the k^- in the numerator and the k^2 -term in the fermion propagator:

$$I_{\text{coll},\emptyset} = -2ig^2 \int \frac{d^D k}{(2\pi)^D} \frac{p_i^-}{(k^- + \delta_{i,n_j})(k^2 - M^2)(-p_i^- k^+ - \Delta_i + i0)}, \quad (\text{B.54})$$

yielding the pole positions

$$k^+ = \frac{-\Delta_i + i0}{p_i^-}, \quad k^+ = \frac{-\mathbf{k}_\perp^2 + M^2 - i0}{k^-}, \quad (\text{B.55})$$

which restrict k^- to positive values as in the case of the massless soft function, see (B.39) and below. We obtain

$$\begin{aligned} I_{\text{coll},\emptyset} &= -\frac{\alpha}{2\pi}\Gamma(\varepsilon)(\mu^2)^\varepsilon \int_0^\infty dz \frac{(M^2 + z\Delta_i)^{-\varepsilon}}{z + \frac{\delta_{i,n_j}}{p_i^-}} \\ &= -\frac{\alpha}{4\pi}\Gamma(1+\varepsilon)\left(\frac{\mu^2}{M^2}\right)^\varepsilon \left(\frac{2}{\varepsilon^2} + \frac{2}{\varepsilon} \log \frac{M^2 p_i^-}{\Delta_i \delta_{i,n_j}} - \frac{\pi^2}{3} + \mathcal{O}(\varepsilon)\right). \end{aligned} \quad (\text{B.56})$$

The zero-bin integral has no closed form in terms of standard functions, its solution is a hypergeometric function. For the correct finite result it is important to take the limit of $\Delta_i \rightarrow 0$ before $\varepsilon \rightarrow 0$. Subtracting the zero-bin contribution from the collinear integral while setting Δ_i and $\delta_{i,n_j}/p_i^-$ to zero wherever possible, we obtain the final result,

$$\begin{aligned} I_{\text{coll}} - I_{\text{coll},\emptyset} &= \frac{\alpha}{4\pi}\Gamma(1+\varepsilon) \left(\frac{2}{\varepsilon^2} + \frac{2}{\varepsilon} \left(1 + \log \left(\frac{\mu^2}{\Delta_i} \right) \right) + 2 \log \left(\frac{\mu^2}{M^2} \right) \left(1 - \log \left(\frac{\Delta_i}{\mu^2} \right) \right) \right. \\ &\quad \left. + \log^2 \left(\frac{\mu^2}{M^2} \right) - \frac{2\pi^2}{3} + 2 \right), \end{aligned} \quad (\text{B.57})$$

in accordance with Eq. (22) of Ref. [46] (up to the prefactor $e^{\gamma_E \varepsilon}$). Eq. (B.57) is indeed independent of the direction j . The collinear integrals can hence be calculated using an arbitrary regularisation direction and the colour algebra can be performed as in the tree-level case.

Photonic part

The photonic SCET_{EW} corrections for massless fermions are obtained from the fact that all SCET_{EW} integrals are scaleless. Their sum can therefore be written as

$$\sum_k \frac{D_k}{\varepsilon_{\text{UV}}^k} - \frac{D_k}{\varepsilon_{\text{IR}}^k}. \quad (\text{B.58})$$

For massless QCD we have obtained

$$\begin{aligned} \mathcal{S}(\{p^2\}) + \sum_i \mathcal{J}(p_i^2) &= \\ &= \frac{\alpha_s \Gamma(1+\varepsilon)}{4\pi} \left(\sum_i \frac{C_i}{\varepsilon_{\text{UV}}^2} + \sum_{i \neq j} \frac{\mathbf{T}_i \cdot \mathbf{T}_j}{2} \left[\frac{1}{\varepsilon_{\text{UV}}} \log \left(\frac{-s_{ij}}{\mu_{\text{UV}}^2} \right) + \frac{1}{2} \log^2 \left(\frac{-s_{ij}}{\mu_{\text{UV}}^2} \right) \right] + \frac{1}{\varepsilon_{\text{UV}}} \sum_i \gamma_i \right) \\ &\quad + \text{UV-finite}, \end{aligned} \quad (\text{B.59})$$

with ‘‘UV-finite’’ given in terms of off-shell regulators. Using (B.58), (B.45), as well as the Abelianisation prescription [180]

$$\alpha_s \rightarrow \alpha, \quad \mathbf{T}_i \rightarrow \sigma_i Q_i, \quad C_F = Q_f^2, \quad C_A = 0, \quad (\text{B.60})$$

yields the photonic SCET corrections for massless fermions:

$$\begin{aligned}
 \mathcal{S}_\gamma + \sum_i J_{\gamma,i}(p_i^2) &= \\
 &= \frac{\alpha\Gamma(1+\varepsilon)}{4\pi} \left(\sum_i \left[\frac{Q_i^2}{\varepsilon_{\text{UV}}^2} + \frac{3}{2} \frac{Q_i^2}{\varepsilon_{\text{UV}}} \right] + \sum_{i \neq j} \sigma_i Q_i \sigma_j Q_j \left[\frac{1}{\varepsilon_{\text{UV}}} \log \frac{-s_{ij}}{\mu_{\text{UV}}^2} + \frac{1}{2} \log^2 \frac{\mu_{\text{UV}}^2}{-s_{ij}} \right] \right. \\
 &\quad \left. - \sum_i \left[\frac{Q_i^2}{\varepsilon_{\text{IR}}^2} + \frac{3}{2} \frac{Q_i^2}{\varepsilon_{\text{IR}}} \right] - \sum_{i \neq j} \sigma_i Q_i \sigma_j Q_j \left[\frac{1}{\varepsilon_{\text{IR}}} \log \frac{-s_{ij}}{\mu_{\text{IR}}^2} + \frac{1}{2} \log^2 \frac{\mu_{\text{IR}}^2}{-s_{ij}} \right] \right). \quad (\text{B.61})
 \end{aligned}$$

To obtain the desired form of the collinear and soft function we have to assign all possible terms in the soft integral to single legs using colour conservation as well as the Sudakov representation of the large invariant s_{ij} ,

$$\log \frac{-s_{ij}}{\mu_{\text{IR}}^2} = \log \frac{\bar{n}_i \cdot p_i}{\mu_{\text{IR}}} + \log \frac{\bar{n}_j \cdot p_j}{\mu_{\text{IR}}} + \log \frac{-n_i \cdot n_j - i0}{2}. \quad (\text{B.62})$$

Subtracting the UV poles, setting $\mu_{\text{UV}} = \mu_1$, and assigning all possible terms to single legs yields

$$\begin{aligned}
 \mathcal{S}_\gamma + \sum_i J_{\gamma,i}(p_i^2) &= \frac{\alpha}{4\pi} \Gamma(1+\varepsilon) \sum_i Q_i^2 \left(-\frac{1}{\varepsilon_{\text{IR}}^2} - \frac{1}{\varepsilon_{\text{IR}}} \left(\frac{3}{2} - 2 \log \frac{\bar{n}_i \cdot p_i}{\mu_{\text{IR}}} \right) \right. \\
 &\quad \left. + \frac{3}{2} \log \frac{\mu_{\text{UV}}^2}{\mu_{\text{IR}}^2} + 2 \log \frac{\mu_{\text{IR}}^2}{\mu_1^2} \log \frac{\bar{n}_i \cdot p_i}{\mu_1} - \frac{1}{2} \log \frac{\mu_{\text{IR}}^2}{\mu_1^2} \right) \\
 &\quad + \frac{\alpha}{4\pi} \Gamma(1+\varepsilon) \sum_{i \neq j} \sigma_i Q_i \sigma_j Q_j \left(\frac{1}{\varepsilon_{\text{IR}}} + \log \frac{\mu_{\text{UV}}^2}{\mu_{\text{IR}}^2} \right) \log \frac{-n_i \cdot n_j - i0}{2}, \quad (\text{B.63})
 \end{aligned}$$

where we used (B.62) in several places. The first two lines are one-particle contributions and contribute to the collinear functions, while the third line yields the photonic part of the soft function.

B.2.2. Gauge boson jet function

The jet functions for the SM gauge bosons are calculated from the diagram:

$$= I_{\text{coll}}(p_i^2, m_{\text{int}}^2, M^2). \quad (\text{B.64})$$

It has the same Lorentz structure as the one in Eq. (B.19). On the level of SU(2) eigenstates there is, however, only one non-vanishing colour configuration for each external particle: An external W^3 with a virtual W^\pm pair and a W^\pm with a W^\pm and W^3 . Decomposing the W^3 into mass eigenstates yields two diagrams in each case.

Concerning the regularisation, the integrals can be calculated in analogy to the fermionic case. Defining the momenta as indicated in Eq. (B.64), we obtain again two terms from the Feynman rule in Eq. (B.22). Unlike in the massless case, they are not equal if $m_{\text{int}} \neq M$. Instead, they switch the role of the gauge bosons:

$$\begin{aligned} I_1(p_i^2, m_{\text{int}}^2, M^2) &= -ig^2 \int d^D k \frac{\bar{n} \cdot (2p_i - k)}{(k^2 - M^2 + i0)[(p_i - k)^2 - m_{\text{int}}^2 + i0](-\bar{n} \cdot k + i0)}, \\ I_2(p_i^2, m_{\text{int}}^2, M^2) &= -ig^2 \int d^D k \frac{\bar{n} \cdot (2p_i - k)}{(k^2 - m_{\text{int}}^2 + i0)[(p_i - k)^2 - M^2 + i0](-\bar{n} \cdot k + i0)} \\ &= I_1(p_i^2, M^2, m_{\text{int}}^2). \end{aligned} \quad (\text{B.65})$$

I_2 can thus be interpreted as “exchange of a gauge boson with mass m_{int} ”. Because the propagators are different, there is also no symmetry factor of $1/2$.

For finite M we obtain (abbreviating $x = m_{\text{int}}^2/M^2$, $w = p_i^2/M^2$)

$$\begin{aligned} I_1 &= -\frac{\alpha}{4\pi} \Gamma(\varepsilon) \left(\frac{\mu^2}{M^2 - \Delta_i} \right)^\varepsilon \int_0^1 dz \frac{(2-z)(1-z+xz-wz(1-z))^{-\varepsilon}}{z + \frac{\delta_{i,n_j}}{p_i^-}} \\ &= -\frac{\alpha}{4\pi} \Gamma(\varepsilon) \left(\frac{\mu^2}{M^2 - \Delta_i} \right)^\varepsilon \left(\int_0^1 dz \frac{2-z}{z + \frac{\delta_{i,n_j}}{p_i^-}} \right. \end{aligned} \quad (\text{B.66})$$

$$\left. -\varepsilon \int_0^1 dz \frac{(2-z) \log(1-z)}{z} - \varepsilon f_S(w, x) + \mathcal{O}(\varepsilon^2) \right)$$

$$= \frac{\alpha}{4\pi} \Gamma(1+\varepsilon) \left(\frac{\mu^2}{M^2} \right)^\varepsilon \left(\frac{1}{\varepsilon} + \frac{2}{\varepsilon} \log \frac{\delta_{i,n_j}}{p_i^-} + 1 - \frac{\pi^2}{3} + f_S(w, x) + \mathcal{O}(\varepsilon^2) \right) \quad (\text{B.67})$$

with f_S defined in (B.5). The zero-bin contribution is the same as in the fermion case because interactions are spin-independent in the soft limit, and we obtain the final result:

$$I_1 - I_{1,\emptyset} = \frac{\alpha}{4\pi} \Gamma(1+\varepsilon) \left(\frac{\mu^2}{M^2} \right)^\varepsilon \left(\frac{2}{\varepsilon^2} + \frac{1}{\varepsilon} + \frac{2}{\varepsilon} \log \frac{M^2}{\Delta_i} + 1 - \frac{2\pi^2}{3} + f_S(w, z) \right). \quad (\text{B.68})$$

Photonic part

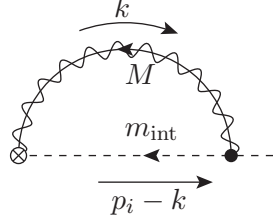
In the case of the W boson, the photonic corrections are obtained in two parts: The IR-finite part is obtained from the SCET diagrams. As explained in more detail in Ref. [44], the W boson is treated as a boosted-heavy-quark-effective-theory (bHQET) field below the low scale μ_1 . The matching corrections between SCET_{EW} and bHQET are obtained from the diagram in (B.64). Because the photon is massless, the integration can be carried out without Δ regulators to yield

$$I_1 = \frac{\alpha}{4\pi} \left(\frac{1}{\varepsilon^2} + \frac{1}{\varepsilon} + \frac{1}{2} \log^2 \frac{\mu^2}{M_W^2} + \log \frac{\mu^2}{M_W^2} + 2 \right). \quad (\text{B.69})$$

The complete gauge-boson jet function is obtained as a sum over all combinations of M and m_{int} , as is demonstrated more explicitly below (“putting the results together”).

B.2.3. Scalar jet function

The scalar collinear integral is obtained from the same diagram as in the fermionic case:



$$= I_{\text{coll}}(p_i^2, m_{\text{int}}^2, M^2), \quad (\text{B.70})$$

Applying the Feynman rules (remember that they are not changed with respect to the SM, because we consider purely collinear interactions) yields the same collinear integral as in the vector-boson case:

$$I_{\text{coll}}(p_i^2, m_{\text{int}}^2, M^2) = -ig^2 \int d^D k \frac{\bar{n} \cdot (2p_i - k)}{(k^2 - M^2 + i0)[(p_i - k)^2 - m_{\text{int}}^2 + i0](-\bar{n} \cdot k + i0)}, \quad (\text{B.71})$$

with p_i^2 equalling the squared mass of the scalar, M is the mass of the exchanged gauge boson, and m_{int} the internal mass of the scalar's isospin partner. Because I_{coll} precisely corresponds to $I_1 + I_2$ in (B.65), we can infer that the result has the same form as in the vector-boson case.

B.2.4. Soft integral

The one-loop soft function is obtained from the integral in Eq. (B.34) with a finite gauge-boson mass M and the offshellnesses replaced by the Δ -regulators:

$$-p_{i/j}^2 \rightarrow \Delta_{i/j}. \quad (\text{B.72})$$

After performing the integrations over k^+ and \mathbf{k}_\perp in the same manner as in the massless case one obtains the integral

$$\mathcal{S} = \sum_{V_a} \frac{\alpha}{2\pi} (\mu^2)^\varepsilon \Gamma(\varepsilon) \sum_{i \neq j} \frac{\mathbf{T}_i^{V_a} \cdot \mathbf{T}_j^{\bar{V}_a}}{2} \int_0^\infty dz \frac{(M_{V_a}^2 + z\Delta_j)^{-\varepsilon}}{\frac{\Delta_i}{s_{ij}} + z} \quad (\text{B.73})$$

with $T_i^{V_a}$ denoting the colour operator associated with gauge boson V_a . The integral in Eq. (B.73) is the same as the zero-bin integral in (B.56), the result reads (with Δ_{ij} set to 0 where possible)

$$\begin{aligned} \mathcal{S} &= \frac{\alpha}{2\pi} \Gamma(1 + \varepsilon) \left(\frac{\mu^2}{M_{V_a}^2} \right)^\varepsilon \sum_{i \neq j} \frac{\mathbf{T}_i^{V_a} \cdot \mathbf{T}_j^{\bar{V}_a}}{2} \left(\frac{1}{\varepsilon^2} + \frac{1}{\varepsilon} \log \frac{M_{V_a}^2 s_{ij}}{\Delta_i \Delta_j} - \frac{\pi^2}{6} + \mathcal{O}(\varepsilon^2) \right) \\ &= \frac{\alpha}{2\pi} \Gamma(1 + \varepsilon) \left(\frac{\mu^2}{M_{V_a}^2} \right)^\varepsilon \left(- \sum_i \frac{\mathbf{T}_i^{V_a} \cdot \mathbf{T}_i^{\bar{V}_a}}{2} \left(\frac{1}{\varepsilon^2} + \frac{2}{\varepsilon} \log \frac{\mu^2}{\Delta_i} + \frac{1}{\varepsilon} \log \frac{M_{V_a}^2}{\mu^2} \right. \right. \\ &\quad \left. \left. + \frac{2}{\varepsilon} \log \frac{\bar{n}_i \cdot p_i}{\mu} - \frac{\pi^2}{6} \right) + \sum_{i \neq j} \frac{\mathbf{T}_i^{V_a} \cdot \mathbf{T}_j^{\bar{V}_a}}{2} \frac{1}{\varepsilon} \log \frac{-n_i \cdot n_j - i0}{2} \right), \quad (\text{B.74}) \end{aligned}$$

where we have split off all one-particle contributions in the last step using that the quantum numbers associated with any of the V_a of course have to be individually conserved.

Photonic part with external masses

For the case of photonic corrections to processes involving massive external particles the soft integral has to be evaluated in bHQET. The result has been given in Eqs. (81) – (83) of Ref. [44] for a finite gauge-boson mass, which is much smaller than the bHQET mass. The result is, however, also valid for an infinitesimal photon mass λ , which we can translate to DimReg using the well-known correspondence

$$\log \lambda^2 \Leftrightarrow \frac{1}{\varepsilon_{\text{IR}}} + \log \mu_{\text{IR}}^2, \quad (\text{B.75})$$

and obtain

$$\mathcal{S}_\gamma = \sum_{\langle ij \rangle} \frac{\alpha \sigma_i Q_i \sigma_j Q_j}{4\pi} \log(2w_{ij}) \left(-\frac{2}{\varepsilon_{\text{UV}}} + \frac{2}{\varepsilon_{\text{IR}}} + 2 \log \frac{\mu_{\text{IR}}^2}{\mu_{\text{UV}}^2} \right) \quad (\text{B.76})$$

with the pseudo-angle

$$w_{ij} = v_i \cdot v_j = \frac{p_i \cdot p_j}{m_i m_j} = \frac{\bar{n}_i \cdot p_i \bar{n}_j \cdot p_j}{m_i m_j} \frac{n_i \cdot n_j}{2}. \quad (\text{B.77})$$

This can be recognised as the result of the QED eikonal integral [143] in the limit of $m_i, m_j \rightarrow 0$.

B.2.5. Putting the results together

The collinear anomalous dimension and matching are obtained as the UV-singular and finite part of the one-particle contributions, respectively. That means we have to add the terms in the first line of Eq. (B.74) to the collinear integrals with the zero bin subtracted and finally sum over the contributions of W, Z, and photon. In addition the respective wavefunction-correction contributions have to be taken into account. They are not changed by SCET_{EW} and can be copied from the SM.

The UV poles reproduce the anomalous dimension of the massless case: All UV-divergent terms depending on M_{V_a} cancel. One can therefore perform the sum over V_a to obtain

$$\begin{aligned} \mathcal{S} &+ \sum_i \left(\sum_{V_a} (I_{\text{coll}}^i(M_{V_a}) - I_{\text{coll},\emptyset}^i(M_{V_a})) + \frac{\delta Z_i}{2} \right) \\ &= \frac{\alpha}{2\pi} \sum_{i \neq j} \frac{\mathbf{T}_i \cdot \mathbf{T}_j}{2} \frac{1}{\varepsilon} \log \frac{-n_i \cdot n_j - i0}{2} - \frac{\alpha}{4\pi} \sum_i C_i^{\text{ew}} \left(\frac{1}{\varepsilon^2} - \frac{2}{\varepsilon} \log \frac{\bar{n}_i \cdot p_i}{\mu} \right) + \sum_i \frac{1}{\varepsilon} \frac{\gamma_i}{2} \\ &+ \text{UV-finite}. \end{aligned} \quad (\text{B.78})$$

The anomalous dimension is given by minus twice the $1/\varepsilon$ coefficient, yielding:

$$\mathbf{\Gamma} = \frac{\alpha}{4\pi} \left(4C_i^{\text{ew}} \log \frac{\bar{n}_i \cdot p_i}{\mu} + \gamma_i \right) \mathbb{1} + \frac{\alpha}{\pi} \sum_{i \neq j} \frac{\mathbf{T}_i \cdot \mathbf{T}_j}{2} \log \frac{-n_i \cdot n_j - i0}{2}. \quad (\text{B.79})$$

The low-scale corrections are obtained from the UV-finite part of the sum of soft and collinear corrections. The soft matching is given by the “irreducible” two-particle contributions in the

last term in Eq. (B.74).

$$\begin{aligned}
 D_S(\mu) &= \frac{\alpha}{4\pi} \sum_{V_a=W,Z,\gamma} \sum_{i \neq j} \frac{\mathbf{T}_i^{V_a} \cdot \mathbf{T}_j^{\bar{V}_a}}{2} \log \frac{\mu^2}{M_{V_a}^2} \log \frac{-n_i \cdot n_j - i0}{2} \\
 &= \frac{\alpha}{4\pi} \sum_{i \neq j} \left(\sigma_i I_i^Z \sigma_j I_j^Z \log \frac{M_W^2}{M_Z^2} + \sigma_i Q_i \sigma_j Q_j \left[-\frac{1}{\varepsilon_{\text{IR}}} + \log \frac{M_W}{\mu_{\text{IR}}^2} \right] \right) \mathbb{1} \log \frac{-n_i \cdot n_j - i0}{2},
 \end{aligned} \tag{B.80}$$

where the last form is special for the case $\mu = M_W$. In addition we used (B.75) for the IR poles.

For each particle the collinear matching is obtained from the one-particle corrections, that is, from the sum of the zero-bin subtracted collinear integral, the field-renormalisation constants, and the one-particle terms of Eq. (B.74). The dependence on the Δ regulators cancels between soft and collinear contributions.

For fermions we obtain

$$D_C^{f_\kappa}(\mu) = \frac{\alpha}{4\pi} \sum_{V_a=W,Z} \left(I_{f_\kappa}^{V_a} \right)^2 D_{V_a}(\mu) \tag{B.81}$$

with $I_{f_\kappa}^{V_a}$ being the coupling of the fermion with gauge boson V_a and the D_{V_a} defined in Eq. (B.85) and the photon-mass regularisation translated to DimReg using Eq. (B.75). Adopting the notation of Ref. [19] we find for the W boson

$$D_C^W(\mu) = \frac{\alpha}{4\pi} \sum_{V_a=W,Z} \sum_{V'_a} \left(I_{WV'_a}^{V_a} \right)^2 \left(F_{V_a}(\mu) + f_S \left(\frac{M_W^2}{M_{V_a}^2}, \frac{M_{V'_a}^2}{M_{V_a}^2} \right) \right) + \frac{\alpha}{4\pi} F_\gamma(\mu) + \frac{\delta Z_W}{2} \Big|_{\text{UV-finite}}, \tag{B.82}$$

where V'_a runs over Z and γ if $V_a = W$. The F_{V_a} are defined in Eq. (B.86).

As already mentioned in Sec. 5.2.6, the low-scale corrections for photons and the Z bosons have to be calculated in the W^3/B basis. For the W^3 contributions one has to use the result of the collinear integral with $M_{V_a} = m_{\text{int}} = M_W$ and $p_i^2 = M_Z^2$ or $p_i^2 = 0$, respectively. The B-boson contributions receive only the field-renormalisation constant contributions and one arrives at

$$\delta \mathcal{M}^{n_W^{(\gamma)} n_B^{(\gamma)} n_B^{(Z)} n_W^{(Z)}} = \left(n_W^{(Z)} D_C^{W^3 \rightarrow Z} + n_W^{(\gamma)} D_C^{W^3 \rightarrow \gamma} + n_B^{(Z)} D_C^{B \rightarrow Z} + n_B^{(\gamma)} D_C^{B \rightarrow \gamma} \right) \mathcal{M}^{n_W^{(\gamma)} n_B^{(\gamma)} n_B^{(Z)} n_W^{(Z)}} \tag{B.83}$$

with $D_C^{W^3/B \rightarrow Z/\gamma}$ given in Eq. (B.89).

B.3. Soft and collinear functions for the Standard Model

In this appendix we collect the final results of the previous section in a more explicit form.

Fermions

For massless fermions with chirality κ the collinear part of the operator corrections yields

$$D_C^{f_\kappa} = \frac{\alpha}{4\pi} \left(\left(I_{f_\kappa}^Z \right)^2 D_Z(\mu_1) + \delta_{\kappa L} \frac{1}{2s_W^2} D_W(\mu_1) + Q_f^2 D_\gamma(\mu_1) \right) \tag{B.84}$$

with the auxiliary functions

$$\begin{aligned}
 D_{W/Z}(\mu_1) &= 2 \log \frac{M_{W/Z}^2}{\mu_1^2} \log \frac{\bar{n} \cdot p}{\mu_1} - \frac{1}{2} \log^2 \frac{M_{W/Z}^2}{\mu_1^2} - \frac{3}{2} \log \frac{M_{W/Z}^2}{\mu_1^2} - \frac{\pi^2}{2} + \frac{9}{4}, \\
 D_\gamma(\mu_1) &= -\frac{c_\varepsilon}{\varepsilon^2} - \frac{c_\varepsilon}{\varepsilon} \left(\frac{3}{2} - 2 \log \frac{\bar{n} \cdot p}{\mu_{\text{IR}}} \right) + 2 \log \frac{\mu_{\text{IR}}^2}{\mu_1^2} \log \frac{\bar{n} \cdot p}{\mu_1} - \frac{1}{2} \log^2 \frac{\mu_{\text{IR}}^2}{\mu_1^2} - \frac{3}{2} \log \frac{\mu_{\text{IR}}^2}{\mu_1^2}. \quad (\text{B.85})
 \end{aligned}$$

Note that these functions already contain the contribution from the respective wavefunction renormalisation constant.

Transverse gauge bosons

For gauge bosons we introduce the functions

$$\begin{aligned}
 F_{W/Z}(\mu_1) &= 2 \log \frac{M_{W/Z}^2}{\mu_1^2} \log \frac{\bar{n} \cdot p}{\mu_1} - \frac{1}{2} \log^2 \frac{M_{W/Z}^2}{\mu_1^2} - \log \frac{M_{W/Z}^2}{\mu_1^2} - \frac{\pi^2}{2} + 1, \\
 F_\gamma(\mu_1) &= 2 \frac{c_\varepsilon}{\varepsilon} \log \frac{\bar{n} \cdot p}{M_W} + 2 \log \frac{\mu_{\text{IR}}^2}{\mu_1^2} \log \frac{\bar{n} \cdot p}{M_W} + \frac{1}{2} \log^2 \frac{M_W^2}{\mu_1^2} - \log \frac{M_W^2}{\mu_1^2} + 2, \quad (\text{B.86})
 \end{aligned}$$

as well as the scalar integral (B.5). The latter, defined in the appendix of [45], can be written in terms of the Passarino–Veltman two-point and three-point standard integrals:

$$\begin{aligned}
 f_S \left(\frac{p^2}{M^2}, \frac{m^2}{M^2} \right) &= - \lim_{r \rightarrow \infty} r \left(C_0(p^2, r, p^2, M^2, m^2, m^2) - C_0(0, r, 0, 0, 0, 0) \Big|_{\mu_{\text{IR}}^2 = M^2} \right) \\
 &\quad + \frac{\pi^2}{2} + B_0(p^2, M^2, m^2) - B_0(0, M^2, 0). \quad (\text{B.87})
 \end{aligned}$$

For the definitions of the B_0 and C_0 integrals see Refs. [143, 190]. In terms of these functions the low scale corrections read

$$\begin{aligned}
 D_C^{W \rightarrow W}(\mu_1) &= \frac{\alpha}{4\pi} \left[\frac{c_w^2}{s_w^2} \left(F_Z + f_S \left(\frac{M_W^2}{M_Z^2}, \frac{M_W^2}{M_Z^2} \right) \right) + \frac{c_w^2}{s_w^2} \left(F_W + f_S \left(1, \frac{M_Z^2}{M_W^2} \right) \right) \right] \\
 &\quad + \frac{\alpha}{4\pi} [F_\gamma + F_W + f_S(1, 0)] + \frac{1}{2} \delta Z_W \Big|_{\mu_{UV} = \mu_1} \quad (\text{B.88})
 \end{aligned}$$

for external W^\pm bosons.

The operator corrections for the Z and the photon depend on the subamplitudes and read

$$\begin{aligned}
 D_C^{W^3 \rightarrow Z}(\mu_1) &= \frac{\alpha}{2\pi s_w^2} \left(F_W + f_S \left(\frac{M_Z}{M_W^2}, 1 \right) \right) + \frac{1}{2} \delta Z_{ZZ} \Big|_{\mu_{UV} = \mu_1} + \frac{1}{2} \frac{s_w}{c_w} \delta Z_{AZ} \Big|_{\mu_{UV} = \mu_1}, \\
 D_C^{W^3 \rightarrow \gamma}(\mu_1) &= \frac{\alpha}{2\pi s_w} (F_W + f_S(0, 1)) + \frac{1}{2} \delta Z_{AA} \Big|_{\mu_{UV} = \mu_1} + \frac{1}{2} \frac{c_w}{s_w} \delta Z_{ZA} \Big|_{\mu_{UV} = \mu_1}, \\
 D_C^{B \rightarrow Z}(\mu_1) &= \frac{1}{2} \delta Z_{ZZ} \Big|_{\mu_{UV} = \mu_1} - \frac{c_w}{s_w} \frac{1}{2} \delta Z_{AZ} \Big|_{\mu_{UV} = \mu_1}, \\
 D_C^{B \rightarrow \gamma}(\mu_1) &= \frac{1}{2} \delta Z_{AA} \Big|_{\mu_{UV} = \mu_1} - \frac{1}{2} \frac{s_w}{c_w} \delta Z_{ZA} \Big|_{\mu_{UV} = \mu_1}. \quad (\text{B.89})
 \end{aligned}$$

Note that the conventions of Ref. [48] imply a factor of 1/2 in the off-diagonal field-renormalisation constants compared to our definition [154], see Eq. (2.30).

Longitudinal gauge bosons/scalars

For the case of scalars the respective functions read

$$D_C^\phi(\mu_1) = \frac{\alpha}{4\pi} \left(\frac{c_w^2 - s_w^2}{4c_w^2 s_w^2} \left(F_Z + f_S \left(\frac{M_W^2}{M_Z^2}, \frac{M_W^2}{M_Z^2} \right) \right) + \frac{1}{4s_w^2} \left(F_W + f_S \left(1, \frac{M_Z^2}{M_W^2} \right) \right) \right. \\ \left. + \frac{1}{4s_w^2} \left(F_W + f_S \left(1, \frac{M_H^2}{M_W^2} \right) \right) + F_\gamma \right) + \delta C_\phi|_{\mu_{UV}=\mu_1} \quad (\text{B.90})$$

with the charged-boson GBET correction factor

$$\delta C_\phi = \delta Z_W + \frac{1}{2} \frac{\delta M_W^2}{M_W^2} - \frac{\Sigma^{W\phi}}{M_W} - \frac{\Sigma_L^{WW}}{M_W^2} \quad (\text{B.91})$$

(see also (3.97)). Similarly to the γ/Z -mixing in the transverse case, one finds different operator corrections for operators containing the ϕ_2 field, depending on whether the external state is a longitudinal Z or a Higgs boson:

$$D_C^{\phi_2 \rightarrow Z_L}(\mu_1) = \frac{\alpha}{4\pi} \left(\frac{1}{4c_w^2 s_w^2} \left(F_Z + f_S \left(1, \frac{M_H^2}{M_Z^2} \right) \right) + \frac{1}{2s_w^2} \left(F_W + f_S \left(\frac{M_Z^2}{M_W^2}, 1 \right) \right) \right) \\ + \delta C_\chi|_{\mu_{UV}=\mu_1} \quad (\text{B.92})$$

with the neutral-boson GBET correction factor

$$\delta C_\chi = \frac{1}{2} \delta Z_{ZZ} + \frac{1}{2} \frac{\delta M_Z^2}{M_Z^2} + i \frac{\Sigma^{Z\chi}}{M_Z} - \frac{\Sigma_L^{ZZ}(M_Z^2)}{M_Z^2(M_Z^2)}. \quad (\text{B.93})$$

For an external Higgs boson one finds

$$D_C^{\phi_2 \rightarrow H}(\mu_1) = \frac{\alpha}{4\pi} \left(\frac{1}{4c_w^2 s_w^2} \left(F_Z + f_S \left(\frac{M_Z^2}{M_H^2}, 1 \right) \right) + \frac{1}{2s_w^2} \left(F_W + f_S \left(\frac{M_H^2}{M_W^2}, 1 \right) \right) \right) \\ + \frac{1}{2} \delta Z_H \Big|_{\mu_{UV}=\mu_1}. \quad (\text{B.94})$$

Bibliography

- [1] **ATLAS** Collaboration, G. Aad et al., *Observation of a new particle in the search for the Standard Model Higgs boson with the ATLAS detector at the LHC*, *Phys. Lett. B* **716** (2012) 1–29, [[arXiv:1207.7214](#)].
- [2] **CMS** Collaboration, S. Chatrchyan et al., *Observation of a New Boson at a Mass of 125 GeV with the CMS Experiment at the LHC*, *Phys. Lett. B* **716** (2012) 30–61, [[arXiv:1207.7235](#)].
- [3] P. W. Higgs, *Broken symmetries and the masses of gauge bosons*, *Phys. Rev. Lett.* **13** (1964) 508–509.
- [4] F. Englert and R. Brout, *Broken symmetry and the mass of gauge vector mesons*, *Phys. Rev. Lett.* **13** (1964) 321–323.
- [5] G. S. Guralnik, C. R. Hagen, and T. W. B. Kibble, *Global Conservation Laws and Massless Particles*, *Phys. Rev. Lett.* **13** (1964) 585–587.
- [6] F. Englert, R. Brout, and M. F. Thiry, *Vector mesons in presence of broken symmetry*, *Nuovo Cim. A* **43** (1966) 244–257.
- [7] P. W. Higgs, *Spontaneous symmetry breakdown without massless bosons*, *Phys. Rev.* **145** (1966) 1156–1163.
- [8] T. W. B. Kibble, *Symmetry breaking in non-Abelian gauge theories*, *Phys. Rev.* **155** (1967) 1554–1561.
- [9] G. Apollinari, O. Brüning, T. Nakamoto, and L. Rossi, *High Luminosity Large Hadron Collider HL-LHC*, *CERN Yellow Rep.* (2015) 1–19, [[arXiv:1705.08830](#)].
- [10] I. Zurbano Fernandez et al., *High-Luminosity Large Hadron Collider (HL-LHC): Technical design report*, .
- [11] **FCC** Collaboration, A. Abada et al., *FCC Physics Opportunities: Future Circular Collider Conceptual Design Report Volume 1*, *Eur. Phys. J. C* **79** (2019) 474.
- [12] **FCC** Collaboration, A. Abada et al., *FCC-ee: The Lepton Collider: Future Circular Collider Conceptual Design Report Volume 2*, *Eur. Phys. J. ST* **228** (2019) 261–623.
- [13] **FCC** Collaboration, A. Abada et al., *FCC-hh: The Hadron Collider: Future Circular Collider Conceptual Design Report Volume 3*, *Eur. Phys. J. ST* **228** (2019) 755–1107.
- [14] **FCC** Collaboration, A. Abada et al., *HE-LHC: The High-Energy Large Hadron Collider: Future Circular Collider Conceptual Design Report Volume 4*, *Eur. Phys. J. ST* **228** (2019) 1109–1382.

- [15] M. Benedikt et al., *Future Circular Hadron Collider FCC–hh: overview and status*, [arXiv:2203.07804](#).
- [16] **CLIC, CLICdp** Collaboration, M. J. Boland et al., *Updated baseline for a staged Compact Linear Collider*, [arXiv:1608.07537](#).
- [17] **CLICdp, CLIC** Collaboration, T. K. Charles et al., *The Compact Linear Collider (CLIC) - 2018 Summary Report*, [arXiv:1812.06018](#).
- [18] **CLIC** Collaboration, J. de Blas et al., *The CLIC Potential for New Physics*, [arXiv:1812.02093](#).
- [19] A. Denner and S. Pozzorini, *One-loop leading logarithms in electroweak radiative corrections. 1. Results*, *Eur. Phys. J. C* **18** (2001) 461–480, [[hep-ph/0010201](#)].
- [20] A. Denner and S. Pozzorini, *One-loop leading logarithms in electroweak radiative corrections. 2. Factorization of collinear singularities*, *Eur. Phys. J. C* **21** (2001) 63–79, [[hep-ph/0104127](#)].
- [21] J. H. Kühn, S. Moch, A. A. Penin, and V. A. Smirnov, *Next-to-next-to-leading logarithms in four fermion electroweak processes at high energy*, *Nucl. Phys. B* **616** (2001) 286–306, [[hep-ph/0106298](#)]. [Erratum: *Nucl.Phys.B* 648, 455–456 (2003)].
- [22] W. Beenakker and A. Werthenbach, *Electroweak two loop Sudakov logarithms for on-shell fermions and bosons*, *Nucl. Phys. B* **630** (2002) 3–54, [[hep-ph/0112030](#)].
- [23] A. Denner, M. Melles, and S. Pozzorini, *Two loop electroweak angular dependent logarithms at high energies*, *Nucl. Phys. B* **662** (2003) 299–333, [[hep-ph/0301241](#)].
- [24] B. Feucht, J. H. Kühn, A. A. Penin, and V. A. Smirnov, *Two loop Sudakov form-factor in a theory with mass gap*, *Phys. Rev. Lett.* **93** (2004) 101802, [[hep-ph/0404082](#)].
- [25] C. W. Bauer, S. Fleming, and M. E. Luke, *Summing Sudakov logarithms in $B \rightarrow X_s \gamma$ in effective field theory.*, *Phys. Rev. D* **63** (2000) 014006, [[hep-ph/0005275](#)].
- [26] C. W. Bauer, S. Fleming, D. Pirjol, and I. W. Stewart, *An effective field theory for collinear and soft gluons: heavy to light decays*, *Phys. Rev. D* **63** (2001) 114020, [[hep-ph/0011336](#)].
- [27] C. W. Bauer and I. W. Stewart, *Invariant operators in collinear effective theory*, *Phys. Lett. B* **516** (2001) 134–142, [[hep-ph/0107001](#)].
- [28] C. W. Bauer, D. Pirjol, and I. W. Stewart, *Soft-collinear factorization in effective field theory*, *Phys. Rev. D* **65** (2002) 054022, [[hep-ph/0109045](#)].
- [29] C. W. Bauer, D. Pirjol, and I. W. Stewart, *On power-suppressed operators and gauge invariance in SCET*, *Phys. Rev. D* **68** (2003) 034021, [[hep-ph/0303156](#)].
- [30] C. W. Bauer and A. V. Manohar, *Shape function effects in $B \rightarrow X_s \gamma$ and $B \rightarrow X_u \ell \bar{\nu}$ decays*, *Phys. Rev. D* **70** (2004) 034024, [[hep-ph/0312109](#)].

-
- [31] D. Pirjol and I. W. Stewart, *A complete basis for power-suppressed collinear ultrasoft operators*, *Phys. Rev. D* **67** (2003) 094005, [[hep-ph/0211251](#)]. [Erratum: *Phys.Rev.D* 69, 019903 (2004)].
- [32] M. Beneke, A. P. Chapovsky, M. Diehl, and T. Feldmann, *Soft-collinear effective theory and heavy to light currents beyond leading power*, *Nucl. Phys. B* **643** (2002) 431–476, [[hep-ph/0206152](#)].
- [33] M. Beneke and T. Feldmann, *Factorization of heavy-to-light form factors in soft-collinear effective theory*, *Nucl. Phys. B* **685** (2004) 249–296, [[hep-ph/0311335](#)].
- [34] T. Becher, M. Neubert, and G. Xu, *Dynamical threshold enhancement and resummation in Drell-Yan production*, *JHEP* **07** (2008) 030, [[arXiv:0710.0680](#)].
- [35] V. Ahrens, A. Ferroglia, M. Neubert, B. D. Pecjak, and L. L. Yang, *Threshold expansion at order α_s^4 for the $t\bar{t}$ invariant mass distribution at hadron colliders*, *Phys. Lett. B* **687** (2010) 331–337, [[arXiv:0912.3375](#)].
- [36] T. Becher and M. D. Schwartz, *Direct photon production with effective field theory*, *JHEP* **02** (2010) 040, [[arXiv:0911.0681](#)].
- [37] T. Becher and M. Neubert, *Drell-Yan production at small q_T , transverse parton distributions and the collinear anomaly*, *Eur. Phys. J. C* **71** (2011) 1665, [[arXiv:1007.4005](#)].
- [38] V. Ahrens, A. Ferroglia, M. Neubert, B. D. Pecjak, and L.-L. Yang, *RG-improved single-particle inclusive cross sections and forward-backward asymmetry in $t\bar{t}$ production at hadron colliders*, *JHEP* **09** (2011) 070, [[arXiv:1103.0550](#)].
- [39] T. Becher, C. Lorentzen, and M. D. Schwartz, *Precision direct photon and W -boson spectra at high p_T and comparison to LHC data*, *Phys. Rev. D* **86** (2012) 054026, [[arXiv:1206.6115](#)].
- [40] S. Fleming, A. H. Hoang, S. Mantry, and I. W. Stewart, *Jets from massive unstable particles: Top-mass determination*, *Phys. Rev. D* **77** (2008) 074010, [[hep-ph/0703207](#)].
- [41] M. D. Schwartz, *Resummation and NLO matching of event shapes with effective field theory*, *Phys. Rev. D* **77** (2008) 014026, [[arXiv:0709.2709](#)].
- [42] C. W. Bauer, S. P. Fleming, C. Lee, and G. F. Sterman, *Factorization of e^+e^- event shape distributions with hadronic final states in soft-collinear effective theory*, *Phys. Rev. D* **78** (2008) 034027, [[arXiv:0801.4569](#)].
- [43] J.-y. Chiu, F. Golf, R. Kelley, and A. V. Manohar, *Electroweak Sudakov corrections using effective field theory*, *Phys. Rev. Lett.* **100** (2008) 021802, [[arXiv:0709.2377](#)].
- [44] J.-y. Chiu, F. Golf, R. Kelley, and A. V. Manohar, *Electroweak corrections in high energy processes using effective field theory*, *Phys. Rev. D* **77** (2008) 053004, [[arXiv:0712.0396](#)].
- [45] J.-y. Chiu, R. Kelley, and A. V. Manohar, *Electroweak corrections using effective field theory: applications to the LHC*, *Phys. Rev. D* **78** (2008) 073006, [[arXiv:0806.1240](#)].

- [46] J.-y. Chiu, A. Fuhrer, A. H. Hoang, R. Kelley, and A. V. Manohar, *Soft-collinear factorization and zero-bin subtractions*, *Phys. Rev. D* **79** (2009) 053007, [[arXiv:0901.1332](#)].
- [47] J.-y. Chiu, A. Fuhrer, R. Kelley, and A. V. Manohar, *Factorization structure of gauge theory amplitudes and application to hard scattering processes at the LHC*, *Phys. Rev. D* **80** (2009) 094013, [[arXiv:0909.0012](#)].
- [48] J.-y. Chiu, A. Fuhrer, R. Kelley, and A. V. Manohar, *Soft-and collinear functions for the Standard Model*, *Phys. Rev. D* **81** (2010) 014023, [[arXiv:0909.0947](#)].
- [49] J. H. Kühn, A. A. Penin, and V. A. Smirnov, *Summing up subleading Sudakov logarithms*, *Eur. Phys. J. C* **17** (2000) 97–105, [[hep-ph/9912503](#)].
- [50] P. Ciafaloni and D. Comelli, *Electroweak evolution equations*, *JHEP* **11** (2005) 022, [[hep-ph/0505047](#)].
- [51] J. H. Kühn, F. Metzler, A. A. Penin, and S. Uccirati, *Next-to-next-to-leading electroweak logarithms for W -pair production at LHC*, *JHEP* **06** (2011) 143, [[arXiv:1101.2563](#)].
- [52] A. Fuhrer, A. V. Manohar, J.-y. Chiu, and R. Kelley, *Radiative corrections to longitudinal and transverse gauge boson and Higgs production*, *Phys. Rev. D* **81** (2010) 093005, [[arXiv:1003.0025](#)].
- [53] A. Fuhrer, A. V. Manohar, and W. J. Waalewijn, *Electroweak radiative corrections to Higgs production via vector boson fusion using soft-collinear effective theory*, *Phys. Rev. D* **84** (2011) 013007, [[arXiv:1011.1505](#)].
- [54] F. Siringo and G. Buccheri, *Electroweak radiative corrections to Higgs production via vector-boson fusion using SCET: numerical results*, *Phys. Rev. D* **86** (2012) 053013, [[arXiv:1207.1906](#)].
- [55] T. Becher and X. Garcia i Tormo, *Electroweak Sudakov effects in W, Z and γ production at large transverse momentum*, *Phys. Rev. D* **88** (2013) 013009, [[arXiv:1305.4202](#)].
- [56] M. Beneke, A. Broggio, C. Hasner, K. Urban, and M. Vollmann, *Resummed photon spectrum from dark matter annihilation for intermediate and narrow energy resolution*, *JHEP* **08** (2019) 103, [[arXiv:1903.08702](#)]. [Erratum: *JHEP* 07, 145 (2020)].
- [57] S. Actis, et al., *RECOLA: REcursive Computation of One-Loop Amplitudes*, *Comput. Phys. Commun.* **214** (2017) 140–173, [[arXiv:1605.01090](#)].
- [58] A. Denner, J.-N. Lang, and S. Uccirati, *Recola2: REcursive Computation of One-Loop Amplitudes 2*, *Comput. Phys. Commun.* **224** (2018) 346–361, [[arXiv:1711.07388](#)].
- [59] G. Bevilacqua, et al., *HELAC-NLO*, *Comput. Phys. Commun.* **184** (2013) 986–997, [[arXiv:1110.1499](#)].
- [60] F. Cascioli, P. Maierhofer, and S. Pozzorini, *Scattering Amplitudes with Open Loops*, *Phys. Rev. Lett.* **108** (2012) 111601, [[arXiv:1111.5206](#)].
- [61] F. Buccioni, et al., *OpenLoops 2*, *Eur. Phys. J. C* **79** (2019) 866, [[arXiv:1907.13071](#)].

-
- [62] M. Grazzini, S. Kallweit, and M. Wiesemann, *Fully differential NNLO computations with MATRIX*, *Eur. Phys. J. C* **78** (2018) 537, [[arXiv:1711.06631](#)].
- [63] S. Frixione, P. Nason, and C. Oleari, *Matching NLO QCD computations with Parton Shower simulations: the POWHEG method*, *JHEP* **11** (2007) 070, [[arXiv:0709.2092](#)].
- [64] T. Sjöstrand, et al., *An introduction to PYTHIA 8.2*, *Comput. Phys. Commun.* **191** (2015) 159–177, [[arXiv:1410.3012](#)].
- [65] J. Alwall, et al., *The automated computation of tree-level and next-to-leading order differential cross sections, and their matching to parton shower simulations*, *JHEP* **07** (2014) 079, [[arXiv:1405.0301](#)].
- [66] E. Bothmann, et al., *A Portable Parton-Level Event Generator for the High-Luminosity LHC*, [arXiv:2311.06198](#).
- [67] J. Bellm et al., *Herwig 7.0/Herwig++ 3.0 release note*, *Eur. Phys. J. C* **76** (2016) 196, [[arXiv:1512.01178](#)].
- [68] W. Kilian, T. Ohl, and J. Reuter, *WHIZARD: Simulating Multi-Particle Processes at LHC and ILC*, *Eur. Phys. J. C* **71** (2011) 1742, [[arXiv:0708.4233](#)].
- [69] M. Chiesa, et al., *Electroweak Sudakov Corrections to New Physics Searches at the LHC*, *Phys. Rev. Lett.* **111** (2013) 121801, [[arXiv:1305.6837](#)].
- [70] E. Bothmann and D. Napoletano, *Automated evaluation of electroweak Sudakov logarithms in Sherpa*, *Eur. Phys. J. C* **80** (2020) 1024, [[arXiv:2006.14635](#)].
- [71] D. Pagani and M. Zaro, *One-loop electroweak Sudakov logarithms: a revisit and automation*, *JHEP* **02** (2022) 161, [[arXiv:2110.03714](#)].
- [72] D. Pagani, T. Vitos, and M. Zaro, *Improving NLO QCD event generators with high-energy EW corrections*, [arXiv:2309.00452](#).
- [73] J. M. Lindert and L. Mai, *Logarithmic EW corrections at one-loop*, [arXiv:2312.07927](#).
- [74] B. Biedermann, et al., *Automation of NLO QCD and EW corrections with Sherpa and Recola*, *Eur. Phys. J. C* **77** (2017) 492, [[arXiv:1704.05783](#)].
- [75] R. Frederix, et al., *The automation of next-to-leading order electroweak calculations*, *JHEP* **07** (2018) 185, [[arXiv:1804.10017](#)]. [Erratum: *JHEP* **11**, 085 (2021)].
- [76] E. Bothmann, D. Napoletano, M. Schönherr, S. Schumann, and S. L. Villani, *Higher-order EW corrections in ZZ and ZZj production at the LHC*, *JHEP* **06** (2022) 064, [[arXiv:2111.13453](#)].
- [77] **OPAL** Collaboration, K. Ackerstaff et al., *Measurement of triple gauge boson couplings from W^+W^- production at $\sqrt{s} = 172$ GeV*, *Eur. Phys. J. C* **2** (1998) 597–606, [[hep-ex/9709023](#)].
- [78] **L3** Collaboration, M. Acciarri et al., *Direct observation of longitudinally polarized W^\pm bosons*, *Phys. Lett. B* **474** (2000) 194–204, [[hep-ex/0001016](#)].

- [79] **DELPHI** Collaboration, P. Abreu et al., *Measurement of trilinear gauge boson couplings WWV , ($V \equiv Z, \gamma$) in e^+e^- collisions at 189 GeV*, *Phys. Lett. B* **502** (2001) 9–23, [[hep-ex/0102041](#)].
- [80] **L3** Collaboration, P. Achard et al., *Measurement of the cross section of W -boson pair production at LEP*, *Phys. Lett. B* **600** (2004) 22–40, [[hep-ex/0409016](#)].
- [81] **ATLAS** Collaboration, M. Aaboud et al., *Measurement of the ZZ production cross section in proton-proton collisions at $\sqrt{s} = 8$ TeV using the $ZZ \rightarrow \ell^-\ell^+\ell'^-\ell'^+$ and $ZZ \rightarrow \ell^-\ell^+\nu\bar{\nu}$ channels with the ATLAS detector*, *JHEP* **01** (2017) 099, [[arXiv:1610.07585](#)].
- [82] **ATLAS** Collaboration, M. Aaboud et al., *Measurement of exclusive $\gamma\gamma \rightarrow W^+W^-$ production and search for exclusive Higgs boson production in pp collisions at $\sqrt{s} = 8$ TeV using the ATLAS detector*, *Phys. Rev. D* **94** (2016) 032011, [[arXiv:1607.03745](#)].
- [83] **ATLAS** Collaboration, M. Aaboud et al., *Measurement of the $W^\pm Z$ boson pair-production cross section in pp collisions at $\sqrt{s} = 13$ TeV with the ATLAS Detector*, *Phys. Lett. B* **762** (2016) 1–22, [[arXiv:1606.04017](#)].
- [84] **ATLAS** Collaboration, G. Aad et al., *Measurement of total and differential W^+W^- production cross sections in proton-proton collisions at $\sqrt{s} = 8$ TeV with the ATLAS detector and limits on anomalous triple-gauge-boson couplings*, *JHEP* **09** (2016) 029, [[arXiv:1603.01702](#)].
- [85] **ATLAS** Collaboration, M. Aaboud et al., *$ZZ \rightarrow \ell^+\ell^-\ell'^+\ell'^-$ cross-section measurements and search for anomalous triple gauge couplings in 13 TeV pp collisions with the ATLAS detector*, *Phys. Rev. D* **97** (2018) 032005, [[arXiv:1709.07703](#)].
- [86] **ATLAS** Collaboration, M. Aaboud et al., *Measurement of $W^\pm Z$ production cross sections and gauge boson polarisation in pp collisions at $\sqrt{s} = 13$ TeV with the ATLAS detector*, *Eur. Phys. J. C* **79** (2019) 535, [[arXiv:1902.05759](#)].
- [87] **ATLAS** Collaboration, G. Aad et al., *Observation of photon-induced W^+W^- production in pp collisions at $\sqrt{s} = 13$ TeV using the ATLAS detector*, *Phys. Lett. B* **816** (2021) 136190, [[arXiv:2010.04019](#)].
- [88] **ATLAS** Collaboration, G. Aad et al., *Search for new phenomena in three- or four-lepton events in pp collisions at $\sqrt{s} = 13$ TeV with the ATLAS detector*, *Phys. Lett. B* **824** (2022) 136832, [[arXiv:2107.00404](#)].
- [89] **CMS** Collaboration, S. Chatrchyan et al., *Measurement of the W^+W^- cross section in pp collisions at $\sqrt{s} = 7$ TeV and limits on anomalous $WW\gamma$ and WWZ couplings*, *Eur. Phys. J. C* **73** (2013) 2610, [[arXiv:1306.1126](#)].
- [90] **CMS** Collaboration, S. Chatrchyan et al., *Study of exclusive two-photon production of W^+W^- in pp collisions at $\sqrt{s} = 7$ TeV and constraints on anomalous quartic gauge couplings*, *JHEP* **07** (2013) 116, [[arXiv:1305.5596](#)].

-
- [91] CMS Collaboration, V. Khachatryan et al., *Measurements of the ZZ production cross sections in the $2\ell 2\nu$ channel in proton–proton collisions at $\sqrt{s} = 7$ and 8 TeV and combined constraints on triple gauge couplings*, *Eur. Phys. J. C* **75** (2015) 511, [[arXiv:1503.05467](#)].
- [92] CMS Collaboration, V. Khachatryan et al., *Measurement of the W^+W^- cross section in pp collisions at $\sqrt{s} = 8$ TeV and limits on anomalous gauge couplings*, *Eur. Phys. J. C* **76** (2016) 401, [[arXiv:1507.03268](#)].
- [93] CMS Collaboration, V. Khachatryan et al., *Measurement of the WZ production cross section in pp collisions at $\sqrt{s} = 13$ TeV*, *Phys. Lett. B* **766** (2017) 268–290.
- [94] CMS Collaboration, V. Khachatryan et al., *Evidence for exclusive $\gamma\gamma \rightarrow W^+W^-$ production and constraints on anomalous quartic gauge couplings in pp collisions at $\sqrt{s} = 7$ and 8 TeV*, *JHEP* **08** (2016) 119, [[arXiv:1604.04464](#)].
- [95] CMS Collaboration, A. M. Sirunyan et al., *Measurements of the $pp \rightarrow ZZ$ production cross section and the $Z \rightarrow 4\ell$ branching fraction, and constraints on anomalous triple gauge couplings at $\sqrt{s} = 13$ TeV*, *Eur. Phys. J. C* **78** (2018) 165, [[arXiv:1709.08601](#)]. [Erratum: *Eur.Phys.J.C* 78, 515 (2018)].
- [96] CMS Collaboration, A. M. Sirunyan et al., *Measurement of vector boson scattering and constraints on anomalous quartic couplings from events with four leptons and two jets in proton–proton collisions at $\sqrt{s} = 13$ TeV*, *Phys. Lett. B* **774** (2017) 682–705, [[arXiv:1708.02812](#)].
- [97] CMS Collaboration, A. M. Sirunyan et al., *Measurements of the $pp \rightarrow WZ$ inclusive and differential production cross section and constraints on charged anomalous triple gauge couplings at $\sqrt{s} = 13$ TeV*, *JHEP* **04** (2019) 122, [[arXiv:1901.03428](#)].
- [98] CMS Collaboration, A. Tumasyan et al., *Measurement of the inclusive and differential WZ production cross sections, polarization angles, and triple gauge couplings in pp collisions at $\sqrt{s} = 13$ TeV*, *JHEP* **07** (2022) 032, [[arXiv:2110.11231](#)].
- [99] B. Mele, P. Nason, and G. Ridolfi, *QCD radiative corrections to Z-boson pair production in hadronic collisions*, *Nucl. Phys. B* **357** (1991) 409–438.
- [100] J. Ohnemus and J. F. Owens, *An order- α_s calculation of hadronic ZZ production*, *Phys. Rev. D* **43** (1991) 3626–3639.
- [101] J. Ohnemus, *An order- α_s calculation of hadronic $W^\pm Z$ production*, *Phys. Rev. D* **44** (1991) 3477–3489.
- [102] J. Ohnemus, *An order- α_s calculation of hadronic W^-W^+ production*, *Phys. Rev. D* **44** (1991) 1403–1414.
- [103] L. J. Dixon, Z. Kunszt, and A. Signer, *Vector boson pair production in hadronic collisions at order α_s : lepton correlations and anomalous couplings*, *Phys. Rev. D* **60** (1999) 114037, [[hep-ph/9907305](#)].

- [104] A. Denner, S. Dittmaier, and R. Schuster, *Radiative corrections to $\gamma\gamma \rightarrow W^+W^-$ in the electroweak Standard Model*, *Nucl. Phys. B* **452** (1995) 80–108, [[hep-ph/9503442](#)].
- [105] A. Denner, S. Dittmaier, M. Roth, and D. Wackerroth, *Predictions for all processes $e^+e^- \rightarrow 4$ fermions $+\gamma$* , *Nucl. Phys. B* **560** (1999) 33–65, [[hep-ph/9904472](#)].
- [106] A. Denner, S. Dittmaier, M. Roth, and D. Wackerroth, *Electroweak radiative corrections to $e^+e^+ \rightarrow W^+W^- \rightarrow 4$ fermions in double pole approximation: the RacoonWW approach*, *Nucl. Phys. B* **587** (2000) 67–117, [[hep-ph/0006307](#)].
- [107] E. Accomando, A. Denner, and A. Kaiser, *Logarithmic electroweak corrections to gauge-boson pair production at the LHC*, *Nucl. Phys. B* **706** (2005) 325–371, [[hep-ph/0409247](#)].
- [108] A. Bredenstein, S. Dittmaier, and M. Roth, *Four-fermion production at $\gamma\gamma$ colliders. 1. Lowest-order predictions and anomalous couplings*, *Eur. Phys. J. C* **36** (2004) 341–363, [[hep-ph/0405169](#)].
- [109] A. Bredenstein, S. Dittmaier, and M. Roth, *Four-fermion production at $\gamma\gamma$ colliders. 2. Radiative corrections in double-pole approximation*, *Eur. Phys. J. C* **44** (2005) 27–49, [[hep-ph/0506005](#)].
- [110] A. Denner, S. Dittmaier, M. Roth, and L. H. Wieders, *Electroweak corrections to charged-current $e^+e^- \rightarrow 4$ fermion processes: technical details and further results*, *Nucl. Phys. B* **724** (2005) 247–294, [[hep-ph/0505042](#)]. [Erratum: *Nucl.Phys.B* 854, 504–507 (2012)].
- [111] A. Bierweiler, T. Kasprzik, J. H. Kühn, and S. Uccirati, *Electroweak corrections to W -boson pair production at the LHC*, *JHEP* **11** (2012) 093, [[arXiv:1208.3147](#)].
- [112] A. Bierweiler, T. Kasprzik, and J. H. Kühn, *Vector-boson pair production at the LHC to $\mathcal{O}(\alpha^3)$ accuracy*, *JHEP* **12** (2013) 071, [[arXiv:1305.5402](#)].
- [113] B. Biedermann, et al., *Next-to-leading-order electroweak corrections to $pp \rightarrow W^+W^- \rightarrow 4$ leptons at the LHC*, *JHEP* **06** (2016) 065, [[arXiv:1605.03419](#)].
- [114] B. Biedermann, A. Denner, S. Dittmaier, L. Hofer, and B. Jäger, *Next-to-leading-order electroweak corrections to the production of four charged leptons at the LHC*, *JHEP* **01** (2017) 033, [[arXiv:1611.05338](#)].
- [115] B. Biedermann, A. Denner, S. Dittmaier, L. Hofer, and B. Jäger, *Electroweak corrections to $pp \rightarrow \mu^+\mu^-e^+e^- + X$ at the LHC: a Higgs background study*, *Phys. Rev. Lett.* **116** (2016) 161803, [[arXiv:1601.07787](#)].
- [116] B. Biedermann, A. Denner, and L. Hofer, *Next-to-leading-order electroweak corrections to the production of three charged leptons plus missing energy at the LHC*, *JHEP* **10** (2017) 043, [[arXiv:1708.06938](#)].
- [117] S. Kallweit, J. M. Lindert, S. Pozzorini, and M. Schönherr, *NLO QCD+EW predictions for $2\ell 2\nu$ diboson signatures at the LHC*, *JHEP* **11** (2017) 120, [[arXiv:1705.00598](#)].

-
- [118] F. Cascioli, et al., *ZZ production at hadron colliders in NNLO QCD*, *Phys. Lett. B* **735** (2014) 311–313, [[arXiv:1405.2219](#)].
- [119] M. Grazzini, S. Kallweit, and D. Rathlev, *ZZ production at the LHC: fiducial cross sections and distributions in NNLO QCD*, *Phys. Lett. B* **750** (2015) 407–410, [[arXiv:1507.06257](#)].
- [120] M. Wiesemann, M. Grazzini, S. Kallweit, and D. Rathlev, *Fully-differential NNLO predictions for vector-boson pair production with MATRIX*, *PoS LL2016* (2016) 072.
- [121] M. Grazzini, S. Kallweit, S. Pozzorini, D. Rathlev, and M. Wiesemann, *W⁺W⁻ production at the LHC: fiducial cross sections and distributions in NNLO QCD*, *JHEP* **08** (2016) 140, [[arXiv:1605.02716](#)].
- [122] M. Grazzini, S. Kallweit, D. Rathlev, and M. Wiesemann, *W[±]Z production at hadron colliders in NNLO QCD*, *Phys. Lett. B* **761** (2016) 179–183, [[arXiv:1604.08576](#)].
- [123] G. Heinrich, S. Jahn, S. P. Jones, M. Kerner, and J. Pires, *NNLO predictions for Z-boson pair production at the LHC*, *JHEP* **03** (2018) 142, [[arXiv:1710.06294](#)].
- [124] M. Grazzini, S. Kallweit, J. M. Lindert, S. Pozzorini, and M. Wiesemann, *NNLO QCD + NLO EW with Matrix+OpenLoops: precise predictions for vector-boson pair production*, *JHEP* **02** (2020) 087, [[arXiv:1912.00068](#)].
- [125] E. Re, M. Wiesemann, and G. Zanderighi, *NNLOPS accurate predictions for W⁺W⁻ production*, *JHEP* **12** (2018) 121, [[arXiv:1805.09857](#)].
- [126] A. Denner, S. Dittmaier, and L. Hofer, *Collier: a fortran-based Complex One-Loop Library in Extended Regularizations*, *Comput. Phys. Commun.* **212** (2017) 220–238, [[arXiv:1604.06792](#)].
- [127] J. M. Cornwall, D. N. Levin, and G. Tiktopoulos, *Derivation of gauge invariance from high-energy unitarity bounds on the S matrix*, *Phys. Rev. D* **10** (1974) 1145. [Erratum: *Phys.Rev.D* **11**, 972 (1975)].
- [128] M. S. Chanowitz and M. K. Gaillard, *The TeV physics of strongly interacting W's and Z's*, *Nucl. Phys. B* **261** (1985) 379–431.
- [129] G. J. Gounaris, R. Kögerler, and H. Neufeld, *Relationship between longitudinally polarized vector bosons and their unphysical scalar partners*, *Phys. Rev. D* **34** (1986) 3257.
- [130] Y.-P. Yao and C. P. Yuan, *Modification of the equivalence theorem due to loop corrections*, *Phys. Rev. D* **38** (1988) 2237.
- [131] A. Ballestrero, E. Maina, and G. Pelliccioli, *W boson polarization in vector boson scattering at the LHC*, *JHEP* **03** (2018) 170, [[arXiv:1710.09339](#)].
- [132] A. Ballestrero, E. Maina, and G. Pelliccioli, *Different polarization definitions in same-sign WW scattering at the LHC*, *Phys. Lett. B* **811** (2020) 135856, [[arXiv:2007.07133](#)].

- [133] A. Denner and G. Pelliccioli, *Polarized electroweak bosons in W^+W^- production at the LHC including NLO QCD effects*, *JHEP* **09** (2020) 164, [[arXiv:2006.14867](#)].
- [134] A. Denner and G. Pelliccioli, *NLO QCD predictions for doubly-polarized WZ production at the LHC*, *Phys. Lett. B* **814** (2021) 136107, [[arXiv:2010.07149](#)].
- [135] A. Denner and G. Pelliccioli, *NLO EW and QCD corrections to polarized ZZ production in the four-charged-lepton channel at the LHC*, *JHEP* **10** (2021) 097, [[arXiv:2107.06579](#)].
- [136] A. Denner, C. Haitz, and G. Pelliccioli, *NLO QCD corrections to polarized diboson production in semileptonic final states*, *Phys. Rev. D* **107** (2023) 053004, [[arXiv:2211.09040](#)].
- [137] D. N. Le and J. Baglio, *Doubly-polarized WZ hadronic cross sections at NLO QCD + EW accuracy*, *Eur. Phys. J. C* **82** (2022) 917, [[arXiv:2203.01470](#)].
- [138] D. N. Le, J. Baglio, and T. N. Dao, *Doubly-polarized WZ hadronic production at NLO QCD+EW: calculation method and further results*, *Eur. Phys. J. C* **82** (2022) 1103, [[arXiv:2208.09232](#)].
- [139] T. N. Dao and D. N. Le, *Enhancing the doubly-longitudinal polarization in WZ production at the LHC*, *Commun. in Phys.* **33** (2023) 223, [[arXiv:2302.03324](#)].
- [140] A. Denner, C. Haitz, and G. Pelliccioli, *NLO EW corrections to polarised W^+W^- production and decay at the LHC*, *Phys. Lett. B* **850** (2024) 138539, [[arXiv:2311.16031](#)].
- [141] A. Denner and S. Rode, *Automated resummation of electroweak Sudakov logarithms in diboson production at future colliders*, [[arXiv:2402.10503](#)].
- [142] M. E. Peskin and D. V. Schroeder, *An Introduction to quantum field theory*. Addison-Wesley, Reading, USA, 1995.
- [143] M. Böhm, A. Denner, and H. Joos, *Gauge theories of the Strong and Electroweak interaction*. Teubner, 2001.
- [144] M. D. Schwartz, *Quantum field theory and the Standard Model*. Cambridge University Press, 3, 2014.
- [145] S. N. Gupta, *Theory of longitudinal photons in quantum electrodynamics*, *Proc. Phys. Soc. A* **63** (1950) 681–691.
- [146] K. Bleuler, *A New method of treatment of the longitudinal and scalar photons*, *Helv. Phys. Acta* **23** (1950) 567–586.
- [147] L. D. Faddeev and V. N. Popov, *Feynman diagrams for the Yang-Mills field*, *Phys. Lett. B* **25** (1967) 29–30.
- [148] G. 't Hooft and M. J. G. Veltman, *Regularization and renormalization of gauge fields*, *Nucl. Phys. B* **44** (1972) 189–213.
- [149] C. G. Bollini and J. J. Giambiagi, *Dimensional Renormalization: The Number of Dimensions as a Regularizing Parameter*, *Nuovo Cim. B* **12** (1972) 20–26.

-
- [150] H. Lehmann, K. Symanzik, and W. Zimmermann, *On the formulation of quantized field theories*, *Nuovo Cim.* **1** (1955) 205–225.
- [151] D. A. Ross and J. C. Taylor, *Renormalization of a unified theory of weak and electromagnetic interactions*, *Nucl. Phys. B* **51** (1973) 125–144. [Erratum: *Nucl.Phys.B* **58**, 643–643 (1973)].
- [152] K. I. Aoki, Z. Hioki, M. Konuma, R. Kawabe, and T. Muta, *Electroweak Theory. Framework of on-shell renormalization and study of higher order effects*, *Prog. Theor. Phys. Suppl.* **73** (1982) 1–225.
- [153] M. Böhm, H. Spiesberger, and W. Hollik, *On the one-loop renormalization of the Electroweak Standard Model and its application to leptonic processes*, *Fortsch. Phys.* **34** (1986) 687–751.
- [154] A. Denner, *Techniques for calculation of electroweak radiative corrections at the one loop level and results for W physics at LEP-200*, *Fortsch. Phys.* **41** (1993) 307–420, [[arXiv:0709.1075](#)].
- [155] A. Denner and T. Sack, *Renormalization of the quark-mixing matrix*, *Nucl. Phys. B* **347** (1990) 203–216.
- [156] M. Baumgart et al., *Snowmass Theory Frontier: Effective Field Theory*, in *Snowmass 2021*, 10, 2022. [[arXiv:2210.03199](#)].
- [157] M. Neubert, *Renormalization theory and effective field theories*, [[arXiv:1901.06573](#)].
- [158] T. Becher and M. Neubert, *Infrared singularities of scattering amplitudes in perturbative QCD*, *Phys. Rev. Lett.* **102** (2009) 162001, [[arXiv:0901.0722](#)]. [Erratum: *Phys.Rev.Lett.* **111**, 199905 (2013)].
- [159] T. Becher, A. Broggio, and A. Ferroglia, *Introduction to Soft-Collinear Effective Theory*, vol. 896. Springer, 2015.
- [160] C. W. Bauer and P. F. Monni, *A numerical formulation of resummation in effective field theory*, *JHEP* **02** (2019) 185, [[arXiv:1803.07079](#)].
- [161] T. Becher and M. Neubert, *Infrared singularities of QCD amplitudes with massive partons*, *Phys. Rev. D* **79** (2009) 125004, [[arXiv:0904.1021](#)]. [Erratum: *Phys.Rev.D* **80**, 109901 (2009)].
- [162] T. Becher and M. Neubert, *On the Structure of Infrared Singularities of Gauge-Theory Amplitudes*, *JHEP* **06** (2009) 081, [[arXiv:0903.1126](#)]. [Erratum: *JHEP* **11**, 024 (2013)].
- [163] V. Ahrens, M. Neubert, and L. Vernazza, *Structure of Infrared Singularities of Gauge-Theory Amplitudes at Three and Four Loops*, *JHEP* **09** (2012) 138, [[arXiv:1208.4847](#)].
- [164] Z. L. Liu and N. Schalch, *Infrared singularities of multileg QCD amplitudes with a massive parton at three loops*, *Phys. Rev. Lett.* **129** (2022) 232001, [[arXiv:2207.02864](#)].

- [165] M. Beneke, M. Garny, R. Szafron, and J. Wang, *Anomalous dimension of subleading-power N -jet operators*, *JHEP* **03** (2018) 001, [[arXiv:1712.04416](#)].
- [166] M. Beneke, M. Garny, R. Szafron, and J. Wang, *Anomalous dimension of subleading-power N -jet operators. Part II*, *JHEP* **11** (2018) 112, [[arXiv:1808.04742](#)].
- [167] T. Becher and G. Bell, *Analytic regularization in soft-collinear effective theory*, *Phys. Lett. B* **713** (2012) 41–46, [[arXiv:1112.3907](#)].
- [168] M. E. Machacek and M. T. Vaughn, *Two-loop renormalization group equations in a general quantum field theory. 1. Wave-function renormalization*, *Nucl. Phys. B* **222** (1983) 83–103.
- [169] J. Davies, F. Herren, C. Poole, M. Steinhauser, and A. E. Thomsen, *Gauge-coupling β -Functions to four-loop order in the Standard Model*, *Phys. Rev. Lett.* **124** (2020) 071803, [[arXiv:1912.07624](#)].
- [170] T. Kinoshita, *Mass singularities of Feynman amplitudes*, *J. Math. Phys.* **3** (1962) 650–677.
- [171] T. D. Lee and M. Nauenberg, *Degenerate systems and mass singularities*, *Phys. Rev.* **133** (1964) B1549–B1562.
- [172] D. A. Kosower, *Antenna factorization in strongly ordered limits*, *Phys. Rev. D* **71** (2005) 045016, [[hep-ph/0311272](#)].
- [173] J. M. Campbell, M. A. Cullen, and E. W. N. Glover, *Four jet event shapes in electron-positron annihilation*, *Eur. Phys. J. C* **9** (1999) 245–265, [[hep-ph/9809429](#)].
- [174] S. Catani and M. Grazzini, *An NNLO subtraction formalism in hadron collisions and its application to Higgs boson production at the LHC*, *Phys. Rev. Lett.* **98** (2007) 222002, [[hep-ph/0703012](#)].
- [175] S. Frixione, Z. Kunszt, and A. Signer, *Three jet cross-sections to next-to-leading order*, *Nucl. Phys. B* **467** (1996) 399–442, [[hep-ph/9512328](#)].
- [176] S. Catani and M. H. Seymour, *A general algorithm for calculating jet cross-sections in NLO QCD*, *Nucl. Phys. B* **485** (1997) 291–419, [[hep-ph/9605323](#)]. [Erratum: *Nucl.Phys.B* 510, 503–504 (1998)].
- [177] S. Dittmaier, *A General approach to photon radiation off fermions*, *Nucl. Phys. B* **565** (2000) 69–122, [[hep-ph/9904440](#)].
- [178] S. Dittmaier, A. Kabelschacht, and T. Kasprzik, *Polarized QED splittings of massive fermions and dipole subtraction for non-collinear-safe observables*, *Nucl. Phys. B* **800** (2008) 146–189, [[arXiv:0802.1405](#)].
- [179] S. Catani, S. Dittmaier, M. H. Seymour, and Z. Trocsanyi, *The dipole formalism for next-to-leading order QCD calculations with massive partons*, *Nucl. Phys. B* **627** (2002) 189–265, [[hep-ph/0201036](#)].

-
- [180] A. Denner and S. Dittmaier, *Electroweak radiative corrections for collider physics*, *Phys. Rept.* **864** (2020) 1–163, [[arXiv:1912.06823](#)].
- [181] S. Dittmaier and C. Schwan, *Non-factorizable photonic corrections to resonant production and decay of many unstable particles*, *Eur. Phys. J. C* **76** (2016) 144, [[arXiv:1511.01698](#)].
- [182] A. Aeppli, F. Cuypers, and G. J. van Oldenborgh, *$O(\Gamma)$ corrections to W pair production in e^+e^- and $\gamma\gamma$ collisions*, *Phys. Lett. B* **314** (1993) 413–420, [[hep-ph/9303236](#)].
- [183] A. Aeppli, G. J. van Oldenborgh, and D. Wyler, *Unstable particles in one loop calculations*, *Nucl. Phys. B* **428** (1994) 126–146, [[hep-ph/9312212](#)].
- [184] E. Mirkes and J. Ohnemus, *W and Z polarization effects in hadronic collisions*, *Phys. Rev. D* **50** (1994) 5692–5703, [[hep-ph/9406381](#)].
- [185] Z. Bern et al., *Left-handed W bosons at the LHC*, *Phys. Rev. D* **84** (2011) 034008, [[arXiv:1103.5445](#)].
- [186] W. J. Stirling and E. Vryonidou, *Electroweak gauge boson polarisation at the LHC*, *JHEP* **07** (2012) 124, [[arXiv:1204.6427](#)].
- [187] M. Hoppe, M. Schönherr, and F. Siegert, *Polarised cross sections for vector boson production with SHERPA*, [[arXiv:2310.14803](#)].
- [188] R. Poncelet and A. Popescu, *NNLO QCD study of polarised W^+W^- production at the LHC*, *JHEP* **07** (2021) 023, [[arXiv:2102.13583](#)].
- [189] A. Denner, S. Dittmaier, and M. Roth, *Non-factorizable photonic corrections to $e^+e^- \rightarrow WW \rightarrow 4$ fermions*, *Nucl. Phys. B* **519** (1998) 39–84, [[hep-ph/9710521](#)].
- [190] G. Passarino and M. J. G. Veltman, *One-loop corrections for e^+e^- annihilation into $\mu^+\mu^-$ in the Weinberg Model*, *Nucl. Phys. B* **160** (1979) 151–207.
- [191] A. Denner and S. Dittmaier, *The complex-mass scheme for perturbative calculations with unstable particles*, *Nucl. Phys. B Proc. Suppl.* **160** (2006) 22–26, [[hep-ph/0605312](#)].
- [192] A. R. Bohm and Y. Sato, *Relativistic resonances: Their masses, widths, lifetimes, superposition, and causal evolution*, *Phys. Rev. D* **71** (2005) 085018, [[hep-ph/0412106](#)].
- [193] D. Y. Bardin, A. Leike, T. Riemann, and M. Sachwitz, *Energy-dependent width effects in e^+e^- annihilation near the Z -boson pole*, *Phys. Lett. B* **206** (1988) 539–542.
- [194] W. Beenakker, et al., *The Fermion loop scheme for finite width effects in e^+e^- annihilation into four fermions*, *Nucl. Phys. B* **500** (1997) 255–298, [[hep-ph/9612260](#)].
- [195] C. W. Bauer and N. Ferland, *Resummation of electroweak Sudakov logarithms for real radiation*, *JHEP* **09** (2016) 025, [[arXiv:1601.07190](#)].
- [196] A. Alloul, N. D. Christensen, C. Degrande, C. Duhr, and B. Fuks, *FeynRules 2.0 - A complete toolbox for tree-level phenomenology*, *Comput. Phys. Commun.* **185** (2014) 2250–2300, [[arXiv:1310.1921](#)].

- [197] A. Denner, J.-N. Lang, and S. Uccirati, *NLO electroweak corrections in extended Higgs sectors with RecoLa2*, *JHEP* **07** (2017) 087, [[arXiv:1705.06053](#)].
- [198] F. Jegerlehner, *Electroweak effective couplings for future precision experiments*, *Nuovo Cim. C* **034S1** (2011) 31–40, [[arXiv:1107.4683](#)].
- [199] S. P. Martin and D. G. Robertson, *Standard model parameters in the tadpole-free pure $\overline{\text{MS}}$ scheme*, *Phys. Rev. D* **100** (2019) 073004, [[arXiv:1907.02500](#)].
- [200] M. E. Machacek and M. T. Vaughn, *Two-loop renormalization group equations in a general quantum field theory. 2. Yukawa couplings*, *Nucl. Phys. B* **236** (1984) 221–232.
- [201] M. E. Machacek and M. T. Vaughn, *Two-loop renormalization group equations in a general quantum field theory. 3. Scalar quartic couplings*, *Nucl. Phys. B* **249** (1985) 70–92.
- [202] L. G. Almeida, et al., *Comparing and counting logs in direct and effective methods of QCD resummation*, *JHEP* **04** (2014) 174, [[arXiv:1401.4460](#)].
- [203] A. H. Mueller, *On the asymptotic behavior of the Sudakov form factor*, *Phys. Rev. D* **20** (1979) 2037.
- [204] J. C. Collins, *Algorithm to compute corrections to the Sudakov form factor*, *Phys. Rev. D* **22** (1980) 1478.
- [205] A. Sen, *Asymptotic behavior of the Sudakov form factor in QCD*, *Phys. Rev. D* **24** (1981) 3281.
- [206] B. Biedermann, A. Denner, and M. Pellen, *Large electroweak corrections to vector-boson scattering at the Large Hadron Collider*, *Phys. Rev. Lett.* **118** (2017) 261801, [[arXiv:1611.02951](#)].
- [207] M. Chiesa, A. Denner, J.-N. Lang, and M. Pellen, *An event generator for same-sign W -boson scattering at the LHC including electroweak corrections*, *Eur. Phys. J. C* **79** (2019) 788, [[arXiv:1906.01863](#)].
- [208] A. Denner, R. Franken, M. Pellen, and T. Schmidt, *Full NLO predictions for vector-boson scattering into Z bosons and its irreducible background at the LHC*, *JHEP* **10** (2021) 228, [[arXiv:2107.10688](#)].
- [209] A. Denner, R. Franken, T. Schmidt, and C. Schwan, *NLO QCD and EW corrections to vector-boson scattering into $W^+ W^-$ at the LHC*, *JHEP* **06** (2022) 098, [[arXiv:2202.10844](#)].
- [210] A. Denner and G. Pelliccioli, *NLO electroweak and QCD corrections to off-shell ttW production at the LHC*, *SciPost Phys. Proc.* **7** (2022) 034, [[arXiv:2110.07447](#)].
- [211] A. Denner, G. Pelliccioli, and C. Schwan, *NLO QCD and EW corrections to off-shell tZj production at the LHC*, *JHEP* **10** (2022) 125, [[arXiv:2207.11264](#)].
- [212] **NNPDF** Collaboration, R. D. Ball et al., *Parton distributions from high-precision collider data*, *Eur. Phys. J. C* **77** (2017) 663, [[arXiv:1706.00428](#)].

- [213] A. Buckley, et al., *LHAPDF6: parton density access in the LHC precision era*, *Eur. Phys. J. C* **75** (2015) 132, [[arXiv:1412.7420](#)].
- [214] **NNPDF** Collaboration, V. Bertone, S. Carrazza, N. P. Hartland, and J. Rojo, *Illuminating the photon content of the proton within a global PDF analysis*, *SciPost Phys.* **5** (2018) 008, [[arXiv:1712.07053](#)].
- [215] A. Manohar, P. Nason, G. P. Salam, and G. Zanderighi, *How bright is the proton? A precise determination of the photon parton distribution function*, *Phys. Rev. Lett.* **117** (2016) 242002, [[arXiv:1607.04266](#)].
- [216] **ALEPH** Collaboration, A. Heister et al., *Measurement of triple gauge boson couplings at LEP energies up to 189 GeV*, *Eur. Phys. J. C* **21** (2001) 423–441, [[hep-ex/0104034](#)].
- [217] **ATLAS** Collaboration, M. Aaboud et al., *Measurement of fiducial and differential W^+W^- production cross-sections at $\sqrt{s} = 13$ TeV with the ATLAS detector*, *Eur. Phys. J. C* **79** (2019) 884, [[arXiv:1905.04242](#)].
- [218] S. Frixione, *A next-to-leading order calculation of the cross-section for the production of W^+W^- pairs in hadronic collisions*, *Nucl. Phys. B* **410** (1993) 280–324.
- [219] T. Gehrmann, et al., *W^+W^- Production at hadron colliders in next-to-next-to-leading order QCD*, *Phys. Rev. Lett.* **113** (2014) 212001, [[arXiv:1408.5243](#)].
- [220] W. Beenakker, A. Denner, S. Dittmaier, R. Mertig, and T. Sack, *High-energy approximation for on-shell W pair production*, *Nucl. Phys. B* **410** (1993) 245–279.
- [221] M. Beccaria, F. M. Renard, and C. Verzegnassi, *Reliability of a high-energy one-loop expansion of $e^+e^- \rightarrow W^+W^-$ in the SM and in the MSSM*, *Nucl. Phys. B* **663** (2003) 394–406, [[hep-ph/0304175](#)].
- [222] J. Baglio, L. D. Ninh, and M. M. Weber, *Full NLO massive gauge boson pair production at the LHC*, in *9th Rencontres du Vietnam: Windows on the Universe*, pp. 215–218, 2013. [[arXiv:1310.3972](#)].
- [223] S. Frixione, P. Nason, and G. Ridolfi, *Strong corrections to WZ production at hadron colliders*, *Nucl. Phys. B* **383** (1992) 3–44.
- [224] J. M. Campbell and R. K. Ellis, *An update on vector boson pair production at hadron colliders*, *Phys. Rev. D* **60** (1999) 113006, [[hep-ph/9905386](#)].
- [225] M. Melles, *Resummation of angular dependent corrections in spontaneously broken gauge theories*, *Eur. Phys. J. C* **24** (2002) 193–204, [[hep-ph/0108221](#)].
- [226] M. Melles, *Electroweak radiative corrections in high-energy processes*, *Phys. Rept.* **375** (2003) 219–326, [[hep-ph/0104232](#)].
- [227] G. Bell, J. H. Kühn, and J. Rittinger, *Electroweak Sudakov logarithms and real gauge boson radiation in the TeV region*, *Eur. Phys. J. C* **70** (2010) 659–671, [[arXiv:1004.4117](#)].
- [228] F. Bloch and A. Nordsieck, *Note on the radiation field of the electron*, *Phys. Rev.* **52** (1937) 54–59.

- [229] M. Ciafaloni, P. Ciafaloni, and D. Comelli, *Electroweak Bloch-Nordsieck violation at the TeV scale: “Strong” weak interactions?*, *Nucl. Phys. B* **589** (2000) 359–380, [[hep-ph/0004071](#)].
- [230] E. Accomando, A. Denner, and S. Pozzorini, *Logarithmic electroweak corrections to $e^+e^- \rightarrow \nu_e\bar{\nu}_e W^+W^-$* , *JHEP* **03** (2007) 078, [[hep-ph/0611289](#)].
- [231] F. Bordry, et al., *Machine parameters and projected luminosity performance of proposed future colliders at CERN*, [arXiv:1810.13022](#).
- [232] A. Robson and P. Roloff, *Updated CLIC luminosity staging baseline and Higgs coupling prospects*, [arXiv:1812.01644](#).
- [233] S. Frixione et al., *Initial state QED radiation aspects for future e^+e^- colliders*, in *Snowmass 2021*, 3, 2022. [arXiv:2203.12557](#).
- [234] E. A. Kuraev and V. S. Fadin, *On radiative corrections to e^+e^- single photon annihilation at high energy*, *Sov. J. Nucl. Phys.* **41** (1985) 466–472.
- [235] M. Cacciari, A. Deandrea, G. Montagna, and O. Nicrosini, *QED structure functions: a systematic approach*, *EPL* **17** (1992) 123–128.
- [236] W. Beenakker et al., *WW cross-sections and distributions*, in *CERN Workshop on LEP2 Physics (followed by 2nd meeting, 15-16 Jun 1995 and 3rd meeting 2-3 Nov 1995)*, 2, 1996. [hep-ph/9602351](#).
- [237] F. Garosi, D. Marzocca, and S. Trifinopoulos, *LePDF: Standard Model PDFs for high-energy lepton colliders*, *JHEP* **09** (2023) 107, [[arXiv:2303.16964](#)].
- [238] **Particle Data Group** Collaboration, R. L. Workman et al., *Review of particle physics*, *PTEP* **2022** (2022) 083C01.
- [239] J. C. Collins, *Renormalization*, vol. 26 of *Cambridge Monographs on Mathematical Physics*. Cambridge University Press, Cambridge, 7, 2023.
- [240] T. Becher and G. Bell, *The gluon jet function at two-loop order*, *Phys. Lett. B* **695** (2011) 252–258, [[arXiv:1008.1936](#)].

Danksagungen

An erster Stelle gilt mein Dank Prof. Ansgar Denner für die Möglichkeit diese Arbeit schreiben zu dürfen, für seine außerordentliche Unterstützung, sein stets offenes Ohr und seine Geduld.

Meinen Kollegen in der TP2 möchte ich danken für viele interessante Diskussionen über so ziemlich jedes erdenkliche Thema, von Physik über Politik bis hin zu Löffeln. Vielen Dank an Timo für die Starthilfe bei der Arbeit mit MoCANLO, sowie an Christopher für viele hilfreiche Ratschläge im Umgang mit git und vielem mehr.

In besonderer Weise danke ich Brigitte und Karina für die großartige Unterstützung in allen bürokratischen Belangen.

Mein besonderer Dank gilt Jean-Nicholas, für seine Hilfe bei der Arbeit mit REPT1L, für die erste Version des symmetrischen Standardmodells, sowie für seine Arbeit an RECOLA.

Vielen Dank an Berrin, Daniele und Christoph für überaus nützliche Korrekturen am Manuskript.

Diese Arbeit entstand zum großen Teil während einer Zeit, die uns alle vor ungewohnte Herausforderungen stellte. Mein großer Dank gilt Viola, die mich in dieser Zeit in unschätzbare Weise unterstützt und ausgehalten hat. Ich möchte weiterhin allen Menschen danken, die mit mir diese Zeit (teilweise räumlich getrennt) geteilt haben, zuvörderst Spieltrieb, auch alias Berstian und die Brandstifter, die Schachspieler vom SB Versbach, Johannes, Thorben, Björn und Hanna. Nicht zuletzt und ganz besonders danke ich meinen Eltern, Johanna, Agnes und Friedhelm.